AN ABSTRACT OF THE THESIS OF

Ivana Radosavljevic for the degree of <u>Doctor of Philosophy</u> in <u>Chemistry</u> presented on <u>December 15, 1998</u>. Title: <u>Synthesis and Structure of New Oxides</u> <u>Containing Bi(III)</u>

Redacted for Privacy

Abstract approved: _____

Arthur W. Sleight

The subject of the research project was exploratory synthesis and structural characterization of Bi(III) containing oxides. Pyrochlore type bismuth titanate was prepared for the first time and its structure was refined from synchrotron X-ray and neutron diffraction data. Several new compounds have been synthesized in the BiM_2AO_6 family (M = divalent cation, A = pentavalent cation). The structures of $BiCa_2VO_6$ and $BiCa_2AsO_6$ have been determined from powder diffraction data. Both compounds are noncentrosymmetric and polar and have been found to be second harmonic generation active. A detailed study of $BiMg_2VO_6$ was performed by variable temperature single crystal diffraction, while the analogous $BiMg_2PO_6$ was refined from neutron diffraction data. Two new copper compounds, $BiCu_2VO_6$ and $BiCu_2AsO_6$ have been prepared and structurally characterized from single crystal diffraction. Other phases prepared in the BiM_2AO_6 family include $BiCd_2VO_6$, $BiZn_2PO_6$ and $BiPb_2VO_6$. A new noncetrosymmetric and polar bismuth cadmium vanadate, $BiCdVO_5$, has been synthesized and shown to be a second harmonic generator.

All the phases in the BiM_2AO_6 family contain $(BiO_2)^-$ infinite chains, $(AO_4)^{3-}$ tetrahedra and interspersed M^{2+} cations. Although built up from the same elements, they exhibit a variety of crystal structures. Bismuth is found in a number of similar coordinations, all of which include four short bonds to oxygens forming the chains. The $(BiO_2)^-$ chains can be related to the $(Bi_2O_2)^{2+}$ layers of the Aurivillius phases. The size of the M^{2+} cation and its bonding preferences appear to be important factors determining the structures of the BiM_2AO_6 phases. The largest M^{2+} cation incorporated into the BiM_2AO_6 compounds is calcium. When the M^{2+} cation has a pronounced covalent character, the nature of the tetrahedral cation appears to have a strong influence on the structure. Thus in the copper series, the three members with different tetrahedral cations have different structures. When the nature of the M^{2+} cation is predominantly ionic, the $(AO_4)^{3-}$ tetrahedra appear to attain the orientation that is the most favorable from the standpoint of efficient packing. In the case of $BiCa_2VO_6$ and $BiCa_2AsO_6$, this leads to all the $(AO_4)^{3-}$ tetrahedra pointing in the same direction along the polar axis of the crystal.

Synthesis and Structure of New Oxides Containing Bi(III)

by

Ivana Radosavljevic

A THESIS

submitted to

Oregon State University

in partial fulfillment of
the requirements for the degree of

Doctor of Philosophy

Completed December 15, 1998
Commencement June 1999

Doctor of Philosophy thesis of Ivana Radosavljevic presented on
December 15, 1998.

APPROVED:

Redacted for Privacy

Major Professor, representing Chemistry

Redacted for Privacy

Head of Department of Chemistry

Redacted for Privacy

Dean of the Graduate School

I understand that my thesis will become part of the permanent collection of
Oregon State University libraries. My signature below authorizes release of my
thesis to any reader upon request.

Redacted for Privacy

Ivana Radosávljevíc, Author

Acknowledgment

I would like to thank my advisor, Professor Arthur Sleight, for his guidance and support during my stay at Oregon State University. I deem myself privileged to have worked for Dr. Sleight. His knowledge and authority have been very inspirational, motivating me to keep trying to do my very best.

I would like to acknowledge my co-workers, members of the Sleight group in the period from 1995 to 1998: Dr. John Evans, Dr. Pat Woodward, Dr. Seung-Tae Hong, Dr. Mary Thundathil, Dr. Matt Hall, Dr. Nazy Khosrovani, Dr. Mark Kennard, Mr. Maddy Thangaraju, Dr. Svetlana Sorokina, Dr. Corinne Marcel, Dr. Martin Attfield, Dr. Claire Closmann, Dr. Xinghua Zhao, Dr. Kameswari Upadhyala, Dr. Alex Yokochi, Ju-Zhou Tao, Tammy Amos, Dong-Keun Lee, Paul Forster, Dr. Niangao Duan and Xiumei Xun.

I would like to take this opportunity to thank Dr. Tom Vogt of Brookhaven National Laboratory for collecting the neutron diffraction data on my samples and Engelene Chrysostom for performing second harmonic generation tests.

Thanks to Prof. Dermot O'Hare of Inorganic Chemistry of Oxford University for his hospitality and to Chemical Crystallography Laboratory of Oxford University for the use of their instruments during the two summers I spent there.

I am fortunate to have two families to thank for their support during the ups and downs of my graduate school. Thanks to my family in Belgrade, Yugoslavia, for their love and everything that I have received from them that made me what I

am today. Thanks to my family in Grants Pass, Oregon, for their support that has

meant so much to me.

Contribution of Authors

This Thesis contains published material co-authored by Dr. John S. O.

Evans and Dr. Arthur W. Sleight.

Table of Contents

Table of Contents (Continued)

Table of Contents (Continued)

Table of Contents (Continued)

Table of Contents (Continued)

List of Figures

List of Figures (Contnued)

List of Figures (Continued)

List of Tables

List of Tables (Continued)

List of Tables (Continued)

List of Tables (Continued)

Ova disertacija je posvecena mojoj porodici,

Mami, Taletu i Jeleni

Synthesis and Structure of New Oxides Containing Bi(III)

Chapter 1

Introduction: Scope and Purpose of the Research Project

---

1. 1. Introduction

Synthetic solid state chemistry has had a tremendous impact on areas ranging from high-tech applications to everyday life in the past several decades. One indicator of its importance is the vast volume of scientific literature published. A more tangible argument requires no proof other than a reflection on things that we use on a daily basis and possibly take for granted, that came as a result of advances in materials chemistry. Our computer memories, magnetic swipe cards, polystyrene coffee cups and kevlar skis were, not so long ago, only samples in laboratories of chemists worldwide.

In order to understand why materials behave the way they do, we need to understand their structure at the microscopic level, for the two are closely related. Understanding the relationships between structure and properties to the extent that would make possible the synthesis of products with desired, prescribed properties is still a challenge before the workers in all the fields that constitute the

multifaceted discipline of materials science. However, huge progress has been made since the days in 1912, when an exceptional group of scientists, including Professor W. von Roentgen, Professor A. Sommerfeld, Privatdozent M. von Laue and doctoral student P. Ewald were at the University of Munich. Ewald was working on his thesis on the interaction of electromagnetic radiation with crystalline matter. The story goes (1) that one day at Café Lutz, which the group frequented, Laue asked Ewald what he thought would happen if the radiation used had a wavelength of the order of interatomic distances in crystals. What they probably did not expect was the birth of a whole new area of science. X-ray diffraction developed to become the most powerful technique used for determination of crystal structures.

The objective of the research project described in this thesis was exploratory synthesis and structural characterization of novel Bi(III) containing oxides. Bi(III) has the electronic configuration of $[Xe]4f^{14}5d^{10}6s^2$. The $6s^2$ electrons are frequently referred to as a lone pair of electrons. Hybridization of the 6s and 6p states results in interesting stereochemistry for Bi(III). This can lead to some interesting and potentially applicable properties. Some of these properties are described in the following sections. The objective was not to give a comprehensive review of Bi(III) containing oxides, but rather to use a few examples to illustrate some properties where Bi(III) plays a significant role.

1. 1. 1. Ionic Conductors

1. 1. 1. 1. Bismuth Oxide, Bi_2O_3

Bismuth oxide exists in four polymorphs (2). The room temperature stable form α-Bi_2O_3 transforms on heating to δ-Bi_2O_3 at 729°C and this phase is stable up to the melting point at 824°C. Cooling may be accompanied by formation of one of the two metastable phases: β-Bi_2O_3 at 650°C or γ-Bi_2O_3 at 639°C (3). These phases transform to α-Bi_2O_3 by 500°C, although γ-Bi_2O_3 may be quenched to room temperature (4, 5). These phase changes are represented schematically in Figure 1. 1.

Heating

α-Bi2O3   729°C   δ-Bi2O3   824°C   Liquid

650°C
β-Bi2O3

by 500°C

γ-Bi2O3
639°C

Cooling
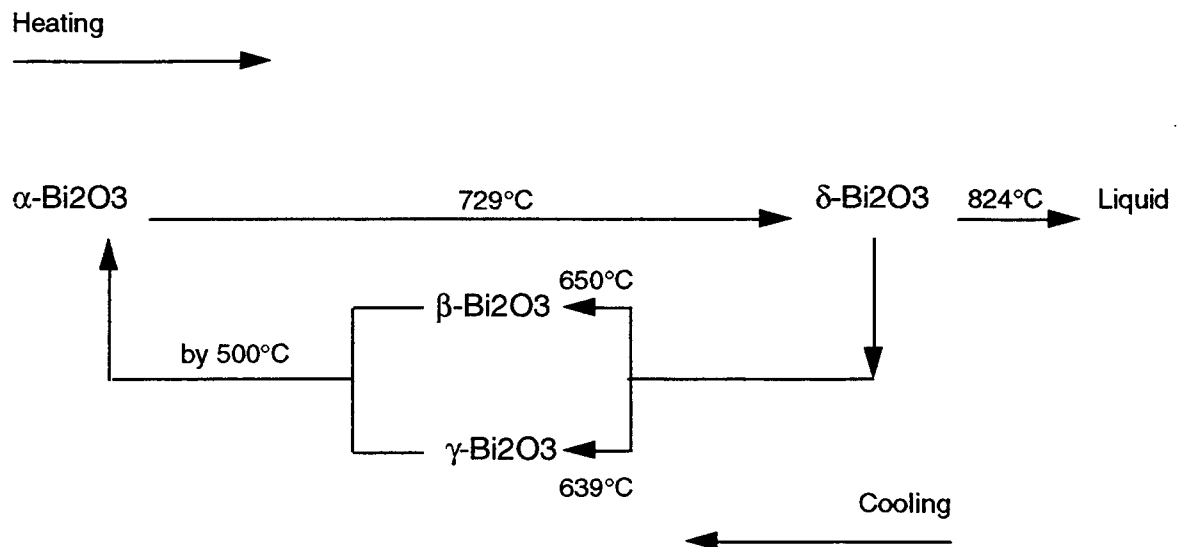
Figure 1. 1. A schematic of phase transitions in Bi_2O_3

The structure of α-Bi_2O_3 was first determined by Sillen (5) and subsequently by Malmros (6) and Harwig (3). It is a monoclinic phase with space group $P2_1/c$. The structure consists of alternating layers of bismuth and oxygen atoms parallel to the (010) plane, with one quarter of oxygen sites vacant. The material can thus be related to a distorted anion deficient fluorite of formula $BiO_{1.5}\varnothing_{0.5}$, where $\varnothing$ represents an anion vacancy.

β-Bi_2O_3 was reported by Sillen (5), Gattow and Schuetze (7) and Harwig (3). It is tetragonal and belongs to the space group $P\bar{4}2_1c$.

Body centered cubic γ-Bi_2O_3 was studied by Schumb and Rittner (8), Levin and Roth (2) and Harwig (3).

The structure of the high temperature δ-Bi_2O_3 has been a subject of numerous studies, owing to its complexity and importance in understanding the high ionic conductivity observed for this phase. Sillen (5) described the structure as fluorite related, with 25% of oxygen atoms missing and vacancies ordered in the <111> direction. Gattow and Schroeder (9) viewed it as a defect fluorite with 25% of oxygen sites missing on a statistical basis. Willis (10, 11) proposed a model where the oxygen atoms are displaced along the <111> directions onto a site of multiplicity four times that of the ideal site, with the occupancy of 3/16. Battle et al. (12) conducted a neutron diffraction study of δ-Bi_2O_3. They found that oxygens were distributed over the regular and interstitial sites in a way that leads to the formation of vacancy strings along the <111> direction.

Studies of the electrical properties of high temperature δ-Bi_2O_3 by Takahashi and Iwahara (13) and Harwig and Gerards (14) showed it to be an excellent ionic conductor with conductivity about three orders of magnitude larger than CaO stabilized ZrO_2 at 750°C (12). This extraordinary feature is compatible with high mobility of oxygen atoms resulting from the high degree of disorder inherent to the structure. In addition, Mairesse (15) suggested that the stereochemistry of Bi^{3+} may play a significant role, in the sense that the highly polarizable cation network in the structure readily accomodates disordering of oxygens and enhances oxygen atom mobility.

Since Takahashi and Iwahara first reported that δ-Bi_2O_3 could be stabilized to lower temperatures by doping with various isovalent and aliovalent cations, numerous series of solid solutions have been prepared in which the face centered cubic structure and the high ionic conductivity have been stabilized as far as room temperature (16).

The stabilizing effect of dopants appears to be related to the contraction of structure of δ-Bi_2O_3 as slightly smaller cations are introduced (17). While the structure is stabilized and the property of high ionic conductivity preserved at lower temperatures, the magnitude of the conductivity somewhat decreases owing to the increasing activation energy for oxygen migration (13).

1. 1. 1. 2. Bismuth Vanadium oxide, $Bi_4V_2O_{11}$

In 1986, Bush and Venetsev [18] reported the synthesis of a novel bismuth vanadate $Bi_4V_2O_{11}$. Abraham et al. [19] performed thermal analysis on this phase and found that it undergoes two phase transitions between room temperature and the melting point, one at 450°C and another at 570°C.

The first structural data on $Bi_4V_2O_{11}$ were reported by Bush and Venetsev [18], who gave an orthorhombic unit cell for this phase. The structure was subsequently re-determined by several authors [20, 21] who all reported orthorhombic symmetry. The most recent structural study was performed using a combination of x-ray, neutron and electron diffraction data by Jourbet et al. [22]. The α-$Bi_4V_2O_{11}$ phase was reported as monoclinic, in space group C2/m. The structure was described as a distorted Aurivillius phase, with bismuth – oxygen $(Bi_2O_2)^{2+}$ layers and oxygen deficient perovskite-like layers with vacancies ordered so that vanadium is alternately in tetrahedral and oxygen deficient octahedral coordination. The structure can thus be formulated as $Bi_2VO_{5.5}Vac_{0.5}$ to emphasize its relationship to Bi_2WO_6.

The room temperature phase transforms via the orthorhombic β-$Bi_4V_2O_{11}$ into tetragonal γ-$Bi_4V_2O_{11}$. This structure was determined by single crystal work by Abraham et al. [23]. γ-$Bi_4V_2O_{11}$ crystallizes in space group I4/mmm and consists of alternating $(Bi_2O_2)^{2+}$ layers and highly distorted oxygen deficient VO_6

octahedra. Both cations are displaced onto sites of higher multiplicities compared to the ideal structure in a disordered manner.

Abraham et al. (19) were the first to report the results of variable temperature electrical conductivity measurements that indicated that γ-$Bi_4V_2O_{11}$ is an exceptional ionic conductor. High oxygen mobility in this phase can be associated with oxygen vacancy and cation disorder that exists in this structure.

This discovery led to considerable efforts in synthetic solid state chemistry going into seeking ways to stabilize the γ-$Bi_4V_2O_{11}$ phase to room temperature. A new family of oxide ion conductors has been developed, known as BIMEVOX (where ME denotes the dopant metal). In these phases, vanadium is substituted by isovalent (Sb^{5+}, Nb^{5+}, Ta^{5+}) or aliovalent cations (Cu^{2+}, Ni^{2+}, Co^{2+}, Zn^{2+}, Ca^{2+}, Sr^{2+}, Fe^{3+}, Ti^{4+}, Mn^{4+}, etc.). A review of the known members of the BIMEVOX family and the effects of composition on electrical conductivity is given by Lazure et al. (24). Comparison of the effects of different dopants shows that the principal factor that enables stabilization and preservation of high conductivity is not the oxidation state of the dopant and hence the number of oxygen vacancies generated. Instead, it appears to be the readiness of the dopant cation to adopt octahedral coordination and undergo a degree of ordering (evidenced by crystallographic studies) that regularizes the diffusion paths for oxide ions.

1. 1. 2. Ferroelectrics and NLO Materials

1. 1. 2. 1. Aurivillius Phases

The most important class of Bi(III) containing ferrolectrics are the Aurivillius phases, named after Bendt Aurivillius who first synthesized and determined the structures of some of these compounds (25, 26, 27). Aurivillius phases are compounds of general formula $Bi_2A_{n-1}B_nO_{3n+3}$, where n ranges from 1 to 5. Their structures consist of $(Bi_2O_2)^{2+}$ layers sandwiched between n perovskite like layers. Some examples of Aurivillius phases are given in Table 1. 1.

Table 1. 1. Examples of Aurivillius Phases

Phase	n	Reference
Bi_2WO_6	1	28
$Bi_2CaNb_2O_9$	2	25
$Bi_3Ti_3O_{12}$	3	26
$Bi_4BaTi_4O_{15}$	4	27
$Bi_4Sr_2Ti_5O_{18}$	5	29

Crystal chemistry of the Aurivillius phases and the possible substitutions into the perovskite layer in terms of the geometrical perovskite tolerance factor

have been discussed by Subbarao (29). Numerous members of the Aurivillius family of compounds exhibit ferroelectricity (30). Displacive mechanism of the ferrolectric transitions in these phases has been described by Newnham et al. (31).

1. 1. 2. 2. Bismuth Tungstate, Bi_2WO_6

Bi_2WO_6 was first reported as a new mineral by Hey and Banister (32) in 1938. They grew single crystals of this phase and deduced from rotation photographs that it was of tetragonal symmetry. The crystal structure was reinvestigated in 1969 by Wolfe et al. (28). They found Bi_2WO_6 to be orthorhombic, with space group B2cb. The latest structural investigations were conducted by Rae et al. (33) by electron diffraction and Knight (34) by high resolution neutron diffraction. The results of both of these studies is that the space group of Bi_2WO_6 is $Pca2_1$.

This structure can be classified as the simplest member of the Aurivillius family $Bi_2A_{n-1}B_nO_{3n+3}$, with n = 1. It consists of $(Bi_2O_2)^{2+}$ layers and perovskite-like layers formed by corner sharing WO_6 octahedra. Each bismuth atom is bonded to six oxygens: four from the $(Bi_2O_2)^{2+}$ layers and two apical oxygens belonging to two different WO_6 octahedra. The WO_6 octahedra are tilted relative to the a axis in alternating directions by about 11° (34). Assuming that the lone pair electrons on Bi^{3+} are located opposite the bonded oxygens, the lone pairs point directly

towards the perovskite-like layer. It is likely that the stereochemical activity of the lone pair influences the tilting of the WO_6 octahedra and the resulting bonding between the two types of layers. The importance of the lone pair effects on the structure of Bi_2WO_6 can be illustrated by the fact that $Bi_{2-x}La_xWO_6$ solid solutions (35) are not isostructural with Bi_2WO_6, despite the similarity of Bi^{3+} and La^{3+} radii (36). $Bi_{2-x}Ln_xWO_6$ (Ln = rare earth) solid solutions (37) in fact have similar structures to that of the high temperature monoclinic polymorph of Bi_2WO_6.

Watanabe studied the polymorphism in Bi_2WO_6 by dilatometry and thermal analysis (38). His analyses showed that Bi_2WO_6 undergoes two reversible phase transitions, one at 662°C and the other at 962°C. The first transition is accompanied by very small changes in enthalpy and dimensions. This suggests that the nature of the change is displacive. X-ray diffraction studies suggest that it apparently occurs without a change in the crystal system. Watanabe (39) attributed this transition to the decrease in the WO6 octahedra tilt angle and the weakening of the two bismuth – oxygen bonds between the $(Bi_2O_2)^{2+}$ layers and the perovskite-like layer. The transition at 962°C, on the other hand, occurs with large thermal and volume changes (38). The structure is monoclinic and belongs to space group P2/c. It contains the $(Bi_2O_2)^{2+}$ layers and isolated WO_4 tetrahedra. Watanabe (39) suggested that this phase transition may be associated with the disappearance of the steric effects of the lone pair electrons at high temperatures. It is a major structural change and a reconstructive phase transition.

Bi_2WO_6 was found to be a second harmonic generation active material (28). It belongs to a polar space group and ferroelectric distortions exist both in the WO_6 octahedra and in the $(Bi_2O_2)^{2+}$ layers. The actual ferrolectric hysteresis, however, has not been measured.

1. 1. 3. Bismuth Molybdate Catalysts

Bismuth molybdates have been used as catalysts for oxidation of propene and butene, ammooxidation of propene, oxidation of methanol and oxidation of carbon monoxide (40, 41, 42, 43).

Although a number of phases have been reported in this system (44), the structures of only three bismuth molybdates are reported in the ICSD database: Bi_2MoO_6, $Bi_2Mo_2O_9$ and $Bi_2Mo_3O_{12}$, while $Bi_{26}Mo_{10}O_{69}$ (45) was reported more recently.

The structure of Bi_2MoO_6 was determined by single crystal diffraction on the naturally occuring mineral koechlinite by van den Elzek and Rieck (46) and subsequently by powder neutron diffraction on a synthetic sample by Teller et al. (47). Bi_2MoO_6 is orthorhombic, belongs to space group $Pna2_1$ and can be described as a n = 1 member of the Aurivillius family $Bi_2A_{n-1}B_nO_{3n+3}$. The high temperature form of Bi_2MoO_6 was characterized by Buttrey et al. (48).

The structure of Bi_2MoO_6 was determined by Chen and Sleight (49). This compound crystallizes in the monoclinic space group $P2_1/n$. It consists of isolated

MoO_4 tetrahedra and eight coordinate bismuth polyhedra that are connected in a way that leads to formation of channels in the structure.

Isolated MoO_4 tetrahedra are also found in the monoclinic $Bi_2Mo_3O_{12}$ structure, detemined by van der Elzen and Rieck (50) and Theobald et al. (51). Bismuth is eight coordinate, but the connectivity of the polyhedra is different from that in $Bi_2Mo_2O_9$.

In an attempt to identify some common structural features of bismuth molybdates that lead to the similar catalytic properties, Depero and Sangaletti (44) have proposed a way to systematically model the structures of the members of this series. They proposed that bismuth molybdates could be thought of as consisting of partially occupied hexagonal nets of cations formed by substitution of Mo^{6+} for Bi^{3+} in cation layers of β-Bi_2O_3. Other authors (48) agree that a fluorite type superstructure is common to these phases. Although the issue of systematizing the structures is still open, it appears that the features that each phase should possess are available oxidizing agent (Mo^{6+}) and an efficient mechanism for oxygen diffusion from the bulk to the surface of the material. The oxidation properties of these materials are thus intimately related to the oxygen mobility observed in other discussed Bi(III) containing phases.

1. 1. 4. Ferroelastics

1. 1. 4. 1. Definition of Ferroelasticity

Ferroelastic materials are those that possess a net spontaneous strain in the absence of mechanical stress or an electric field. In addition, they possess two or more orientations of the net strain between which they can be switched by application of mechanical stress (52, 53).

Ferroelasticity can occur in crystals that possess other types of ferroic properties, such as ferroelectrics and ferromagnets (54). In a ferroelastic ferroelectric, the two properties may be coupled in the sense that a change in the polarization vector induces a change in the strain vector and vice versa. Examples of such compounds are potasium dihydrogen phosphate, KH_2PO_4 and barium titanate, $BaTiO_3$ (55). A compound that is a pure ferroelastic is bismuth vanadate, $BiVO_4$ (56).

1. 1. 4. 2. Bismuth vanadium oxide, $BiVO_4$

The first structural studies of naturally occuring $BiVO_4$, mineral pucherite, were published by de Jonge et al. (57). The structure was determined by Quarashi and Barnes (58, 59), who described it as orthorhombic, space group

Pnca. Laboratory synthesis of this phase, however, gave a phase with different structure (56).

Bierlein and Sleight discovered ferroelasticity in $BiVO_4$ at room temperature (56). By optical examination of the crystal they showed that it undergoes a transition to a paraelastic phase at 225°C. This phase transition could not be detected by thermal analysis, suggesting that it was probably of low energy, displacive nature. Variable temperature diffraction studies of $BiVO_4$ were performed by Sleight et al (60) and David et al (61). According to these studies, room temperature $BiVO_4$ is monoclinic, space group I2/a. Vanadium is tetrahedral and bismuth is found in an eightfold coordination. The high temperature phase is tetragonal, space group $I4_1/a$. On the basis of their structural studies, both groups proposed a mechanism for the ferroelastic transition in $BiVO_4$. They found that the principal change is the displacement of bismuth atoms along the [001] direction, where they move closer to the oxygens on one side of the coordination sphere and away from those on the opposite side. This distortion can again be attributed to the steric effect of the lone pair electrons on Bi^{3+}, which is not possible in the high temperature tetragonal phase due to symmetry constraints (60).

Monoclinic $BiVO_4$ has been patented as a base for orange-yellow pigments (62).

1. 1. 5. High Temperature Superconductors

An important class of Bi(III) containing compounds is the high temperature superconductors. One family of materials can be represented by the general formula $(BiO)_2Sr_2Ca_{n-1}Cu_nO_{2n+2}$. Members with n = 1, $Bi_2Sr_2CuO_6$ (63), n = 2, $Bi_2Sr_2CaCu_2O_8$ (64) and n = 3, $Bi_2Sr_2Ca_2Cu_3O_{10}$ (65) have been prepared as crystalline single phases. Layered structures of high temperature superconducting cuprates have been reviewed by several authors (65, 66). Structures of bismuth containing phases exhibit incommensurate modulations (67, 68, 69, 70, 71, 72) and are therefore considerably more complex. Studies of this feature appear to indicate that the modulation occurs primarily due to the Bi(III) displacements that enable the formation of three short bonds to oxygen and a less symmetric environment preferred by this cation. Bi(III), however, does not seem to play an active role in the superconductivity mechanism. An exception to this is the $BaPb_{1-x}Bi_xO_3$ system (73), where bismuth does play a key role through mixed valence effects.

1. 2. Systems Investigated

The systems investigated in this project and the single phase products

obtained and further characterized are summarized in Table 1. 3.

Table 1. 3. Phase Systems Investigated in the Research Project

System	Product obtained
$Bi^{III}/Ti^{IV}/O$	$Bi_2Ti_2O_7$
$Bi^{III}/Ca^{II}/V^{V}/O$	$BiCa_2VO_6$
$Bi^{III}/Ca^{II}/As^{V}/O$	$BiCa_2AsO_6$
$Bi^{III}/Ca^{II}/P^{V}/O$	
$Bi^{III}/Mg^{II}/V^{V}/O$	$BiMg_2VO_6$
$Bi^{III}/Mg^{II}/P^{V}/O$	$BiMg_2PO_6$
$Bi^{III}/Sr^{II}/V^{V}/O$	
$Bi^{III}/Sr^{II}/As^{V}/O$	
$Bi^{III}/Sr^{II}/P^{V}/O$	
$Bi^{III}/Cd^{II}/V^{V}/O$	$BiCd_2VO_6$, $BiCdVO_5$
$Bi^{III}/Cu^{II}/V^{V}/O$	$BiCu_2VO_6$
$Bi^{III}/Cu^{II}/As^{V}/O$	$BiCu_2AsO_6$
$Bi^{III}/Ni^{II}/V^{V}/O$	
$Bi^{III}/Co^{II}/V^{V}/O$	
$Bi^{III}/Zn^{II}/V^{V}/O$	
$Bi^{III}/Zn^{II}/P^{V}/O$	$BiZn_2PO_6$
$Bi^{III}/Pb^{II}/V^{V}/O$	$BiPb_2VO_6$

The objective of the work on the Bi_2O_3 – TiO_2 system was the synthesis of the pyrochlore phase $Bi_2Ti_2O_7$. Preparation of this compound and the refinement of its structure are described in Chapter 2.

Exploratory synthesis in the Bi_2O_3 – CaO – V_2O_5 system resulted in the discovery of a new bismuth calcium vanadate, $BiCa_2VO_6$. Ab initio solution of the structure of this compound from laboratory X-ray diffraction data is the topic of Chapter 3.

The attempt to synthesize the corresponding phosphate was not successful. Bismuth calcium arsenate $BiCa_2AsO_6$, however, was prepared and its structure refined, as described in Chapter 4.

The attempts to prepare $BiSr_2AO_6$ phases (A = V, As, P) were not successful. The obtained products were inhomogeneous mixtures of known compounds.

Structural reinvestigations of $BiMg_2AO_6$ (A = V, P) are the subjects of Chapters 5 and 6, respectively.

The work on Bi_2O_3 – CdO – V_2O_5 system gave two compounds, $BiCd_2VO_6$ and $BiCdVO_5$. Some details about $BiCd_2VO_6$ are given in section 3.6. Structural characterization of $BiCdVO_5$ from single crystal X-ray diffraction is described in Chapter 7.

Synthesis of a new bismuth copper vanadate, $BiCu_2VO_6$, as a polycrystalline material and single crystals and the determination of its structure are the topic of Chapter 8.

Structural work on a new bismuth copper arsenate, $BiCu_2AsO_6$ is the subject of Chapter 9.

Attempts to synthesize analogous compounds of Ni^{2+} and Co^{2+} resulted in formation of known materials.

Bismuth zinc phosphate, $BiZn_2PO_6$ was prepared in the polycrystalline form, while single crystal growth was not successful. Structural investigations of this phase from laboratory X-ray diffraction data did not give results beyond the determination of the unit cell. Synthesis of the corresponding vanadate did not yield the expected product. However, it was found that Zn could be isostructurally substituted into $BiCu_2VO_6$, up to the composition of $Bi(Cu_{1/3}Zn_{2/3})_2VO_6$.

Synthesis of bismuth lead vanadate, $BiPb_2VO_6$ was successful. The attempt at ab initio structure solution from high resolution synchrotron X-ray diffraction data gave the unit cell, space group symmetry, but only partial structure. Crystal growth resulted in formation of twinned crystals, not suitable for structure determination.

A comparative analysis of the BiM_2AO_6 structures and the final conclusions are the subject of Chapter 10.

1. 3. References

1. M. J. Buerger, Crystal Structure Analysis, John Wiley and Sons, New York, N.Y., 1960.

2. E. M. Levin and R. S. Roth, *J. Res. Nat. Bur. Stand.* 68A, 189 (1969)

3. H. A. Harwig, *Z. Anorg. Allg. Chem.*, 444, 151 (1978)

4. H. A. Harwig, Thesis, State University Utrecht, The Netherlands, 1977.

5. L. G. Sillen, *Ark. Kemi Mineral. Geol.*, 12A, 1 (1937)

6. G. Malmros, *Acta Chem. Scand.*, 24, 384 (1970)

7. G. Gattow and D. Schuetze, *Z. Anorg. Allg. Chem.*, 328, 44 (1964)

8. W. C. Schumb and E. S. Rittner, *J. Amer. Chem. Soc.*, 65, 1055 (1943)

9. G. Gattow and H. Schroeder, *Z. Anorg. Allg. Chem.*, 318, 176 (1962)

10. B. T. M. Willis, *Proc. Roy. Soc.*, A274, 134 (1963)

11. B. T. M. Willis, *Acta Cryst.*, 18, 75 (1965)

12. P. D. Battle, C. R. A. Catlow, J. Drennan and A. D. Murray, *J. Phys.* C16, L561 (1983)

13. T. Takahashi and H, Iwahara, *Mat. Res. Bull.*, 13, 1447 (1978)

14. H. A. Harwig and A. G. Gerards, *J. Solid State Chem.*, 26, 265 (1978)

15. G. Mairesse, in Fast Ion Transport in Solids, ed. by B. Scrosati, Kluver, Amsterdam, The Netherlands, 1993.

16. P. Shuk, H. D. Wiemhoefer, U. Guth, W. Goepel and M. Greenblatt, *Solid State Ionics*, 89, 179 (1996)

17. M. J. Verkerk and A, J, Burggraaf, *J. Electrochem. Soc.*, 75, 128 (1980)

18. A. A. Bush and Yu. N. Venetsev, *Russ. J. Inorg. Chem.*, 769, 31, 5 (1986)

19. F. Abraham, M. F. Debruille-Gresse, G. Mairesse and G. Nowogrocki, *Solid State Ionics*, 28-30, 529 (1988)

20. K. B. R. Varma, G. N. Subbanna, T. N. Guru Row and C. N. R. Rao, *J. Mater. Res.*, 5, 2718 (1990)

21. M. Touboul, J. Lokaj, L. Tessier, V. Kettman and V. Vrabel, *Acta Cryst..*, C48, 1176 (1992)

22. O. Joubert, A. Jouanneaux and M. Ganne, *Mat. Res. Bull.*, 29, 12, 175 (1994)

23. F. Abraham, J. C. Boivin, G. Mairesse and G. Nowogrocki, *Solid State Ionics*, 40-41, 934 (1190)

24. S. Lazure, Ch. Vernochet, R. N. Vannier, G. Nowogrocki and G. Mairesse, *Solid State Ionics*, 90, 117 (1990)

25. B. Aurivillius, *Ark. Kemi*, 1, 54, 463 (1949)

26. B. Aurivillius, *Ark. Kemi*, 1, 58, 499 (1949)

27. B. Aurivillius, *Ark. Kemi*, 2, 37, 519 (1949)

28. R. W. Wolfe, R. E. Newnham and M. I. Kay, *Solid State Comm.*, 7, 1797 (1969)

29. E. C. Subbarao, *J. Amer. Chem. Soc.*, 45, 4, 166 (1962)

30. E. C. Subbarao, *J. Chem. Phys.*, 34, 2, 695 (1961)

31. R. E. Newnham, R. W. Wolfe and J. F. Dorrian, *Mat. Res. Bull.*, 6, 1029 (1971)

32. M. H. Hey and F. A. Bannister, *Mineral. Mag.*, 25, 41 (1938)

33. A. D. Rae, J. G. Thompson and R. L. Withers, *Acta Cryst.* B 47, 870 (1991)

34. K. S. Knight, *Mineral. Mag.*, 56, 399 (1992)

35. A. Watanabe, Y. Sekikawa and F. Izumi, *J. Solid State Chem.*, 41, 138 (1982)

36. A. Watanabe, *Mat. Res. Bull.*, 15, 1473 (1980)

37. R. D. Shannon, *Acta Cryst.* A32, 751 (1976)

38. A. Watanabe, *J. Solid State Chem.*, 41, 160 (1982)

39. A. Watanabe, *Mat. Res. Bull.*, 19, 877 (1984)

40. T. Tsunoda, T. Hayakawa, T. Kameyama and K. Takehira, *J. Chem. Soc. Farad. Trans.*, 91, 1117 (1995)

41. L. C. Glaeser, J. F. Brazdil, M. A. Hazle, M. Mehicic and R. K. Grasseli, *J. Chem. Soc. Farad. Trans.*, 81, 2903 (1985)

42. R. K. Grasseli and J. F. Burrington, *Adv. Catal.*, 30, 133 (1981)

43. D. H. Galvan, S. Fuentes, M. Alvalosborja, L. Cotaaraiza, E. A. Early, M. B. Maple and J. Cruzreyes, *J. Phys. Condens. Matter*, 5, A217 (1993)

44. L. E. Depero and L. Sangaletti, *J. Solid State Chem.*, 119, 428 (1995)

45. D. J. Buttrey, T. Vogt, G. P. A. Yap and A. L. Rheingold, *Mat. Res. Bull.*, 32, 7, 947 (1997)

46. A. F. van den Elzek and G. D. Rieck, *Acta Cryst.* B29, 2436 (1973)

47. R. G. Teller, J. F. Brazdil, R. K. Grasseli and J. D. Jorgensen, *Acta Cryst.* C40, 2001 (1984)

48. D. J. Buttrey, T. Vogt, U. Wildgruber and W. R. Robinson, *J. Solid State Chem.*, 111, 118 (1994)

49. H. Y. Chen and A. W. Sleight, *J. Solid State Chem.*, 63, 70 (1986)

50. A. F. van den Elzek and G. D. Rieck, *Acta Cryst.* B29, 2433 (1973)

51. F. Theobald, A. Laarif and A. W. Hewat, *Mat. Res. Bull.*, 20, 653 (1985)

52. K. Aizu, *J. Phys. Soc. Japan*, 27, 2, 387 (1969)

53. K. Aizu, *J. Phys. Soc. Japan*, 28, 3, 706 (1970)

54. R. E. Newnham, Structure – Property Relations, Springer – Verlag, New York, 1975.

55. S. C. Abrahams, *Mat. Res. Bull.*, 6, 881 (1971)

56. J. D. Bierlein and A. W. Sleight, *Solid State Comm.*, 16, 69 (1975)

57. W. F. de Jong and J. J. de Lange, *Amer. Mineral.*, 21, 809 (1936)

58. M. M. Qarashi and W. H. Barnes, *Amer. Mineral.*, 37, 423 (1952)

59. M. M. Qarashi and W. H. Barnes, *Amer. Mineral.*, 38, 489 (1953)

60. A. W. Sleight, H. Y. Chen, A. Ferretti and D. E. Cox, *Mat. Res. Bull.*, 14, 1571 (1979)

61. W. I. F. David, A. M. Glazer and A. W. Hewat, *Phase Transitions*, 1, 155, (1979)

62. Balducci et al., U. S. Patent N° 4,230,500

63. C. C. Torrardi et al., *Phys. Rev. B*, 38, 225 (1988)

64. M. A. Subramanian, C. C. Torardi, J. C. Calabrese, J. Gopalakrishnan, K. J. Morrissey, T. R. Askew, R. B. Flippen, U. Chowdry and A. W. Sleight, *Science*, 239, 1015 (1988)

65. A. W. Sleight, *Science*, 242, 1519 (1988)

66. B. Raveau, in High-T$_c$ Superconductivity 1996: Ten Years after the Discovery, 109, Kluwer Academic Publishers, Amsterdam, The Netherlands, 1997.

67. Y. Gao, P. Lee, P. Coppens, M. A. Subramanian and A. W. Sleight, *Science*, 241 954 (1988)

68. C. C. Torardi, J. B. Parise, M. A. Subramanian, J. Gopalakrishnan and A. W. Sleight, *Physica C*, 157, 115 (1989)

69. Y. Le Page, W. R. McKinnon, J. M. Tarascon and P. Barboux, *Phys. Rev. B*, 40, 10 (1989)

70. A. I. Beskrovnyi, M. Dlouha, Z. Jirak and S. Vratislav, *Physica C*, 171, 19 (1990)

71. A. A. Levin, Yu. I. Smolin and Yu. F. Shepelev, *J. Phys.:Condens. Matter*, 6, 3539 (1994)

72. N. Jakubowicz, O. Perez, D. Grebille and H. Leligny, *J. Solid State Chem.*, 139, 194 (1998)

73. A. W. Sleight, J. L. Gillson and P. E. Bierstedt, *Solid State Commun.*, 7, 299 (1969)

Chapter 2

Synthesis and Structure Refinement
of Pyrochlore – Type Bismuth Titanate

2. 1. Introduction

Compounds with the pyrochlore structure have been extensively studied owing to a wide variety of chemical compositions as well as interesting and potentially applicable properties they exhibit. Comprehensive reviews of structural features and properties of pyrochlores can be found in literature (1,2).

Phases of the general formula $A_2B_2O_7$ form a family of compounds isostructural with the mineral pyrochlorite, $(NaCa)(NbTa)O_6F$. Pyrochlores most commonly contain the combinations of oxidation states of $A^{3+}_2B^{4+}_2O_7$ or $A^{2+}_2B^{5+}_2O_7$. Variations of these basic formulations by substitutions onto either or both cation sites, such as $A^{2+}A^{4+}B_2O_7$, $A_2B^{3+}B^{5+}O_7$, $A^{1+}A^{3+}B^{4+}B^{6+}O_7$ or $A^{2+}A^{3+}B^{4+}B^{5+}O_7$ are also known (2,3). In addition, the pyrochlore structure is such that it tolerates a degree of deficiency on the A cation and oxygen sites, giving rise to defect pyrochlores .

The pyrochlore structure was first determined by von Gaertner (4). The ideal structure belongs to the space group $Fd\bar{3}m$. There are eight molecular units

per unit cell and four types of crystallographically unique sites. Atomic positions

for ideal pyrochore are given in Table 2.1. These positions are given with respect

to the origin choice 2 in space group $Fd\bar{3}m$, and this choice of origin will be

consistently used throughout this chapter. Figure 2.1 respresents the ideal

pyrochlore structure. In this figure, A cations are represented by purple spheres,

B cations as blue distorted octahedra and oxygen atoms are red.
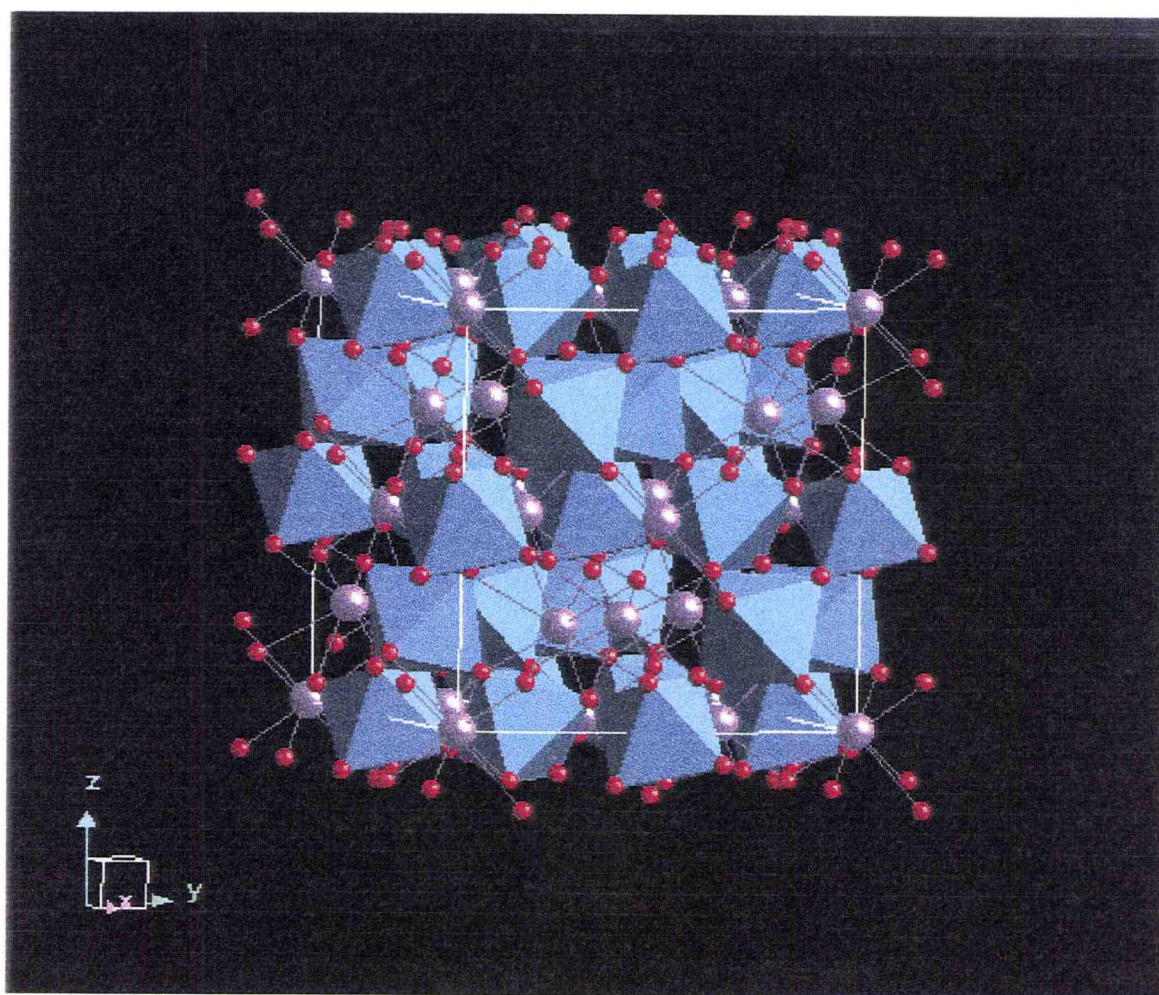
Figure 2.1. Ideal pyrochlore structure

Table 2.1. Atomic Positions for the Ideal Pyrochlore Structure

Atom	Site	Symmetry	Coordinates
A	16c	$\bar{3}m$	0, 0, 0
B	16d	$\bar{3}m$	1/2, 1/2, 1/2
O	48f	mm	1/8, 1/8, x
O'	8a	$\bar{4}3m$	1/8, 1/8, 1/8

There is only one positional parameter x to be determined. Nikiforov (5) developed a set of mathematical relationships that can be used to calculate the unknown oxygen coordinate from the known lattice parameter and the ionic radii of the constituent cations. These relationships are based on the hard sphere model and strict additivity of ionic radii and therefore cannot be applied to compositions containing highly polarizable cations (e.g. Bi^{3+}, Pb^{2+}).

The A cations in the ideal pyrochlore structure have a coordination number of eight. The coordination geometry can be described as a cube distorted along the threefold axis. The two bonds along this axis are unequal to the remaining six, which form a puckered ring with the midplane parallel to the crystallographic (111) plane. B cations are located in a trigonal antiprismatic environment. The exact degree of distortion of the two coordination geometries from the ideal cube and the ideal tetrahedron, respectively, is determined by the oxygen parameter x.

For x = 0.375, BO_6 coordination polyhedra would be regular octahedra; for x = 0.4375, AO_8 polyhedra would be regular cubes (6). Since there are no sites of cubic symmetry in the structure, actual x parameters lie between these two limiting values. The connectivity of AO_8 and BO_6 coordination polyhedra to form the pyrochlore structure has been described in several ways. Bystrom (7) described it as consisting of a framework of corner shared BO_6 octahedra, with A atoms occupying the interstitial sites. Jona et al. (8), Aleshin and Roy (9) and Longo et al. (10) described it as an oxygen deficient fluorite structure, with the BO_6 polyhedra sharing corners to give the framework of the composition $(B_2O_6)_\infty$ while the remaining oxygens and the A cations occupy the interstices in this framework. Sleight (11) viewed the pyrochlore structure as consisting of two interpenetrating networks. B cations are in a sixfold coordination, sharing corners to form the (B_2O_6) network. A cations are in a twofold coordination, bonded only to the oxygens on the special position, forming the A_2O' network. This description facilitates the rationalization of the relatively high degree of tolerance of the pyrochlore structure towards both the A cation and O' deficiency.

Owing to the multitude of the chemical compositions attainable and a number of structural modifications exhibited, pyrochlores can display various interesting and applicable properties. Detailed reviews of the applications of pyrochlores are given in references 1 and 2.

2. 2. Stability Field of Pyrochlores

The large number of known pyrochlore phases has made possible certain generalizations in regard to the necessary conditions for the formation of this structure. Stability fields for pyrochlores have been constructed on the basis of radius ratios of constituent cations. According to these studies, the pyrochlore structure should form and be stable for r_A^{3+}/r_B^{4+} between 1.46 and 1.80 at ambient pressure (1). However, the upper limit can be extended by high pressure synthesis methods (12). Radius ratio arguments cannot be viewed as universal, since they do not take into account the nature of the cations. For example, La^{3+} and Bi^{3+} have very different electron configurations and, despite their similar radii, $La_2Zr_2O_7$ and $La_2Hf_2O_7$ are pyrochlores, while $Bi_2Zr_2O_7$ and $Bi_2Hf_2O_7$ are not (13). Lanthanum titanate has not been produced in the pyrochlore structure (14), while we have prepared pyrochlore type bismuth titanate (15). It can be expected that the radius ratio conditions for formation of the pyrochlore structure should be to a lesser degree applicable to Bi^{3+} and other lone pair cations. These species are highly polarizable and their radii are not easily defined, since they depend on the coordination environment of these cations in specific compounds.

Table 2.1 contains the known $Bi_2B_2O_7$ phases, B^{4+} radii, r_{Bi}^{3+}/r_B^{4+} ratios, electronegativitites of B cations and the differences in electronegativities between B cations and oxygen.

Table 2.2. Known Pyrochlores of the $Bi_2B_2O_7$ Formula

Composition	B^{4+}	r_{Bi}^{3+}/r_B^{4+}	χ_B	$\Delta\chi_{B-O}$
$Bi_2Pt_2O_7$	0.625	1.776	2.28	1.16
$Bi_2Os_2O_7$	0.630	1.762	2.2	1.24
$Bi_2Ru_2O_7$	0.620	1.790	2.2	1.24
$Bi_2Rh_2O_{6.8}$	0.600	1.85	2.28	1.16
$Bi_2Ir_2O_7$	0.625	1.776	2.20	1.24
$Bi_2Ti_2O_7$	0.605	1.835	1.54	1.90
α- $Bi_2Sn_2O_7$	0.690	1.609	1.96	1.48
$Bi_2Zr_2O_7$	0.720	1.54	1.33	2.11
$Bi_2Hf_2O_7$	0.71	1.56	1.3	2.14

Data in Table 2.2 reveal certain inconsistencies between the reported structures and the predictions based on the radius ratio stability fields. $Bi_2Rh_2O_{6.8}$ and $Bi_{1.74}Ti_2O_{6.62}$ are outside the stability region and yet they form the ideal pyrochlore structure and one very closely related to it, respectively. $Bi_2Sn_2O_7$, $Bi_2Zr_2O_7$ and $Bi_2Hf_2O_7$ fall within the stability field. Although their structures appear to be related to pyrochlore, they are sufficiently different that they are still unknown.

Wang et al. (16) suggested that the formation of Bi^{3+} containing pyrochlores might be related to the extent of coupling of bismuth $6s^2$ electrons in the structure. Another approach is to relate the distortion from the ideal pyrochlore structure to the relative electronegativity of Bi and the B cation. If electronegativity of the B cation is large and its bonds to oxygen have a pronounced covalent character, there is a competition between Bi and B for orbital overlap with the oxygen atom they both bond to. The most favorable way for Bi to achieve maximum overlap is to remain on its ideal position on the threefold axis. If electronegativity of B is low and its bonds to oxygen are largely ionic in nature, the competition between Bi and B for overlap with the oxygen between them does not occur and Bi is free to displace off its ideal position on the threefold axis onto a site more favorable for a lone pair cation. This gives rise to distorted pyrochlore structure. Data in Table 2.2 show that the B – O bonds have a more ionic character when B = Ti, Sn, Zr and Hf. According to the above arguments, these phases should not form ideal pyrochlore structures, and indeed they do not.

A correlation between the stereochemical activity of the lone pair electrons and the electrical conductivity of the bismuth(III) containing pyrochlores has recently been discussed by Ismunandar (28).

2. 3. Bi_2O_3 - TiO_2 System

Studies of the Bi_2O_3 - TiO_2 system have been reported by numerous authors. Known and characterized phases in this system include $Bi_4Ti_3O_{12}$, first synthesized and investigated by Aurivillius (17), $Bi_2Ti_4O_{11}$, reported by Subbarao (18) and $Bi_{12}TiO_{20}$, identified by Levin and Roth (19). Existence of the pyrochlore phase, $Bi_2Ti_2O_7$, in this system has been an issue of interest and some controversy. Aleshin and Roy (9) indicated the formation of a pyrochlore-type phase in the solid state reaction of Bi_2O_3 and $2TiO_2$, heated at 750°C/48hr and 1225°C/22hr. No information were given concerning the purity of the obtained product or the structural details of the pyrochlore phase. Shimada et al. (20) reported the growth of $Bi_2Ti_2O_7$ single crystals in the Bi_2O_3 -V_2O_5 - TiO_2 system. Crystals were grown from a melt that contained 13% mol V_2O_5 and an addition of 10% mol ZnO. The cubic unit cell parameter found from a powder X-ray diffraction pattern was a = 20.68 Å. However, the description of the obtained crystals as reddish-brown indicates that the composition was not pure bismuth titanate. Barsukova et al. (21) performed a study of hydrothermal crystallization of bismuth titanium oxides; $Bi_2Ti_2O_7$ was not synthesized. Knop et al. (22) carried out a solid state reaction of Bi_2O_3 + $2TiO_2$ at 950°C/16hr and 1000°C/24hr. X-ray diffraction pattern of the obtained product contained extra peaks that precluded cubic indexing. They also studied a series of $(Y_{1-x}Bi_x)_2Ti_2O_7$ solid solutions with x ranging from 0.2 to 0.8. Samples with compositions up to x = 0.75 were cubic pyrochlores with the unit cell parameter linearly increasing with increasing

bismuth content. Extrapolation of these data to x = 1 yields a cell parameter of a = 10.354 Å for pure $Bi_2Ti_2O_7$. Bamberger et al. (23) studied several sets of bismuth containing lanthanide dititanates $(Ln_{1-x}Bi_x)_2Ti_2O_7$ (Ln = La to Lu and Y, except Ce, Pm and Eu). Extrapolation of their data to pure $Bi_2Ti_2O_7$ gives a cubic lattice parameter of 10.354 ± 0.008 Å.

The available literature information seems to indicate that the attempts to prepare a pure bismuth titanate with the pyrochlore structure by solid state reactions, hydrothermal syntheses and crystal growth have not been successful. High temperature solid state reactions, in particular, give mixed bismuth titanates. A solution precipitation technique was therefore employed to synthesize essentially single phase pyrochlore type bismuth titanate.

2. 4. Experimental

Initial attempts to synthesize bismuth titanate by solution precipitation method were performed by using the stoichiometric quantities of 0.1M acetone solutions of bismuth (III) nitrate pentahydrate (Aldrich, 98+%) and titanium (IV) butoxide (Alfa Aesar, 99+%). X-ray diffraction patterns of the obtained products indicated the presence of considerable quantities of the bismuth rich phase $Bi_4Ti_3O_{12}$. Subsequent syntheses were therefore modified and a 10% molar excess of titanium was used. The two acetone solutions were vigorously stirred to achieve homogeneity and then mixed together. The mixture was hydrolyzed at

50°C with constant stirring and dropwise addition of ammonium hydroxide, while the pH value was monitored. The white precipitate that formed immediately upon mixing the two solutions turned into a voluminous, gel-like white slurry as the mixture was neutralized. After most of acetone had evaporated, the beaker was removed from the hot plate, lightly covered and left overnight. This resulted in the formation of dry tan-colored granules that were then ground, placed in an alumina crucible and heated at 600°C for 16 hours. The final product was a light tan-colored powder.

The X-ray diffraction pattern of samples made in this way at a 1 : 1 Bi : Ti ratio showed that a face centered cubic phase dominated, but peaks of $Bi_4Ti_3O_{12}$ were also present. It was found that these extra peaks could be eliminated by using extra titanium in the synthesis. For the sample used for detailed structural analysis, a 10% molar excess of titanium relative to 1 : 1 Bi : Ti ratio was used. Very weak peaks of $Bi_2Ti_4O_{11}$ and TiO_2 were present in this sample. Heating samples at 650°C or higher resulted in the decomposition of the pyrochlore phase to form $Bi_4Ti_3O_{12}$ and $Bi_2Ti_4O_{11}$.

Laboratory X-ray diffraction was used to monitor the content of the obtained products. Patterns were recorded on a Siemens D5000 powder diffractometer with a Kevex detector and vertical Soller slits. Synchrotron X-ray diffraction data for structure refinement were collected on line X7A of the National Synchrotron Light Source at Brookhaven National Laboratory. The wavelength used was 0.50275 Å. The sample was in a 0.2 mm capillary and an absorption

correction was applied. Neutron diffraction data were collected on line BT-1 at the NIST Center for Neutron Research using a wavelength of 1.5402 Å and an array of 32 He-3 detectors at 3° intervals. Details of both data collections are given in Table 2.3.

Table 2.3. Details of Synchrotron X-ray and Neutron Diffraction Data

Quantity	X-ray Diffraction Data	Neutron Diffraction Data
Empirical formula	$Bi_{1.74}Ti_2O_{6.62}$	$Bi_{1.74}Ti_2O_{6.62}$
Formula weight (amu)	566.005	565.403
Z	8	8
Calc. density (g/cm^3)	6.768	6.770
Space group	$Fd\bar{3}m$ (227), origin#2	$Fd\bar{3}m$ (227), origin#2
Unit cell parameter, a (Å)	10.35691(11)	10.35233(17)
Wavelength (λ)	0.50275	1.5402
Data range (° 2θ)	4.5 - 38	10-150
Zero point (° 2θ)	0.0087(2)	-0.0501(18)
Step size (° 2θ)	0.005	0.005
Number of variables	36	27
R_p (%)	1.88	4.11
wR_p (%)	1.80	5.03
$R_F{}^2$ (%)	6.07	5.50
χ^2 (%)	2.204	1.059

2. 5. Structural Analysis

The obtained X-ray diffraction pattern showed that, in addition to a phase of face centered cubic symmetry with a cell edge of about 10.35 Å, the sample also contained very small quantities of $Bi_2Ti_4O_{11}$ and TiO_2. Both of these phases were included in the Rietveld refinements of the diffraction data. All refinements and bond lengths and angles calculations were carried out using the GSAS suite of programs (24). Bond valence calculations were performed using the program Eutax (25, 26).

Inspection of the X–ray diffraction pattern of bismuth titanate immediately suggested that this phase was not an ideal pyrochlore. There was no line splitting indicating non-cubicity, but the intensities of certain reflections were indicative of a departure form the ideal structure as described in the Introduction. Firstly, reflections such as 442 and 644, although allowed by the general reflection conditions of the space group $Fd\bar{3}m$, can be considered forbidden for the pyrochlore structure, since isotropic atoms at positions 16c, 16d, 48f and 8a do not contribute to them. These reflections are present in the observed pattern of bismuth titanate. Secondly, reflections (hkl): $h + k + l = 4n$ satisfy the special reflection conditions for sites 48f and 8b only. Therefore, in an ideal pyrochlore structure their intensities are due solely to the scattering on oxygens. The intensities observed for these reflections appear to be larger than the values calculated for the case where only oxygens contribute to them. Apart from these

two classes, calculated and observed intensities are in good agreement. Some of these examples are given in Table 2.4.

Table 2.4. Comparison of Observed and Calculated Intensities for Some Bismuth Titanate Reflections

hkl	I (obs)	I (calc)	Note
111	890	847	
220	137	1.3	Oxygen reflection
311	780	590	
222	10300	9600	
400	4644	5335	
331	934	958	
442	362	0	Forbidden reflect.
620	272	23	Oxygen reflection
644	34	0	Forbidden reflect.
660	450	29	Oxygen reflection

Isotropic refinement of bismuth titanate as an ideal pyrochlore (Model 1) did not give good results. Zero intensity is calculated for reflections 442 (Figure 2.2.a) and 644. The agreement factor is $R_F^2 = 13.04\%$.

Fits to the forbidden reflections improve if the thermal displacement factor for bismuth is is allowed to vary anisotropically (Figure 2.2.b, Model 2). The agreement factor decreases to is $R_F^2 = 10.65\%$. The thermal ellipsoid obtained for bismuth, although positive, has a physically unacceptable shape (Figure 2.3). Its real mean displacements are 0.1154(8) Å in directions parallel to the (111) plane and 0.0183(5) Å along the threefold axis. These dimensions suggest that the model would probably be improved if bismuth were statically displaced in directions perpendicular to the threefold axis.
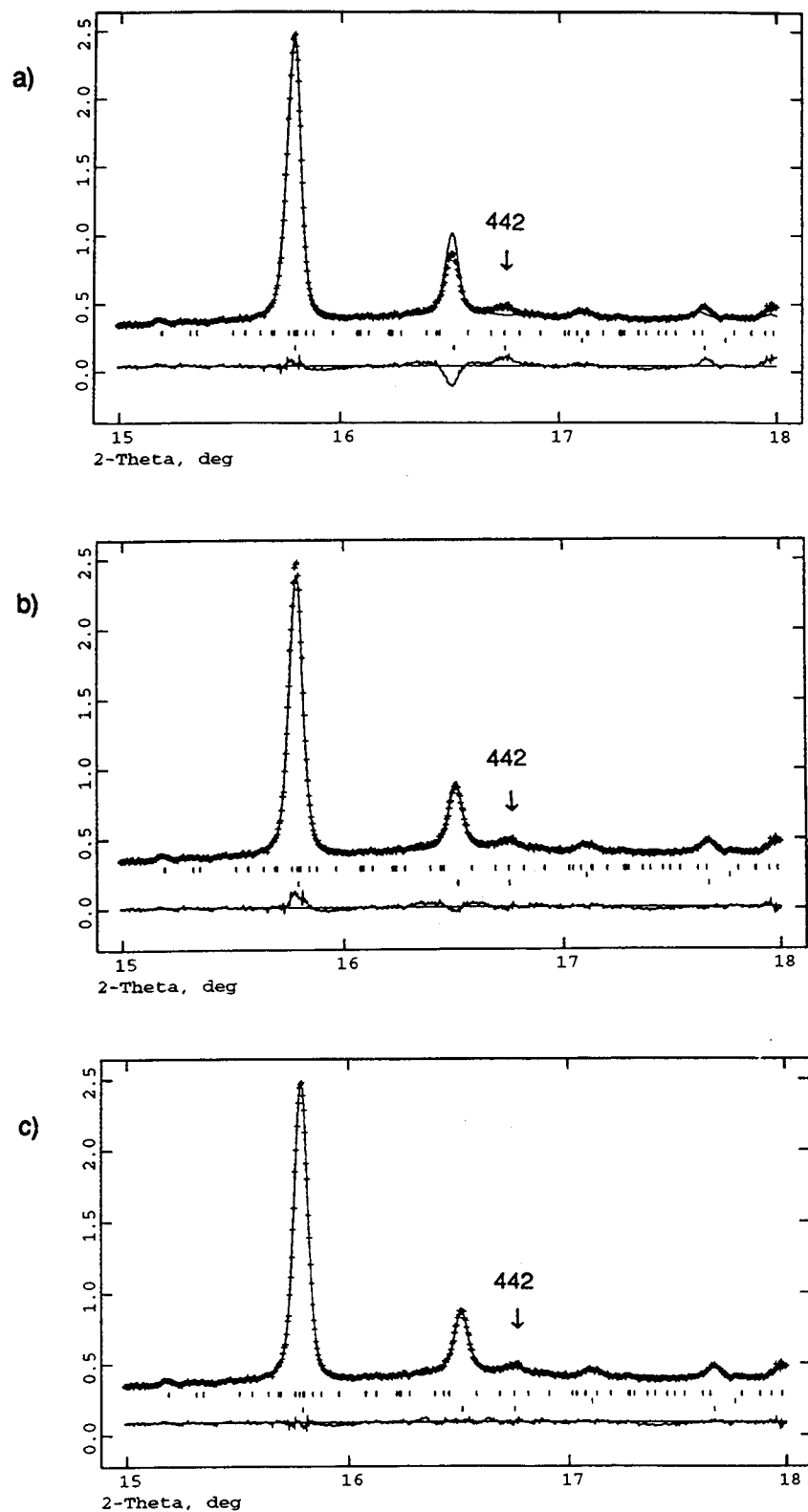
Figure 2.2. The Fit to the Forbidden 442 Reflection Using Different Models
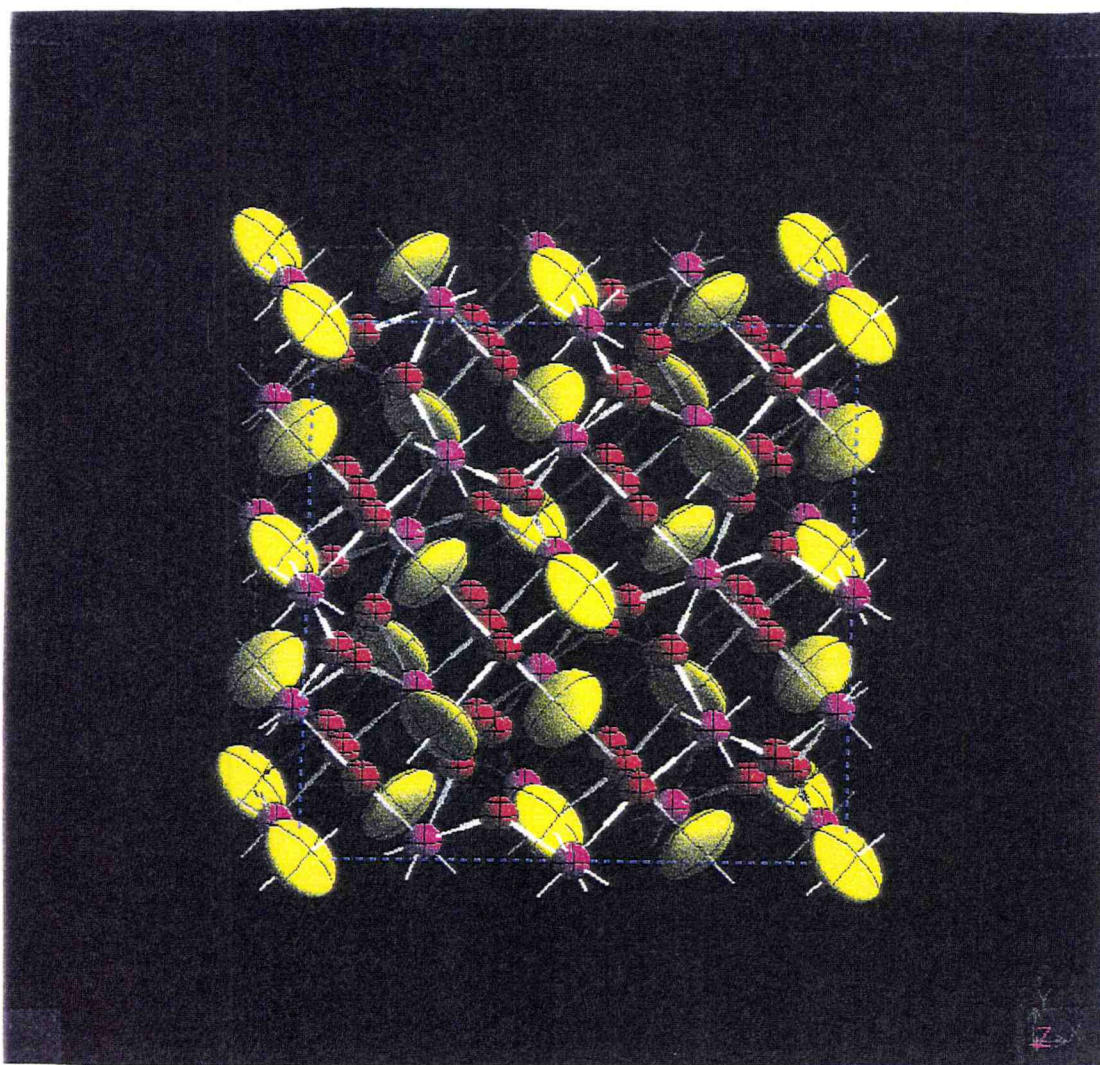
Figure 2.3. Result of the anisotropic refinement of Bi^{3+} on the ideal site

If bismuth is placed on site 96h in a disordered manner and its temperature factor refined isotropically (Model 3), the fit to the observed data significantly improves (Figure 2.2.c). An agreement factor of R_F^2 = 6.07% is obtained. An inversion center is physically not a very plausible location for a lone pair cation. In this model, bismuth is displaced off its ideal position on the center of inversion. A short summary of the relevant parameters for the three models is given in Table 2.5.

It should be noted that bismuth can alternatively be placed onto 96g site, which is also in the (111) plane. This model did not give as good results as the one with bismuth on 96h. The reason for this may be in that the position g moves bismuth off the threefold axis directly towards one of the six equatorial oxygen atoms, whereas the position h moves in a direction half way between two oxygens. Either way, bismuth atom is moved off the center of inversion by 0.38 Å in the (111) plane. However, in the case of $Sn_{2-x}^{2+}(Nb_{2-y}^{5+}Sn_y^{4+})O_{7-x-y/2}$ and $Sn_{2-x}^{2+}(Ta_{2-y}^{5+}Sn_y^{4+})O_{7-x-y/2}$ (27), Sn^{2+} cations placed in either position h or g gave equally good fits to the observed data.

Table 2.5. Results of the Bismuth Titanate Refinement Using Different Models

Model	$\chi 2$	R_F^2 (%)	Note
1	6.299	13.04	No intensity calculated for 442, 644, ...
2	4.514	10.56	Unacceptable shape of thermal ellipsoids
3	2.204	6.07	

All subsequent refinement was performed using Model 3. It immediately became apparent that the bismuth site was not fully occupied, and its occupancy, as well as that of O(4), was refined. The refinements based on the X-ray and neutron data gave very similar results for the bismuth positional and occupational parameters. Neither data would give a stable refinement if the occupation factor and thermal parameter value for O(4) were simultaneously refined. The occupation factor for this oxygen was therefore constrained to achieve charge balance, but its thermal parameter was refined. The agreement between observed and calculated diffraction patterns is shown in Figures 2.4 and 2.5. Final parameters are shown in Table 2.6, and some interatomic distances and angles are given in Table 2.7.

Table 2.6. Atomic Fractional Coordinates, Occupancies and Isotropic Thermal Parameters

Atom	Site	x/a	y/b	z/c	Occup.	U_{iso} (Å^2)
Bi (1)	96h	0	0.02745(4)	0.97255(4)	0.145(1)	0.0129(2)
Ti (2)	16d	0.5	0.5	0.5	1	0.0189(4)
O (3)	48f	0.125	0.125	0.43126(9)	1	0.0181(2)
O (4)	8a	0.125	0.125	0.125	0.624(1)	0.0234(9)

Table 2.7. Selected Interatomic Distances (Å) and Bond Angles (°)

	O (3)	O (4)
Bi (1)	2.2868(6) x 2	2.27710(3) x 2
	2.6517(7) x 2	
	2.9722(7) x 2	
Ti (2)	1.9635(3) x 2	
O (3) - Bi (1) - O (3)	72.86(1)	
O (3) - Bi (1) - O (4)	88.00(2) x 2	
	108.60(2) x 2	
O (4) - Bi (1) - O (4)	159.667(1)	
O (3) - Ti (2) - O (3)	92.49(4)	
	87.51(4)	
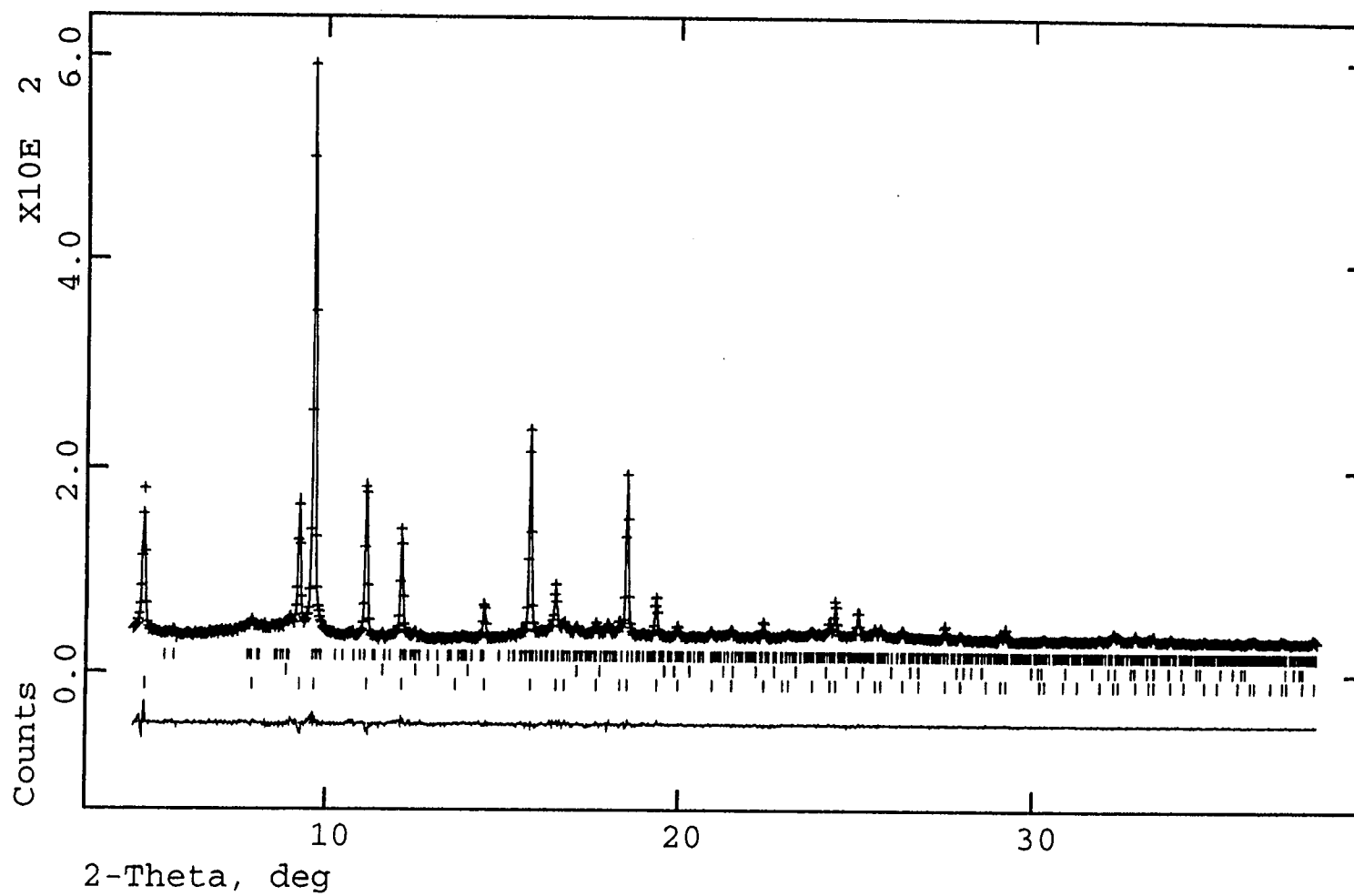
Figure 2.4. The Rietveld refinement of synchrotron X-ray diffraction data for bismuth titanate
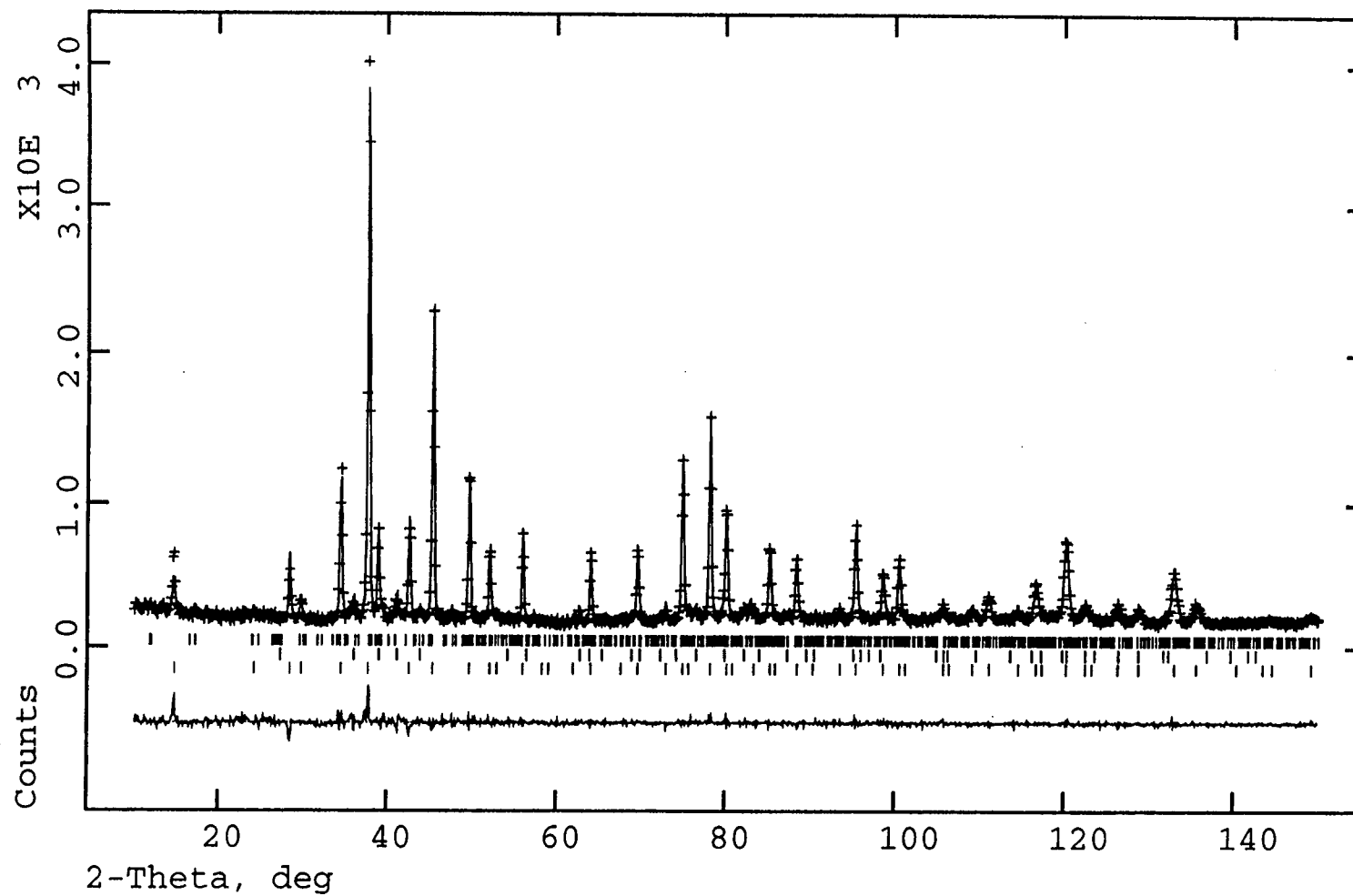
Figure 2.4. The Rietveld refinement of neutron diffraction data for bismuth titanate

2. 6. Discussion

Refinement of fractional occupancies showed bismuth titanate to be both bismuth and oxygen defficient. The obtained occupancy values correspond to the molecular formula $Bi_{1.75}Ti_2O_{6.62}$.

Lattice parameter of a = 10.352 Å is in excellent agreement with the values predicted for $Bi_2Ti_2O_7$ by extrapolation of yttrium bismuth and lanthanide bismuth titanates (12, 14).

The coordination environment of Ti is shown in Figure 2.6. The O(3) - Ti(2) - O(3) angles of 87.5° and 92.5° reflect a relatively small degree of distortion of the octahedral symmetry. The six oxygen atoms are equidistant at 1.964 Å. This value is in good agreement with the Ti - O distance of 1.97 Å reported for $Sm_2Ti_2O_7$, which has the ideal pyrochlore structure (22). Calculated total bond valence for titanium in this environment is 4.016. TiO_6 polyhedra share corners to form the strongly bound $(Ti_2O_6)^{4-}$ network.
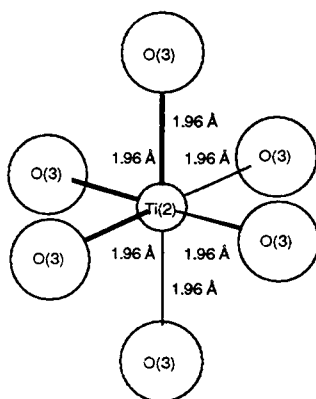
Figure 2.6. Coordination environment of titanium
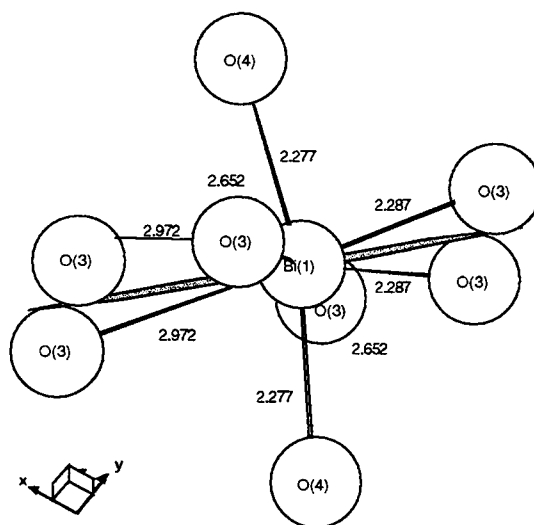
Figure 2.7.a. Coordination of bismuth viewed parallel to the (111) plane
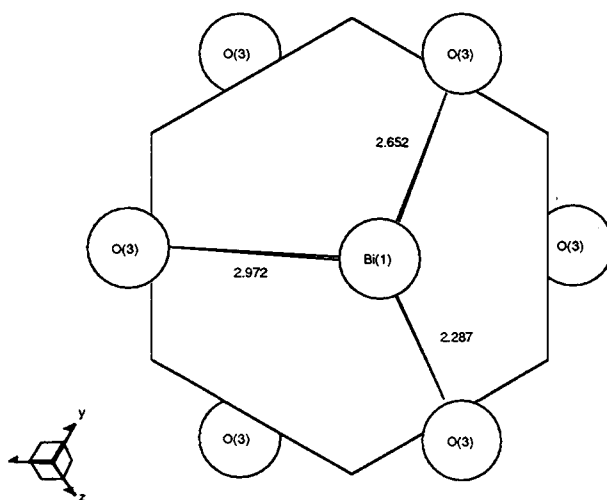
Figure 2.7.b. Coordination of bismuth viewed along the three-fold axis

Two different views of the coordination of Bi are shown in Figure 2.7. Two shorter bonds (2.277 Å) are to O(4) atoms, with which Bi forms $(Bi_2O)^{4+}$ network. The remaining six are longer internetwork bonds to O(3) atoms. While in the ideal pyrochlore structure these would be equidistant, in bismuth titanate there are three pairs of equal bond lengths, with the average being 2.631 Å. The disordered displacement of bismuth yields a better placement for its lone pair, which presumably points between the two oxygens at 2.97 Å (Figure 2.7.b). Total bond valence for bismuth in this environment is 3.005.

Thus, it appears that bismuth titanate is very closely related to the ideal pyrochlore structure and that the departure therefrom is caused mainly by the presence of a lone pair cation.

2. 7. References

1. M. A. Subramanian, G. Aravamudan and G. V. Subba Rao, Prog. Solid State Chem., 15, 55 (1983)

2. M. A. Subramanian and A. W. Sleight, Handbook on the Physics and Chemistry of Rare Earths, Vol. 16, Elsevier Science Publishers B. V., 1993.

3. R. A. McCauley and F. A. Hummel, J. Solid State Chem., 33, 99 (1980)

4. H. von Gaertner, Neues Jahrb. Mineral. Geol. Palaeontol., Ref. 61,1 (1930)

5. L. G. Nikiforov, Sov. Phys. Cystallogr., 17, 2, 347 (1972)

6. R. A. McCauley, J. Appl. Phys., 51, 1, 290 (1980)

7. Bystrom, Ark. Kemi Min. Geol., 18A, 1 (1945)

8. F. Jona, G. Shirane and R. Pepinsky, Phys. Rev., 98, 4 (1955)

9. E. Aleshin and R.Roy, J. Am. Ceram. Soc., 45, 1, 18 (1965)

10. J. M. Longo, P. M. Raccah and J. B. Goodenough, Mater. Res. Bull., 4, 191 (1969)

11. A. W. Sleight, Inorg. Chem., 7, 9, 1704 (1968)

12. R. D. Shannon and A. W. Sleight, Inorg. Chem., 7, 1649 (1968)

13. S. L. Sorokina and A. W. Sleight, Mat. Res. Bull., 33, 7, 1077 (1998)

14. O. Knop, F. Brisse and L. Castelliz, Can. J. Chem., 47, 971 (1969)

15. I. Radosavljevic, J. S. O. Evans and A. W. Sleight, J. Solid State Chem., 136, 63 (1998)

16. X. Wang, H. Wang and X. Yao, J. Am. Ceram. Soc., 80, 10, 2745 (1997)

17. Aurivillius, Ark. Kemi, 1, 499 (1949)

18. E. C. Subbarao, J. Am. Ceram. Soc.,45, 564 (1962)

19. E. M. Levin and R. S. Roth, J. Res. Nat. Bur. Stand., 68A, 2, 197 (1964).

20. S. Shimada, K. Kodaira and T. Matsushita, J. Cryst. Growth, 41, 317 (1977)

21. M. L. Barsukova, V. A. Kuznetsov, A. N. Lobachev and Yu. V. Shaldin, *J. Cryst. Growth,* 13/14, 530 (1972).

22. O. Knop, F. Brisse and L. Castelliz, *Can. J. Chem.,* 13, 118 (1969)

23. C. E. Bamberger, H. W. Dunn, G. M. Begun and S. A. Landry, *J. Solid State Chem.,* 58, 114 (1985)

24. A. C. Larson and R. B. von Dreele, LANSCE, Los Alamos National Laboratory, Los Alamos, N.M., 1994.

25. I.D. Brown and D. Altermatt, *Acta Cryst.* Sect B 41, 244 (1985)

26. N.E. Brese and M. O'Keeffe, *Acta Cryst.* Sect B47, 192 (1991)

27. T. Birchall and A. W. Sleight, *J. Solid State Chem.,* 13, 118 (1975)

28. Ismunandar, B. J. Kennedy and B. A. Hunter, *Mat. Res. Bull.,* in press

Chapter 3

Synthesis and Structure of A New Bismuth Calcium Vanadate, $BiCa_2VO_6$

3. 1. Introduction

Exploratory synthesis of quaternary oxides in the $Bi_2O_3 - CaO - V_2O_5$ system has led to the discovery of some interesting materials. Known and characterized phases in this system include $BiCaVO_5$ (1), $BiCa_4V_3O_{13}$ (2), $BiCa_9V_4O_{28}$ (3,4,5), $Bi_2CaV_2O_9$ (6) and $Bi_6Ca_{18}V_{22}O_{82}$ (7) and $BiCa_2VO_6$ (8).

$BiCaVO_5$ was reported by Boje and Mueller – Buschbaum in 1993. It crystallizes in the orthorhombic space group Pbca (#61) and has the lattice parameters of a = 11.2022(25) Å, b = 5.4283(15) Å and c = 15.5605(19) Å.

In 1993 Huang and Sleight reported the crystal structure of the apatite related $BiCa_4V_3O_{13}$. This phase belongs to the hexagonal space group $P6_3$ (#173). This compound contains bismuth / calcium disorder over two six coordinate sites. The third calcium site is nine coordinate, while vanadium is tetrahedral. The two types of calcium coordination polyhedra share faces to form chains parallel to the threefold axis. This structure is related to that of apatite, except for the loss of the inversion center. Its space group belongs to the non

centrosymmetric crystal class 6 (9) and the compound can therefore exhibit properties such as second harmonic generation and ferroelectricity.

Lazoryal et al. reported the synthesis of $BiCa_9V_4O_{28}$ in 1990. They studied a series of compounds of the formula $RCa_9(VO_4)_7$, where R = Y, Bi or a lanthanide. Their X-ray diffraction and infrared spectroscopy experiments have indicated that $BiCa_9V_7O_{28}$, as well as the other members of the series, is essentially isostructural with mineral whitlockite, $Ca_3(VO_4)_2$. Non linear optical properties in this material have been observed and patented (3).

3. 2. Structure Solution from Powder Data – A Brief Overview

X–ray diffraction (XRD) is the most important technique used for structural characterization of crystalline materials. Whether the experiment is carried out on a single crystal or a polycrystalline sample, the obtained diffraction pattern stores the same information. The two approaches differ to a great extent, though, in how easily and reliably this information can be extracted and processed. New structures reported from single crystal data significantly outnumber those from powder data. Figure 3.1 represents the number of reported structures solved ab initio from powder diffraction data in the past decade.
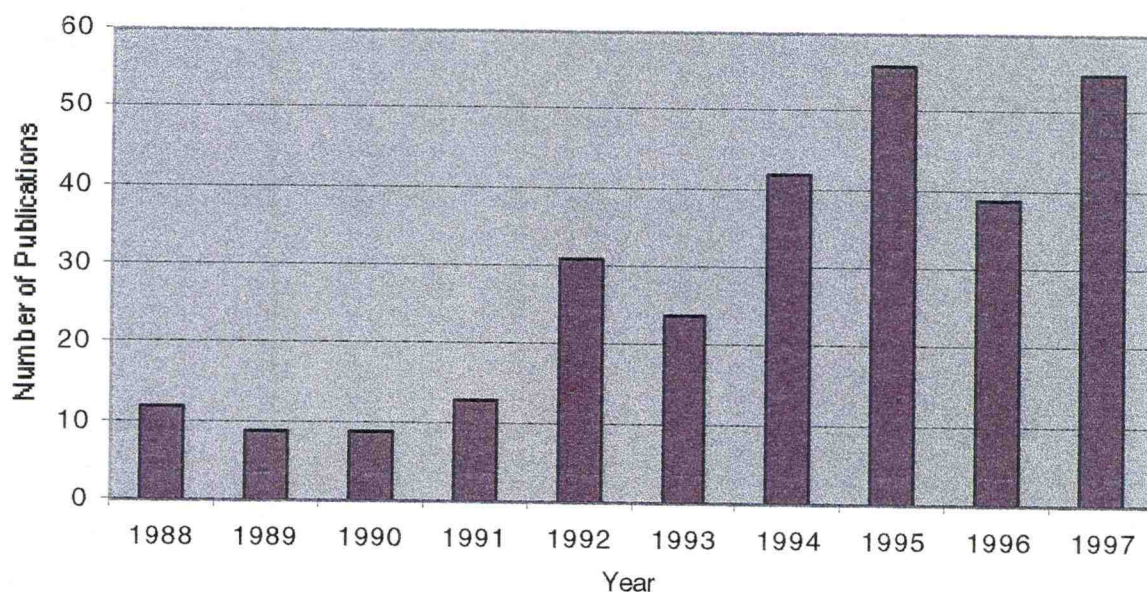
Figure 3.1. Number of ab initio structure determinations from powder X-ray diffraction data

Some of the first structural determinations from powder X-ray diffraction data are those of heteropoly acids (10) published in 1933. The structure of β – plutonium metal reported by Zachariasen and Ellinger (11) in 1963 is considered to be the first successful ab initio structure determination from powder data. Despite the enormous progress achieved both in instrumentation and computational techniques, the increase of the crystal structures solved from powder data has been very gradual.

The diffraction phenomenon is a three dimensional one. In a single crystal experiment, methods of experimental detection are such that the structural information is collected while maintaining the three dimensional spatial

distribution. In the case of powder diffraction, the scattered intensity is measured as a function of only one coordinate, the 2θ or Bragg angle. The three dimensional space in which diffraction occurs is reduced to one dimension in which it is recorded and, consequently, some information is lost. This is primarily manifested in the peak overlap observed in powder diffraction patterns. Peak overlap can be accidental or due to instrumental limitations (such as insufficient resolution) and properties of the crystal structure itself (such as the unit cell size and symmetry). In addition, background may not be easily estimated with a high degree of accuracy. Both of these factors create grave difficulties in assigning reliable individual intensity values, particularly in the groups of overlapping reflections. Unambiguous I(hkl) values are necessary for all widely used methods of structure solution, although some fundamentally different approaches have been under development lately.

The steps involved in an ab initio structure determination from powder data include the following:

1. Pattern indexing, unit cell and space group determination

2. Pattern decomposition

3. Structure solution

4. Structure refinement

Pattern indexing in ab initio structure determinations is frequently carried out by autoindexing. Autoindexing procedures involve determination of the unit cell parameters from the positions of the observed reflections. Ease of obtaining

a satisfactory indexing depends on the resolution of the data used, accuracy in determining the peak positions and the size and symmetry of the unit cell. There are a number of computer programs available (12, 13, 14). A typical algorithm consists of assigning provisional indices to several peaks in the low two theta region, calculating a trial cell and using it to generate the peak positions in the entire region. A figure of merit is calculated, on which basis a proposed solution may be accepted or rejected. Two distinctly different approaches exist in regard to crystal symmetry. Some programs seek a solution in higher symmetry crystal systems and gradually distort the cell to achieve satisfactory indexing. Other programs look for a solution in the triclinic system and then apply cell reduction routine to arrive at the correct symmetry. When the correct unit cell is found, one or more possible space groups can be determined from the systematic absences in the pattern. This step, fairly straightforward in single crystal work, can be made more difficult by the peak overlap of the powder pattern.

Pattern decomposition is the procedure of extracting structure factor moduli for all reflections from a powder pattern. In addition to the peak overlap, the main difficulties arise from significant background and preferred orientation. The available computer programs (15, 16) are mainly based on either Pawley or Le Bail algorithms, although other approaches exist as well. The Pawley method (17) involves pattern fitting with unit cell, intensities, background and profile function as parameters refined in a least squares procedure. When substantial peak overlap is present in the pattern, this algorithm faces a problem of high

correlation of peak intensities. As a result, negative intensities may be assigned to certain reflections, while others may be significantly overestimated to compensate. The Le Bail (18) technique overcomes this problem by equipartitioning intensities of overlapping reflections. The program Extra (15) uses the Le Bail algorithm to extract structure factor moduli starting from known unit cell parameters and space group. Profile fitting in several least square cycles is carried out, with the scale factor, cell parameters, zero point, background coefficients and the parameters of the selected profile function refined. Once the pattern is decomposed into a series of (hkl) reflections and associated structure factor moduli, the structure solution process becomes essentially the same as that used in single crystal work.

Two commonly used techniques are the Patterson method and direct methods. The Patterson method employs a function that uses only structure factor moduli and does not depend on phases. Each peak in the Patterson map computed with this function represents an interatomic vector in the unit cell, while the height of the peak is proportional to the product of the atomic numbers of the two atoms connected by that vector weighted by its multiplicity. The properties of the Patterson method suggest that it should be particularly suitable for structures containing a small number of strong scatterers relative to the number of lighter atoms. A good example of this is $\alpha - CrPO_4$, the first structure solved from synchrotron powder data (19). Direct methods are statistical methods based on two properties of electron density: positivity and atomicity. Owing to these

restraints, structure factor phases can in principle be derived directly from the observed structure factor moduli. Various probabilistic relationships have been developed that yield trial phases from which an electron density map is calculated. The generated diffraction pattern is compared to the observed one and a residual is calculated on which basis the proposed structure is accepted or rejected. Mathematical details of the probabilistic relationships employed by direct methods can be found in (20) and references therein.

In addition to these two, there are a number of different techniques for structure solution. A completely different kind of approach is used in Monte Carlo and simulated annealing methods. Structure solution by Monte Carlo method starts from a random distribution of atoms in the unit cell. The starting model is taken through a number of so-called Monte Carlo steps, that is, translations and rotations of rigid structural fragments and random displacements of individual atoms. After each such move, a diffraction pattern is generated and compared to the observed one. Calculated residual is compared to that from the previous step and on the basis of the difference, the model is accepted or rejected. Simulated annealing is in principle very similar to Monte Carlo method, the main difference being in the procedure of accepting and rejecting models.

Structure refinement by the Rietveld method is a whole pattern least squares fitting procedure, in which the refined variables include the parameters of the structural model as well as instrumental ones. For a pattern recorded in a step mode, an intensity value $y_{c,i}$ is calculated for each step. It is assumed that

the total intensity observed at each step results from contributions from Bragg reflections and background, so the calculated intensity $y_{c,i}$ has the form (21):

$$y_{c,i} = s\Sigma_{hkl}\ L_{(hkl)}|F_{(hkl)}|^2\Phi P_{(hkl)}A + y_{b,i}$$

where: s = scale factor

$L_{(hkl)}$ = Lorentz, polarization and multiplicity factor

Φ = profile function

$P_{(hkl)}$ = preferred orientation function

A = absorption correction

$y_{b,i}$ = background

The agreement between the observed and calculated profiles is expressed through the value of the residual, the quantity that is minimized in the course of the refinement by an iterative least squares procedure. Some of the widely used structural refinement software packages include GSAS (22), Rietan (23) and Fullprof (24).

3. 3. Experimental

A polycrystalline sample of $BiCa_2VO_6$ was synthesized by solid state reaction using Bi_2O_3 (Cerac, 99.999%), $CaCO_3$ (Mallinckrodt, reagent grade) and NH_4VO_3 (Johnson Matthey, 99+ %). The mixture was thoroughly ground, fired at 950°C for 30 hours in an alumina crucible and then cooled to room temperature

at a rate of 5°/minute. The pale yellow product was analyzed using an SX-50 electron microprobe. The analysis confirmed a single phase product with a Bi : Ca : V ratio of 1 : 2 : 1. $BiCa_2VO_6$ melts congruently, for the X-ray diffraction pattern of ground crystals obtained by melting and slow-cooling was identical to that of the polycrystalline sample.

All powder x-ray diffraction patterns were collected using Cu K_a radiation on a Siemens D5000 diffractometer with vertical Soller slits and an energy dispersive Kevex detector. The x-ray diffraction pattern for autoindexing purposes was collected in the 2θ region from 2° to 90° (step size = 0.02°, step time = 8 s) on a sample that contained a small amount of Si standard NBS 640b. The pattern for structure solution by direct methods was recorded under the same conditions, but without Si. X-ray diffraction data for Rietveld refinement were collected in the range from 2° to 150°, using a step size of 0.02° and a step time of 10 s. Details of the data collection are given in Table 3.1.

Neutron diffraction data were collected on a 15 gram sample of $BiCa_2VO_6$ at Brookhaven National Laboratory using the high resolution powder diffractometer at beam line H1A of the high flux beam reactor with a wavelength of 1.8857 Å. Details of the neutron diffraction data collection are given in Table 3.1.

Second harmonic generation effect was sought using a Nd^{3+}:YAG laser with a wavelength of 1064 nm.

3. 4. Structure Solution

Accurate 2θ values of the observed reflections in the X-ray diffraction pattern of $BiCa_2VO_6$ were obtained by fitting the peaks using a pseudo - Voigt peak shape, with the program Profile (ref) within the Siemens Diffract/AT suite (25). A calibration curve $\Delta2\theta = f(2\theta)$ was constructed from the observed and calculated Si reflections. Appropriate corrections were applied to BiCa2VO6 peak positions to correct for the zero point and sample height errors. The first thirty reflections were used as the input for the autoindexing program Visser (12). Autoindexing gave a solution with a figure of merit of $M_{20} = 227$ and suggested an orthorhombic cell: a = 8.893 Å, b = 11.955 Å and c = 5.545 Å. These cell parameters were refined using the program Refcel (26) and the obtained values were: a = 8.894(1) Å, b = 11.955(2) Å and c = 5.544(1) Å. The pattern was indexed and the inspection of the reflection conditions (hkl: h + k = 2n, 0kl: k = 2n, h0l: l = 2n, hk0: h + k = 2n, h00: h = 2n, 0k0: k = 2n, 00l: l = 2n) suggested two possible space groups: $Cmc2_1$ (#36) and Cmcm (#63).

The number of formula units per unit cell was determined by comparison with $Bi_2CaV_2O_9$ and $BiCaVO_5$, on the basis of known unit cell volumes and cell contents of these phases. A value of Z = 4 was obtained.

Structure factor moduli were extracted using the program Extra (15). Peak fitting in both space groups $Cmc2_1$ and Cmcm gave an agreement factor of R = 19.53%. Direct methods were applied by using the program Sirpow (27). Structure solution in the non-centrosymmetric space group $Cmc2_1$ gave a

combined figure of merit of $C_{FoM} = 0.830$ and $R = 10.02\%$. Slightly poorer agreement factors of $C_{FoM} = 0.713$ and $R = 11.50\%$ were obtained for the space group Cmcm. In all cases only metal sites were sought. Three cation positions were found, one each for Bi, Ca and V. These three sites were used as a partial structure for the calculation of difference Fourier maps in order to locate oxygen atoms. Ten peaks were sought and four among them were identified as oxygens based on their positions relative to cations.

The structure was then refined using the Rietveld method and the GSAS software suite (22). X-ray diffraction pattern was fitted by refinement of a total of 44 variables: scale factor, zero point, lattice parameters, 4 profile coefficients, 12 background terms, 16 positional parameters and 7 isotropic temperature factors. An excellent agreement to the observed diffraction pattern was achieved, with the final agreement factors of $R_p = 7.41\%$, $wR_p = 10.22\%$, $R_F^2 = 4.43\%$, $R_F = 2.35\%$ and $\chi^2 = 4.88$. The obtained model was used as the starting point for neutron diffraction data refinement. A total of 38 variables was refined: scale factor, zero point, lattice parameters, 5 profile coefficients, 9 background terms, 15 positional parameters and 4 isotropic temperature factor. The obtained agreement factors were: $R_p = 9.39\%$, $wR_p = 12.10\%$, $R_F^2 = 12.11\%$, $R_F = 7.73\%$ and $\chi^2 = 8.199$. It seems that the main obstacle to achieving an even better fit to the neutron diffraction data was the inability to fully overcome the difficulties arising from highly asymmetric peak profiles rather than a flaw in the structural model, since the structure independent Le Bail fit to the observed pattern gave

agreement factors very similar to those from the Rietveld refinement. Observed, calculated and difference profiles for X-ray diffraction data are given in Figure 3.2.a, while those for neutron diffraction data are in Figure 3.2.b.

Rietveld refinements of both data sets were carried out in the centrosymmetrical space group Cmcm without giving satisfactory results. In addition, a second harmonic generation signal of intensity of about 1.5 times that of KDP was observed, confirming the lack of an inversion center in the $BiCa_2VO_6$ structure.

Table 3.1. Details of X-ray and Neutron Diffraction Data Collection and Refinement for $BiCa_2VO_6$

Quantity	X-ray Diffraction Data	Neutron Diffraction Data
a (Å)	8.89315(7)	8.8946(3)
b (Å)	11.9608(1)	11.9663(4)
c (Å)	5.54594(5)	5.5445(2)
Zero point (° 2θ)	- 0.0025(3)	0.0085(3)
Wavelength (λ)	1.54056	1.8857
Data range (° 2θ)	10 - 150	10 - 150
Step size (° 2θ)	0.02	0.05
Time per step (s)	10	300
Number of data points	6999	2802
Number of reflections	372	207
Number of variables	44	38
R_p (%)	7.41	9.39
wR_p (%)	10.22	12.10
R_F^2 (%)	4.43	12.11
R_F (%)	2.35	7.73
χ^2	4.88	8.199
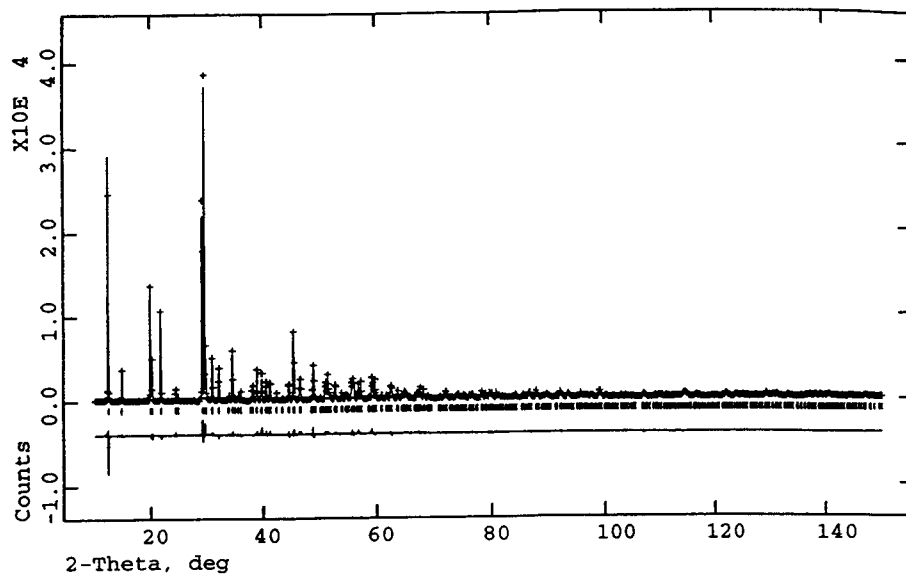
Figure 3.2.a. Results of the Rietveld Refinement of $BiCa_2VO_6$ from X-ray Diffraction Data
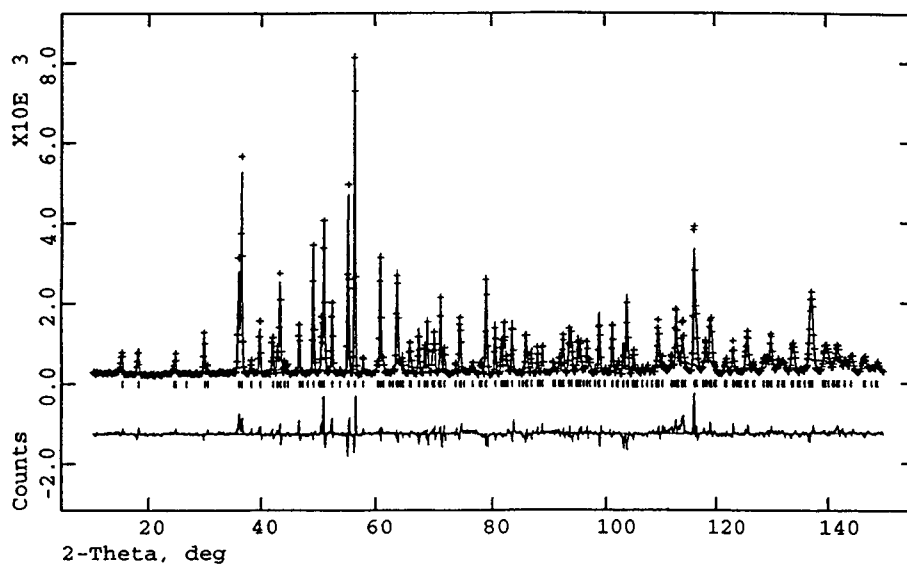
Figure 3.2.b. Results of the Rietveld Refinement of $BiCa_2VO_6$ from Neutron Diffraction Data

3. 5. Description of Structure

A view of the unit cell of $BiCa_2VO_6$ is shown in Figure 3.3. The structure can be viewed as consisting of covalently bound $(BiO_2)^-$ infinite chains and VO_4^{3-} tetrahedra with charge balance provided by interspersed Ca^{2+} cations. The unit cell dimensions of $BiCa_2VO_6$ are very similar to those of other known orthorhombic phases of the BiA_2MO_6 family (28, 29, 30, 31). Of all of these phases, it is $BiMg_2VO_6$ (28) that bears the most resemblance to $BiCa_2VO_6$. $BiMg_2VO_6$ belongs to the primitive centrosymmetric space group Pmcn, while the systematic absences in the $BiCa_2VO_6$ pattern clearly indicate that the structure is C – centered. The structure of $BiMg_2VO_6$ is the subject of Chapter 5, while a detailed comparison between these two phases is given in Chapter 10.

$BiCa_2VO_6$ contains seven atoms in the asymmetric unit. Their positions and isotropic temperature factors are given in Table 3.2. Selected bond distances and angles are given in Table 3.3.
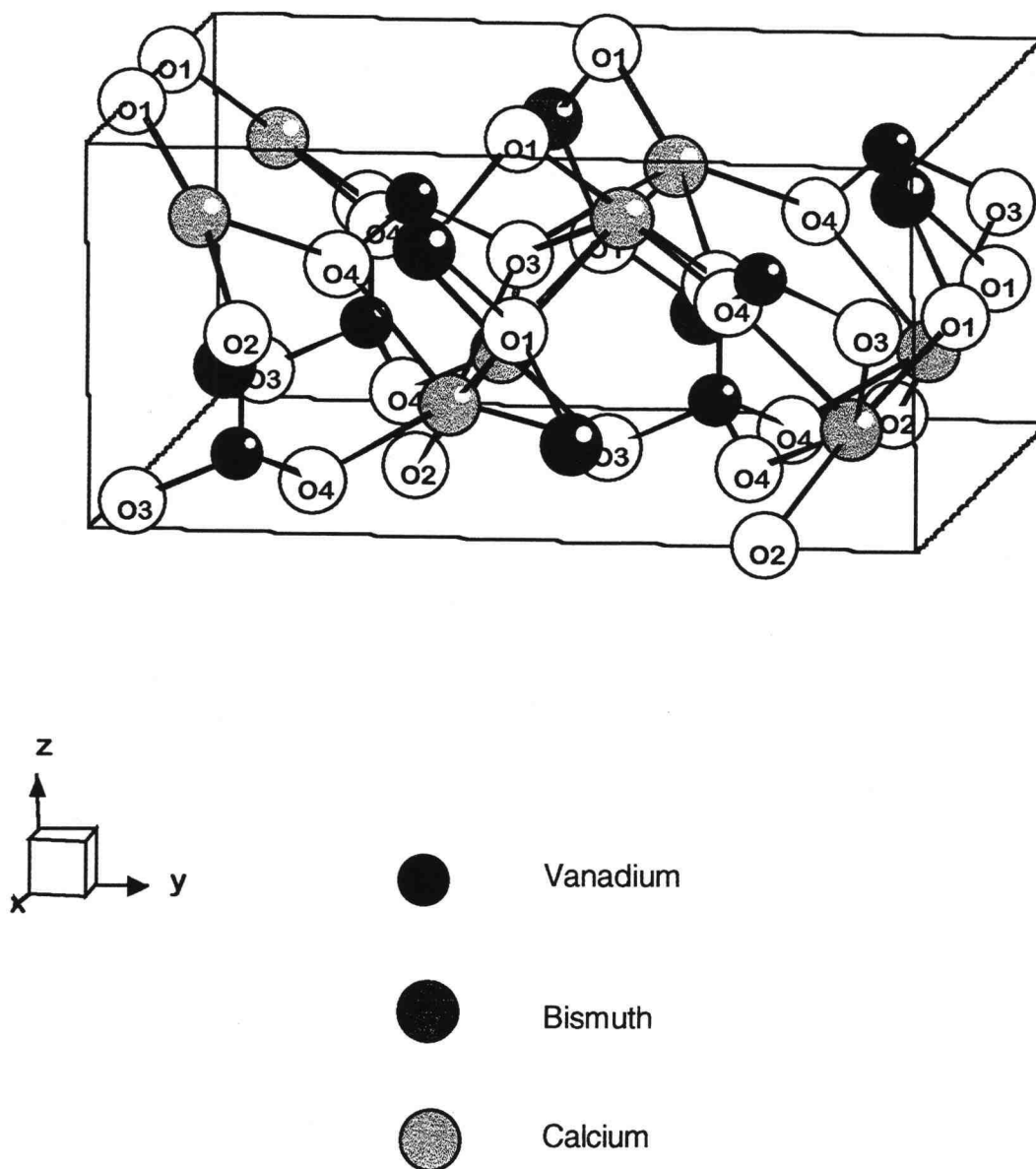
Figure 3.3. A view of the unit cell of $BiCa_2VO_6$

Table 3.2. Atomic Coordinates and Isotropic Thermal Parameters for $BiCa_2VO_6$

Atom	x/a	y/b	z/c	U_{iso} (Å)
Bi	0.5	0.0894(6)	0.25	0.00998(87)
V	0	0.181(2)	0.199(4)	0.0126(9)
Ca	0.2999(4)	0.3927(3)	0.242(1)	0.017(1)
O (1)	0.3492(4)	0.9970(3)	0.492(1)	0.0108(8)
O (2)	0	0.8168(3)	0.005(1)	0.00(1)
O (3)	0	0.9481(4)	0.568(1)	0.013(1)
O (4)	0.1548(4)	0.2472(3)	0.079(1)	0.0126(8)

Table 3.3. Selected Interatomic Distances (Å) and Bond Angles (°) for $BiCa_2VO_6$

	O (1)	O (2)	O (3)	O (4)
Bi	2.196(5) x 2	3.040(5)		3.008(5) x 2
	2.219(5) x 2			
V		1.696(23)	1.711(24)	1.720(15) x 2
Ca	2.285(7)	2.393(6)	2.780(6)	2.539(6)
	2.331(7)		2.622(7)	2.349(7)

O (1) - Bi - O (1)..........77.83(9) x 2

O (1) - Bi - O (1)..........75.4(2)

O (1) - Bi - O (1)..........74.5(2)

O (2) - Bi - O (4)..........71.1(2) x 2

O (4) - Bi - O (4)..........54.5(1)

O (2) - V - O (3)..........116(1)

O (2) - V - O (4)..........112.4(9) x 2

O (3) - V - O (4) ....104.5(9) x 2

O (4) - V - O (4) ....106(1)

O (1) - Ca - O (1)..........73.8(2)

O (1) - Ca - O (2)..........166.2(2)

O (1) - Ca - O (3)..........101.9(2)

O (1) - Ca - O (3)..........80.7(2)

O (1) - Ca - O (4)..........90.5(3)

O (1) - Ca - O (4)..........108.6(2)

The coordination of Bi^{3+} is typical of a lone pair cation (Figure 3.4.a). On one side of bismuth, there are four bonds to oxygens at about 2.2 Å. Distorted square pyramids that Bi forms with these four oxygens share edges parallel to the (100) direction to form $(BiO_2)^-$ chains that run parallel to the c axis (Figure 3.4.b). On the opposite side of Bi^{3+}, there are three more bonds to oxygens belonging to the VO_4 tetrahedra, at about 3 Å. The bond valence sum for bismuth in this environment is 3.15. Calcium is in a sevenfold coordination (Figure 3.5), with bond lengths ranging from 2.28 Å to 2.78 Å. The bond valence sum for calcium in this environment is 1.96. Vanadium is in a distorted tetrahedral environment, with bond lengths from 1.70 Å to 1.72 Å and angles from 106° to 116° (Figure 3.6). The bond valence sum for vanadium in this environment is 5.12. It appears that the non-centrosymmetric arrangement of the VO_4 tetrahedra leads to a more efficient packing along the y axis in $BiCa_2VO_6$ compared to the same direction in $BiMg_2VO_6$. The larger size of Ca^{2+} relative to Mg^{2+} might be expected to give rise to an increase in all three cell edges. However, the b axis in $BiCa_2VO_6$ is actually smaller.

The space group of $BiCa_2VO_6$ belongs to the non-centrosymmetric crystal class mm2 and the compounds therefore can, at least from the structural point of view, be considered a ferroelectric with the polar axis being the c axis. The alternating shorter and longer bonds in the (BiO_2)- chains can be viewed as a ferroelectric distortion. However, the biggest change in the $BiCa_2VO_6$ structure to switch polarity would be the rotations of VO_4 tetrahedra. They all lpoint in the

same direction along the polar axis. Ferroelectric switching would involve the rotation of the tetrahedra so that they all point in the opposite direction along the c axis. The centrosymmetric space group Cmcm, found for $BiMg_2VO_6$ at high temperatures, could be regarded as a paraelectric form of $BiCa_2VO_6$. At this time, we have no evidence that $BiCa_2VO_6$ can be switched in an electric field or that a transition to a paraelectric form occurs below the melting point.
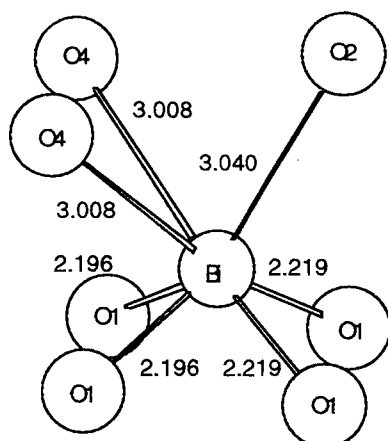
Figure 3.4.a. Coordination environment of Bi^{3+} in $BiCa_2VO_6$
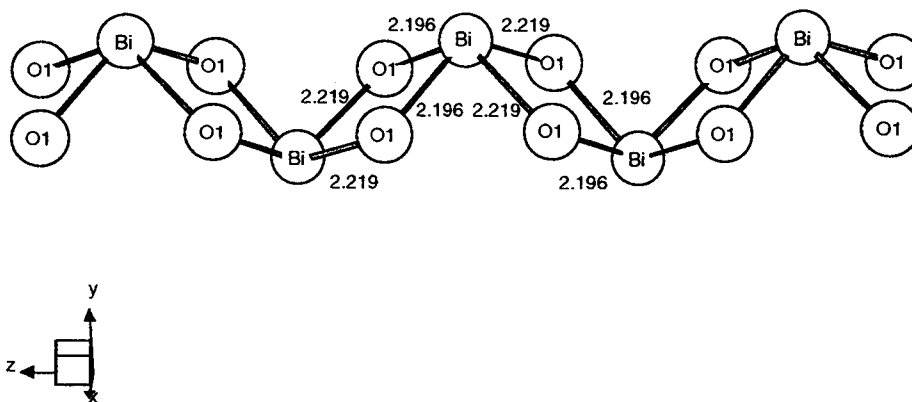
Figure 3.4.b. $(BiO_2)^-$ chains in $BiCa_2VO_6$
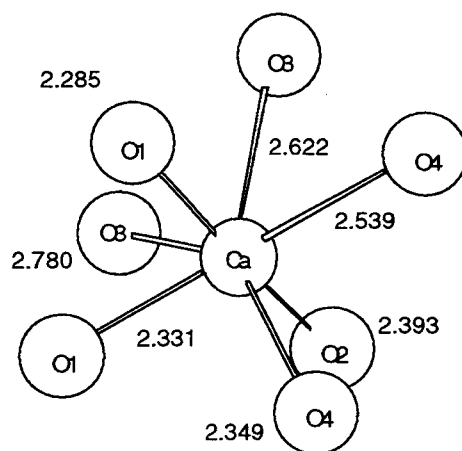
Figure 3.5. Coordination environment of Ca^{2+} in $BiCa_2VO_6$
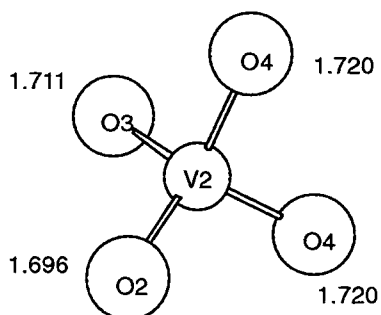
Figure 3.6. Coordination environment of V^{5+} in $BiCa_2VO_6$

3. 6. Bismuth Cadmium Vanadate, $BiCd_2VO_6$

$BiCd_2VO_6$ was synthesized by a solid state reaction of reaction Bi_2O_3 (Cerac, 99.999%), CdO (Mallinckrodt, reagent grade) and NH_4VO_3 (Johnson Matthey, 99+ %). The mixture was thoroughly ground and fired at 800°C for 30 hours in an alumina crucible. The bright orange product was analyzed using an SX-50 electron microprobe. The analysis confirmed a Bi : Cd : V ratio of 1 : 2 : 1. Attempts to grow single crystals of $BiCd_2VO_6$ were not successful.

Powder X-ray diffraction data were collected using Cu K_a radiation on a Siemens D5000 diffractometer with vertical Soller slits and an energy dispersive Kevex detector. The pattern for the Rietveld refinement was collected in the 2θ region from 2° to 150°, with a step size of 0.02° and a step time of 8 s. Details of data collection are given in Table 3.4.

The appearance of the powder X-ray pattern of $BiCd_2VO_6$ showed certain similarities with that of $BiCa_2VO_6$. The first five reflections were therefore indexed by analogy with $BiCa_2VO_6$ and the cell dimensions were refined using the program Refcel (26) and by a Le Bail fit (18) within the GSAS suite (22). The agreement of the obtained unit cell with the observed reflections was very good, except for three very weak reflections marked with asterisks in Figure 3.7.

Table 3.4. Details of X-ray Diffraction Data Collection and Refinement for $BiCd_2VO_6$

Quantity	X-ray Diffraction Data
a (Å)	8.64363(7)
b (Å)	11.4587(1)
c (Å)	5.64649(5)
Zero point (° 2θ)	- 0.0108(5)
Wavelength (λ)	1.54056
Data range (° 2θ)	10 - 150
Step size (° 2θ)	0.02
Time per step (s)	8
Number of data points	6999
Number of reflections	338
Number of variables	40
R_p (%)	11.04
wR_p (%)	14.87
R_F^2 (%)	10.50
R_F (%)	5.78
χ^2	12.03
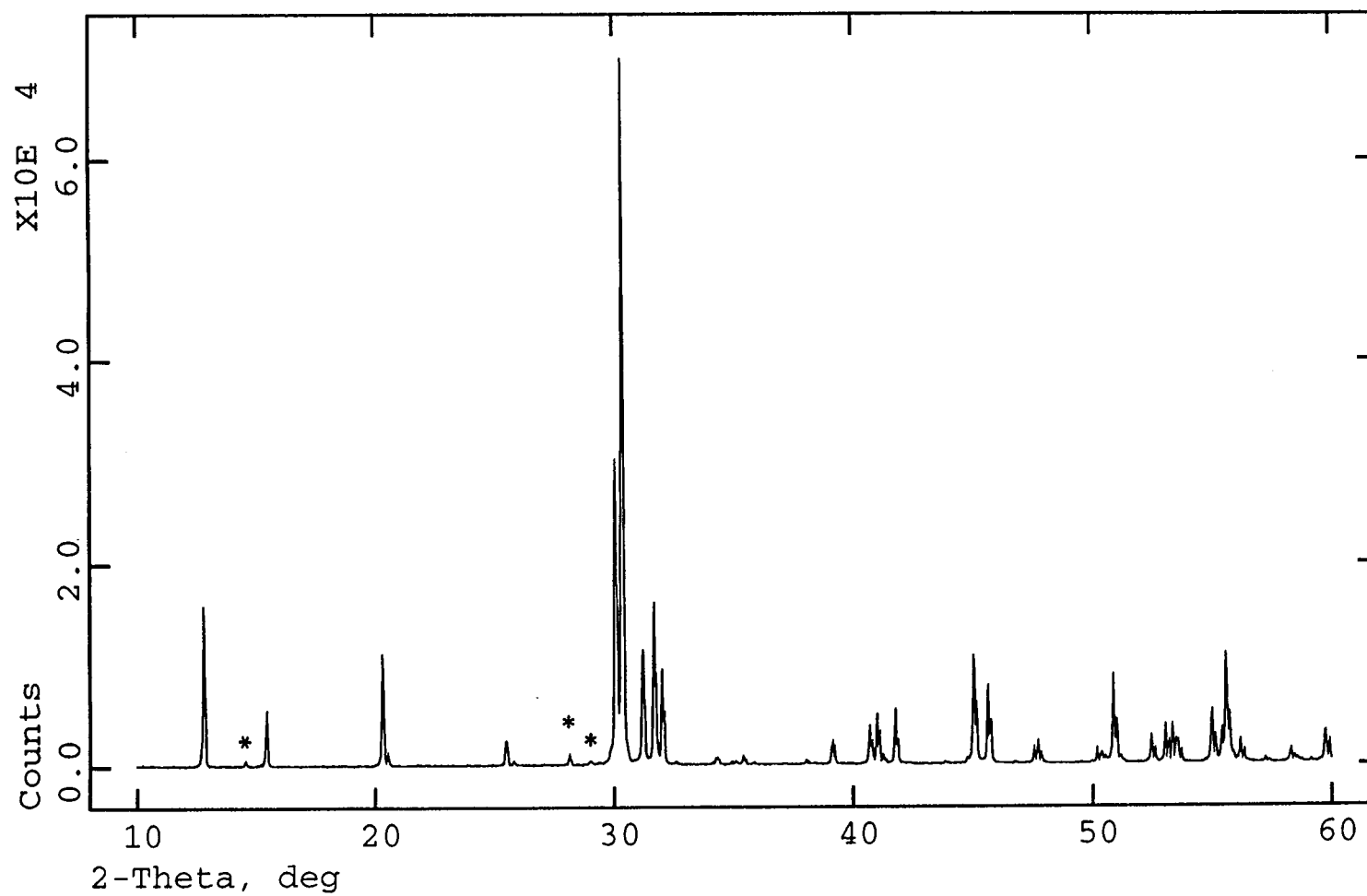
Figure 3.7. The observed X-ray diffraction pattern of $BiCd_2VO_6$ (up to 60° 2θ)

Searches for the possible impurities in the JCPDS database did not give any results. The attempts to account for the extra peaks by lowering the symmetry to primitive orthorhombic and monoclinic were not successful. The 2θ regions from $14.0°$ to $15.0°$ and from $27.6°$ to $29.2°$ were therefore excluded from the observed pattern and the Rietveld refinements were carried out in the C-centered space groups Cmcm and $Cmc2_1$. The starting model used in space group $Cmc2_1$ was $BiCa_2VO_6$ and in space group Cmcm the high temperature form of $BiMg_2VO_6$. Table 3.5 summarizes the course of the Rietveld refinements in the two space groups.

Table 3.5. The Rietveld Refinements of $BiCd_2VO_6$

Cmc2_1			Cmcm		
Parameters refined	Number of parameters	Agreement factors	Parameters refined	Number of parameters	Agreement factors
General	20	$\chi^2 \sim 37$ $R_F^2 \sim 22$	General	20	$\chi^2 \sim 94$ $R_F^2 \sim 48$
General and positions	36	$\chi^2 \sim 12$ $R_F^2 \sim 12$	General and positions	29	$\chi^2 \sim 25$ $R_F^2 \sim 23$
General, positions and U_{iso}	43	$\chi^2 \sim 11$ $R_F^2 \sim 11$	General, positions and U_{iso}	35	

Isotropic temperature factors both for the cations and the oxygen atoms in the space group Cmcm refined to valued that do not make physical sense; they were up to two orders of magnitude larger than the expected values. This strongly suggested that the space group Cmcm is incorrect. The Rietveld refinement in space group $Cmc2_1$ gave a physically plausible model. The obtained observe, calculated and difference profiles are shown in Figure 3.8. The atomic positions and isotropic temperature factors are given in Table 3.6. The model presented here is the one with the isotropic temperature factors on oxygen atoms equated.

Table 3.6. Atomic Coordinates and Isotropic Thermal Parameters for $BiCd_2VO_6$

Atom	x/a	y/b	z/c	U_{iso} (Å)
Bi	0.5	0.0952(1)	0.25	0.0114(3)
V	0	0.1654(4)	0.224(2)	0.006(1)
Ca	0.2941(1)	0.3855(1)	0.243(1)	0.0134(4)
O (1)	0.359(1)	1.011(2)	0.494(6)	0.011(2)
O (2)	0	0.798(2)	0.011(3)	0.011(2)
O (3)	0	0.995(1)	0.737(8)	0.011(2)
O (4)	0.181(1)	0.201(6)	0.127(2)	0.011(2)
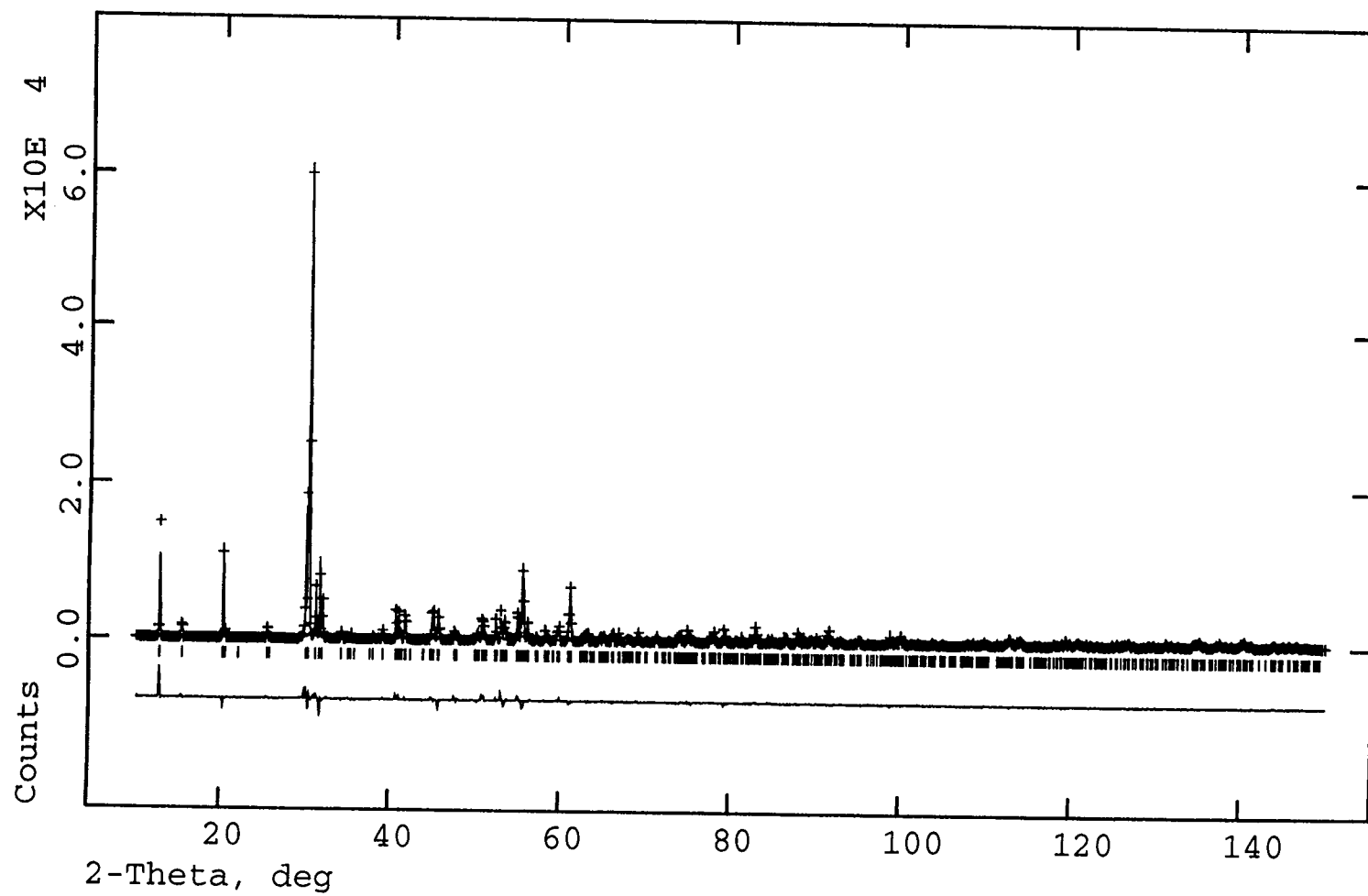
Figure 3.8. The observed, calculated and difference profiles for $BiCd_2VO_6$

$BiCd_2VO_6$ thus appears to be isostructural with $BiCa_2VO_6$. Two obstacles to obtaining a better refinement and more structural details are the inability to collect neutron diffraction data owing to the presence of cadmium, and the inability to grow single crystals of $BiCd_2VO_6$.

3. 7. References

1. J. Boje and Hk. Muller-Buschbaum, *Z. Anorg. Allg. Chem.*, 619, 521 (1993)

2. J. Huang and A. W. Sleight, *J. Solid State Chem.*, 104, 52 (1993)

3. W. Sleight and J. Huang, US Patent No 5202891 (1993)

4. Lazoryak, L. O. Dmitrienko and S. V. Grechkin, *Russ. J. Inorg. Chem.*, 35, 5, (1990)

5. J. S. O. Evans, J. Huang and A. W. Sleight, in preparation

6. J. S. O. Evans and A. W. Sleight, in preparation

7. J. S. O. Evans and A. W. Sleight, in preparation

8. I. Radosavljevic, J. S. O. Evans and A. W. Sleight, *J. Solid State Chem.*, 137, 143 (1998)

9. International Tables for Crystallography, Vol. 4, ed. by T. Hahn, D. Reidel Publishing Company, Dodrecht, The Netherlands, 1983.

10. J. F. Keggin, *Nature*, 131, 908 (1933)

11. W. H. Zachariasen and F. H. Ellinger, *Acta Cryst.*, 16, 5, 329 (1963)

12. J. W. Visser, J. Appl. Cryst. 2, 89 (1969)

13. P. E. Werner. L. Erriksson and M. Westdahl, *J. Appl. Cryst.*, 18, 367 (1985)

14. A. Boultif and D. Louer, *J. Appl. Cryst.*, 24, 987 (1991)

15. A. Altomare, M. C. Burla, G. Cascarno, C.Giacovazzo, A. Guagliardi, A. G. G. Moliterni and G. Polidori, *J. Appl. Cryst.* 28, 842 (1995)

16. Profil Program, J. K. Cockroft, Department of Crystallography, Birkbeck College, London, 1994.

17. G. S. Pawley, *J. Appl. Cryst.*, 19, 440 (1981)

18. A. Le Bail, H. Duroy and J. L. Fourquet, *Mat. Res. Bull.*, 23, 447 (1988)

19. J. P. Attfield, A. W. Sleight and A. K. Cheetam, *Nature*, 322 (1986)

20. Fundamentals of Crystallography, ed. by C. Giacovazzo, Oxford University Press, Oxford, England, 1995.

21. The Rietveld Method, ed. by R. A. Young, Oxford University Press, 1993.

22. A. C. Larson, R. B. von Dreele, LANSCE, Los Alamos National Lab, Los Alamos, NM, 1994.

23. F. Izumi, H. Asano, H. Murata and N. Watanabe, *J. Appl. Cryst.*, 20, 411 (1987)

24. J. Rodriguez Caravajal, in Collected Abstracts of Powder Diffraction Meeting, p. 127, Toulouse, 1990.

25. Profile Version 1.1, Diffract/AT Software Package Version 3.2, 1985.

26. Refcel Program, J. K. Cockroft, Department of Crystallography, Birkbeck College, London, 1985.

27. A. Altomare, G. Cascarno, C.Giacovazzo, A. Guagliardi, M. C. Burla, G. Polidori, M. Camalli, *J. Appl. Cryst.* 27, 435 (1994)

28. J. Huang, A. W. Sleight, *J. Solid State Chem.* 100, 170 (1992)

29. J. Huang, Q. Gu, A. W. Sleight, *J. Solid State Chem.* 105, 599 (1993)

30. I. Radosavljevic, J. S. O. Evans and A. W. Sleight, *J. Comp. Alloys*, in press

31. F. Abraham, M. Ketatni, G. Mairesse and B. Mernari, *Eur. J. Solid State Inorg. Chem.*, 31, 313 (1994)

Chapter 4

Synthesis and Structure of a New Bismuth Calcium Arsenate, $BiCa_2AsO_6$

4. 1. Introduction

Bismuth calcium vanadate $BiCa_2VO_6$ has recently been synthesized and structurally characterized (1). This compound crystallizes in the noncentrosymmetric polar space group $Cmc2_1$. It has been found to exhibit non linear optical properties. Possible isostructural compounds were therefore sought. Arsenic and vanadium have very similar radii (2) and are both often found in tetrahedral coordination. Synthesis and crystal structure determination of bismuth calcium arsenate $BiCa_2AsO_6$ were therefore carried out.

4. 2. Experimental

A polycrystalline sample of $BiCa_2AsO_6$ was synthesized by solid state reaction from Bi_2O_3 (Cerac, 99.999%), $CaCO_3$ (Mallinckrodt, analytical reagent) and As_2O_5 (Johnson Matthey Electronics, 99.99%). Stoichiometric quantities of reagents were ground together into a mixture that was then heated at 980°C for 20 hours and then cooled to room temperature at a rate of 10°/minute. Pale tan colored powder was obtained. Powder X-ray diffraction data were collected on

a Siemens D5000 diffractometer with vertical Soller slits and an energy-dispersive Kevex detector, using Cu K_α radiation. The 2θ range of $2°$ to $150°$ was scanned in $0.02°$ increments, with a counting time of 8 seconds per step. Neutron diffraction data were collected on line BT1, the high resolution powder diffractometer at the Center for Neutron Research at NIST, using the Cu (311) monochromator ($\lambda = 1.5401$ Å), a 15' in-pile Soller collimator and an array of 32 He-3 detectors at $5°$ intervals. Details of x-ray and neutron diffraction data collections are given in Table 4.1.

Second harmonic generation effect was sought using a Nd^{3+}:YAG laser with a wavelength of 1064 nm.

Table 4.1. Details of X-ray and Neutron Diffraction Data Collection for $BiCa_2AsO_6$

Quantity	X-ray Diffraction Data*	Neutron Diffraction Data
a (Å)	8.88479(8)	8.8817(4)
b (Å)	11.97231(11)	11.9721(5)
c (Å)	5.54532(5)	5.5424(2)
Zero point (° 2θ)	-0.1078(4)	-0.053(4)
Wavelength (λ)	1.54056	1.5401
Data range (° 2θ)	10 - 150	10 – 160
Step size (° 2θ)	0.02	0.05
Number of data points	6999	2999
Number of reflections	368	393
Number of variables	20	41
R_p (%)	6.44	4.65
wR_p (%)	9.63	5.87
R_F^2 (%)	n/a	6.95
R_F (%)	n/a	4.91

* Le Bail fit to the observed x-ray diffraction pattern

4. 3. Structure Analysis

The X–ray diffraction pattern of $BiCa_2AsO_6$ was compared to that observed for $BiCa_2VO_6$. The similarities between the two patterns are obvious (Figure 4.1). The first ten peaks of $BiCa_2AsO_6$ were therefore assigned the indices of their vanadate counterparts and the cell edges were refined using the program Refcel (3) starting from the orthorhombic unit cell of $BiCa_2VO_6$. More accurate cell parameters were determined by fitting the entire pattern using the Le Bail algorithm (4) within the GSAS suite (5). The obtained cell parameters were a = 8.88479(8) Å, b = 11.97231(11) Å and c = 5.54532(5) Å. The final Le Bail fit is shown in Figure 4.2. The pattern was the inspected for the systematic absences, which indicated two possible space groups, $Cmc2_1$ (N° 36) and Cmcm (N° 63). The structure of $BiCa_2AsO_6$ thus appeared to be either isostructural or very closely related to that of $BiCa_2VO_6$

Rietveld refinement (6) of $BiCa_2AsO_6$ x-ray diffraction data was carried out using the $BiCa_2VO_6$ structure as the initial model. Although a good fit to the observed data and satisfactory agreement factors were obtained, the refinement would not converge due to the large shifts of positional parameters of oxygens O (1).

Rietveld refinement performed on the neutron diffraction data in space group $Cmc2_1$ readily converged, resulting in the final agreement factors of wR_p = 5.78%, R_p = 4.58% and R_F = 4.91%. Observed, calculated and difference curves for neutron diffraction data are shown in Figure 4.3.a.
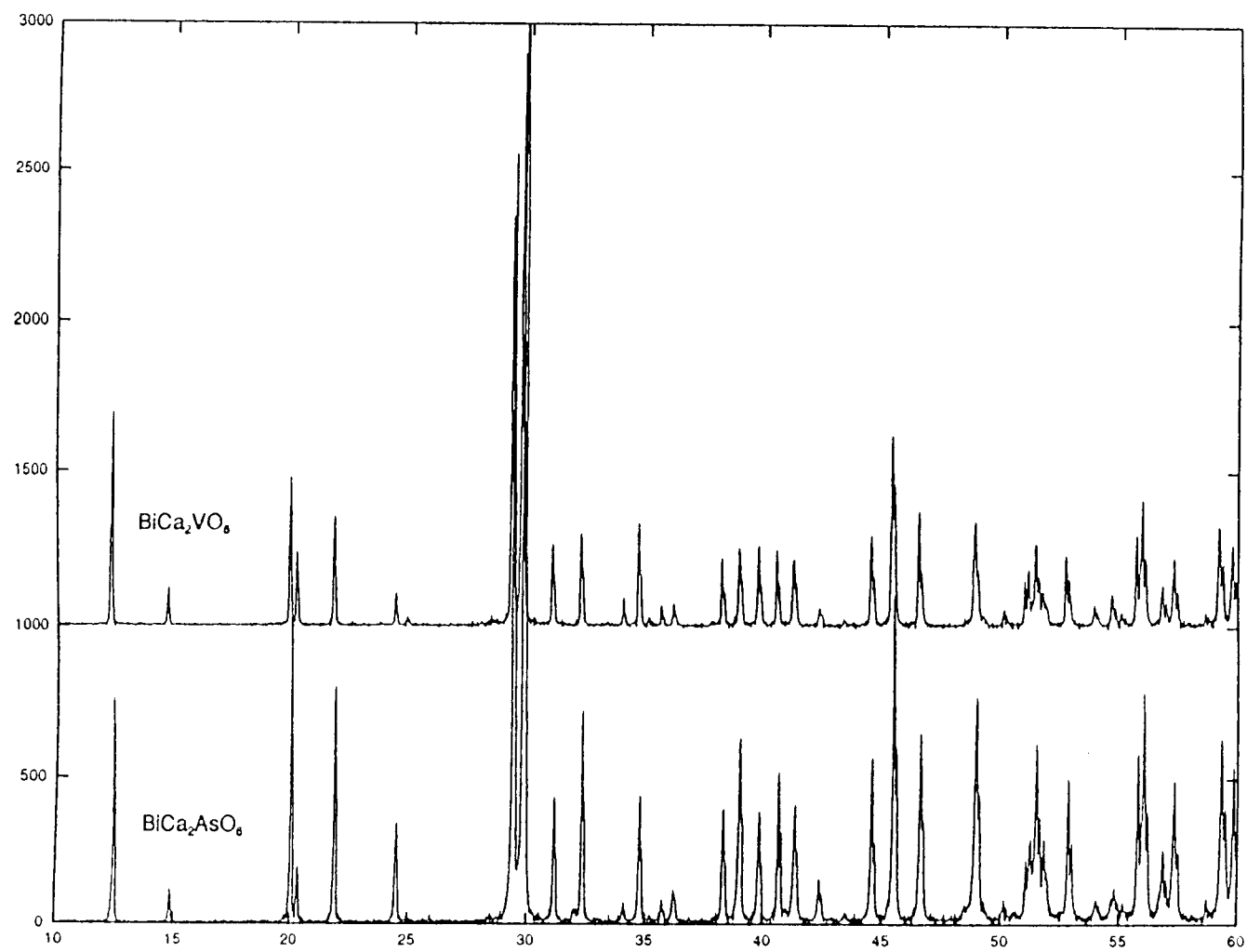
Figure 4.1. A comparison of the X-ray diffraction patterns of $BiCa_2AsO_6$ and $BiCa_2VO_6$
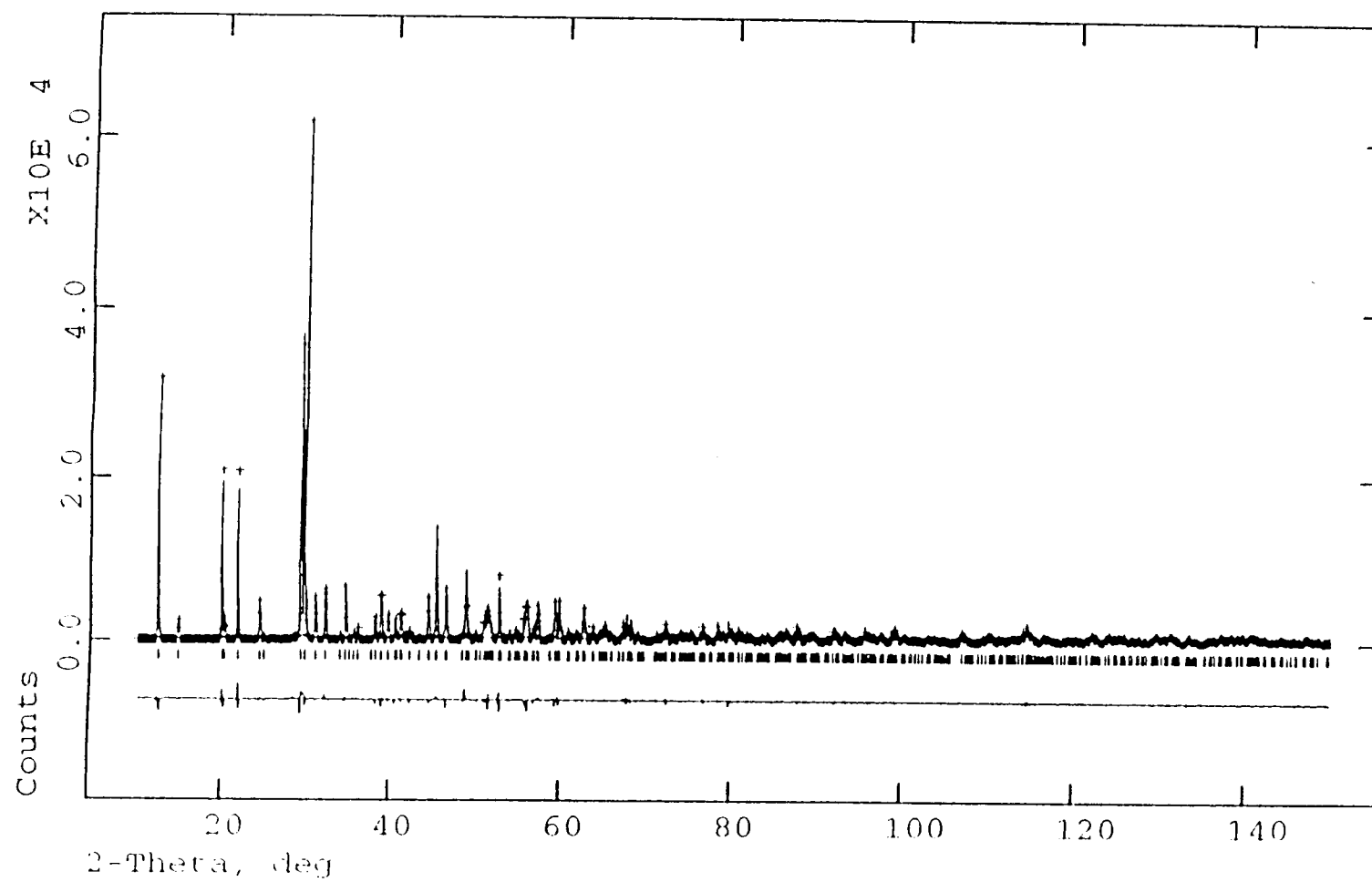
Figure 4.2. The Le Bail fit to $BiCa_2AsO_6$ X-ray diffraction data

BiCa2AsO6, space group C m c 21
Lambda 1.5401 A
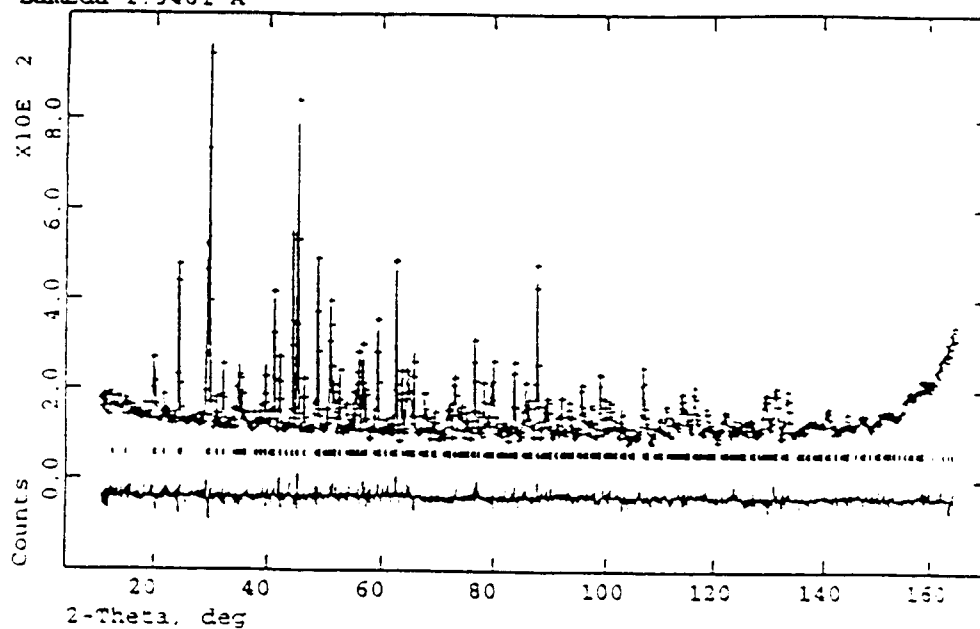
Figure 4.3.a. The Rietveld refinement of the $BiCa_2AsO_6$ neutron diffraction data in space group $Cmc2_1$

BiCa2AsO6, space group C m c m
Lambda 1.5401 A
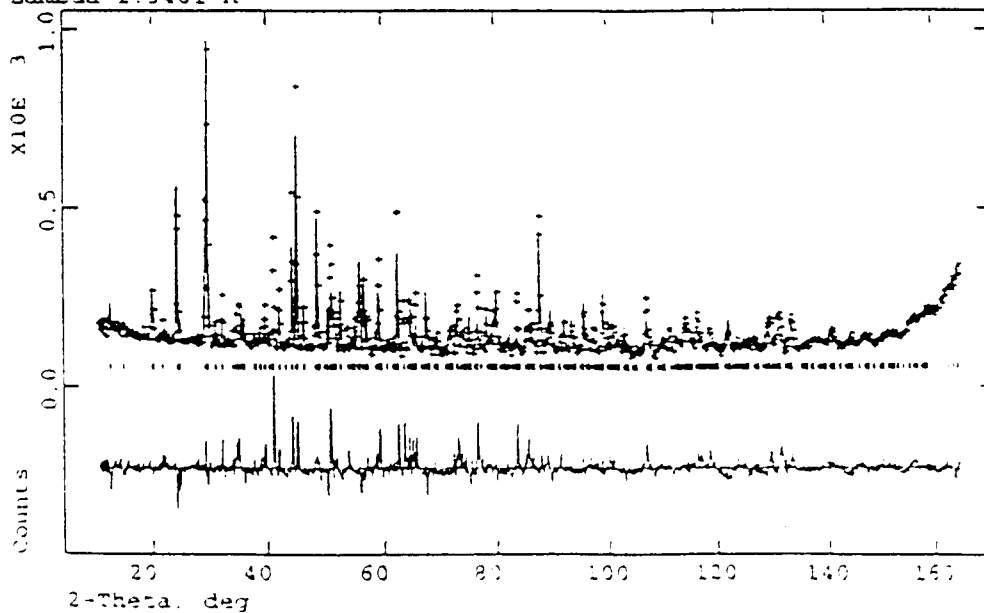
Figure 4.3.b. The Rietveld refinement of the $BiCa_2AsO_6$ neutron diffraction data in space group $Cmcm$

Refinement of neutron diffraction data was also carried out in the centrosymmetrical space group Cmcm. No satisfactory agreement between the observed and calculated patterns was achieved, as can bee seen in Figure 4.3.b. $BiCa_2AsO_6$ was found to be second harmonic generation active. This property confirms the lack of a center of symmetry in this structure.

4. 4. Discussion

Atomic fractional coordinates, isotropic structure factors and bond valence sums (7) for $BiCa_2AsO_6$ are given in Table 4.2. A view of the $BiCa_2AsO_6$ structure is shown in Figure 4.4. Lattice parameters of $BiCa_2AsO_6$ (a = 8.882 Å, b = 11.972 Å, c = 5.542 Å) are very similar to those of $BiCa_2VO_6$ (a = 8.895 Å, b = 11.966 Å, c = 5.544 Å), as can be expected for isostructural substitution of $^{IV}As^{5+}$ (r = 0.335 Å) for $^{IV}V^{5+}$ (r = 0.355 Å). $(BiO_2)^-$ one-dimensional infinite chains extend along the z axis. VO_4^{3-} tetrahedra are found in a non-centrosymmetrical arrangement, all pointing in the same direction along the z axis, the polar axis of the crystal. Ca^{2+} cations adopt an irregular seven coordinate site between these units.

Coordination of bismuth is shown in Figure 4.5. Bi^{3+} has a coordination environment consisting of four shorter (2 x 2.160 Å, 2 x 2.240 Å) and three longer bonds (3.104 Å, 2 x 3.064 Å). Such an asymmetric arrangement is typical of lone pair cations. The four short bonds participate in formation of the $(BiO_2)^-$ chains along the z axis, found in all the members of the BiA_2MO_6 family that we

have reported (8, 9, 10, 11, 12). The three longer bonds that complete the coordination of bismuth are to oxygens of AsO_4 tetrahedra.

Coordination of arsenic in $BiCa_2AsO_6$ is shown in Figure 4.6. Arsenic bonds to four oxygen atoms in a slightly distorted tetrahedral coordination. Bond distances range from 1.67 Å to 1.70 Å and angles from 104° to 114°.

Coordination of calcium in $BiCa_2AsO_6$ is shown in Figure 4.7. Calcium bonds to seven oxygen atoms, two from the $(BiO_2)^-$ chains and five from the AsO_4^{3-} units. Bond lengths range from 2.30 Å to 2.76 Å.

Table 4.2. Atomic Coordinates, Isotropic Thermal Parameters and bond valence sums for $BiCa_2AsO_6$

Atom	x/a	y/b	z/c	U_{iso} (Å²)	BV sums
Bi	0.5	0.0884(3)	0.25	0.0082(8)	3.19
As	0	0.1822(4)	0.695(1)	0.0122(10)	5.05
Ca	0.3022(4)	0.3932(4)	0.237(1)	0.0132(9)	1.94
O (1)	0.3491(4)	0.9981(4)	0.485(1)	0.0099(7)	2.26
O (2)	0	0.8198(4)	0.002(1)	0.0098(11)	2.02
O (3)	0	0.9469(4)	0.567(1)	0.0117(14)	1.78
O (4)	0.1547(4)	0.2432(3)	0.084(1)	0.0160(8)	1.90

Table 4.3. Selected Interatomic Distances (Å) and Bond Angles (°) for $BiCa_2AsO_6$

	O (1)	O (2)	O (3)	O (4)
Bi	2.160(5) x 2	3.104(5)		3.064(5) x 2
	2.240(5) x 2			
As		1.673(7)	1.702(7)	1.674(4) x 2
Ca	2.297(7)	2.372(6)	2.617(7)	2.378(6)
	2.334(7)		2.764(6)	2.552(7)

O (1) - Bi - O (1)..........78.0(1) x 2

O (1) - Bi - O (1)..........76.7(3)

O (1) - Bi - O (1)..........73.5(2)

O (2) - Bi - O (4)..........71.6(2) x 2

O (4) - Bi - O (4)..........53.4(2)

O (2) - V - O (3)..........113.8(3)

O (2) - V - O (4)..........112.0(2) x 2

O (3) - V - O (4) ....104.0(2) x 2

O (4) - V - O (4) ....110.4(4)

O (1) - Ca - O (1)..........73.5(2)

O (1) - Ca - O (2)..........166.3(3)

O (1) - Ca - O (3)..........101.4(2)

O (1) - Ca - O (3)..........80.7(2)

O (1) - Ca - O (4)..........89.2(2)

O (1) - Ca - O (4)..........107.7(2)
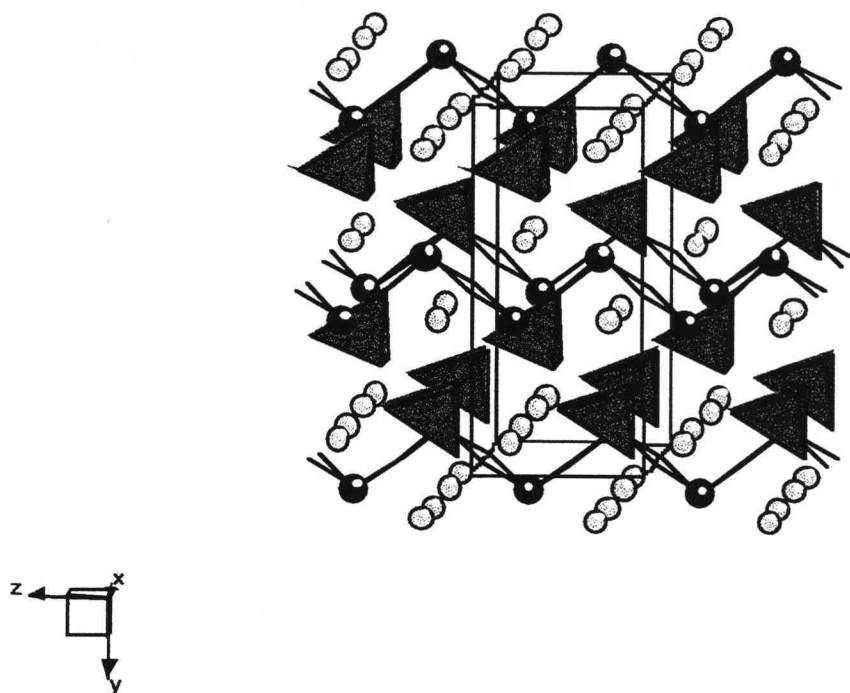
Figure 4.4. A view of the BiCa$_2$AsO$_6$ structure
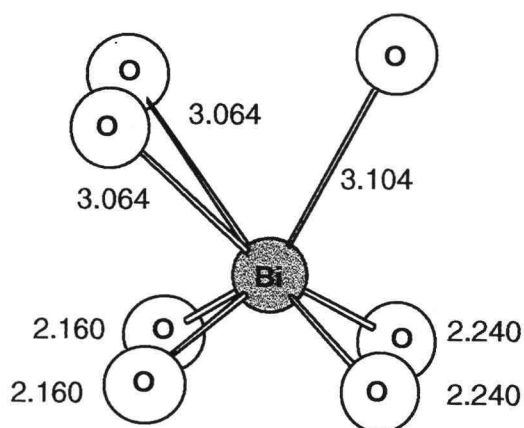
Figure 4.5. Coordination environment of bismuth in BiCa$_2$AsO$_6$
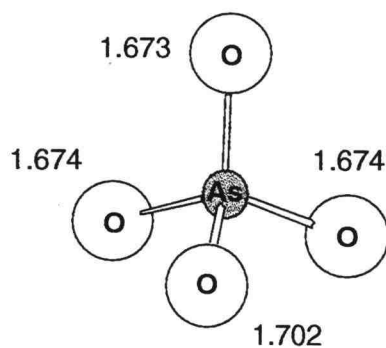
Figure 4.6. Coordination environment of arsenic in $BiCa_2AsO_6$
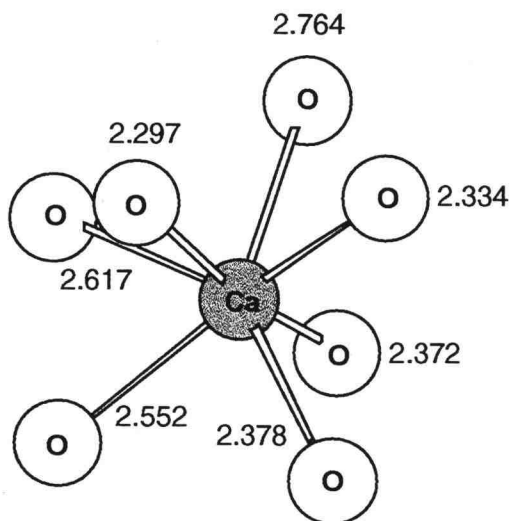
Figure 4.7. Coordination environment of calcium in $BiCa_2AsO_6$

4. 5. References

1. I. Radosavljevic, J. S. O. Evans and A. W. Sleight, *J. Solid State Chem.*, 137, 143 (1998)

2. R. D. Shannon, *Acta Cryst.*, 32, 751 (1976)

3. Refcel Program, J. K. Cockroft, Department of Crystallography, Birkbeck College, London, 1995.

4. A. Le Bail, H. Duroy and J. L. Fourquet, *Mat. Res. Bull.*, 23, 447 (1988)

5. A. C. Larson, R. B. von Dreele, LANSCE, Los Alamos National Lab, Los Alamos, NM, 1994.

6. H. M. Rietveld, *J. Appl. Cryst.*, 2, 65 (1969)

7. N. E. Brese and M. O. Keeffe, *Acta Cryst.*, B47, 192 (1991)

8. J. Huang, A. W. Sleight, *J. Solid State Chem.* 100, 170 (1992)

9. J. Huang, Q. Gu, A. W. Sleight, *J. Solid State Chem.* 105, 599 (1993)

10. I. Radosavljevic, J. S. O. Evans and A. W. Sleight, *J. Alloys Comp.*, in press

11. I. Radosavljevic, J. S. O. Evans and A. W. Sleight, *J. Solid State Chem.*, 141, 149 (1998)

12. F. Abraham, M. Ketatni, G. Mairesse and B. Mernari, *Eur. J. Solid State Inorg. Chem.*, 31, 313 (1994)

Chapter 5

Variable Temperature X-ray Diffraction Study of Bismuth Magnesium Vanadate, $BiMg_2VO_6$

5. 1. Introduction

The room temperature structure of $BiMg_2VO_6$ solved from single crystal data was reported in 1992 (1). The compound was reported as C-centered orthorhombic, with unit cell dimensions of a = 7.9136(6) Å, b = 12.246(2) Å, c = 5.544(2) Å and space group C m c m (N° 63). In the rest of this Chapter this space group will be referred to in the setting Amma. A somewhat problematic detail in this structure was the size and shape of the thermal ellipsoid of one of the oxygen atoms. The position of this particular atom with respect to the symmetry elements present in this space group suggested that one of the possible ways to explain the shape of its thermal ellipsoid would be an inaccuracy in the proposed model. In particular, the questionable detail was whether the unit cell was centered, as reported, or primitive orthorhombic.

The purpose of this study was to gain a better insight into this situation.

5. 2. Experimental

Single crystals of $BiMg_2VO_6$ were grown from Bi_2O_3 flux in a platinum crucible. Bi_2O_3 (Atomergic Chemetals, 99.9%), MgO (Aldrich, 99+%) and NH_4VO_3 (Johnson Mathey, 99.99%) were mixed in 2:2:1 molar ratio. The mixture was heated at 700°C for 12 hours, at 800°C for 6 hours and at 1000°C for 1 hour. It was cooled to 500°C at a rate of 0.05° per hour and then furnace cooled to room temperature. Yellow needle shaped crystals were obtained.

Preliminary structural studies were carried out using an Enraf − Nonius DIP 2000 image plate diffractometer with Mo radiation, equipped with an Oxford Cryosystems nitrogen gas cryostream. Oscillation photographs of several different crystals were taken in 3° intervals, with exposure time of 900 seconds. Two data sets were collected, one at room temperature and the other at 150K. In both cases sixty frames were recorded at 3° intervals, with an exposure time of 900 seconds per frame. The obtained images were processed using the XDisplayF, Denzo and Scalepack programs of the HKL software suite (2). Details about these data collections are given in Table 5.1.

Table 5.1. Data Collections Using DIP 2000 Image Plate Diffractometer

Instrument	Enraf – Nonius DIP 2000 image plate diffractometer	
Wavelength (λ)	0.71073	0.71073
Temperature	298	150
N° of independent reflect.	663	661
N° of reflect. > 3 σ I	461	510
R_{merge} (%)	13.6	12.7
Space group	Pmcn	Pmcn

The purpose of these data collections was to use the advantages of an image plate detector to resolve the existing uncertainty in regard to the presence or absence of cell centering in this structure. These analyses confirmed the presence of (hkl): k + l = 2n+1 reflections in both data sets, indicating that at 150K and room temperature the structure was primitive, rather than centered orthorhombic. After these preliminary investigations, a more detailed study was performed on a selected crystal of 0.1 x 0.1 x 0.3 mm in dimensions.

Variable temperature X-ray diffraction experiments were conducted on an Enraf – Nonius Mach3 diffractometer with Cu radiation. Data collections were performed at 100 K, 150 K, 200 K, 250 K, 300 K and 350 K. Temperature was adjusted and controlled using an Oxford Cryosystems nitrogen gas cryostream.

Temperatures are estimated to be accurate to 0.1°. Twenty five reflections were located from a combination of automated search routines and polaroid photographs. These reflections were centered and indexed to the primitive orthorhombic cell expected. Data collection was then performed in the theta range from 2 to 75°. The same reflection centering file and collection conditions were used at all subsequent temperatures. Data sets were processed using RC93 software (3). Structure refinements were performed using the Oxford Crystals suite (4).

Details about the crystal and general data collection conditions are given in Table 5.2. Temperature dependent parameters of data collections and refinements are given in Table 5.3.

Table 5.2 Crystal and Data Collection Data

Crystal size (mm)	0.1 x 0.1 x 0.3
Crystal shape	needle
Crystal color	yellow
Crystal system	orthorhombic
Diffractometer	Enraf – Nonius CAD4
Radiation	Cu
Theta range (°)	2 - 75
Scan mode	two theta - omega
h range	0 - 6
k range	0 - 9
l range	0 - 15
Number of centering reflections	25
Theta min. of centering reflections	6.68
Theta max. of centering reflections	46.15
Number of intensity standards	3 (checked every 100 reflections)
Number of orientation standards	2 (checked every 60 minutes)

Table 5.3. Structure Refinement Details as a Function of Temperature

	100 K	150 K	200 K	250 K	300 K	350 K
Space group	Pmcn	Pmcn	Pmcn	Pmcn	Pmcn	Amma*
Z	4	4	4	4	4	4
Density (g/cm³)	5.136	5.134	5.130	5.126	5.120	5.116
N° reflections	530	529	528	520	480	318
N° parameters	56	56	56	56	56	33
Extinction	11.7(13)	11.0(13)	16.2(18)	15.6(19)	17.7(23)	1.9(7)
Scale factor	2.49(4)	2.47(4)	2.57(4)	2.52(5)	2.58(5)	1.78(5)
R (%)	5.75	6.88	6.00	6.99	6.66	8.83
wR (%)	6.68	7.46	6.62	7.43	7.76	10.98

* Identical results for the 350 K data were obtained by refining the structure in space group Pmcn using the necessary constraints

5. 3. Structural Analysis

Analysis of the diffraction images taken both at 150 K an at room temperature gave an orthorhombic cell of a ~ 5.4 Å, b ~ 7.9 Å and c ~ 12.2 Å and indicated the reflection conditions of (h00): h = 2n, (0k0): k = 2n, (00l): l = 2n, (h0l): l = 2n and (hk0): h+k = 2n. There were clearly no systematic absences for the (hkl) class of reflections, suggesting two possible primitive orthorhombic space groups Pmcn (#62) and P 21 c n (#33). Since a negative second harmonic generation test for $BiMg_2VO_6$ had been reported by Huang and Sleight (1), the refinements in this work were carried out in the centrosymmetric space group.

The six data sets collected between 100 K and 350 K were also inspected for the presence of (hkl): k + l = 2n + 1 reflections. The absence of such reflections would indicate an additional A centering condition. The following trends were found: the number of observed (hkl): k + l = 2n reflections, which would be allowed in both primitive and centered space groups ("A – reflections") remains essentially unchanged with temperature; the number of (hkl): k + l = 2n + 1 reflections, allowed in the primitive, but forbidden in the centered space group ("P – reflections") gradually decreases as a function of temperature and they disappear at the temperature of 350 K. The intensity of "P – reflections" decreases with temperature at a higher rate than that of "A – reflections". These trends are illustrated in Figures 5.1 and 5.2. In Figure 5.2 the summed intensities of all the 'P' and 'A' reflections measured are plotted separately as a function of increasing temperature.
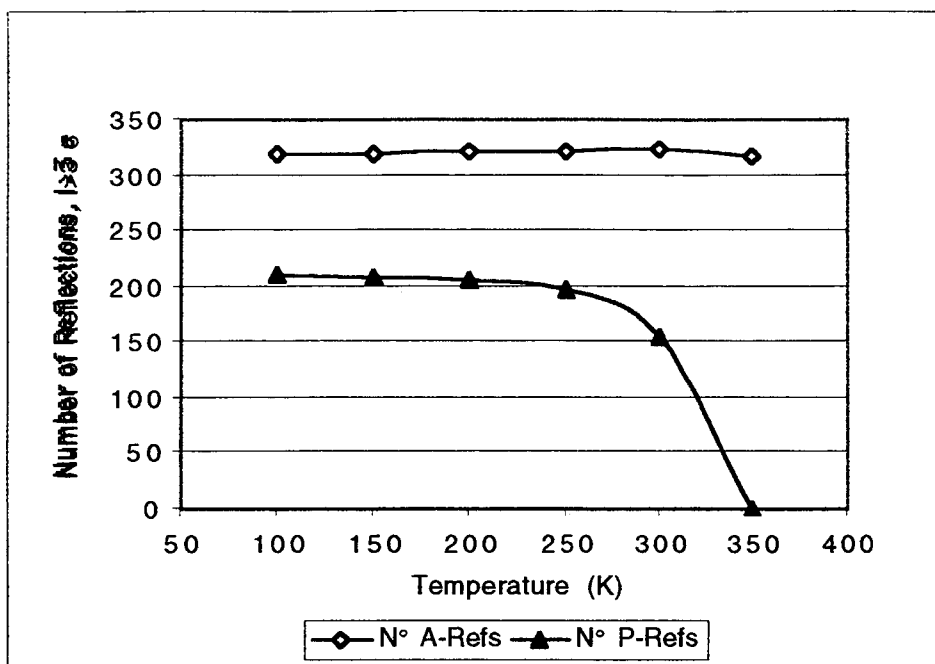
Figure 5.1. Number of A- and P-reflections as a function of temperature
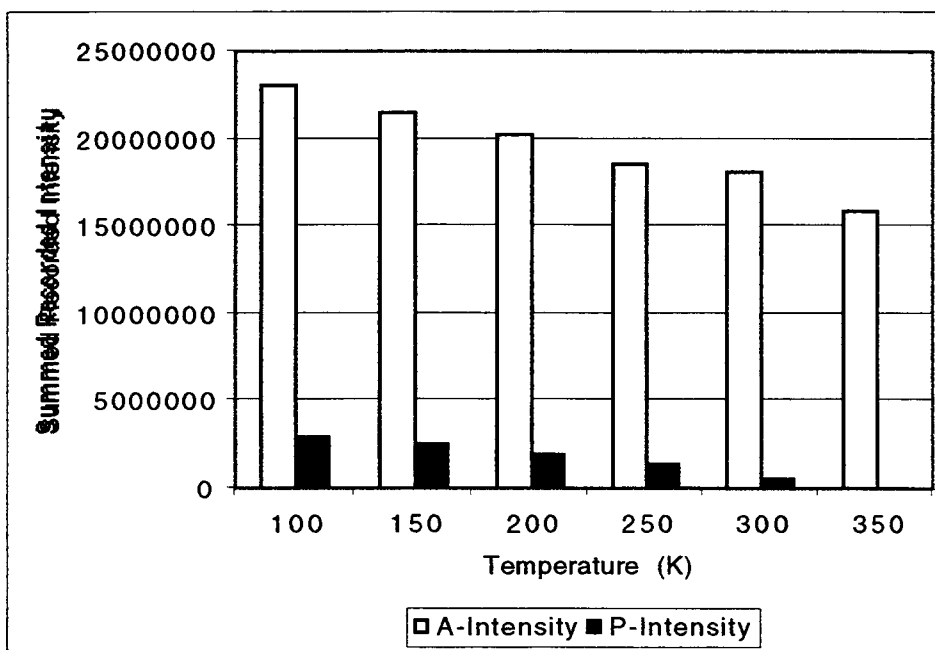
Figure 5.2. Intensity of A- and P-reflections as a function of temperature

The data represented in these figures indicates that $BiMg_2VO_6$ undergoes a phase transition from the primitive space group Pmcn to its centered supergroup Amma somewhere between 300 K and 350 K. Structure refinements at 100 K, 150 K, 200 K, 250 K and 300 K were performed in space group P c m n. At 350 K, the free refinement in Pmcn did not give a satisfactory fit, but space group Amma gave good results. This data set was also refined in the primitive space group, using the necessary constraints on the positions and temperature factor components of Mg(1) and Mg(2), as well as O(3) and O(4) atoms. These two refinements gave identical results, as expected.

Preliminary structure refinements were carried out with each data set independently and all gave satisfactory agreement factors for full anisotropic refinements. However, the scale factor, extinction parameter, absorption and temperature factors were highly correlated, hence a more systematic approach should be applied to ensure consistency and in order for the parameters obtained for different temperatures to be compared in a meaningful way. The following refinement strategy was applied to all data sets:

1. Refinement of positional parameters and isotropic temperature factors, keeping scale factor fixed and extinction parameter at zero. The obtained temperature factors were checked for the increasing trend with increasing temperature

2. Application of an absorption correction (5), making sure that the corrections at different temperatures did not vary to a significant extent

3. Further refinement of positional parameters and isotropic temperature factors

4. Refinement of positional parameters and anisotropic temperature factors

5. Full anisotropic refinement, including scale factor and extinction parameter

6. Application of an optimal weighting scheme

The final agreement factors each temperature are given in Figure 5.3. Scale factors and extinction parameters obtained for different temperatures are shown in Figure 5.4.
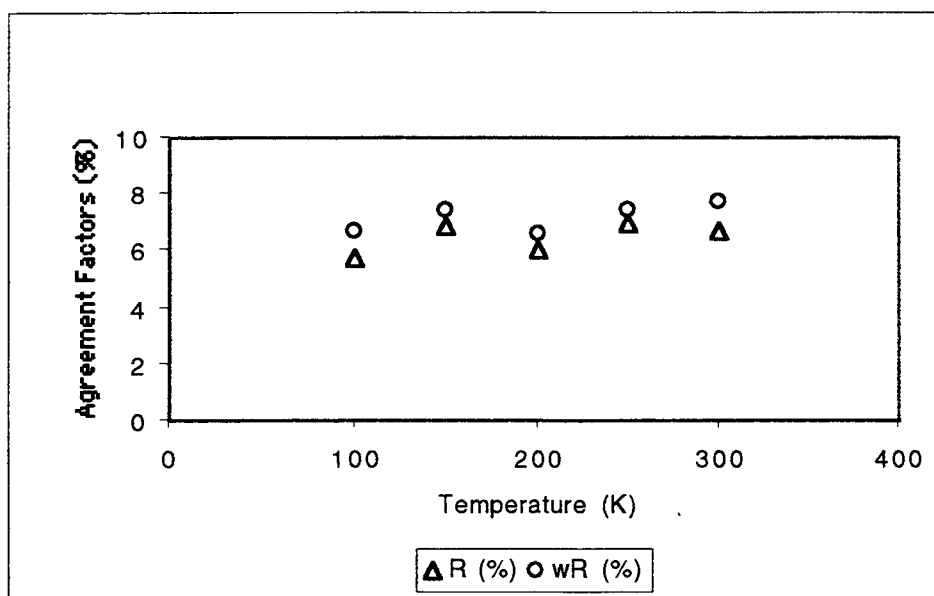
Figure 5.3. Agreement factors obtained for structure refinements as a function of temperature
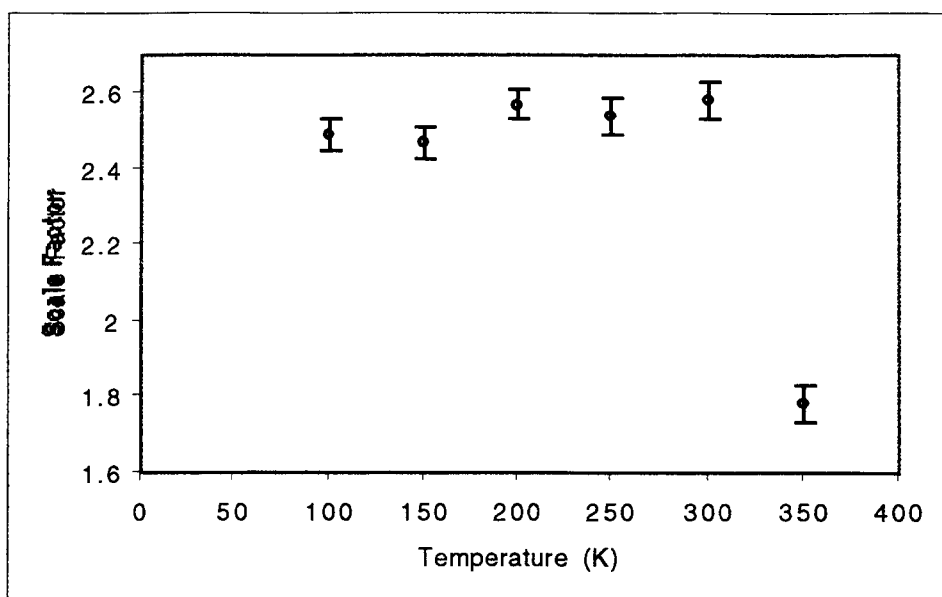
Figure 5.4.a. Scale factor as a function of temperature
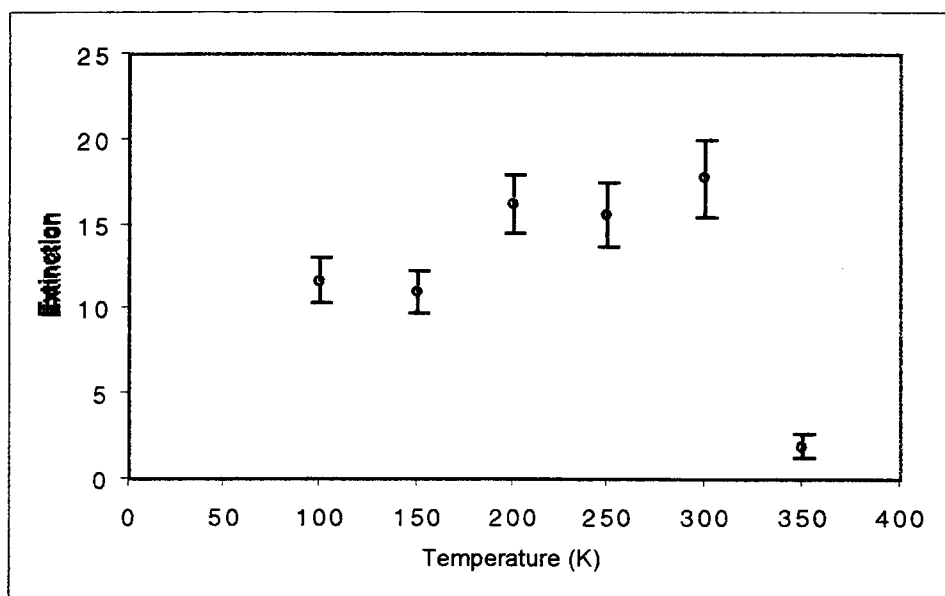
Figure 5.4.b. Extinction parameter as a function of temperature

Unit cell parameters increase smoothly with temperature, as shown in Table 4 and Figures 5.5.a – 5.5.d.

Table 5.4. Variation of Unit Cell Parameters as a Function of Temperature

T(K)	a (Å)	b (Å)	c (Å)	V (Å³)
100	5.4405(2)	7.9122(2)	12.2214(4)	526.09(3)
150	5.4404(2)	7.9128(2)	12.2261(4)	526.32(3)
200	5.4411(2)	7.9142(1)	12.2313(3)	526.70(3)
250	5.4420(2)	7.9152(2)	12.2384(3)	527.16(3)
300	5.4431(2)	7.9160(2)	12.2475(3)	527.72(3)
350	5.4449(4)	7.9169(5)	12.2522(7)	528.15(6)

The increase in all four cases follows a smooth trend, suggesting that the nature of the structural change is displacive. This and the inability to find a transition by differential scanning calorimetry suggest that this phase transition is displacive.

Atomic positions at different temperatures are given in Tables 5.5.a – 5.5.f. The variation of bond lengths as a function of temperature is given in Tables 5.6.a – 5.6.c and in Figures 5.6.a – 5.6.c.
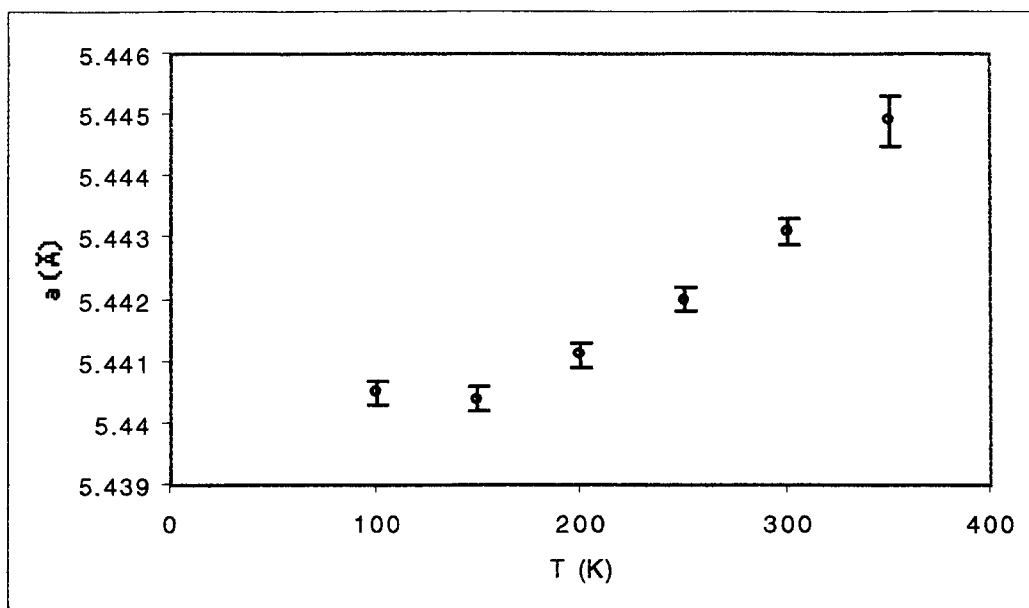
Figure 5.5.a. Variation of the unit cell *a* axis with temperature
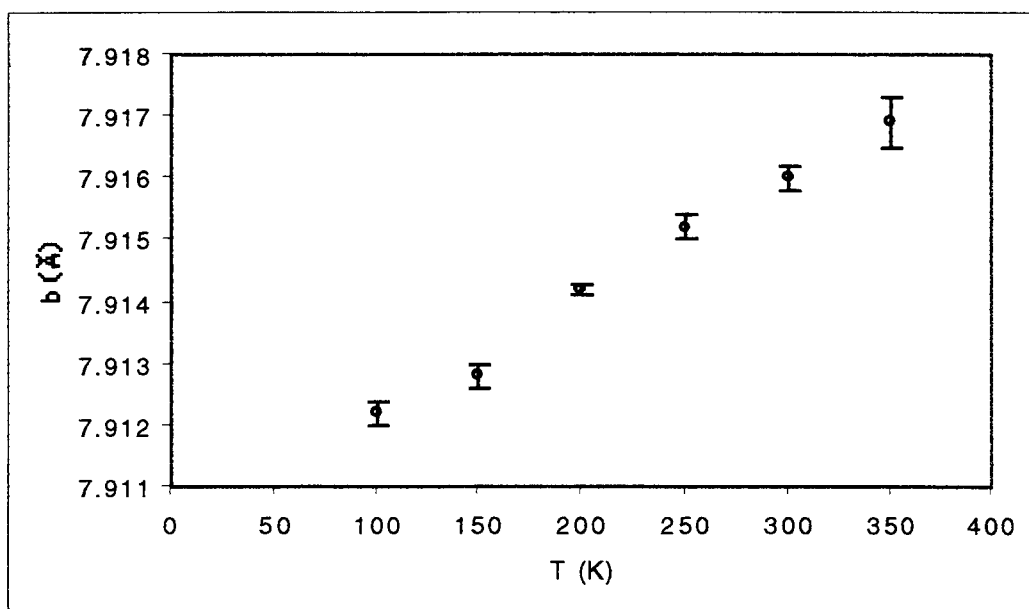
Figure 5.5.b. Variation of the unit cell *b* axis with temperature
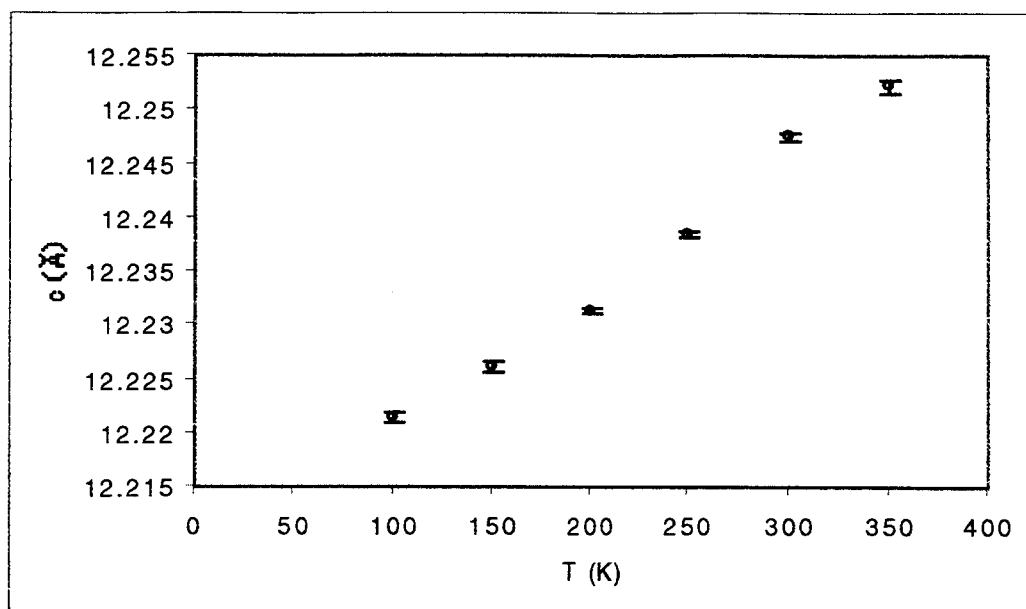
Figure 5.5.c. Variation of the unit cell *c* axis with temperature
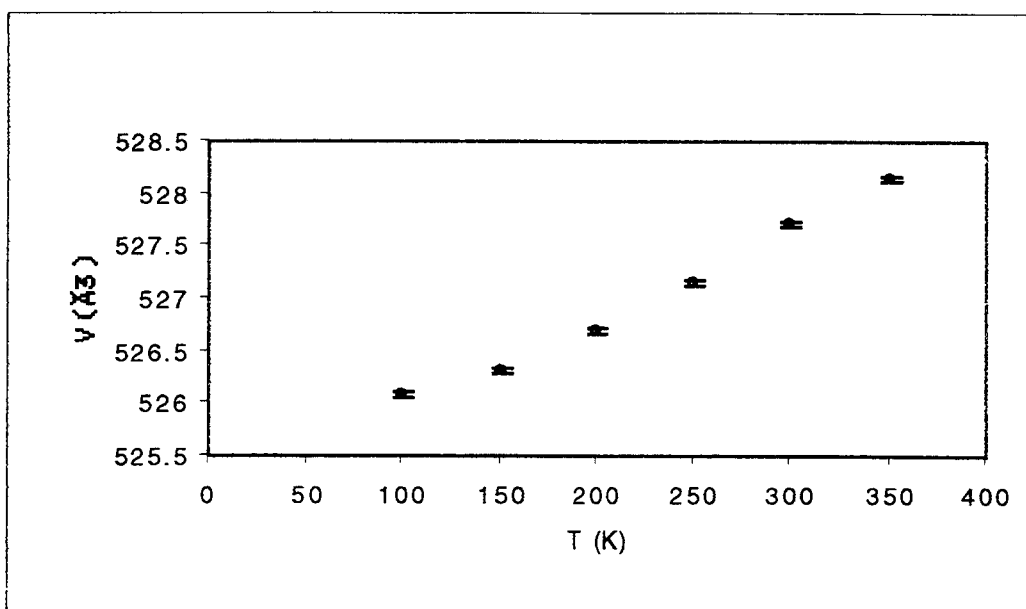
Figure 5.5.d. Variation of the unit cell volume with temperature

Table 5.5.a. Atomic Fractional Coordinates at 100K

Atom	x/a	y/b	z/c
Bi	0.75	-1.0105(1)	0.90782(5)
V	0.25	-0.9829(3)	0.6981(3)
Mg(1)	0.75	-0.697(1)	1.0845(4)
Mg(2)	1.25	-0.688(1)	0.9068(4)
O(1)	-0.007(2)	-0.9937(7)	0.6172(9)
O(2)	1.001(1)	-0.8335(9)	0.9941(4)
O(3)	0.25	-1.140(1)	0.7928(9)
O(4)	0.75	-1.292(2)	0.7409(9)

Table 5.5.b. Atomic Fractional Coordinates at 150K

Atom	x/a	y/b	z/c
Bi	0.75	-1.0099(1)	0.90791(6)
V	0.25	-0.9834(4)	0.6983(4)
Mg(1)	0.75	-0.696(1)	1.0853(5)
Mg(2)	1.25	-0.689(1)	0.9068(4)
O(1)	-0.008(3)	-0.994(1)	0.618(1)
O(2)	1.003(1)	-0.834(2)	0.9946(6)
O(3)	0.25	-1.140(2)	0.792(1)
O(4)	0.75	-1.293(2)	0.739(1)

Table 5.5.c. Atomic Fractional Coordinates at 200K

Atom	x/a	y/b	z/c
Bi	0.75	-1.0089(1)	0.90787(6)
V	0.25	-0.9853(4)	0.6979(4)
Mg(1)	0.75	-0.696(1)	1.0856
Mg(2)	1.25	-0.690(1)	0.9069(4)
O(1)	-0.008(2)	-0.9948(9)	0.618(1)
O(2)	1.001(1)	-0.835(1)	0.9955(5)
O(3)	0.25	-1.144(2)	0.791(1)
O(4)	0.75	-1.296(2)	0.737(1)

Table 5.5.d. Atomic Fractional Coordinates at 250K

Atom	x/a	y/b	z/c
Bi	0.75	-1.0076(1)	0.90794(7)
V	0.25	-0.9874(4)	0.6974(4)
Mg(1)	0.75	-0.695(1)	1.0863(6)
Mg(2)	1.25	-0.690(1)	0.9076(6)
O(1)	-0.008(3)	-0.995(1)	0.618(1)
O(2)	1.002(2)	-0.835(1)	0.9958(8)
O(3)	0.25	-1.147(2)	0.790(2)
O(4)	0.75	-1.299(2)	0.735(2)

Table 5.5.e. Atomic Fractional Coordinates at 300K

Atom	x/a	y/b	z/c
Bi	0.75	-1.00489(9)	0.90796(8)
V	0.25	-0.9920(4)	0.6973(5)
Mg(1)	0.75	-0.694(1)	1.0875(6)
Mg(2)	1.25	-0.691(1)	0.9081(6)
O(1)	-0.009(3)	-0.997(1)	0.618(1)
O(2)	1.001(2)	-0.834(1)	0.9972(6)
O(3)	0.25	-1.56(3)	0.787(2)
O(4)	0.75	-1.307(3)	0.732(2)

Table 5.5.f. Atomic Fractional Coordinates at 350K

Atom	x/a	y/b	z/c
Bi	0.75	-1.00	0.9082(2)
V	0.25	-1.00	0.6962(9)
Mg(1)	0.75	-0.691(2)	1.088(1)
Mg(2)	0.75	-0.691(2)	1.912(1)
O(1)	-0.019(8)	-1.00	0.617(3)
O(2)	1.00	-0.833(3)	1.00
O(3)	0.25	-1.160(6)	0.785(4)
O(4)	0.25	-1.160(6)	0.715(4)

Table 5.6.a. Variation of the Bi-O Bonds as a Function of Temperature

T (K)	$d_{1(Bi-O)}$ (Å)	$d_{2(Bi-O)}$ (Å)
100	2.223(6)	2.188(6)
150	2.229(8)	2.179(8)
200	2.219(7)	2.181(7)
250	2.212(11)	2.183(11)
300	2.214(10)	2.194(10)
350	2.208(15)	2.208(15)
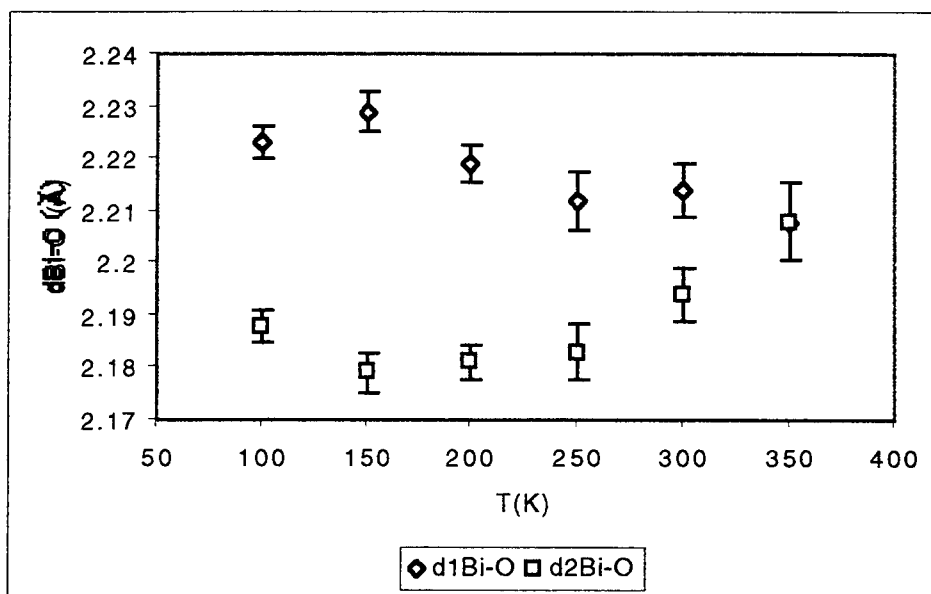
Figure 5.6.a. Variation of the Bi-O Bonds as a function of temperature

Table 5.6.b. Variation of the V-O Bonds as a Function of Temperature

T (K)	$d_{1(V-O)}$ (Å)	$d_{2(VO)}$ (Å)	$d_{3(V-O)}$ (Å)
100	1.71(1)	1.70(1)	1.68(1)
150	1.71(1)	1.69(1)	1.69(1)
200	1.71(1)	1.70(1)	1.69(1)
250	1.71(1)	1.70(2)	1.70(2)
300	1.71(1)	1.70(2)	1.70(2)
350	1.76(4)	1.66(4)	1.66(4)
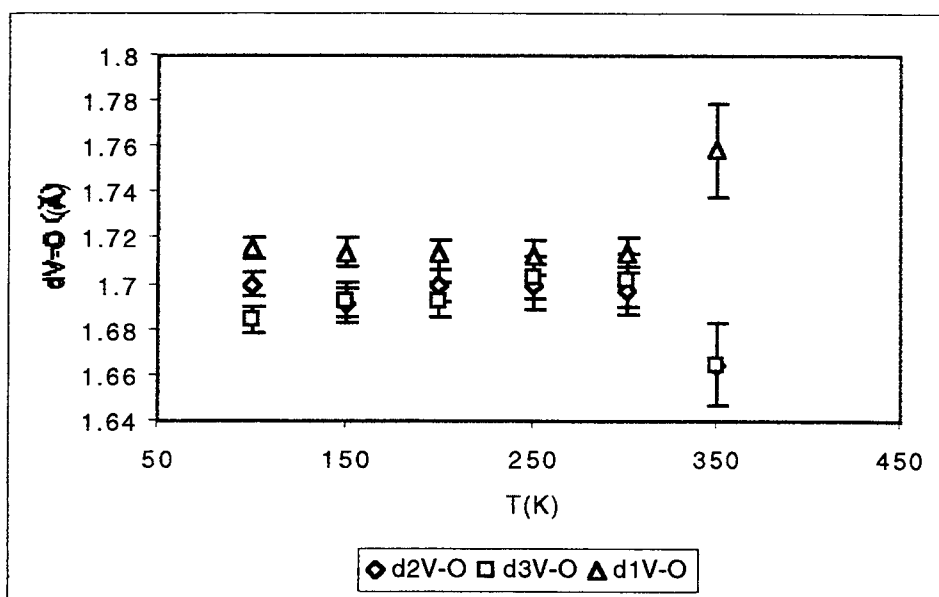
Figure 5.6.b. Variation of the V-O bonds as a function of temperature

Table 5.6.c. Variation of the Mg-O Bonds as a Function of Temperature

T (K)	$d_{1(Mg-O)}$ (Å)	$d_{2(Mg-O)}$ (Å)	$d_{3(Mg-O)}$ (Å)
100	2.04(1)	2.064(8)	1.98(1)
150	2.04(1)	2.07(1)	1.98(2)
200	2.04(1)	2.071(9)	1.96(2)
250	2.03(1)	2.08(1)	1.96(2)
300	2.04(1)	2.08(1)	1.94(3)
350	1.98(3)	2.06(2)	1.95(6)
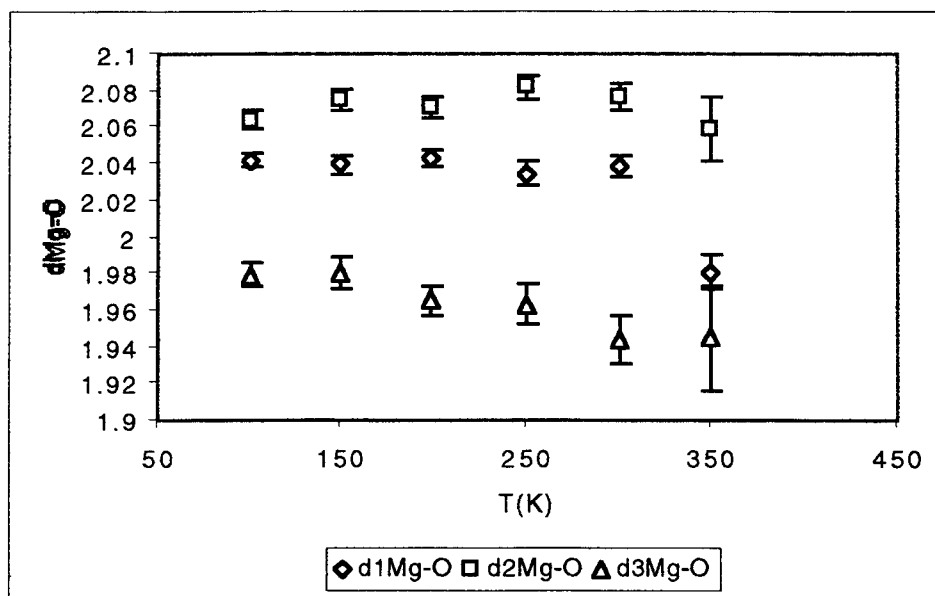
Figure 5.6.c. Variation of the Mg-O bonds as a function of temperature
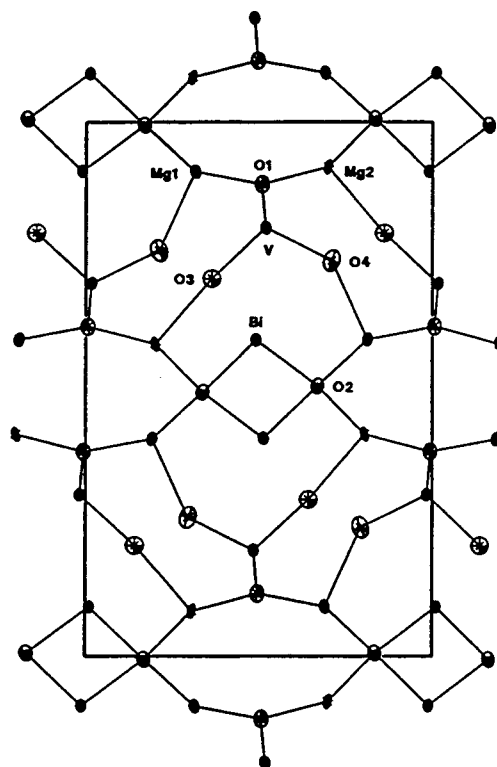
Figure 5.7.a. $BiMg_2VO_6$ structure at 100 K
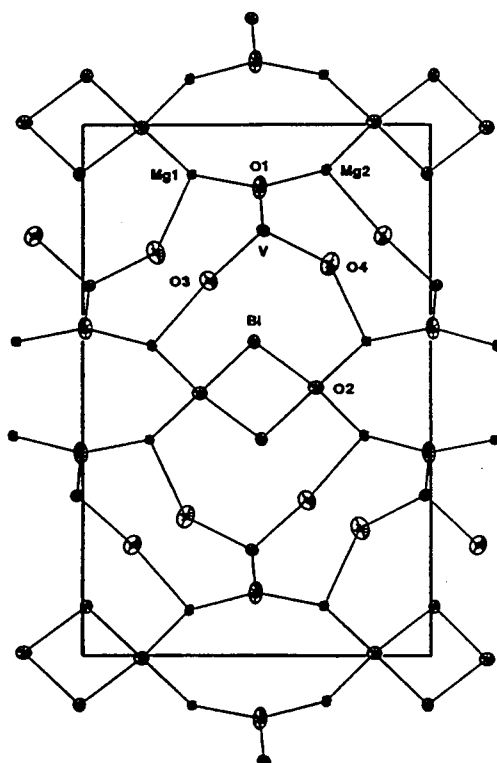
Figure 5.7.b. $BiMg_2VO_6$ structure at 150 K
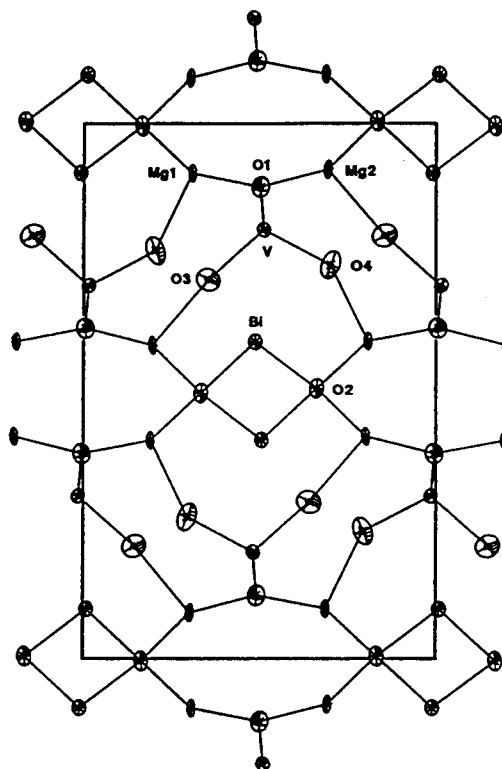
Figure 5.7.c. BiMg$_2$VO$_6$ structure at 200 K
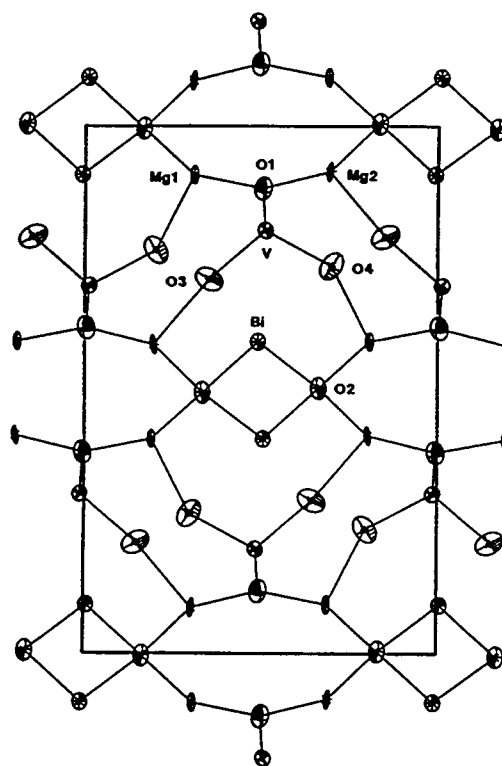
Figure 5.7.d. BiMg$_2$VO$_6$ structure at 250 K
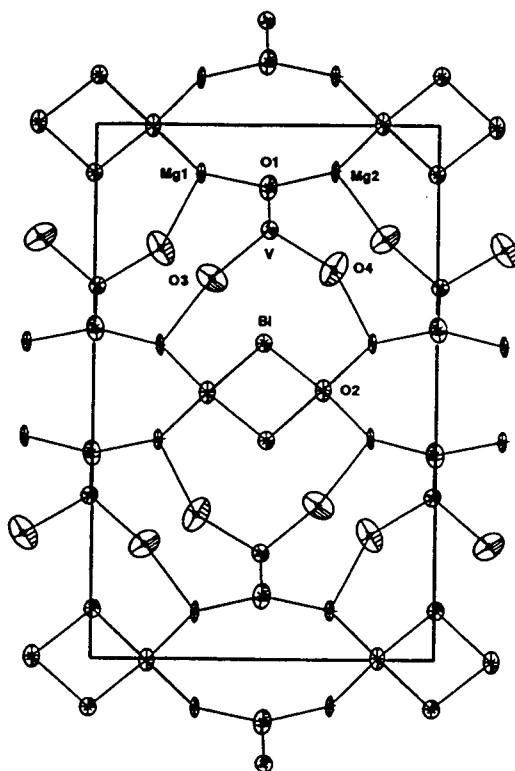
Figure 5.7.e. BiMg$_2$VO$_6$ structure at 300 K
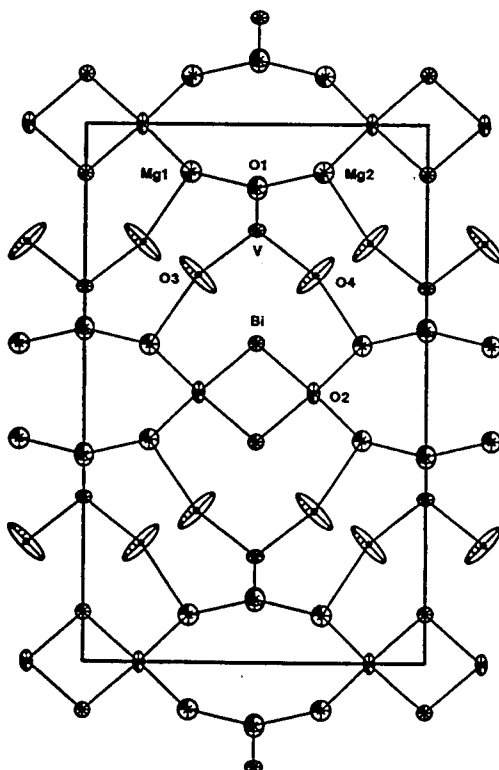
Figure 5.7.f. BiMg$_2$VO$_6$ structure at 350 K

Figures 5.7.a – 5.7.f show the anisotropic thermal ellipsoid representation of the structures obtained at different temperatures. It appears that the most striking, although not the only, difference among them is the size of the thermal ellipsoids on O(3) and O(4) atoms. Table 5.7 summarizes the calculated isotropic equivalents of anisotropic temperature factors for all atoms. They are plotted as a function of temperature in Figure 5.8.

Table 5.7. Isotropic Equivalent of Thermal Displacement Factors as a Function of Temperature

T (K)	Bi	V	Mg(1)	Mg(2)	O(1)	O(2)	O(3)	O(4)
100	0.0068(5)	0.0073(7)	0.009(1)	0.009(1)	0.013(2)	0.010(1)	0.013(2)	0.019(2)
150	0.0087(5)	0.0095(8)	0.011(1)	0.009(1)	0.019(2)	0.009(1)	0.017(2)	0.022(2)
200	0.0119(5)	0.0121(7)	0.014(1)	0.013(1)	0.019(2)	0.015(2)	0.023(2)	0.028(3)
250	0.0142(6)	0.0151(9)	0.015(2)	0.015(2)	0.023(2)	0.016(2)	0.028(4)	0.034(4)
300	0.0169(6)	0.0179(9)	0.017(2)	0.017(2)	0.025(2)	0.018(2)	0.038(4)	0.046(4)
350	0.010(1)	0.016(2)	0.022(3)	0.022(3)	0.030(6)	0.016(3)	0.062(8)	0.062(8)
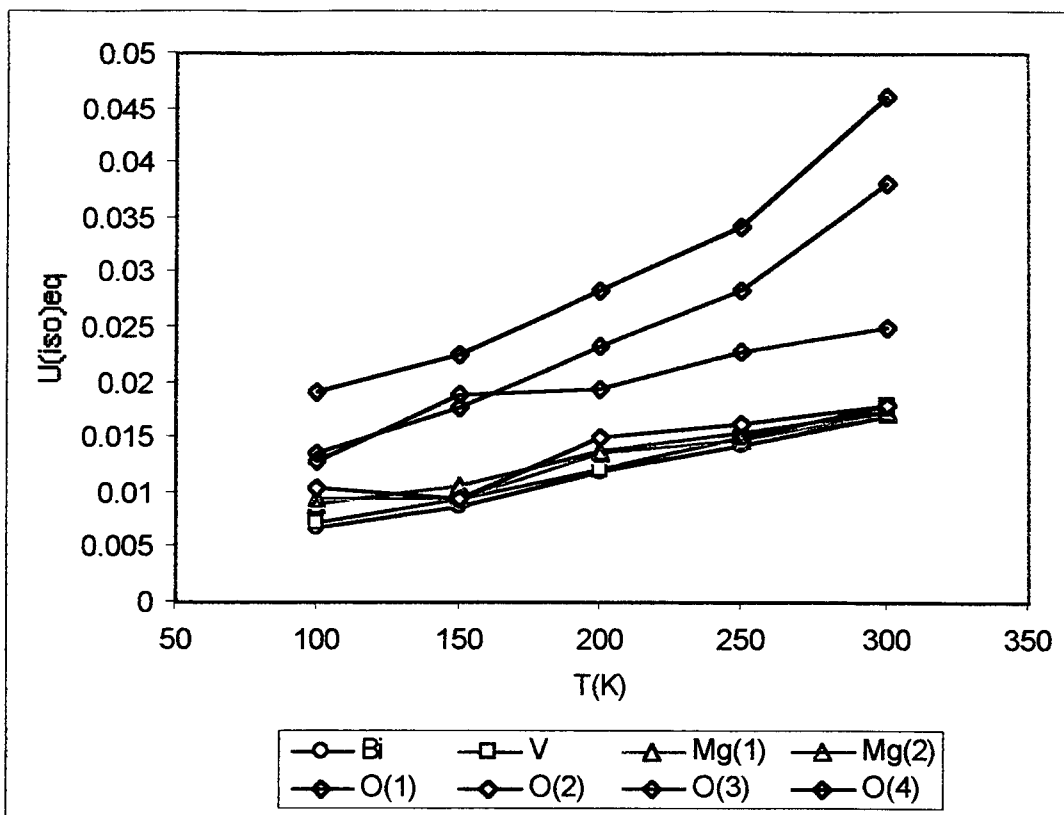
Figure 5.8. Isotropic equivalents of the temperature factors as a function of temperature

The plot shows that there is a clear division of atoms in this structure into two classes, on the basis of the rate of change of their temperature factors. Thermal factors of O(3) and O(4) increase at very similar rates, about three times faster than the other atoms, indicating that the key role of these atoms in the phase transition in question.

The phase transition in $BiMg_2VO_6$ can be described in terms of the emergence of a mirror plane perpendicular to the y axis, which gives rise to an additional A centering in the structure. In the centered structure O(3) and O(4) become crystallographically equivalent, as do Mg(1) and Mg(2). Bi, V and O(1)

move onto this mirror plane, while O(2) moves onto the twofold axis generated by this plane. These tendencies are reflected in the way that atomic coordinates change with increasing temperature. At the same time, thermal displacements of atoms increase. Table 5.8 summarizes the thermal displacements of atoms expressed as real principal axes of their thermal ellipsoids. It should be noted that the direction cosines for these axes do not change significantly as a function of temperature. This can be seen by the projections of thermal ellipsoids in Figure 5.7.

Table 5.8. Principal Thermal Ellipsoid Axes as a Function of Temperature

	100 K	150 K	200 K	250 K	300 K	350 K
Bi	0.0048	0.0066	0.0095	0.0115	0.0143	0.0097
	0.0075	0.0093	0.0128	0.0151	0.0178	0.0101
	0.0082	0.0103	0.0134	0.0159	0.0187	0.0106
V	0.0045	0.0066	0.0088	0.0113	0.0150	0.0096
	0.0078	0.0083	0.0116	0.0147	0.0172	0.0167
	0.0095	0.0137	0.0159	0.0195	0.0216	0.0219
Mg(1)	0.0026	0.0035	0.0025	0.0016	0.0025	0.0004
	0.0104	0.0063	0.0173	0.0194	0.0227	0.0166
	0.0139	0.0223	0.0220	0.0255	0.0270	0.0499
Mg(2)	0.0044	0.0036	0.0025	0.0034	0.0044	0.0004
	0.0087	0.0045	0.0159	0.0176	0.0209	0.0166
	0.0154	0.0203	0.0220	0.0232	0.0261	0.0499
O(1)	0.0057	0.0089	0.0109	0.0154	0.0155	0.0224
	0.0101	0.0183	0.0158	0.0158	0.0176	0.0279
	0.0231	0.0295	0.0318	0.0368	0.0418	0.0404
O(2)	0.0078	0.0070	0.0103	0.0094	0.0127	0.0047
	0.0105	0.0096	0.0135	0.0131	0.0141	0.0206
	0.0134	0.0119	0.0214	0.0264	0.0271	0.0251
O(3)	0.0079	0.0144	0.0130	0.0189	0.0273	0.0055
	0.0162	0.0175	0.0252	0.0232	0.0278	0.0420
	0.0171	0.0210	0.0320	0.0435	0.0593	0.1412
O(4)	0.0134	0.0145	0.0166	0.0207	0.0265	0.0055
	0.0178	0.0240	0.0255	0.0357	0.0425	0.0420
	0.0263	0.0290	0.0432	0.0461	0.0691	0.1412

The phase transition itself can be viewed as a cooperative effect of changes of atomic positions and thermal displacements. One way that this may be thought of is as follows. The changing atomic positions of O(3) and O(4) can be monitored by calculating the distance between, for example, O(4) and the position of O(3) reflected in the mirror plane that will eventually appear in the structure. This distance decreases with temperature, as indicated in the second column of Table 5.10. When this distance becomes smaller than half of the sum of the longest real ellipsoid semiaxes on O(3) and O(4), the two atoms can be considered to have become one crystallographic site. This model is not intended to be universal, but it appears to be one of the possible ways to view the changes that the $BiMg_2VO_6$ structure undergoes with increasing temperature. The proposed definition of the phase transition can then be applied in this particular case. The above described trends are illustrated in Figure 9. The decreasing curve represents the distance between O(4) and the O(3) 'symmetry equivalent'. The increasing curve represents the average value of the ellipsoid semiaxes for these two atoms. The two curves intersect at 320 K. Under the simple assumption that the lower temperature trend can be extrapolated as the transition temperature is approached, this temperature can be viewed as the approximate phase transition temperature.

Table 5.9. Variation of Oxygen Positional Parameters and Thermal Dsplacements Leading to the Phase Transition

T(K)	d(O3-O4)	U(O3)	U(O4)	1/2U(O2)	1/2U(O3)	Σ1/2U	1/2Σ1/2U
100	0.68(2)	0.13(2)	0.16(1)	0.06(1)	0.080(5)	0.14(1)	0.070(5)
150	0.65(2)	0.14(2)	0.17(2)	0.07(1)	0.08(1)	0.15(1)	0.075(5)
200	0.59(2)	0.18(2)	0.21(2)	0.09(1)	0.10(1)	0.19(1)	0.095(5)
250	0.53(3)	0.21(2)	0.21(2)	0.10(1)	0.10(1)	0.20(1)	0.100(5)
300	0.37(3)	0.24(2)	0.24(2)	0.12(1)	0.12(1)	0.24(1)	0.120(5)
350	0	0.37(4)	0.37(3)	0.18(2)	0.18(2)	0.36(1)	0.18(1)

$y = -1E{-}05x^2 + 0.0043x + 0.3729$

$y = 2E{-}06x^2 - 0.0005x + 0.1066$

d(O3-O4)   1/2S1/2U
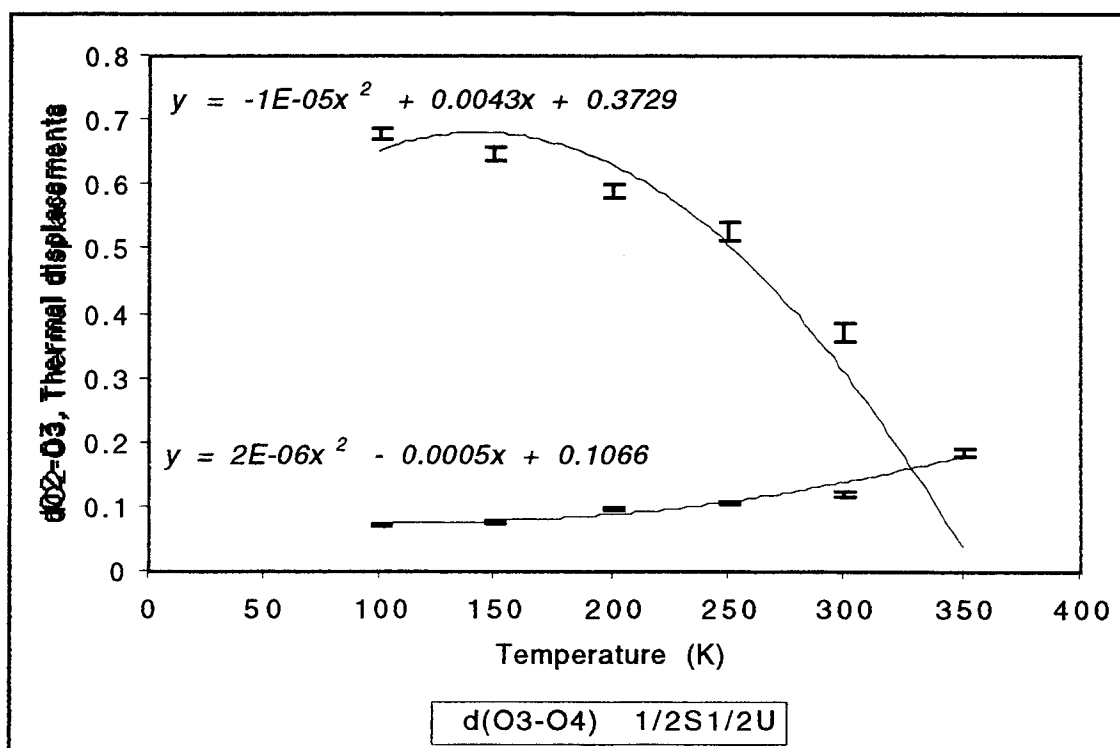
Figure 5.9. Variation of oxygen positional parameters and thermal displacements leading to the phase transition

5. 4. References

1. J. Huang, A. W. Sleight, *J. Solid State Chem.* 100, 170 (1992)

2. Z. Otwinowski and W. Minor, "Processing of X-Ray Diffraction Data in Oscillation Mode", in *Methods in Enzymology*, 276, C.W. Carter, Jr. and R.M. Sweet, Eds., Academic Press (1996)

3. RC93 Software, Chemical Crystallography Laboratory, University of Oxford, Oxford (1993)

4. Oxford Crystals, D.J. Watkin, J.R. Carruthers and P.W. Betteridge, Chemical Crystallography Laboratory, University of Oxford, Oxford (1985)

5. D. Stewart and N. Walker, *Acta Cryst.* Sect. A 39, 158 (1983)

Chapter 6

Neutron Diffraction Study of Bismuth Magnesium Phosphate, $BiMg_2PO_6$

6. 1. Introduction

Shortly after the structure of $BiMg_2VO_6$ was published (1), $BiMg_2PO_6$ and $BiMg_2AsO_6$ were prepared and reported as centered orthorhombic, isostructural with the vanadate compound (2). The structure of $BiMg_2PO_6$ was solved from single crystal data and the Rietveld refinement of the powder X-ray diffraction pattern was found to agree with the single crystal results. $BiMg_2AsO_6$ was refined from X-ray diffraction data only.

The structural models for both compounds exhibited the same problematic detail in that the thermal ellipsoids on two oxygen atoms were of unusual size and shape. The same feature had been reported for $BiMg_2VO_6$. In this case, the problem was resolved by variable temperature single crystal X-ray diffraction experiments that showed that the compound is, in fact, primitive orthorhombic at room temperature. This work is detailed in Chapter 5. The subject of the present Chapter is the refinement of $BiMg_2PO_6$ structure from neutron diffraction data.

6. 2. Experimental

A 10 g polycrystalline sample of $BiMg_2PO_6$ was synthesized by heating an intimately ground mixture of Bi_2O_3 (Cerac, 99.999%), MgO (Aldrich, 99+ %) and $(NH_4)_2HPO_4$ (Mallinckrodt, 99.99%) in a platinum crucible at 400°C for 2 hours to decompose $(NH_4)_2HPO_4$, at 700°C for 12 hours, at 800°C for 12 hours and at 1000°C for 12 hours. The obtained product was a white powder.

Powder X-ray diffraction data were collected on a Siemens D5000 diffractometer with vertical Soller slits and an energy-dispersive Kevex detector, using Cu K_α radiation. The 2θ range from 2° to 150° was scanned in 0.02° increments, with a counting time of 8 seconds per step. Neutron diffraction data were collected on line BT1, the high resolution powder diffractometer at the Center for Neutron Research at NIST, using the Cu (311) monochromator (λ = 1.5401 Å), a 15' in-pile Soller collimator and an array of 32 He-3 detectors at 5° intervals. Details of neutron diffraction data collections are given in Table 6.1.

The Rietveld refinements were performed using the GSAS suite of programs (3).

Table 6.1. Details of Neutron Diffraction data Collection for $BiMg_2PO_6$

Quantity	Neutron Diffraction Data
a (Å)	5.2743(1)
b (Å)	7.8088(2)
c (Å)	11.8948(3)
Zero point (° 2θ)	-0.065(1)
Wavelength (λ)	1.5401
Data range (° 2θ)	10 – 160
Step size (° 2θ)	0.05
Number of data points	2999
Number of reflections	601
Number of variables	47
R_p (%)	5.96
wR_p (%)	7.60
R_F^2 (%)	2.76
R_F (%)	2.27

6. 3. Structural Analysis

Inspection of the obtained X-ray diffraction pattern revealed the presence of a small amount of Bi_2O_3 in addition to the orthorhombic phase of approximate unit cell dimensions of a ~ 5.3 Å, b ~ 7.8 Å and c ~ 11.9 Å. Bi_2O_3 was therefore included as a second phase in all the subsequent diffraction data analyses. Inspection of the X-ray diffraction pattern showed that these data would not be sufficient to distinguish between the centered and the primitive orthorhombic structure of $BiMg_2PO_6$. In other words, the weak reflections that violate the centering condition ('P – reflections') that are mainly due to the scattering on oxygen atoms are not observed. Figure 6.1 represents a low angle portion of the observed X-ray diffraction pattern. The marked 2θ positions correspond to the d-spacings of some of the non-overlapping 'P – reflections'.
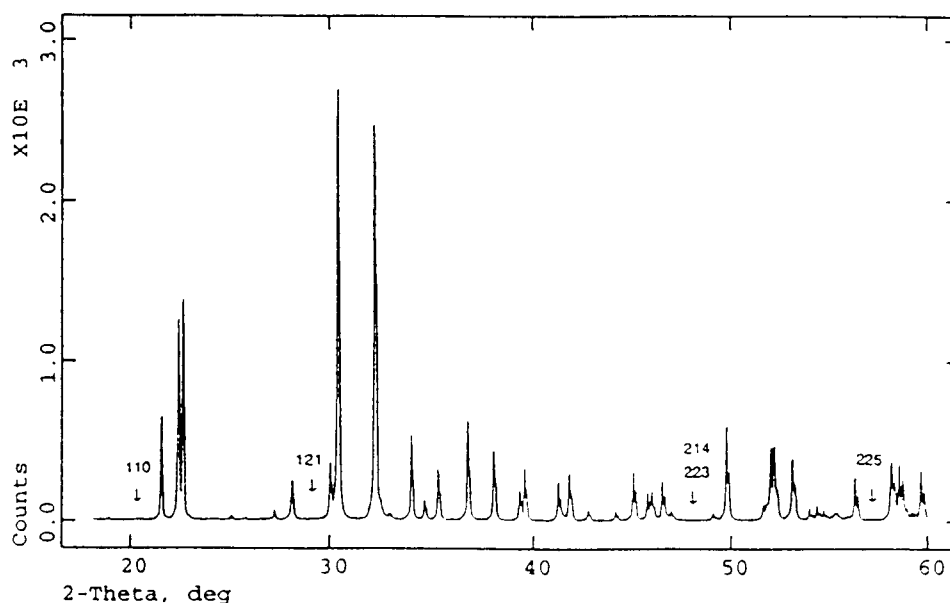
Figure 6.1. Observed X-ray diffraction pattern of $BiMg_2PO_6$

Inspection of the neutron diffraction pattern indicated the presence of certain reflections that are allowed in the primitive orthorhombic space group Pmcn, but forbidden in the centered space group Amma. The presence of the second phase makes the identification of such reflections difficult, especially at higher angles. Some reflections that can be indexed with certainty, since they are not overlapping with other $BiMg_2PO_6$ or Bi_2O_3 peaks, are listed in Table 6.2 and shown in Figure 6.2.

Table 6.2. Observed 'P – reflections' in $BiMg_2PO_6$

Reflection (hkl)	d_{hkl} (Å)	$2\theta_{hkl}$ (°)
110	4.3708	20.3015
121	3.0343	29.4122
223	1.9139	47.3895
214	1.9129	47.4153
225	1.6094	57.1921

These reflections violate the centering condition and the Rietveld refinement of $BiMg_2PO_6$ was therefore carried out in space group Pmcn. The obtained agreement factors are given in Table 6.1. The observed, calculated and difference patterns are shown in Figure 6.3.
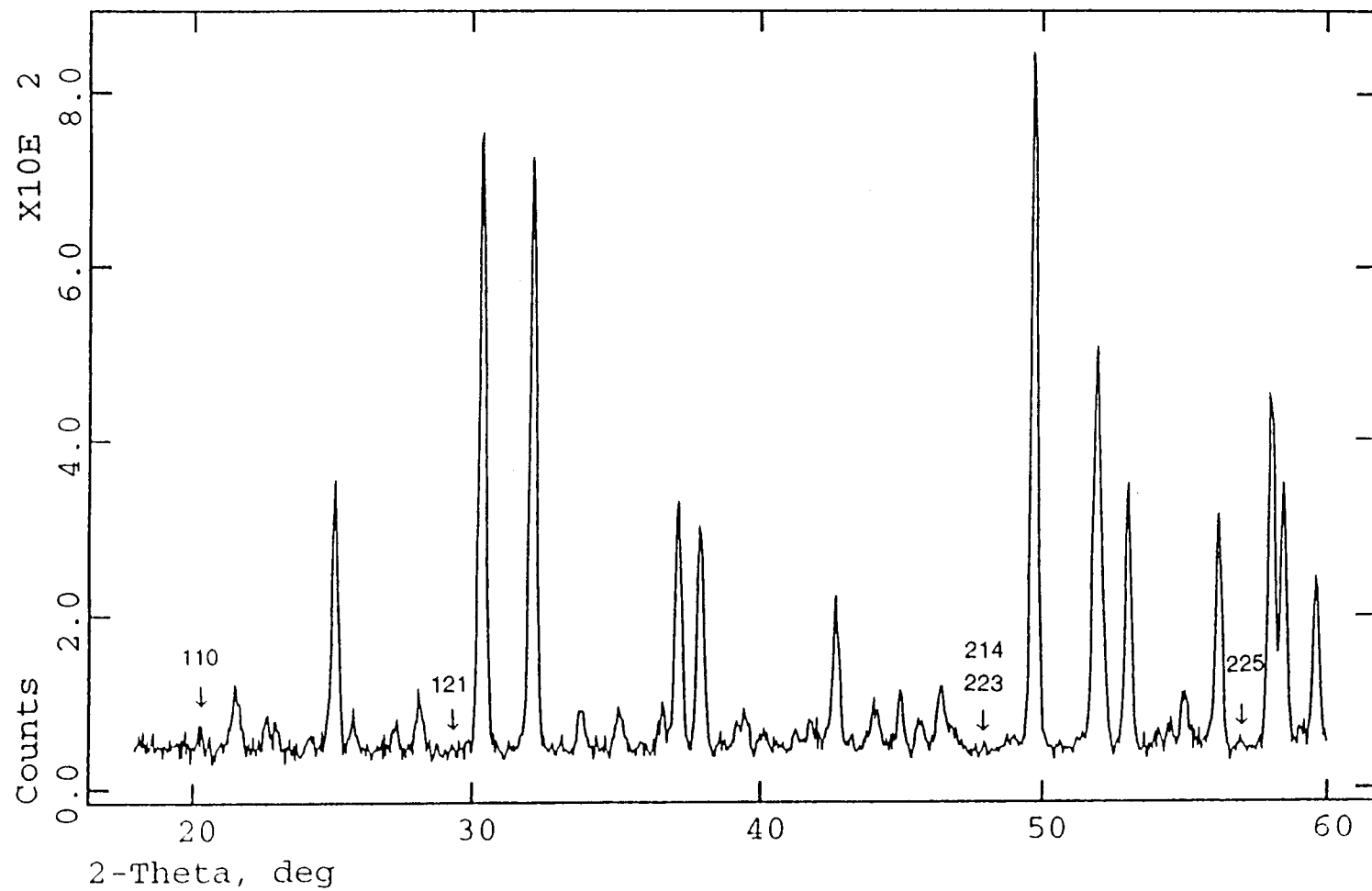
Figure 6.2. Observed 'P – reflections' in $BiMg_2PO_6$
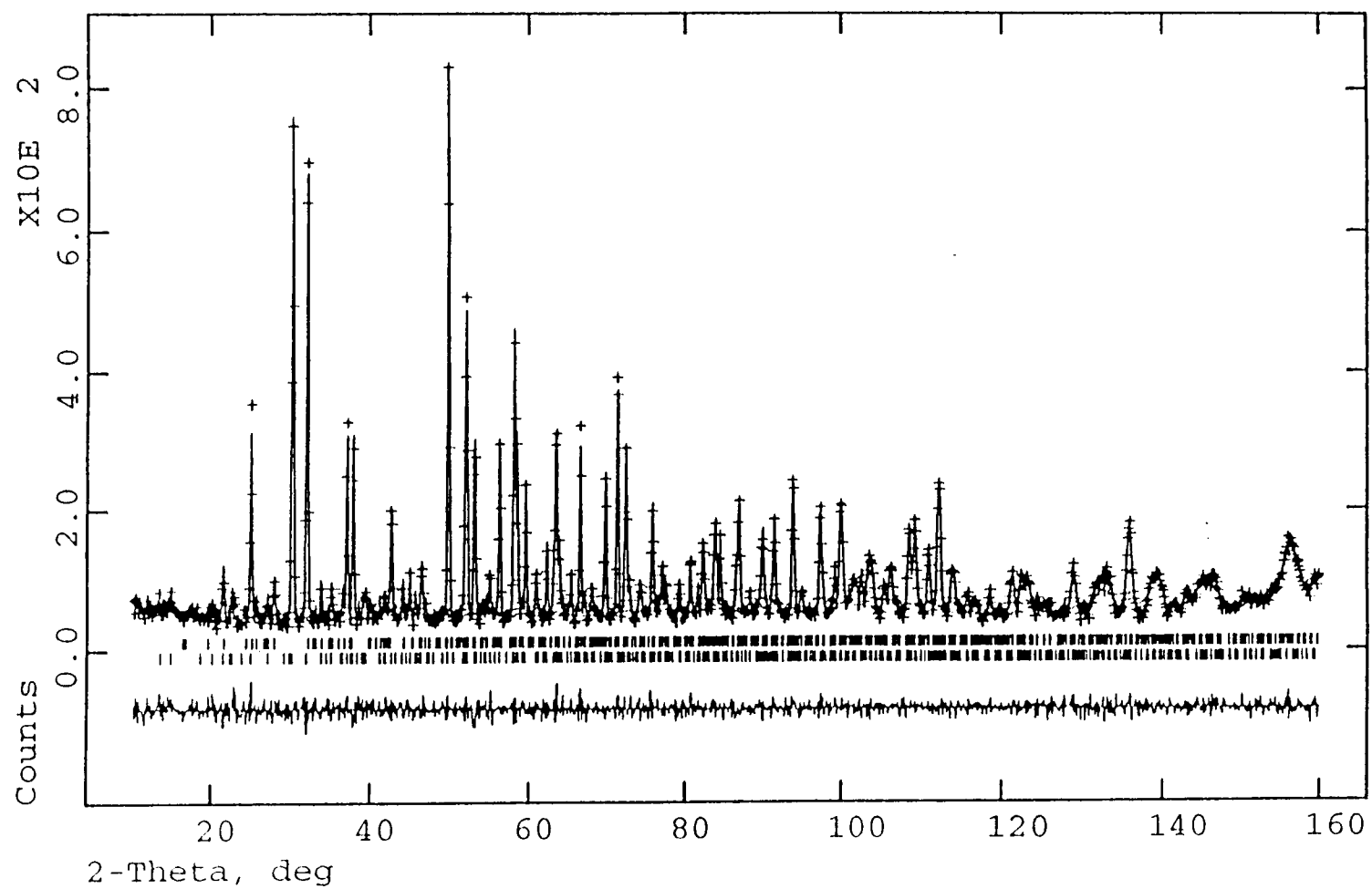
Figure 6.3. The Rietveld refinement of neutron diffraction data for $BiMg_2PO_6$

6. 4. Discussion

The obtained atomic positions and isotropic temperature factors are given in Table 6.3. Selected bond distances and lengths are in Table 6.4. A view of the $BiMg_2PO_6$ structure is given in Figure 7.4.

Table 6.3. Atomic Positions and Isotropic Temperature Factors for $BiMg_2PO_6$

Atom	x/a	y/b	z/c	U_{iso} ($Å^2$)
Bi	0.75	-0.997(1)	0.9024(2)	0.0127(5)
P	0.25	-1.001(2)	0.697(3)	0.0197(8)
Mg(1)	0.75	-0.695(1)	1.034(6)	0.021(2)
Mg(2)	1.25	-0.6982(9)	0.9070(4)	0.002(1)
O(1)	0.0043(4)	-0.9992(9)	0.6226(1)	0.0128(4)
O(2)	997 (1)	-0.8295(2)	0.9941(3)	0.0072(4)
O(3)	0.25	-1.1484(8)	0.7685(5)	0.014(1)
O(4)	0.75	-1.330(1)	0.7343(6)	0.029(1)

$BiMg_2PO_6$ is isostructural with $BiMg_2VO_6$. At room temperature, the structure is primitive orthorhombic and may be expected to undergo a centering displacive phase transition at higher temperatures.

Table 6.4. Selected Bond Lengths (Å) and Angles (°) for $BiMg_2PO_6$

	O (1)	O (2)	O (3)	O (4)
Bi		2.144(8) x 2		
		2.264(7) x 2		
P	1.567(3) × 2		1.45(1)	1.57(1)
Mg(1)	2.040(9) × 2	2.119(9) × 2	1.95(1)	
Mg(2)	2.083(8) × 2	1.974(8) × 2		1.97(1)

O (2) - Bi - O (2)..........75.0(4)

O (2) - Bi - O (2)..........74.34(9) × 2

O (2) - Bi - O (2)..........116.5(1) × 2

O (1) - P - O (1)..........111.5(3)

O (1) - P - O (3)..........110.0(7) × 2

O (1) - P - O (4) ....106.6(7) × 2

O (3) - P - O (4) ....112.1(4)

O (1) - Mg(1) - O (1)..........82.2(5)

O (1) - Mg(1) - O (2)..........91.8(3) × 2

O (2) - Mg(1) - O (3)..........99.9(4) × 2

O (1) - Mg(2) - O (1)..........80.2(4)

O (1) - Mg(2) - O (2)..........92.4(2) × 2

O (2) - Mg(2) - O (4)..........100.2(3) × 2
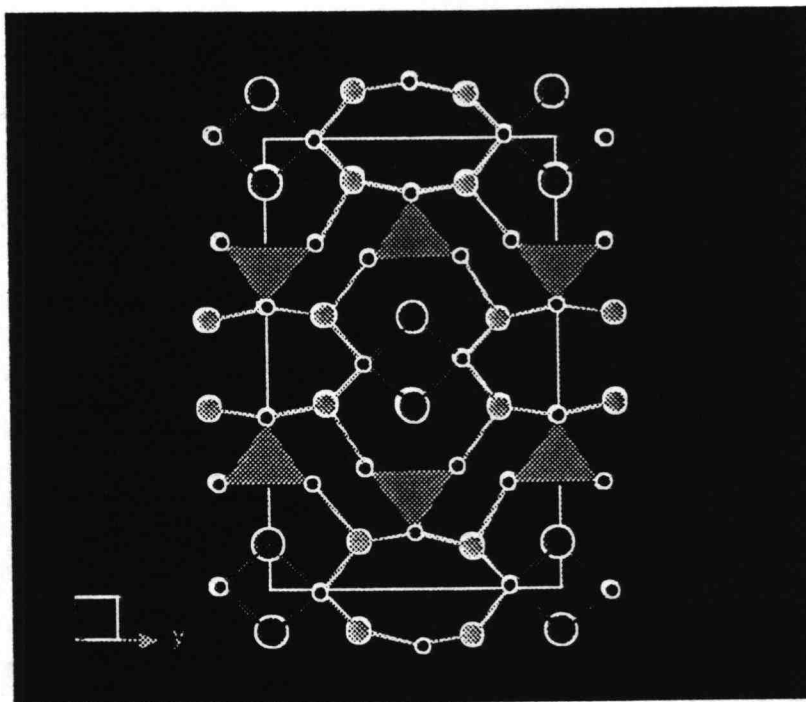
Figure 6.4. A view of the BiMg$_2$PO$_6$ structure

The degree of departure from cell centering in the BiMg$_2$PO$_6$ structure at room temperature is smaller than in BiMg$_2$VO$_6$. This can be seen by comparing Figures 6.4 and 10.7.a. Such a trend could be expected on the basis of previous reports (1, 2), since the isotropic thermal factor for the problematic tetrahedral oxygen was 3.3(3) Å^2 in BiMg$_2$PO$_6$ and 2.2(3) Å^2 in BiMg$_2$PO$_6$.

This work illustrates the value of neutron diffraction relative to X-ray diffraction data in resolving subtle structural details that arise mainly from oxygen atoms.

6. 5. References

1. J. Huang, A. W. Sleight, *J. Solid State Chem.* 100, 170 (1992)

2. J. Huang, Q. Gu, A. W. Sleight, *J. Solid State Chem.* 105, 599 (1993)

3. A. C. Larson, R. B. von Dreele, LANSCE, Los Alamos National Lab, Los Alamos, NM, 1994.

Chapter 7

Synthesis and Structure of a New Bismuth Copper Vanadate, $BiCu_2VO_6$

7. 1. Introduction

The $Bi_2O_3 - CuO - V_2O_5$ system contains a number of known compounds. Some of the interesting copper containing ternary oxides in this system include long range antiferromagnet Bi_2CuO_4 (1, 2) and copper – vanadium bronzes of the formulas $Cu_xV_2O_5$, $Cu_xV_4O_{11}$ and $Cu_xV_{12}O_{29}$ (3, 4, 5). In the course of the work on the BIMEVOX (6) phases described in more detail in the Introduction, Abraham et al. have substituted copper(II) into $Bi_4V_2O_{11}$ and obtained a high perfomance oxide ion conductor.

The first quaternary oxide in this diagram was reported by Deacon et al. (7) in 1994. They have synthesized and determined the crystal structure of $Bi_4Cu_3V_2O_{14}$. This compound is triclinic and crystallizes in space group P–1. Bismuth(III) is in an eightfold coordination, with four short and four long bonds ranging from 2.24Å to 3.05Å. Vanadium(V) is tetrahedral. There are two unique copper(II) atoms. One is in a distorted square pyramidal (4 + 1) environment, while the other is in distorted octahedral (4 + 2) coordination. Pairs of CuO_5 and CuO_6 polyhedra share an edge, resulting in the copper – copper distances of

about 3 Å. These units are linked together and with the VO_4 tetrahedra by corner sharing.

A hollandite type bismuth copper vanadate of the composition $Bi_{1.9}Cu_4V_4O_{16}$ was reported by Feldmann and Mueller-Buschbaum (8).

In 1994, Abraham et al. (9) reported the synthesis and crystal structure of a new bismuth copper phosphate, $BiCu_2PO_6$. This compound is orthorhombic, with unit cell parameters of a = 11.776(1) Å, b = 5.1730(6) Å and c = 7.7903(6) Å and crystallizes in space group Pnma. This indicates that it is likely to be related to the previously reported $BiMg_2MO_6$ (M = V, As, P) series and $BiCa_2VO_6$ that we have prepared and characterized. Indeed, the structure of $BiCu_2PO_6$ features one dimensional (BiO_2)- chains and tetrahedral pentavalent cations found in both calcium and magnesium compounds. It has copper atoms in distorted square planar coordination, similar to five coordinate magnesium atoms in $BiMg_2MO_6$. A new feature is the interaction between CuO_5 units to form dimers of the formula (Cu_2O_8).

In the case of calcium and magnesium compounds, phases with the same divalent and different pentavalent cations are isostructural. In order to determine whether this would be the case for a divalent transition metal such as copper(II), we have synthesized and characterized bismuth copper vanadate, $BiCu_2VO_6$ (10).

7. 2. Experimental

The polycrystalline sample of $BiCu_2VO_6$ was synthesized by the solid state reaction of Bi_2O_3 (Atomergic Chemetals, 99.9%), CuO (Cerac, 99.9%) and NH_4VO_3 (Johnson Matthey, 99.99%). Stoichiometric quantities of the reagents were ground and heated in an alumina crucible at 750°C for 20 hours. Single crystal growth was carried out by melting a small amount of the polycrystalline sample at 1000°C, slow cooling it to 600°C at a rate of 3°C per hour and to room temperature at a rate of 5°C per minute. Dark brown needle shaped crystals with well developed faces were obtained. The chemical composition of several crystals was analyzed using an SX-50 electron microprobe. The results confirmed the Bi:Cu:V ratio of 1:2:1.

Preliminary powder X-ray diffraction work was done on the patterns recorded on a Siemens D5000 diffractometer with vertical Soller slits and a Kevex detector.

Single crystal X-ray diffraction data were collected both at room temperature and at 150 K. Both data sets were collected on an Enraf Nonius DIP 2000 image plate diffractometer with Mo radiation, using the same collection method. A total of sixty frames, each corresponding to a 3° oscillation interval, were recorded with exposure time of 900 seconds per frame. The obtained data sets were processed using XDisplayF, Denzo and Scalepack programs of the HKL software suite (11). A total of 13944 reflections were measured at room temperature and merged to 3326 unique reflections with an agreement factor of R_{merge} = 9.0%. At 150K, a total of 13889 reflections were

measured and merged to 3371 unique reflections with an agreement factor of R_{merge} = 9.7%.

Structure solution and refinement of both data sets were performed using the Oxford Crystals suite (12). Details about the crystal, data collection and refinement are given in Tables 7.1 and 7.2.

Table 7.1. Crystal Data for $BiCu_2VO_6$

Chemical formula	$BiCu_2VO_6$	
Crystal color	Dark brown	
Crystal size (mm)	0.1 x 0.1 x 0.3	
Crystal system	monoclinic	
Space group	$P2_1/n$	
Z	12	
Temperature (K)	298	150
a (Å)	13.471(1)	13.453(1)
b (Å)	7.812(1)	7.808(1)
c (Å)	15.760(1)	15.753(1)
β (°)	113.10(1)	113.12(1)
V (Å³)	1525.51	1521.77
Density (g/cm³)	6.311	6.327

Table 7.2. Data Collection and Refinement

Diffractometer	Enraf Nonius DIP2000	Enraf Nonius DIP2000
Temperature (K)	298	150
Wavelength (Å)	0.71073	0.71073
N° measured reflect.	13944	13889
N° independent reflect.	3326	3371
Cut-off	I > 4σI	I > 4σI
N° observed reflect.	2067	2061
N° parameters	122	122
N° reflect./ N° param.	16	16
$\Delta\rho_{min}$ (e⁻/Å³)	-5.18	-7.31
$\Delta\rho_{max}$ (e⁻/Å³)	+6.03	+6.12
Extinction parameter	88.5(5)	105.0(5)
Goodness-of-Fit, S	1.13	1.08
R (%)	8.35	7.78
wR (%)	7.50	8.17

Powder diffraction data for Rietveld refinement were collected on a Siemens D5000 diffractometer using Cu K_α radiation. The scan was performed in the range from 2 to 100° 2θ, using a step size of 0.02° and a step count time of 8 seconds. Rietveld refinement was performed using the GSAS software suite (13).

7. 3. Solution and Refinement of Structure

Powder X-ray diffraction pattern of $BiCu_2VO_6$ showed certain similarities, particularly in the low two theta region, with the pattern of the known compound $BiCa_2VO_6$. The Miller indices of the first five reflections in the $BiCa_2VO_6$ pattern (110, 200, 111, 201, 020) were therefore assigned to the corresponding peaks in the $BiCu_2VO_6$ pattern (Figure 7.1). Accurate two theta values for these reflections were obtained by peak fitting using the program Profile (14). Together with the cell parameters of $BiCa_2VO_6$, they were then used for cell refinement with the program Refcel (15). The full range of the pattern was indexed with the obtained cell parameters and the space group Pnam, the primitive orthorhombic space group related to that of $BiCa_2VO_6$. Although the high and the medium intensity reflections indexed with a very good agreement, there still remained a number of low intensity peaks that remained unaccounted for (Figure 7.2).
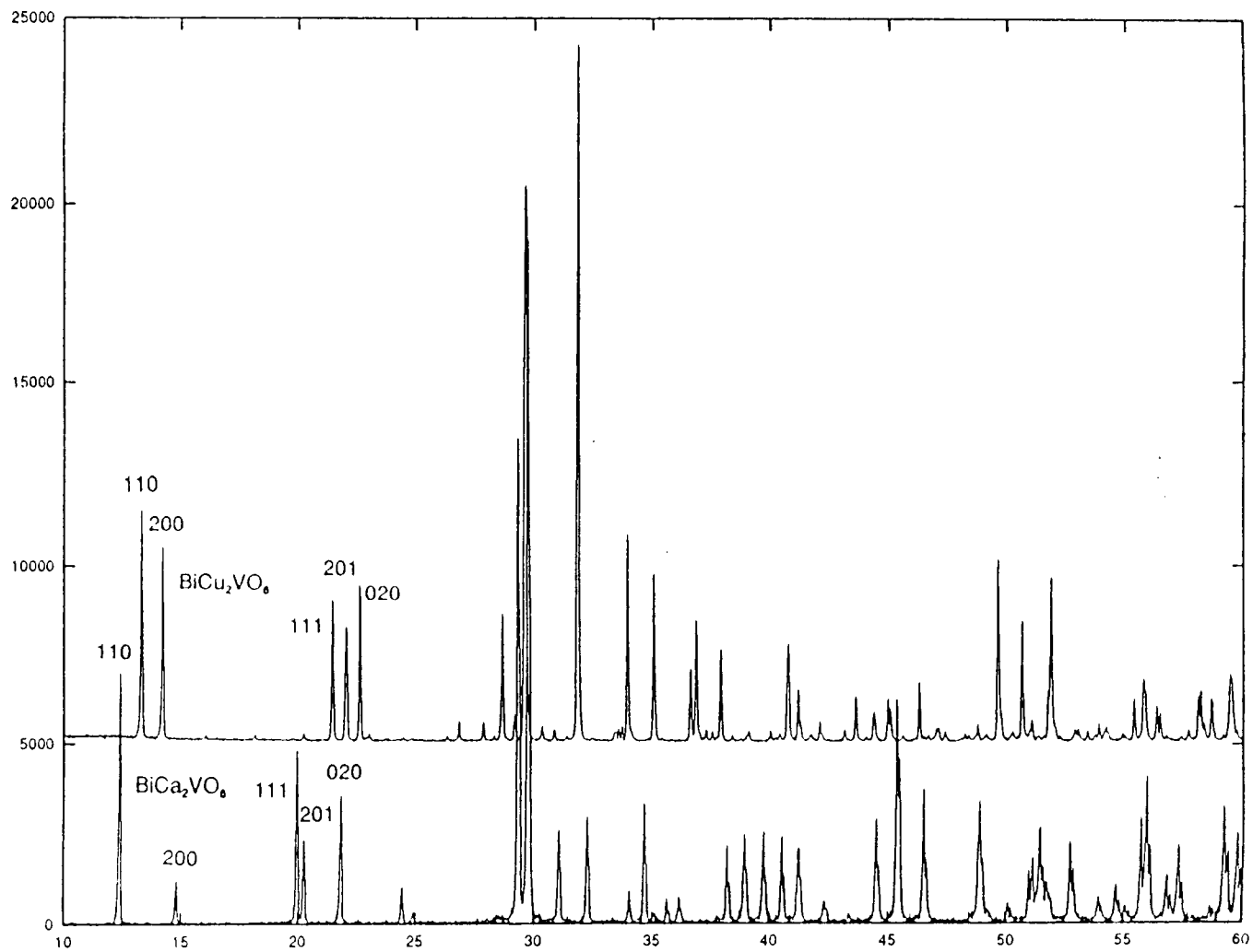
Figure 7.1. A comparison of the powder X-ray diffraction patterns of $BiCu_2VO_6$ and $BiCa_2VO_6$
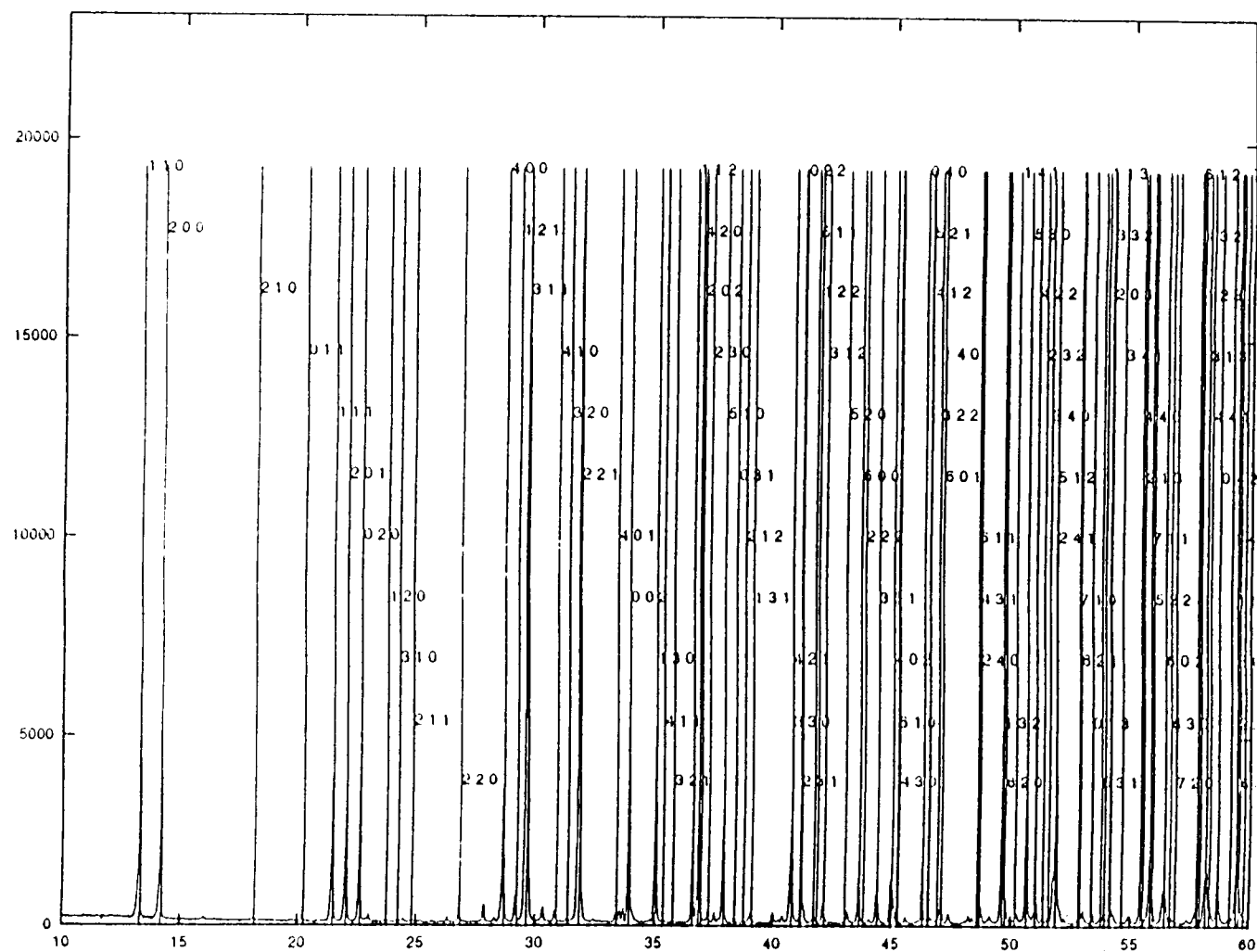
Figure 7.2. Indexing of the $BiCu_2VO_6$ powder diffraction pattern in a primitive orthorhombic space group

rtho   Hist 1
ambda 1.5406 A, L-S cycle   39   Obsd. and Diff. Profiles

2-Theta, deg   X10E 1

rtho   Hist 1
ambda 1.5406 A, L-S cycle   39   Obsd. and Diff. Profiles

2-Theta, deg   X10E 1
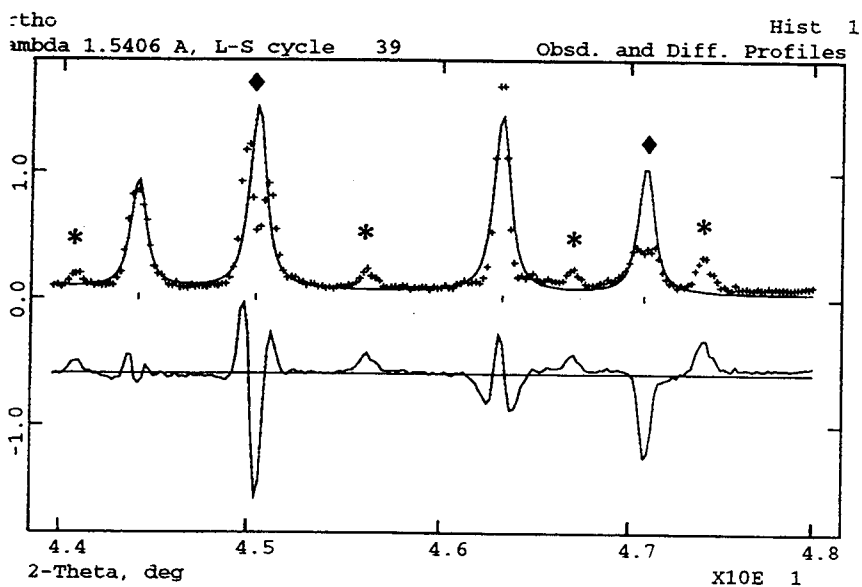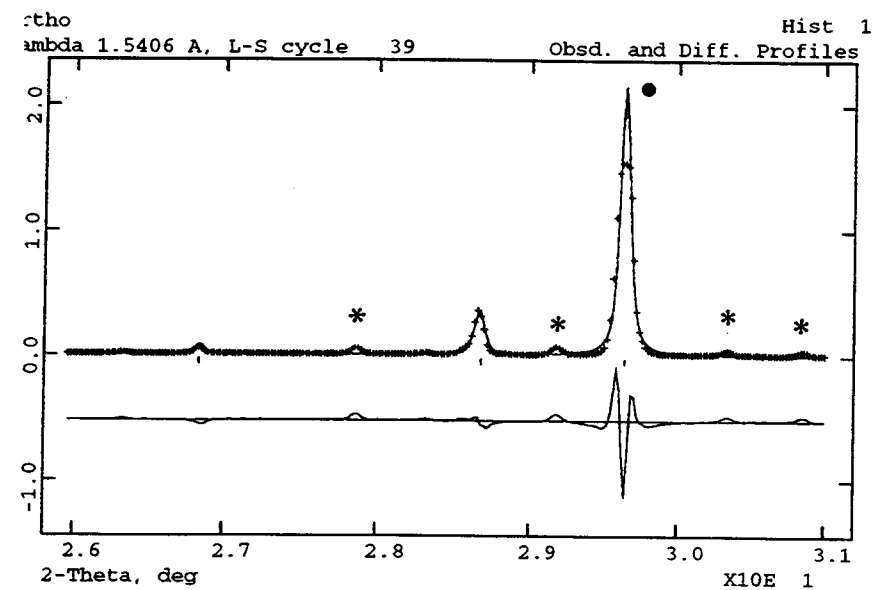
Figure 7.3. Features of the powder X-ray diffraction pattern of $BiCu_2VO_6$ indicating monoclinic symmetry

This primitive orthorhombic cell was used to fit the pattern using the Le Bail algorithm (16) within the GSAS suite (13). The typical disagreements found between the observed and the fitted pattern and the corresponding difference curves are shown in Figure 7.3. It is obvious that some reflections (marked with *) are not predicted at all. For peaks such as the ones at approximately 45 and 47 degrees 2θ (marked with ♦) only one reflection is predicted, while the observed profiles clearly indicate peak overlap. Finally, the reflection observed at about 29.6 degrees 2θ (marked with ●) does not appear split, but the shape of the difference curve suggests that there may in fact be more than one reflection present. The results of the Le Bail fit suggested that BiCu2VO6 may be monoclinic, but probably related to the obtained orthorhombic cell with the parameters: a =12.4140, b = 7.8247, c = 5.268.

Structural investigation was resumed by single crystal work using an image plate diffractometer. Preliminary oscillation photographs were taken on several $BiCu_2VO_6$ crystals and they gave consistent indexing to a monoclinic cell that was refined from the sixty diffraction images collected on the selected crystal. The obtained cell had the parameters of: a = 13.471(1) Å, b = 7.812(1) Å, c = 15.760(1) Å and β = 113.10(1)°. The systematic absences in the pattern (h00: h=2n, 0k0: k=2n, 00l: l=2n, h0l: l=2n) suggested space group $P2_1/n$ (#14). Structure solution was initiated by direct methods using the program SIR92 (17). Three bismuth, six copper and three vanadium unique sites were found. Subsequent Fourier difference map syntheses revealed eighteen oxygen sites, thus completing the asymmetric unit of 30 atoms.

A full matrix refinement of a total of 122 parameters (scale factor, extinction parameter, 90 positional parameters, 30 isotropic temperature factors) was performed. Agreement factors achieved were R = 13.19% and wR = 15.14%. An empirical absorption correction using the program Difabs (18) was then applied. Further refinement and the application of an optimal weighting scheme (third order Chebyshev polynomial) led to the final agreement factors of R = 8.35% and wR = 7.50%. The obtained atomic positional parameters, temperature factors and bond valence sums (21, 22) are given in Table 7.3.

Table 7.3. Positional Parameters, Temperature Factors and Bond Valence Sums for $BiCu_2VO_6$

Atom	x	y	z	U_{iso} ($Å^2$)	BV Sum
Bi(1)	0.40756(7)	0.0116(1)	0.06077(7)	0.0043(3)	2.97
Bi(2)	0.62129(7)	-0.0112(1)	0.28720(7)	0.0038(3)	3.11
Bi(3)	0.41265(7)	0.0111(1)	0.38016(7)	0.0036(3)	3.14
Cu(1)	0.5878(3)	0.3183(4)	0.4470(3)	0.0073(7)	2.14
Cu(2)	0.5762(2)	-0.3140(4)	0.4443(3)	0.0054(7)	2.05
Cu(3)	0.4301(3)	-0.2915(4)	0.2326(3)	0.0071(7)	2.12
Cu(4)	0.4461(3)	0.3041(4)	0.2396(3)	0.0078(7)	1.97
Cu(5)	0.5765(2)	-0.3171(4)	0.1010(3)	0.0046(7)	2.10
Cu(6)	0.5841(2)	0.3221(4)	0.1046(3)	0.0057(7)	2.07
V(1)	0.3081(3)	0.4991(6)	0.3466(3)	0.0083(8)	5.13

Table 7.3 (Continued)

V(2)	0.6924(3)	0.5197(6)	0.3158(3)	0.0056(8)	5.39
V(3)	0.3103(3)	-0.5214(6)	0.0405(3)	0.0082(9)	5.14
O(1)	0.504(1)	0.175(2)	-0.002(2)	0.003(3)	2.18
O(2)	0.518(1)	0.176(3)	0.170(2)	0.009(4)	2.14
O(3)	0.513(1)	-0.171(2)	0.172(2)	0.007(4)	2.18
O(4)	0.522(1)	-0.158(2)	0.337(2)	0.005(4)	2.45
O(5)	0.534(1)	0.163(2)	0.347(2)	0.007(4)	2.39
O(6)	0.493(2)	-0.170(2)	0.497(2)	0.011(4)	2.20
O(7)	0.622(1)	0.507(3)	0.534(1)	0.016(4)	2.20
O(8)	0.350(2)	0.323(3)	0.306(2)	0.013(4)	1.95
O(9)	0.342(2)	-0.329(3)	0.301(2)	0.024(5)	2.07
O(10)	0.329(1)	-0.012(2)	0.185(1)	0.010(3)	1.91
O(11)	0.593(1)	0.502(3)	0.364(1)	0.008(3)	2.15
O(12)	0.751(1)	0.210(2)	0.155(1)	0.008(4)	1.91
O(13)	0.628(1)	-0.498(3)	0.196(1)	0.011(4)	2.15
O(14)	0.715(1)	-0.125(2)	0.147(1)	0.006(3)	2.00
O(15)	0.392(1)	-0.501(2)	0.160(1)	0.006(3)	2.06
O(16)	0.614(1)	-0.495(2)	0.029(1)	0.007(3)	1.97
O(17)	0.716(2)	-0.131(3)	0.511(2)	0.027(5)	1.75
O(18)	0.758(1)	0.214(2)	0.523(2)	0.010(4)	1.89

Data collection at 150 K was performed in order to check whether the compound would undergo a phase transition to a structure of lower symmetry at low temperatures. No change in the space group was indicated. The cell parameters have somewhat decreased: a = 13.453(1) Å, b = 7.808(1) Å, c = 15.753(1) Å and β = 113.12(1)°. The room temperature structure was used as the initial model for low temperature data refinement and the final agreement factors obtained were R = 7.78% and wR = 8.17%.

The structure obtained from the single crystal data was used as the initial model for the Rietveld refinement of powder diffraction data. The purpose of this refinement was mainly to confirm the structure as well as the purity of the powder sample. Atomic positional parameters were therefore kept fixed. The scale factor, diffractometer zero point, lattice parameters, background and profile coefficients were initially refined. The observed data were then corrected for the surface roughness effects using the method of Suortti (19), while the isotropic thermal factors were kept at values typical for this type of materials. Cation temperature factors were subsequently allowed to refine freely, while those of oxygens were constrained to vary with the same shifts. During the final cycles of refinement a total of 35 parameters were varied, giving the proile agreement factors of R_p = 8.77%, wR_p = 12.05% and R_f^2 = 7.66%. Details of the refinement are given in Table 7.4. Observed, calculated and difference profiles are shown in Figure 7.4.

Table 7.4. Powder X-ray Diffracion Data Collection and Refinement

Diffractometer	Siemens D5000
Temperature (K)	298
Wavelength (Å)	1.5406
Scan range ($°2\theta$)	12 - 100
Step size (°)	0.02
Step time (s)	8
Number of data points	4399
Number of observed reflections	1624
Number of variables	35
N° observations/N° parameters ratio	46
χ^2	4.66
R_p (%)	8.77
wR_p (%)	12.05
R_F (%)	5.21
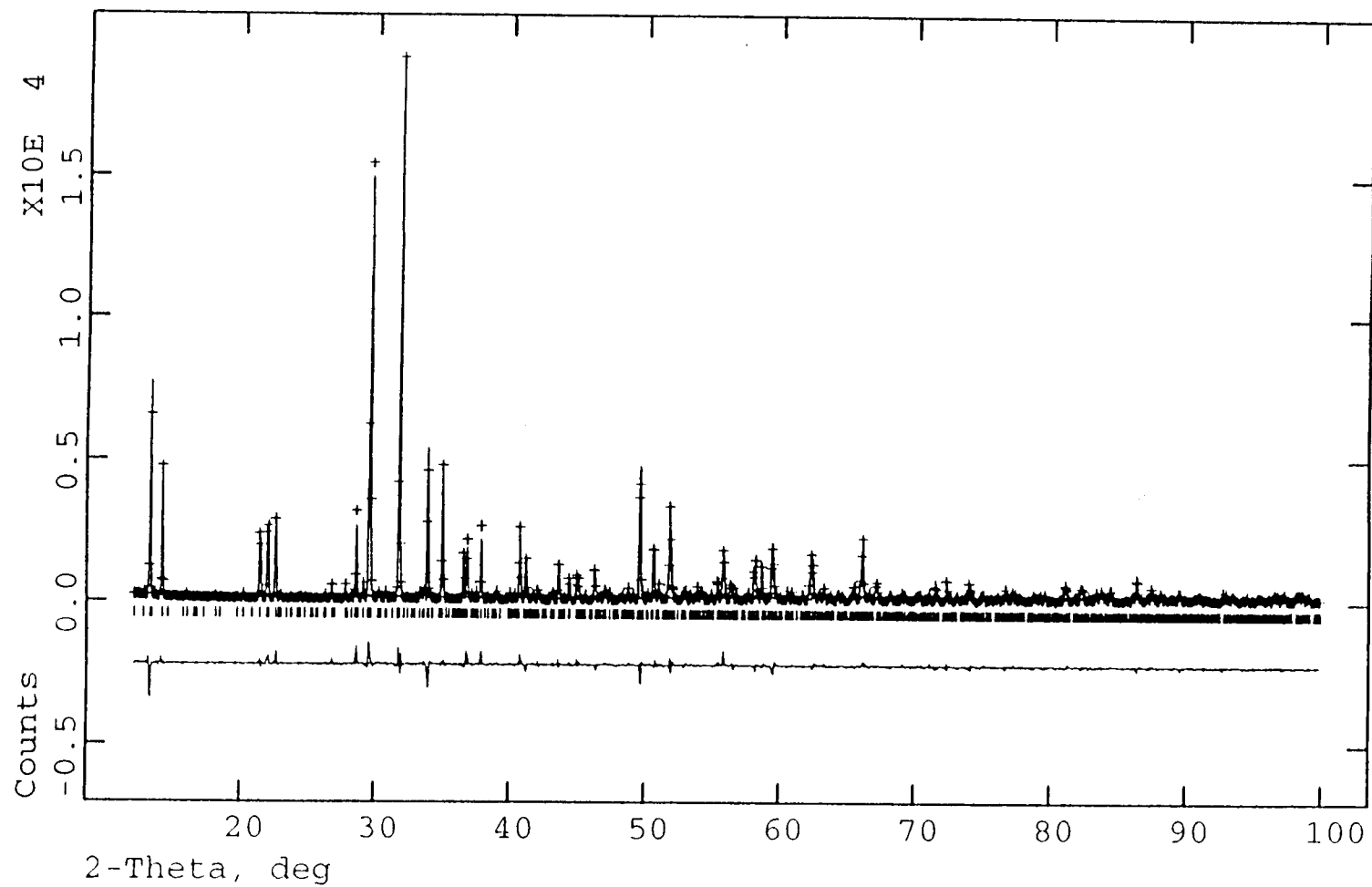
Figure 7.4. Observed, calculated and difference profiles for $BiCu_2VO_6$

7. 4. Description of Structure

The structure of $BiCu_2VO_6$, shown in Figure 7.5.a, is more complex than that of other BiA_2MO_6 phases. All the members of the BiA_2MO_6 family reported so far can be described using an orthorhombic cell of approximate dimensions of 12 Å × 8 Å × 5 Å. In $BiCu_2VO_6$, the space group has dropped to P21/n, and the volume of the monoclinic cell is three times the volume of the related orthorhombic cell. The b axis remains the same, the c axis in the monoclinic structure increases by a factor of three, while the a axes of the two cells are connected by the relationship:

$$a_{ortho}/a_{mono} = \sin \beta_{mono}$$

associated with the distortion of the β angle from 90° to 113.10°. The similarities of the two cells are illustrated in Figures X-5a and X-5b. The number of unique crystallographic sites for each atomic species is tripled relative to the number of unique sites in the related orthorhombic phases $BiCu_2PO_6$ (9) and $BiCu_2AsO_6$ (20). Selected bonds and distances, as well as the bond valence sums calculated using the program Eutax (21, 22) are given in Table 7.5.
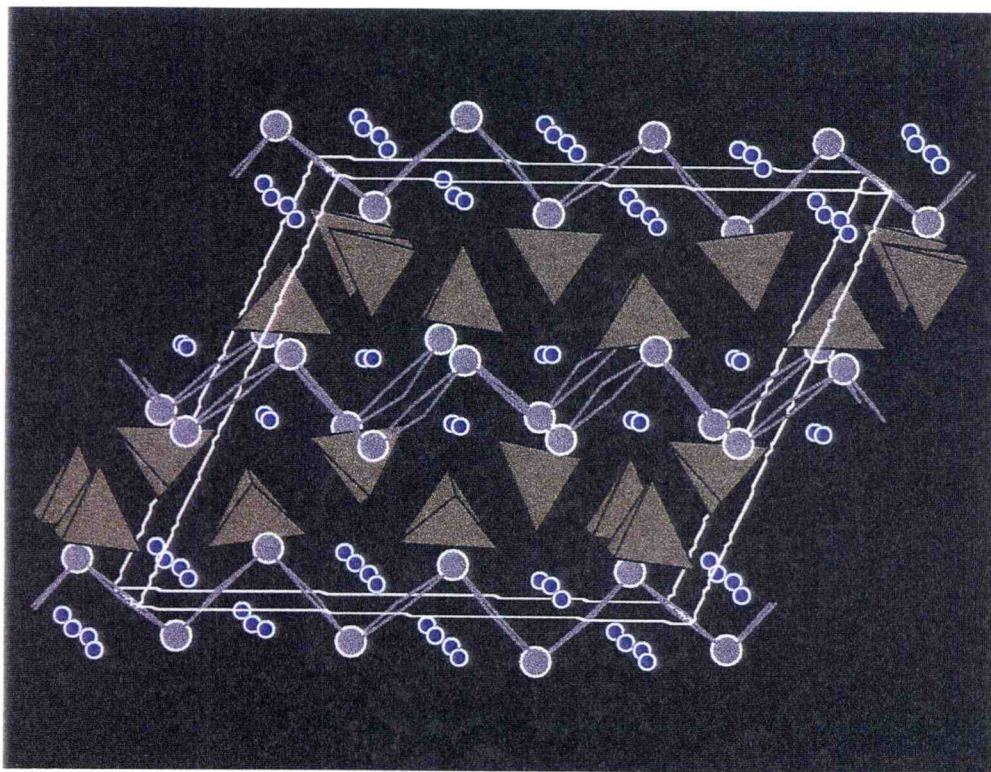
Figure 7.5.a. A view of the BiCu$_2$VO$_6$ structure
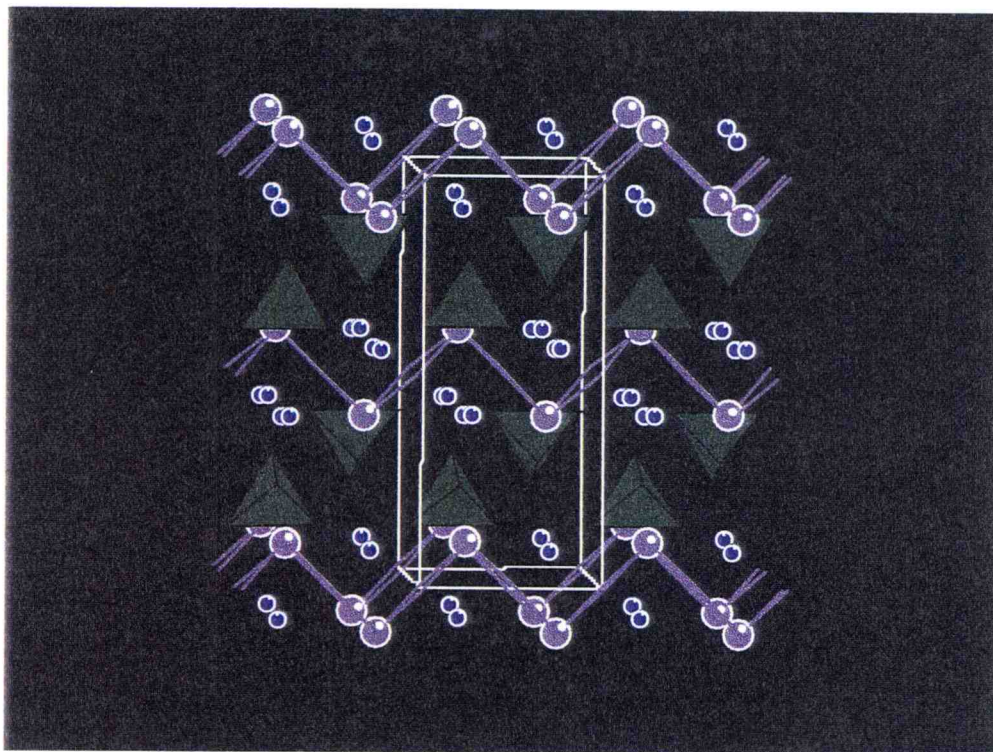
Figure 7.5.b. A view of the BiCu$_2$PO$_6$ structure

Table 7.5. Selected Bond Lenghts (Å) and Angles (°) for $BiCu_2VO_6$

Atom	Bond Lengths (Å)		Bond Angles (°)	
Bi(1)	-O(2)	2.195(21)	O(1)-Bi(1)-O(1)	73.1(6)
	-O(3)	2.268(20)	O(1)-Bi(1)-O(3)	113.1(7)
	-O(1)	2.296(21)	O(2)-Bi(1)-O(10)	78.6(7)
	-O(1)	2.302(21)	O(2)-Bi(1)-O(18)	86.0(7)
	-O(10)	2.571(19)		
	-O(18)	2.841(19)		
Bi(2)	-O(4)	2.129(20)	O(2)-Bi(2)-O(5)	72.8(8)
	-O(3)	2.218(20)	O(2)-Bi(2)-O(4)	111.4(7)
	-O(5)	2.237(21)	O(3)-Bi(2)-O(12)	87.2(7)
	-O(2)	2.340(21)	O(3)-Bi(2)-O(14)	64.7(7)
	-O(12)	2.707(19)		
	-O(14)	3.080(19)		
Bi(3)	-O(6)	2.227(27)	O(4)-Bi(3)-O(6)	73.8(9)
	-O(6)	2.236(26)	O(5)-Bi(3)-O(6)	111.6(8)
	-O(5)	2.242(20)	O(4)-Bi(3)-O(8)	121.4(8)
	-O(4)	2.280(20)	O(4)-Bi(3)-O(9)	59.0(7)
	-O(8)	2.689(19)	O(4)-Bi(3)-O(10)	70.3(7)
	-O(10)	2.834(19)		
	-O(9)	2.926(20)		

Table 7.5 (Continued)

Cu(1)	-O(5)	1.896(22)	O(5)-Cu(1)-O(11)	90.8(8)
	-O(7)	1.941(23)	O(6)-Cu(1)-O(7)	98.4(8)
	-O(11)	1.962(20)	O(7)-Cu(1)-O(11)	81.7(8)
	-O(6)	2.012(26)	O(7)-Cu(1)-O(18)	89.4(8)
	-O(18)	2.280(19)		
Cu(2)	-O(7)	1.914(23)	O(4)-Cu(2)-O(11)	89.7(8)
	-O(4)	1.980(21)	O(4)-Cu(2)-O(7)	88.4(9)
	-O(11)	1.982(21)	O(7)-Cu(2)-O(11)	81.7(8)
	-O(6)	1.990(26)	O(6)-Cu(2)-O(17)	87.3(9)
	-O(17)	2.265(25)		
Cu(3)	-O(9)	1.917(29)	O(3)-Cu(3)-O(4)	81.9(9)
	-O(4)	1.924(20)	O(4)-Cu(3)-O(9)	86(1)
	-O(15)	1.942(19)	O(9)-Cu(3)-O(10)	85.3(8)
	-O(3)	1.974(21)	O(9)-Cu(3)-O(15)	98.2(9)
	-O(10)	2.525(19)	O(4)-Cu(3)-O(10)	82.9(7)
	-O(11)	2.852(19)		
Cu(4)	-O(15)	1.923(19)	O(11)-Cu(4)-O(15)	90.0(9)
	-O(8)	1.955(25)	O(2)-Cu(4)-O(5)	86.3(9)
	-O(5)	1.972(21)	O(8)-Cu(4)-O(15)	97.3(8)
	-O(2)	2.002(22)	O(5)-Cu(4)-O(8)	83.3(9)
	-O(11)	2.668(19)	O(4)-Cu(4)-O(10)	82.9(7)
	-O(10)	2.871(20)		

Table 7.5 (Continued)

Cu(5)	-O(1)	1.879(23)	O(3)-Cu(5)-O(13)	95.0(8)
	-O(13)	1.980(20)	O(1)-Cu(5)-O(3)	84.0(9)
	-O(16)	1.981(20)	O(1)-Cu(5)-O(16)	97.3(8)
	-O(3)	2.007(21)	O(1)-Cu(5)-O(14)	90.4(9)
	-O(14)	2.284(17)	O(3)-Cu(5)-O(14)	85.7(7)
Cu(6)	-O(13)	1.933(22)	O(2)-Cu(6)-O(13)	95.7(9)
	-O(2)	1.962(22)	O(1)-Cu(6)-O(16)	94.7(9)
	-O(1)	1.966(23)	O(13)-Cu(6)-O(16)	81.6(8)
	-O(16)	1.999(19)	O(12)-Cu(6)-O(13)	92.7(7)
	-O(12)	2.242(18)	O(12)-Cu(6)-O(16)	95.0(7)
V(1)	-O(9)	1.669(27)	O(8)-V(1)-O(10)	109(1)
	-O(8)	1.712(22)	O(7)-V(1)-O(9)	110(1)
	-O(10)	1.721(17)	O(8)-V(1)-O(9)	107(1)
	-O(7)	1.741(20)	O(9)-V(1)-O(10)	111(1)
V(2)	-O(14)	1.610(17)	O(13)-V(2)-O(14)	109(1)
	-O(12)	1.652(21)	O(12)-V(2)-O(14)	108.7(9)
	-O(13)	1.744(20)	O(11)-V(2)-O(13)	108.6(8)
	-O(11)	1.789(18)	O(12)-V(2)-O(13)	110(1)
V(3)	-O(18)	1.638(19)	O(15)-V(3)-O(17)	109(1)
	-O(17)	1.669(25)	O(16)-V(3)-O(17)	110(1)
	-O(16)	1.774(18)	O(15)-V(3)-O(18)	108(1)
	-O(15)	1.783(18)	O(15)-V(3)-O(16)	112.1(8)

In $BiCu_2VO_6$ there are six crystallographically unique Cu sites showing two different types of coordination environments. Four copper atoms are in a five fold distorted square pyramidal coordination (Figure 7.6). They form four bonds to the basal oxygens at about 2 Å and one to the apical oxygen at about 2.3 Å. Pairs of square pyramids share an edge to form (Cu_2O_8) dimers, which then share two corners to form the quadrimer units of the formula (Cu_4O_{14}), shown in Figure 7.7. The intradimer copper-copper distance is about 2.8 Å, very similar to the dimers found in $BiCu_2PO_6$ and $BiCu_2AsO_6$. The remaining two copper sites are six coordinate distorted octahedral (Figure 7.8), with bond lengths ranging from 2.2 Å (equatorial oxygens) to about 3 Å (axial oxygens). These octahedra alternately share an edge and a corner forming rows that run perpendicular to the $(BiO_2)^-$ chains (Figure 7.9). Copper-copper distance between the edge sharing octahedra is 3.17 Å, while that between the corner sharing ones is 4.66 Å.

Bismuth atoms form one dimensional $(BiO_2)^-$ chains parallel to the z axis, found in all the known BiM_2AO_6 phases. There are three unique bismuth sites (Figure 7.10). Two of them are six coordinate. They form four short bonds to the oxygens in the $(BiO_2)^-$ chains at about 2.2 - 2.3 Å and two more bonds to oxygens at distances between 2.6 and 3.1 Å. The third bismuth atom is located near the six coordinate copper atoms, and consequently there are more oxygen atoms in its vicinity. In addition to the four short bonds to the oxygens in the $(BiO_2)^-$ chains, there are three additional bonds to oxygens ranging in length from 2.7 to 3.0 Å. All BiA_2MO_6 phases have $(BiO_2)^-$ chains with four short bonds

to oxygens at about 2.2 Å – 2.3 Å. The longer bismuth – oxygen bonds found in $BiCu_2VO_6$ are longer than those found in the calcium and magnesium series. In $BiCu_2PO_6$, however, there is a fifth bismuth – oxygen distance at about 2.6 Å (9).

Vanadium in $BiCu_2VO_6$ is in a distorted tetrahedral environment, with bond angles ranging from 105° to 113°. $(VO_4)^{3-}$ tetrahedra share all of their corners with the copper coordination polyhedra in a way that makes it possible to view this structure as consisting of sheets shown in Figure 7.11. Copper coordination polyhedra and the $(BiO_2)^-$ chains form slabs parallel to the (100) plane; the linkage along the x direction is provided by the $(VO_4)^{3-}$ tetrahedra. Very similar sheets are found in the orthorhombic $BiCu_2PO_6$. In most of the BiA_2MO_6 compounds there is only one type of MO_4 tetrahedron from a crystallographic point of view, and this tetrahedron lies on a symmetry element, usually a mirror plane. This results in the tetrahedra having definite orientations with respect to the crystallographic axes. In $BiCu_2VO_6$ none of the three distinct VO_4 tetrahedra lie on any symmetry element and thus they do not point in directions along the axes of the unit cell.
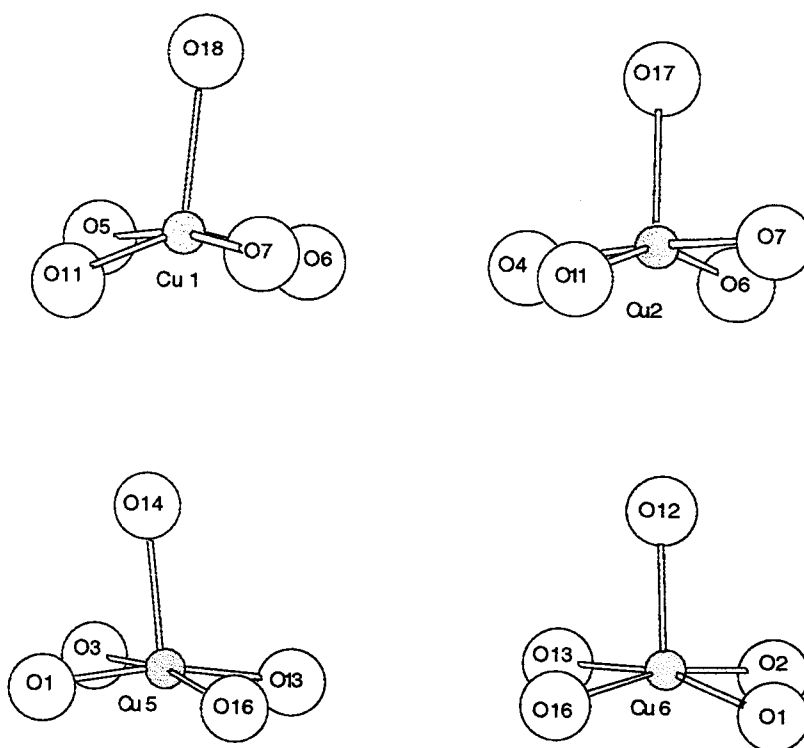
Figure 7.6. Five coordinate copper atoms in $BiCu_2VO_6$
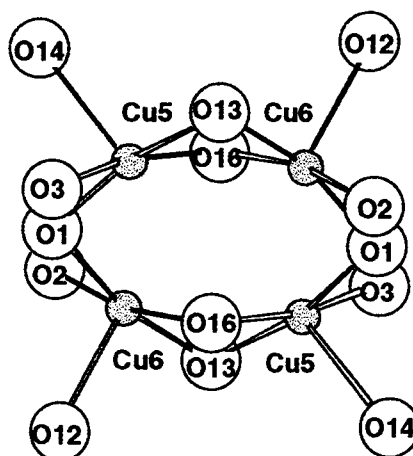
Figure 7.7. Quadrimer units in $BiCu_2VO_6$
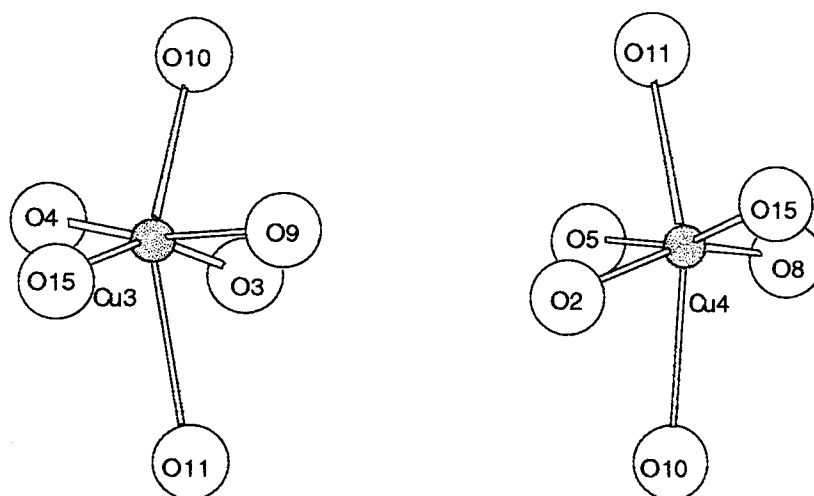
Figure 7.8. Six coordinate copper atoms in $BiCu_2VO_6$
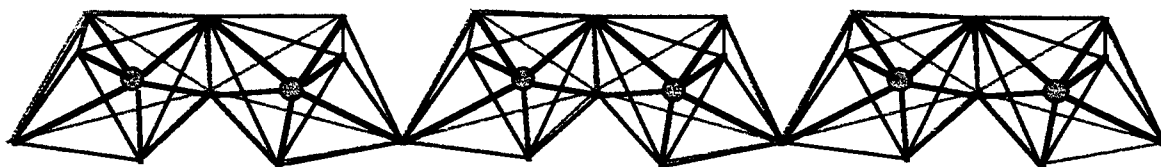
Figure 7.9. Corner and edge sharing of CuO6 units in $BiCu_2VO_6$
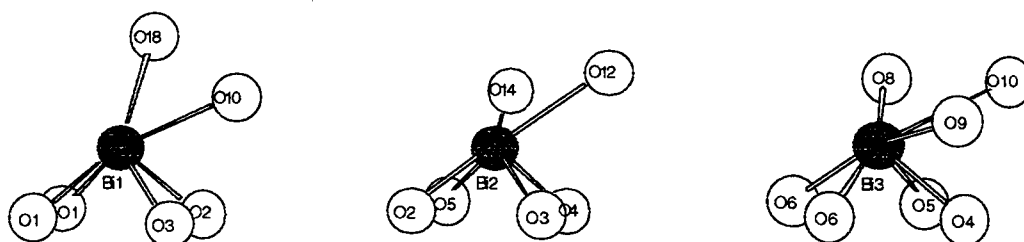
Figure 7.10. Coordination of bismuth atoms in $BiCu_2VO_6$
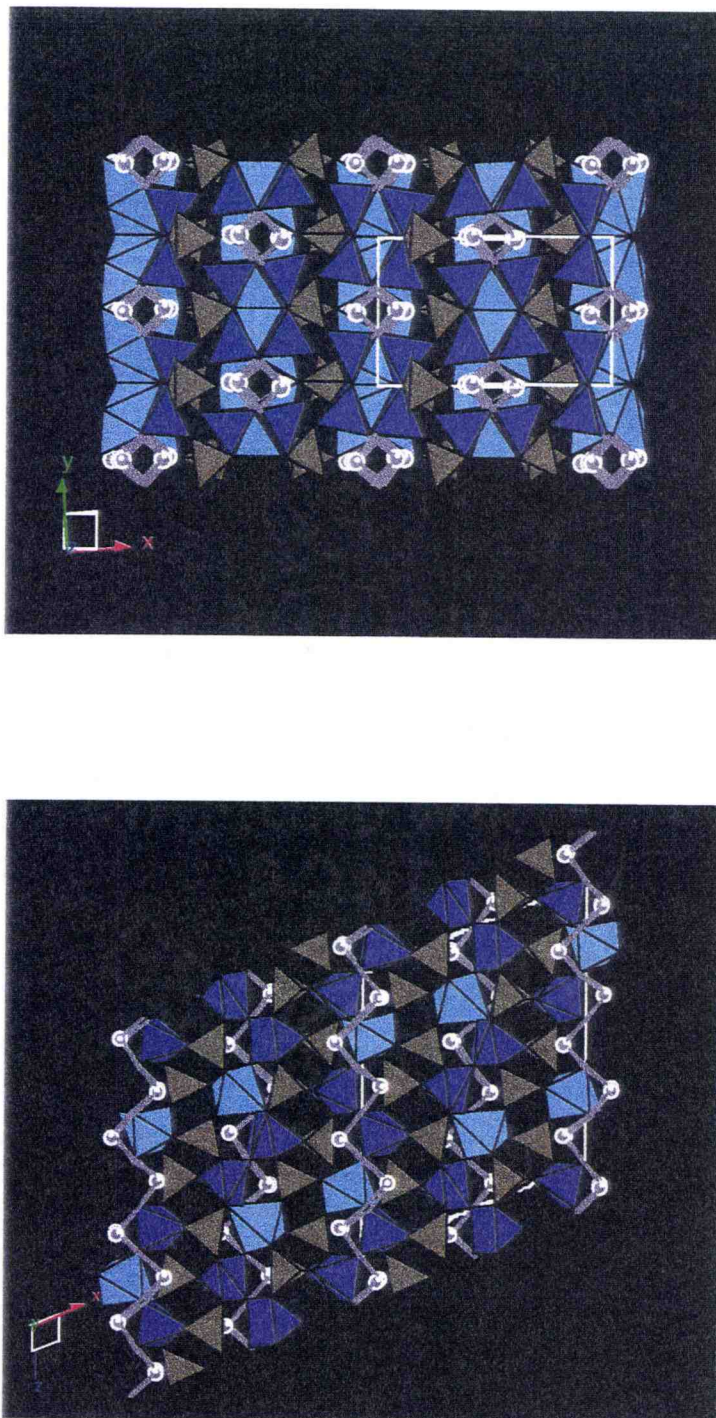
Figure 7.11. Two views of the sheet structure of $BiCu_2VO_6$

7. 5. References

1. E. W. Ong, G. H. Kwei, R. A. Robinson, B. L. Ramakrishna and R. B. von Dreele, *Phys. Rev. B*, 42, 4255 (1990)

2. J. L. Garcia Munoz, J. Caravajal Rodriguez, F. Sapina, M. J. Sanchis, R. Ibanez and D. Beltran Porter, *J. Phys.*, 2, 2205 (1990)

3. J. Galy, D. Lavaud, A. Casalot and P. Hagenmueller, *J. Solid State Chem.*, 2, 531 (1970)

4. J. Galy and D. Lavaud, *Acta Cryst.*, 27, 1005 (1971)

5. K. Kato, E. Takayama Muromachi and Y. Kanke, *Acta Cryst.*, 45, 1841 (1989)

6. F. Abraham, J. C. Boivin, G. Mairesse and G. Nowogrocki, *Solid State Ionics*, 40-41, 934 (1990)

7. G. B. Deacon, B. M. Gatehouse and G. N. Ward, *Acta Cryst.*, C50, 1178 (1990)

8. J. Feldmann and Hk. Mueller Buschbaum, *Zeitschrift fur Naturforschung*, B50, 1163 (1995)

9. F. Abraham, M. Ketatni, G. Mairesse and B. Mernari, *Eur. J. Solid State Inorg. Chem.*, 31, 313 (1994)

10. I. Radosavljevic, J. S. O. Evans and A. W. Sleight, *J. Solid State Chem.*, 141, 149 (1998)

11. Z. Otwinowski and W. Minor, "Processing of X-Ray Diffraction Data in Oscillation Mode", in *Methods in Enzymology*, 276, C.W. Carter, Jr. and R.M. Sweet, Eds., Academic Press (1996)

12. Oxford Crystals, D.J. Watkin, J.R. Carruthers and P.W. Betteridge, Chemical Crystallography Laboratory, University of Oxford, Oxford (1985)

13. A. C. Larson, R. B. Von Dreele, LANSCE, Los Alamos National Lab, Los Alamos, NM, 1994.

14. Profile Version 1.1, Diffract/AT Software Package Version 3.2, 1985.

15. Refcel Program, J. K. Cockroft, Department of Crystallography, Birkbeck College, London, 1995.

16. A. Le Bail, H. Duroy and J. L. Fourquet, *Mat. Res. Bull.*, 23, 447 (1988)

17. A. Altomare, G. Cascarano, C. Giacovazzo, A. Guagliardi, M.C. Burla, G. Polidori and M. Camalli, *J. Appl. Cryst.*, 27, 435 (1994)

18. D. Stewart and N. Walker, *Acta Cryst. Sect.* A 39, 158 (1983)

19. P. Suortti, *J. Appl. Cryst.*, 5, 325 (1972)

20. I. Radosavljevic, J. S. O. Evans and A. W. Sleight, *J. Alloys and Comp.* , in press

21. I.D. Brown and D. Altermatt, *Acta Cryst.* Sect B 41, 244 (1985)

22. N.E. Brese and M. O'Keeffe, *Acta Cryst.* Sect B47, 192 (1991)

Chapter 8

Synthesis and Structure of a New Bismuth Copper Arsenate, $BiCu_2AsO_6$

8. 1. Introduction

In the course of structural studies of the members of the BiM_2AO_6 family, the vanadate, the arsenate and the phosphate compounds in calcium and magnesium series were found to be isostructural. This was, however, not the case in the copper series. $BiCu_2PO_6$ was reported as orthorhombic (1), while $BiCu_2VO_6$ belongs to the monoclinic crystal system (2). $BiCu_2AsO_6$ is the first quaternary compound to be reported in the of Bi_2O_3 - CuO - As_2O_5 phase system (3). The present Chapter gives details of its synthesis and structural characterization.

8. 2. Experimental

A powder mixture of Bi_2O_3 (Atomergic Chemetals, 99.9%), CuO (Cerac, 99.9%) and As_2O_5 (Johnson Matthey, 99.99%) was ground and heated at 800°C for 15 hours in an alumina crucible. The obtained dark green powder was subsequently melted at 1000°C, slow cooled to 600°C at a rate of 3°C per hour

and to room temperature at a rate of 5°C per minute. Dark green elongated needle shaped crystals were obtained.

Single crystal x-ray diffraction data were collected on an Enraf Nonius DIP 2000 image plate diffractometer using Mo radiation. Data were collected in 3° rotation intervals on a total of 60 frames, covering a 180° angular range with exposure time of 900 seconds per frame. Data processing was carried out using XDisplayF, Denzo and Scalepack programs of the HKL software suite (4). A total of 3081 reflections were measured and merged to 447 unique reflections with merging agreement factors of: R_{lin} = 7.0%, R_{sq} = 7.8%, χ^2 = 1.12.

Structure solution and refinement were performed using the Oxford Crystals suite (5). Further details about the crystal, data collection and refinement are given in Tables 8.1, 8.2 and 8.3.

Table 8.1. Crystal Data for $BiCu_2AsO_6$

Chemical formula	$BiCu_2AsO_6$
Crystal color	Dark green
Crystal size (mm)	0.1 x 0.1 x 0.3
Crystal system	orthorhombic
Space group	Pnma
a ($\AA$)	12.253(1)
b ($\AA$)	5.280(1)
c ($\AA$)	7.577(1)
V ($\AA^3$)	490.20
Z	4
Density (g/cm^3)	6.870

Table 8.2. Single Crystal Data Collection for $BiCu_2AsO_6$

Diffractometer	Enraf Nonius DIP 2000
Temperature (K)	298
Wavelength (Å)	0.71073
Number of measured reflections	3081
Number of independent reflections	447
Number of observed reflections	411
Criterion for observed reflections	$I > 3\sigma I$
Range of h	0-5
Range of k	0-9
Range of l	0-14
R_{merge} (%)	7.0

Table 8.3. Structure Refinement Data for $BiCu_2AsO_6$

Method	Full matrix least squares on /F/
Number of parameters	40
Number of reflections used	411
Absorption correction	Difabs
Weighting polynomial coefficients	0.932, -0.563, 0.633
$\Delta\rho_{min}$ (e$^-$/Å^3)	-2.78
$\Delta\rho_{max}$ (e$^-$/Å^3)	+3.15
Extinction parameter	31.6(5)
Goodness of fit indicator, S	1.10
R (%)	5.28
wR (%)	3.14

8. 3. Structural Analysis

The observed diffraction pattern was indexed on an orthorhombic unit cell. Refinement of cell parameters from the sixty recorded images gave the following values: $a = 12.253(1)$ Å, $b = 5.280(1)$ Å and $c = 7.577(1)$ Å. Inspection of the systematic absences ($h00$: $h=2n$, $0k0$: $k=2n$, $00l$: $l=2n$, $h0l$: $l=2n$, $hk0$: $h+k=2n$) indicated two possible space groups: Pnma (#62) and $Pn2_1a$ (#33). This suggested possible similarities with the structure of $BiCu_2PO_6$ which crystallizes in space group Pnma (1). Structure solution was therefore first performed in this space group. However, attempts to refine the structure of $BiCu_2AsO_6$ starting with parameters from the $BiCu_2AsO_6$ structure were not successful.

Solution of $BiCu_2AsO_6$ structure was achieved by direct methods using SIR92 (6). All cation sites were found and the oxygen atoms were located by subsequent difference Fourier map syntheses.

A full matrix refinement of a total of 40 parameters (scale factor, extinction parameter, 18 positional parameters, 16 anisotropic and 4 isotropic temperature factors) was performed. Agreement factors achieved were $R = 7.34\%$ and $wR = 8.46\%$. An empirical absorption correction using the program Difabs (7) was then applied. The final agreement factors for the isotropic model were $R = 5.48\%$ and $wR = 3.65\%$. Allowing the metal temperature factors to refine anisotropically while the oxygens were kept isotropic led to the agreement factors of $R = 5.28\%$ and $wR = 3.14\%$. Additional details of the refinement are

given in Table 8.3. Refinement of the $BiCu_2AsO_6$ structure was also attempted in the non-centrosymmetric space group $Pn2_1a$ (#33), but no significant change occurred.

8. 4. Results and Discussion

Atomic positional and thermal factors obtained in the refinement are given in Table 8.4. The components of the anisotropic temperature factors for cations are given in Table 8.5. Selected bond lengths and angles in Table 8.6. Bond valence calculations performed using the program Eutax (8, 9) gave good agreement with the expected values (Table 8.4).

Table 8.4. Atomic Positions, Temperature Factors and Bond Valence Sums for BiCu₂AsO₆

Atom	x	y	z	U_{iso} (Å²)*	BV sum
Bi	0.44464(5)	0.75000	0.85390(8)	0.0014(4)	3.09
Cu(1)	0.6946(2)	0.75000	0.9575(3)	0.003(1)	2.04
Cu(2)	0.3734(2)	0.75000	0.2867(3)	0.004(1)	1.94
As	0.6287(1)	0.75000	0.4741(2)	0.0010(8)	5.16
O(1)	0.5037(9)	0.75000	0.560(2)	0.007(3)	1.91
O(2)	0.5885(6)	0.499(2)	0.888(1)	0.006(2)	2.17
O(3)	0.2005(6)	0.499(2)	0.9479(9)	0.007(2)	2.10
O(4)	0.376(1)	0.25000	0.742(2)	0.019(3)	1.77

Table 8.5. Components of the Anisotropic Temperature Factors for Cations

Atom	U_{11}	U_{22}	U_{33}	U_{23}	U_{13}	U_{12}
Bi(1)	0.0020(4)	0.0012(4)	0.0010(3)	-0.0001(3	0.0000	0.0000
As(2)	0.003(1)	0.0022(8)	0.0002(8)	-0.0002(6)	0.0000	0.0000
Cu(3	0.004(1)	0.008(1)	0.001(1)	-0.0020(9)	0.0000	0.0000
Cu(4)	0.004(1)	0.004(1)	0.008(1)	0.0024(8)	0.0000	0.0000

---

* Isotropic equivalent of the anisotropic temperature factors for cations

Table 8.6. Selected Bond Lengths (Å) and Angles (°) for $BiCu_2AsO_6$

	O(1)	O(2)	O(3)	O(4)
Bi	2.343(11)	2.220(8) x 2		2.899(6) x 2
		2.393(8) x 2		
Cu(1)		1.931(8) x 2	1.976(9) x 2	2.435(14)
Cu(2)	2.614(12)	1.922(8) x 2	2.008(9) x 2	
As	1.663(11)		1.698(9) x 2	1.637(15)

O(1)-Bi-O(2)	146.2(2)
O(2)-Bi-O(2)	111.6(1) x 2
O(2)-Bi-O(2)	73.3(4) x 2
O(1)-Bi-O(4)	79.1(3) x 2
O(2)-Bi-O(4)	73.8(3)
O(1)-As-O(2)	109.9(4)
O(3)-As-O(3)	102.6(6)
O(1)-As-O(4)	111.1(6)
O(3)-As-O(4)	111.5(3)

O(2)-Cu(1)-O(2)	86.7(5)	O(2)-Cu(2)-O(2)	86.3(5)
O(2)-Cu(1)-O(3)	94.7(4)	O(2)-Cu(2)-O(3)	94.5(3)
O(2)-Cu(1)-O(4)	91.0(3)	O(2)-Cu(2)-O(4)	99.5(3)
O(3)-Cu(1)-O(3)	93.3(2)	O(3)-Cu(2)-O(3)	81.9(5)
O(3)-Cu(1)-O(4)	83.6(3)	O(3)-Cu(2)-O(4)	119.5(3)

Figure 8.1 shows a view of the structure of $BiCu_2AsO_6$ which can be described in terms of three structural elements: $(BiO_2)^-$ infinite chains running parallel the y axis, $(AsO_4)^{3-}$ tetrahedra and interspersed Cu^{2+} cations.
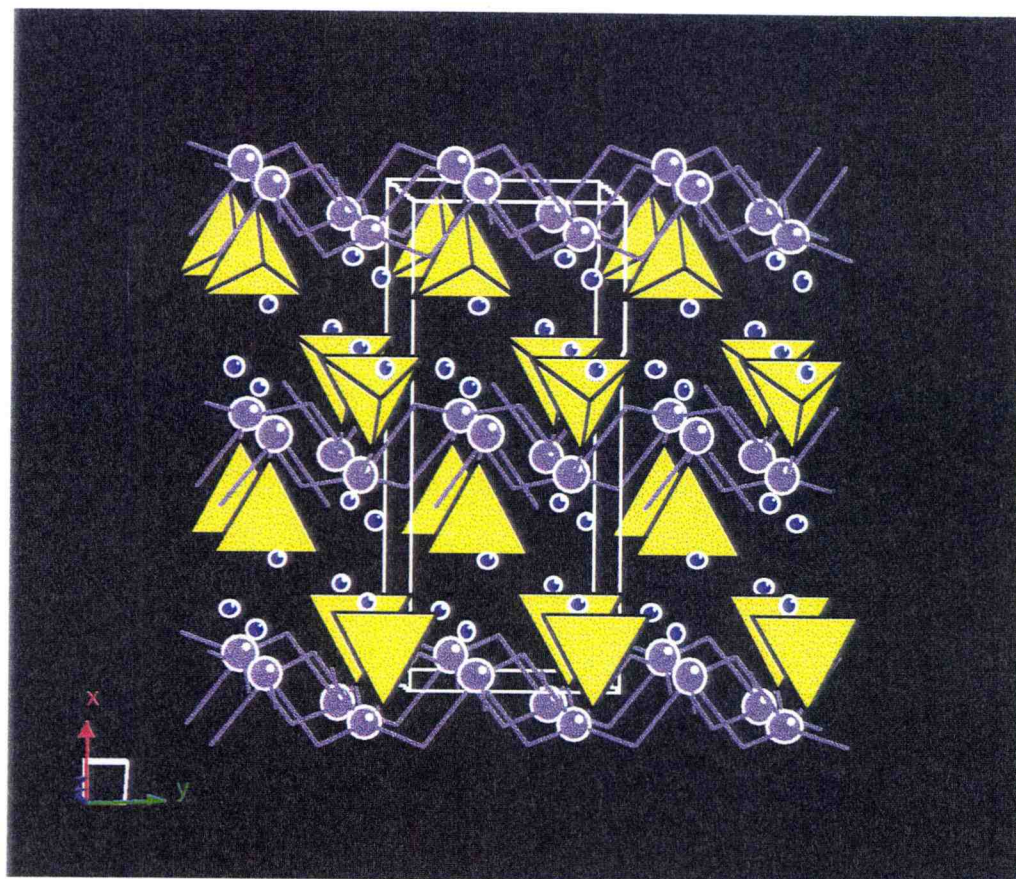
Figure 8.1. A view of the $BiCu_2AsO_6$ structure

In $BiCu_2AsO_6$, as well as in $BiCu_2PO_6$, there are two crystallographically unique Cu sites. The copper coordination geometries in both cases can be viewed as distorted square pyramids. In the CuO_5 square pyramids of $BiCu_2AsO_6$, bonds to basal oxygens (ranging from 1.92 Å to 2.01 Å) are shorter than those to apical oxygens (2.44 Å for Cu(1) and 2.61 Å for Cu(2)). Coordination environments of these two cations are shown in Figure 8.2. The two square pyramids share an edge along their bases to form a (Cu_2O_8) dimeric unit (Figure 8.3.a). The intradimer copper-copper distance is 2.92 Å, which is considerably longer than it would be for regular square pyramids sharing an edge (~ 2.77 Å). Inspection of the thermal ellipsoids of the three cations indicates that the slight decrease of the agreement factors for the anisotropic compared to the isotropic model arises mainly from allowing a larger displacement of copper atoms along the bonds to the apical oxygens in the square pyramid than to the basal ones.
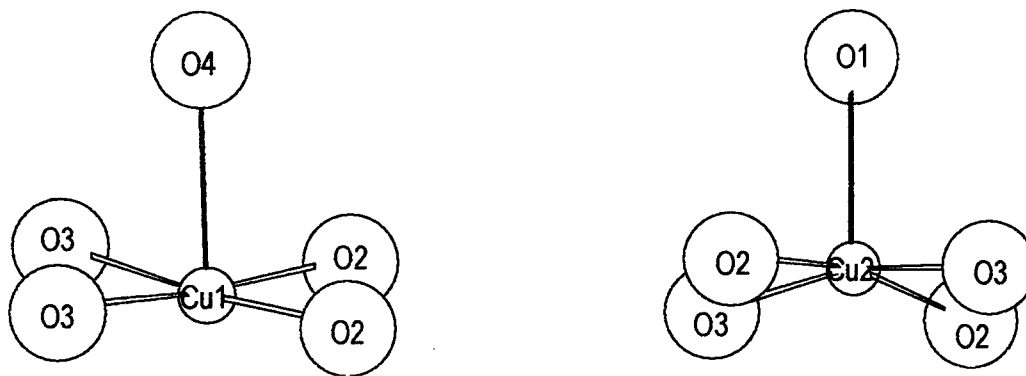
Figure 8.2. Coordination environments of copper atoms in $BiCu_2AsO_6$
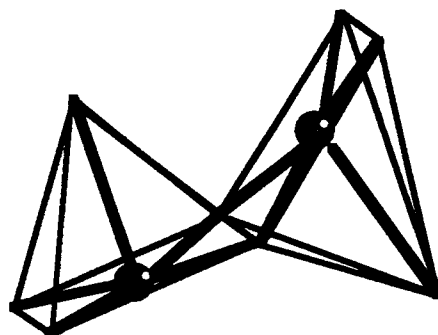
Figure 8.3.a. (Cu_2O_8) dimers in $BiCu_2AsO_6$
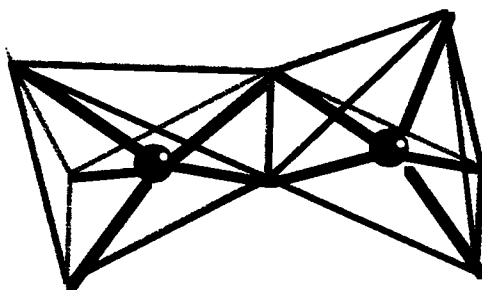
Figure 8.3.b. (Cu_2O_8) dimers in $BiCu_2PO_6$

Arsenic in $BiCu_2AsO_6$ is in a four fold distorted tetrahedral environment, with bond angles ranging from 102.6 to 111.5 degrees. The $(AsO_4)^{3-}$ tetrahedra share all of their corners with the (Cu_2O_8) dimers, forming a three dimensional framework.

Bismuth is in a distorted seven coordinate environment typical of a lone pair cation (Figure 8.4). There are four short bonds to the oxygens of the $(BiO_2)^-$ chains (2 x 2.22 Å, 2 x 2.39 Å). These oxygens are further shared with the corners of the basal planes of the (Cu_2O_8) dimers. The coordination sphere of bismuth is completed by three oxygen atoms belonging to $(AsO_4)^{3-}$ tetrahedra; two of these are relatively long range interactions (at about 2.90 Å), while the remaining one is at 2.34 Å. This short bond can be viewed as the principal interaction between the bismuth-oxygen chains and the $(AsO_4)^{3-}$ tetrahedra. Owing to the lone pair electrons on Bi^{3+}, this cation usually has two, three or four short bonds which are never opposite one another. The coordination of Bi^{3+} in $BiCu_2AsO_6$, as well as in $BiCu_2PO_6$, is unusual in having five short bonds.
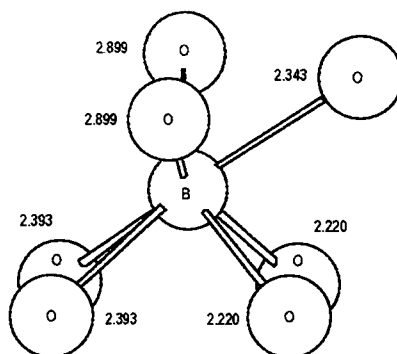
Figure 8.4. Coordination of bismuth in $BiCu_2AsO_6$

8. 5. Comparison of $BiCu_2AsO_6$ to $BiCu_2PO_6$

The structures of $BiCu_2AsO_6$ and $BiCu_2PO_6$ are compared in Figure 8.5. Both structures are projected along the axis parallel to the $(BiO_2)^-$ chains. The placement of the MO_4 tetrahedra and the Cu cations, as well as the orientation of the $(BiO_2)^-$ chains are different in $BiCu_2AsO_6$ and $BiCu_2PO_6$. The orientation of the MO_4 tetrahedra is very different as well. These differences explain why the structure of $BiCu_2AsO_6$ could not be refined starting with the parameters from the $BiCu_2PO_6$ structure despite the similar cell dimensions and the same space group.

The copper atoms in $BiCu_2AsO_6$ and $BiCu_2PO_6$ have very similar five fold coordinations. In both compounds, their environments can be described as distorted square pyramids that share an edge to form the (Cu_2O_8) dimeric units. The connectivity within the dimers, however, is different in the two cases. In $BiCu_2AsO_6$, the apical oxygens in the dimer are in a trans arrangement, while in $BiCu_2PO_6$ they are in a cis arrangement, as shown in Figures 8.3.a and 8.3.b. These differences between the structures of $BiCu_2AsO_6$ and $BiCu_2PO_6$ are also reflected in the cell edges of the two compounds. The cell volume of $BiCu_2AsO_6$ is larger than that of $BiCu_2AsO_6$, as expected. Nonetheless, the c axis is shorter in $BiCu_2AsO_6$, 7.577 Å, compared to 7.790 Å for $BiCu_2PO_6$. Apparently, the placement of cations and the orientations of the tetrahedra and chains leads to better packing along the c axis in $BiCu_2AsO_6$.
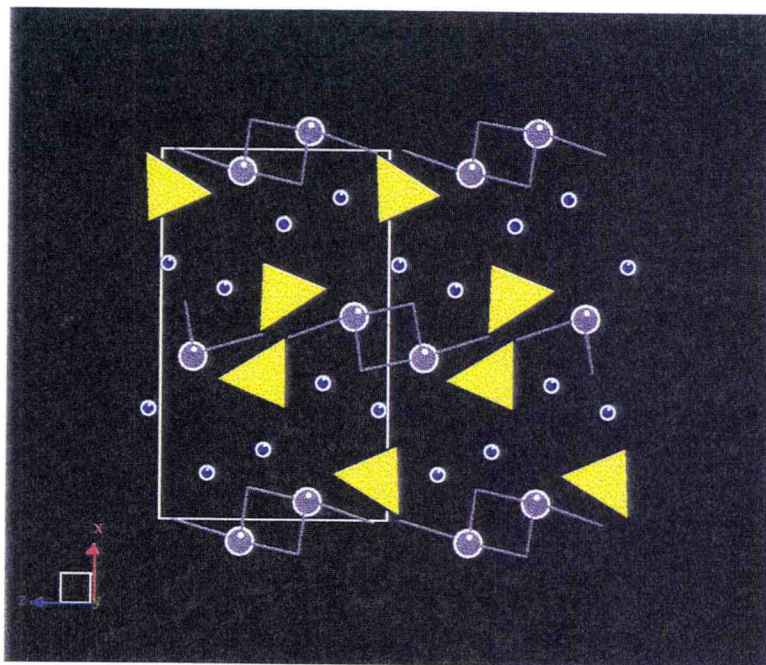
Figure 8.5.a. A view of the BiCu$_2$AsO$_6$ parallel to the (010) plane
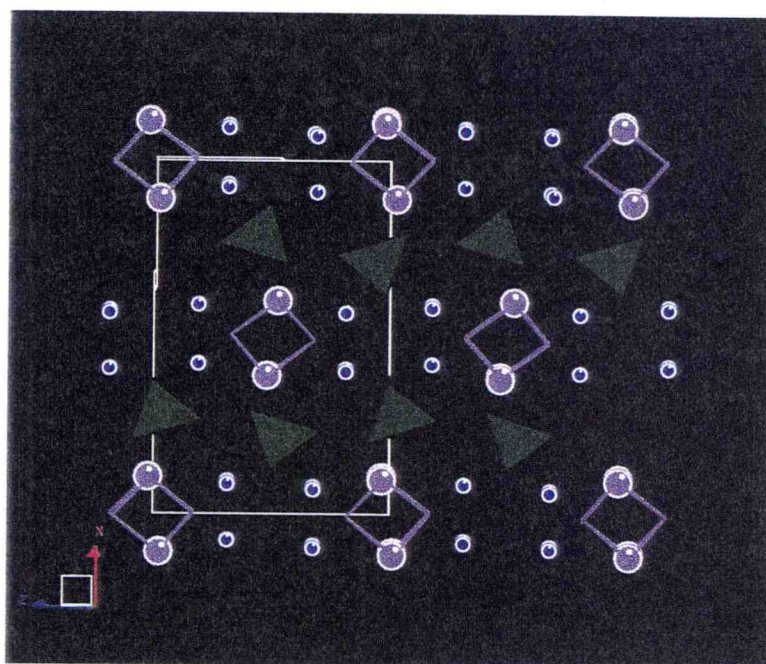
Figure 8.5.b. A view of the BiCu$_2$PO$_6$ parallel to the (010) plane

8. 6. References

1. F. Abraham, M. Ketatni, G. Mairesse and B. Mernari, *Eur. J. Solid State Inorg. Chem.* 31, 313 (1994)

2. Radosavljevic, J.S.O. Evans and A.W. Sleight, *J.Solid State Chem*, 141, 149 (1998)

3. Radosavljevic, J.S.O. Evans and A.W. Sleight, *J. Alloys and Comp.*, in press

4. Z. Otwinowski and W. Minor, "Processing of X-Ray Diffraction Data in Oscillation Mode", in Methods in Enzymology, 276, C.W. Carter, Jr. and R.M. Sweet, Eds., Academic Press, 1996.

5. D.J. Watkin, J.R. Carruthers and P.W. Betteridge, Chemical Crystallography Laboratory, University of Oxford, Oxford (1985)

6. A. Altomare, G. Cascarano, C. Giacovazzo, A. Guagliardi, M.C. Burla, G. Polidori and M. Camalli, *J. Appl. Cryst*, 27, 435 (1994)

7. D. Stewart and N. Walker, *Acta Cryst.*, Sect. A 39, 158 (1983)

8. I.D. Brown and D. Altermatt, *Acta Cryst.*, Sect B 41, 244 (1985)

9. N.E. Brese and M. O'Keeffe, *Acta Cryst.*, Sect B47, 192 (1991)

Chapter 9

Synthesis and Structure of a New Bismuth Cadmium Vanadate, BiCdVO$_5$

9. 1. Introduction

Noncentrosymmetric oxide of the formula BiCa$_4$V$_3$O$_{13}$ was reported by Huang and Sleight in 1994 (1). The attempt to synthesize a cadmium analog of this compound was not successful. However, a new oxide BiCdVO$_5$ was prepared in the process. This Chapter describes the characterization of this compound and its comparison to BiCaVO$_5$, reported by Boje and Mueller – Buschbaum (2).

9. 2. Experimental

Single crystals of BiCdVO$_5$ were initially obtained during the growth of BiCd$_4$V$_3$O$_{13}$ crystals from melt. An intimately ground mixture of Bi$_2$O$_3$ (99.975%, Alfa Aesar), CdO (reagent grade, J. T. Baker) and NH$_4$VO$_3$ (99%, Alfa Aesar) containing the molar ratio of Bi : Cd : V of 1 : 4 : 3 was heated to 900°C, held at this temperature for one hour, slow cooled to 500°C at a rate of 3° per hour and then furnace cooled to room temperature. Optical inspection of the reaction

mixture revealed the presence of bright yellow crystals with two distinct habits, suggesting the presence of two different phases. Platelets with well developed faces were analyzed using an SX-50 electron microprobe and a ratio Bi : Cd : V of 1 : 1 : 1 was found.

A polycrystalline sample of $BiCdVO_5$ was prepared by a solid state reaction of the stiochiometric quantities of Bi_2O_3 (Cerac, 99.999%), CdO (Mallinckrodt, reagent grade) and NH_4VO_3 (Johnson Matthey, 99+ %). The mixture was heated in an alumina crucible at 800°C for a total 45 hours with intermediate grinding.

Preliminary single crystal X-ray diffraction investigation was carried out on several crystals using an Enraf – Nonius DIP 2000 image plate diffractometer with Mo radiation. Rotation photographs were taken in 3° intervals with an exposure time of 600 seconds.

Data were collected from a single crystal of 0.50 x 0.14 x 0.03 mm attached to a quartz fiber on a Siemens SMART three circle diffractometer with graphite monochromatized Mo K_α radiation and a CCD area detector. Omega scans were used in such a way that an initial 180° scan range consisting of 10 second frames in 3° intervals was followed by three further 120° and 90° scans with offsets in phi of 88° and 180°, respectively. This collection strategy samples the sphere in reciprocal space up to approximately 60° in 2θ. Unit cell dimensions were refined using the centroid values of 324 reflections with θ angles between

13.66° and 27.34°. At 100K an initial 180° scan range consisting of 10 second frames in 3° intervals was followed by three further 120° and 180° scans with offsets in phi of 88° and 180°, respectively. This collection strategy samples the sphere in reciprocal space up to approximately 60° in 2θ. Unit cell dimensions were refined using the centroid values of 426 reflections with θ angles between 13.69° and 28.42°. Multi scan absorption correction was applied to the data based on the 010 and 0-10 faces of the crystal using the program XPREP (3). Raw frame data were integrated using the SAINT program (4). Temperature control was achieved using an Oxford Cryosystem nitrogen flow cooling device. Temperatures are estimated to be accurate and stable to ± 0.1 K. Details about the crystal and data collections are given in Table 9.1 and Table 9.2.

Powder X-ray diffraction data were collected in order to confirm the composition of the polycrystalline sample. All patterns were recorded on a Siemens D5000 diffractometer with vertical Soller slits, using CuK_α radiation.

Second harmonic generation test was performed using a Nd^{3+}:YAG laser with a wavelength of 1064 nm.

Table 9.1. Crystal Data for $BiCdVO_5$

Chemical formula	$BiCdVO_5$	
Crystal color	Bright yellow	
Crystal size (mm)	0.50 x 0.14 x 0.03	
Crystal shape	plate	
Crystal system	orthorhombic	
Space group	$P c 2_1 n$	
Z	8	
Temperature (K)	298	100
a (Å)	5.505(2)	5.4958(8)
b (Å)	11.699(4)	11.677(2)
c (Å)	14.276(4)	14.271(2)
V (Å^3)	919.5	915.9
Density (g/cm^3)	6.536	6.562

Table 9.2. Single Crystal Data Collection and Refinement

Diffractometer	Siemens SMART CCD single crystal diffractometer	
Temperature (K)	298	100
Wavelength (Å)	0.71073	0.71073
N° measured reflect.	4791	6451
N° independent reflect.	1078	1077
h range	0 - 7	0 - 7
k range	0 - 15	0 - 15
l range	0 - 18	0 - 18
N° observed reflect.	1078	1077
N° parameters	146	146
N° reflect./ N° param.	7	7
$\Delta\rho_{min}$ (e$^-$/Å^3)	+ 3.33	+ 4.48
$\Delta\rho_{max}$ (e$^-$/Å^3)	- 3.95	- 4.32
Extinction parameter	22.4(16)	22.8(16)
Goodness-of-Fit, S	1.04	1.00
R (%)	4.17	4.35
wR (%)	4.47	5.10

9. 3. Structural Analysis

Preliminary rotation photographs were indexed using the programs XdisplayF and Denzo of the HKL suite (5). The obtained unit cell was orthorhombic with approximate dimensions of a = 5.5 Å, b = 11.7 Å and c = 14.3 Å. Comparison of these cell dimensions with known materials in the ICSD database initially suggested that $BiCdVO_5$ might be isostructural with $BiCaVO_5$ reported by Boje and Mueller − Buschbaum (2). Examination of reflection conditions, however, revealed the systematic absences (hk0): h + k = 2n, (0kl): l = 2n, (h00): h = 2n, (0k0): k = 2n and (00l): l = 2n, suggesting space groups $Pc2_1n$ (# 33) and Pcmn (#62) as possibilities. These extinction conditions clearly indicate that $BiCdVO_5$ is not isostructural with $BiCaVO_5$.

Structure solution was carried out by direct methods using the program SIR92 (6) within the Oxford Crystals suite (7). Initial structure solution in the non-centrosymmetric polar space group $Pc2_1n$ gave an agreement factor of R = 13.27%, while solution in its centrosymmetric supergroup Pcmn was significantly less satisfactory with R = 22.86%. A positive second harmonic generation test confirmed the absence of a center of symmetry in this compound. Structure refinement was therefore resumed only in the noncentrosymmetric space group. Two atoms of each cation species and six oxygens were found by direct methods and the asymmetric unit was completed by locating four more oxygens by difference Fourier maps. A full matrix least squares refinement was performed

with a total of 146 varied parameters: 48 positional parameters, 96 components of the anisotropic temperature factors, an extinction parameter and a scale factor. The final agreement factors obtained for the room temperature data were $R = 4.17\%$ and $wR = 4.47\%$. The room temperature structure was used as a starting model for the refinement of 100K data, since there were no indications that a structural change occurred at low temperatures. Details of the refinement are given in Table 9.2.

9. 4. Description of Structure

Atomic positions, isotropic equivalents of temperature factors and bond valence sums for $BiCdVO_5$ are given in Table 9.3. Components of the anisotropic temperature factors are given in Table 9.4. Selected bond lengths and angles are given in Table 9.5.

A view of the unit cell of $BiCdVO_5$ is shown in Figure 9.1. The structure consists of bismuth – oxygen ribbons parallel to the x axis, CdO_6 distorted octahedral units and VO_4 tetrahedra.
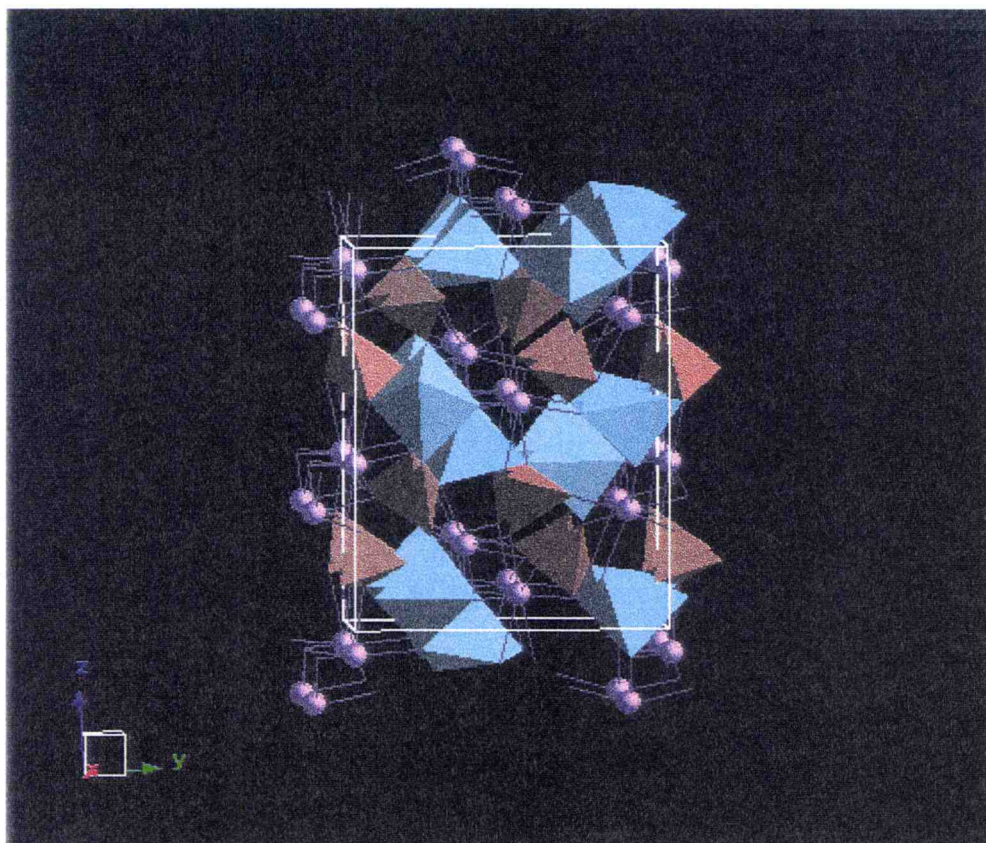
Figure 9.1. A unit cell of $BiCdVO_6$

Table 9.3. Atomic Positions and Isotropic Equivalents of Temperature Factors for BiCdVO$_5$ at Room Temperature

Atom	x	y	z	U$_{iso,eq}$
Bi(1)	-0.7437(1)	0.0329(1)	0.41326(7)	0.0124(2)
Bi(2)	-0.2692(1)	-0.1171(1)	0.30115(4)	0.0100(2)
Cd(1)	-0.24012)	-0.1117(2)	0.54368(8)	0.0131(3)
Cd(2)	-0.7867(2)	-0.2696(1)	0.4129(1)	0.0087(3)
V(1)	-0.2702(6)	0.2117(3)	0.3440(4)	0.0125(8)
V(2)	0.2089(6)	0.0635(3)	0.1547(3)	0.0081(7)
O(1)	-0.519(2)	-0.1229(9)	0.4199(6)	0.010(2)
O(2)	0.139(2)	0.010(1)	0.2643(8)	0.021(2)
O(3)	0.338(2)	0.199(1)	0.1575(8)	0.017(2)
O(4)	0.435(2)	0.720(1)	0.0649(8)	0.022(3)
O(5)	0.415(3)	0.979(1)	0.102(10	0.034(3)
O(6)	0.134(2)	0.572(1)	0.1633(8)	0.018(3)
O(7)	0.861(2)	0.251(1)	0.2421(7)	0.016(2)
O(8)	0.947(3)	0.066(1)	0.0821(9)	0.018(3)
O(9)	0.971(3)	0.789(1)	0.1356(9)	0.027(3)
O(10)	0.482(2)	0.397(1)	0.0857(6)	0.010(2)

Table 9.4. Anisotropic Temperature Factor Components for BiCdVO$_5$

	U$_{11}$	U$_{22}$	U$_{33}$	U$_{23}$	U$_{13}$	U$_{12}$
Bi(1)	0.0132(3)	0.0123(4)	0.0119(4)	-0.0002(3)	0.0002(2)	-0.0007(2)
Bi(2)	0.0142(3)	0.0105(4)	0.0071(3)	0.0020(4)	-0.0000(2)	0.0012(4)
Cd(1)	0.0155(6)	0.0184(7)	0.0088(5)	0.0013(9)	0.0012(4)	-0.0050(5)
Cd(2)	0.0069(5)	0.0102(6)	0.0101(6)	0.0006(5)	0.0007(4)	0.0022(6)
V(1)	0.015(1)	0.010(2)	0.016(2)	0.001(1)	0.001(1)	-0.004(4)
V(2)	0.016(1)	0.006(2)	0.007(1)	-0.001(1)	0.004(1)	-0.002(1)
O(1)	0.020(6)	0.008(6)	0.007(4)	-0.000(5)	0.000(3)	0.004(4)
O(2)	0.015(6)	0.038(8)	0.019(5)	0.002(6)	0.004(4)	-0.004(6)
O(3)	0.015(5)	0.015(6)	0.025(6)	-0.002(5)	0.001(5)	0.004(5)
O(4)	0.024(6)	0.026(7)	0.019(6)	-0.000(5)	0.004(5)	-0.002(5)
O(5)	0.042(9)	0.029(8)	0.051(9)	-0.016(7)	0.021(7)	0.001(7)
O(6)	0.029(7)	0.010(6)	0.022(6)	-0.000(5)	-0.003(5)	-0.002(5)
O(7)	0.026(6)	0.023(6)	0.011(5)	0.003(5)	-0.004(4)	-0.013(6)
O(8)	0.027(7)	0.017(6)	0.025(6)	-0.009(5)	-0.013(5)	-0.002(5)
O(9)	0.027(7)	0.037(8)	0.024(6)	0.006(6)	-0.007(5)	0.008(6)
O(10)	0.008(5)	0.012(5)	0.011(5)	-0.005(4)	0.002(3)	0.001(4)

Table 9.5. Selected Bond Lengths (Å) and Angles (°) for BiCdVO$_5$

Atom	Bond Lengths (Å)		Bond Angles (°)	
Bi(1)	-O(1)	2.20(1)	O(1) - Bi(1) - O(2)	96.3(4)
	-O(2)	2.24(1)	O(1) - Bi(1) - O(6)	72.1(4)
	-O(6)	2.40(1)	O(2) - Bi(1) - O(6)	80.8(4)
	-O(10)	2.19(1)	O(1) - Bi(1) - O(10)	77.9(5)
	-O(4)	2.84(1)	O(2) - Bi(1) - O(10)	74.0(4)
	-O(5)	2.92(1)		
	-O(8)	2.94(1)		
Bi(2)	-O(1)	2.18(1)	O(1) - Bi(2) - O(3)	86.2(4)
	-O(3)	2.13(1)	O(1) - Bi(2) - O(6)	73.6(4)
	-O(6)	2.31(1)	O(1) - Bi(2) - O(10)	79.9(4)
	-O(10)	2.33(1)	O(3) - Bi(2) - O(10)	73.2(4)
	-O(7)	2.63(1)	O(6) - Bi(2) - O(10)	84.9(4)
	-O(2)	2.75(1)		
	-O(9)	2.92(1)		
Cd(1)	- O(1)	2.35(1)	O(1) - Cd(1) - O(8)	84.9(4)
	- O(4)	2.60(1)	O(5) - Cd(1) - O(8)	83.5(5)
	- O(5)	2.24(1)	O(1) - Cd(1) - O(9)	92.5(5)
	- O(8)	2.43(1)	O(4) - Cd(1) - O(9)	84.5(5)
	- O(9)	2.16(1)	O(5) - Cd(1) - O(10)	81.2(5)
	- O(10)	2.22(1)	O(8) - Cd(1) - O(9)	92.6(5)

Table 9.5 (Continued)

Cd(2)	- O(1)	2.26(1)	O(3) - Cd(2) - O(4)	94.8(4)
	- O(3)	2.33(1)	O(3) - Cd(2) - O(7)	85.3(4)
	- O(4)	2.32(1)	O(4) - Cd(2) - O(8)	97.1(5)
	- O(7)	2.37(1)	O(7) - Cd(2) - O(8)	85.5(4)
	- O(8)	2.31(1)	O(4) - Cd(2) - O(10)	81.0(4)
	- O(10)	2.32(1)	O(7) - Cd(2) - O(10)	96.4(4)
V(1)	- O(4)	1.73(1)	O(4) - V(1) - O(6)	107.6(7)
	- O(6)	1.72(1)	O(4) - V(1) - O(7)	110.7(6)
	- O(7)	1.69(1)	O(6) - V(1) - O(7)	109.7(7)
	- O(9)	1.72(1)	O(4) - V(1) - O(9)	112.7(7)
			O(6) - V(1) - O(9)	105.0(7)
			O(7) - V(1) - O(9)	111.0(7)
V(2)	- O(2)	1.73(1)	O(2) - V(2) - O(3)	113.5(6)
	- O(3)	1.74(1)	O(2) - V(2) - O(5)	110.1(8)
	- O(5)	1.69(1)	O(3) - V(2) - O(5)	105.7(7)
	- O(8)	1.78(1)	O(2) - V(2) - O(8)	110.7(6)
			O(3) - V(2) - O(8)	109.2(6)
			O(5) - V(2) - O(8)	107.2(8)

There are two crystallographically unique bismuth atoms. Both are seven coordinate, with bond lengths ranging from 2.1 Å to 3.0 Å (Figure 9.2). This coordination is different from that in $BiCaVO_5$, where Bi^{3+} forms five short bonds (2.1 Å to 2.5 Å) in a distorted tetragonal pyramidal geometry and has two more long contacts (3.4 Å) on the opposite side. There are, however, similarities with the $BiCa_2AO_6$ (A = V, As) phases, where bismuth is found in 4 + 3 (approximately 4 x 2.2 Å and 3 x 3 Å) environment. The coordination polyhedra of bismuth in $BiCdVO_5$ can be described as cuboids, with oxygen atoms at seven vertices and the lone pair at the eighth one. These polyhedra share edges to form ribbons that run approximately parallel to the x axis of the crystals (Figure 9.3.a). This feature is very different from the $(BiO_2)^-$ chains found in the BiM_2AO_6 phases, mainly because the edge sharing that gives rise to the formation of the ribbons does not involve solely the four short bismuth – oxygen bonds. Bismuth coordination polyhedra in $BiCaVO_5$, however, form ribbons of the same type, with a similar degree of irregularity (Figure 9.3.b).

Both vanadium sites in $BiCdVO_5$ are tetrahedral, with bond lengths from 1.68 Å to 1.77 Å and angles from 105° to 113°.
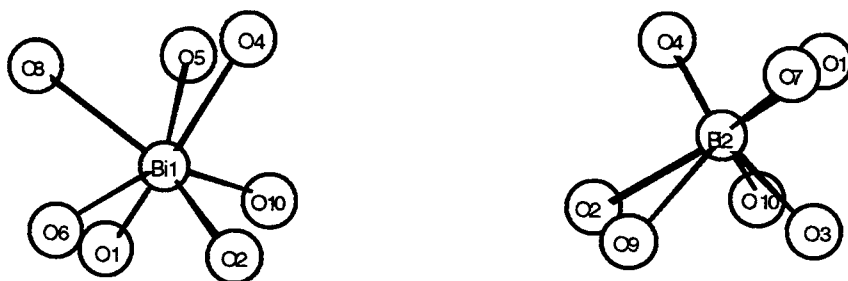
Figure 9.2. Coordination environment of Bi atoms
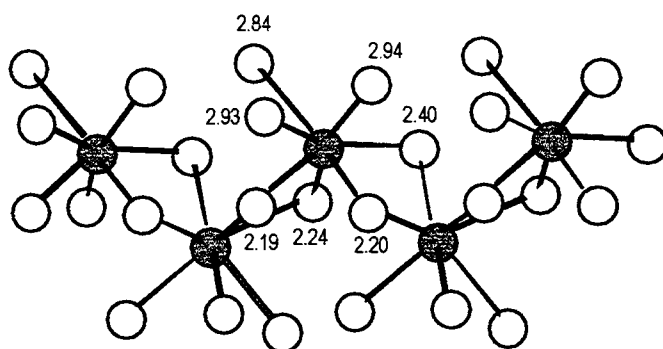
Figure 9.3.a. Bismuth – oxygen ribbons in $BiCdVO_5$
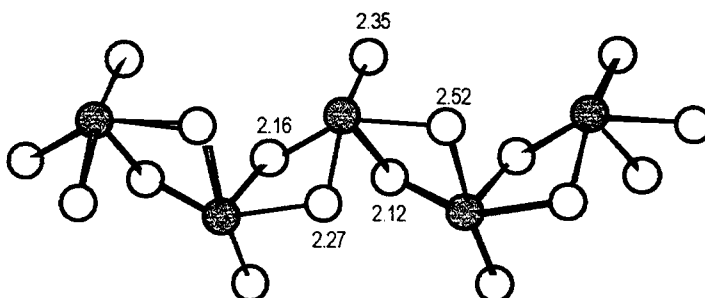
Figure 9.3.b. Bismuth – oxygen ribbons in $BiCaVO_5$

BiCdVO$_5$ has two unique cadmium sites. They are both distorted octahedra, with bond lengths ranging from 2.2 Å to 2.6 Å (Figure 9.4). Pairs of Cd(1)O$_6$ – Cd(2)O$_6$ octahedra share an edge to form the Cd$_2$O$_{10}$ units shown in Figure 9.5. These units are linked in the xy plane by corner sharing and thus form puckered layers approximately perpendicular to the z axis (Figure 9.6.a). The closest Cd – Cd distance is 3.6 Å. In contrast, calcium in BiCaVO$_5$ is seven coordinate and its coordination polyhedra also form puckered sheets approximately perpendicular to the z axis (Figure 9.6.b). These sheets are different from those in BiCdVO$_5$ in that the connectivity in the xy plane results solely from edge sharing of CaO$_7$ polyhedra.

It appears that the different bonding preferences of cadmium and calcium are the main cause of the differences in BiCdVO$_5$ and BiCaVO$_5$ structures. The ionic radii of Ca and Cd might have been considered sufficiently similar for the two materials to be isostructural (8). Simple calculations of bond valence sums (9, 10) reveal, however, that the bonding requirements of calcium and cadmium in these oxides are sufficiently different that the structural differences observed are not unexpected. Table 9.6 shows a comparison of calculated valence sums for the divalent cations in BiCdVO$_5$ and BiCaVO$_5$ compounds with the values obtained for hypothetical materials in which Cd is exchanged for Ca in the BiCaVO$_5$ structure and Ca for Cd in BiCdVO$_5$ structure.

Table 9.6. Bond Valence Calculations Comparing the $BiCdVO_5$ and $BiCaVO_5$ Structures

Structure	Cd bond valence sum		Ca bond valence sum	
$BiCdVO_5$	$^{VI}Cd(1)$	2.02	$^{VI}Ca(1)$	2.40
	$^{VI}Cd(2)$	1.96	$^{VI}Ca(2)$	2.32
$BiCaVO_5$	$^{VII}Cd(1)$	1.72	$^{VII}Ca(1)$	2.04

Bond valence arguments demonstrate that cadmium placed in a seven coordinate environment of calcium in $BiCaVO_5$ would be overbonded, while calcium would be underbonded in the six-fold coordination of cadmium in $BiCdVO_5$. The different crystal structures that the two compounds adopt, despite the similarity of the ionic radii, can be related to different bonding preferences of cadmium and calcium.
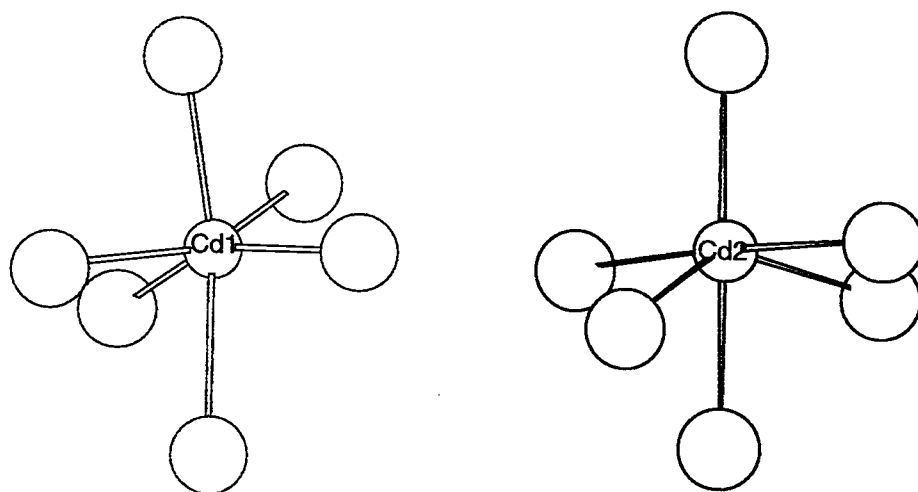
Figure 9.4. Distorted octahedral coordination of Cd(1) and Cd(2)
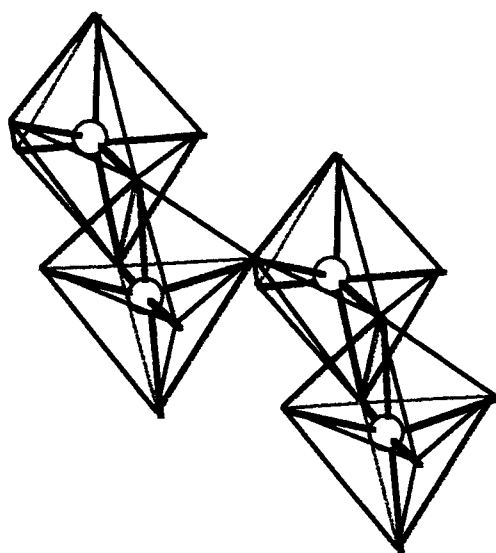
Figure 9.5. Edge and corner sharing of CdO$_6$ octahedra

a) Cd-O

b) Ca-O
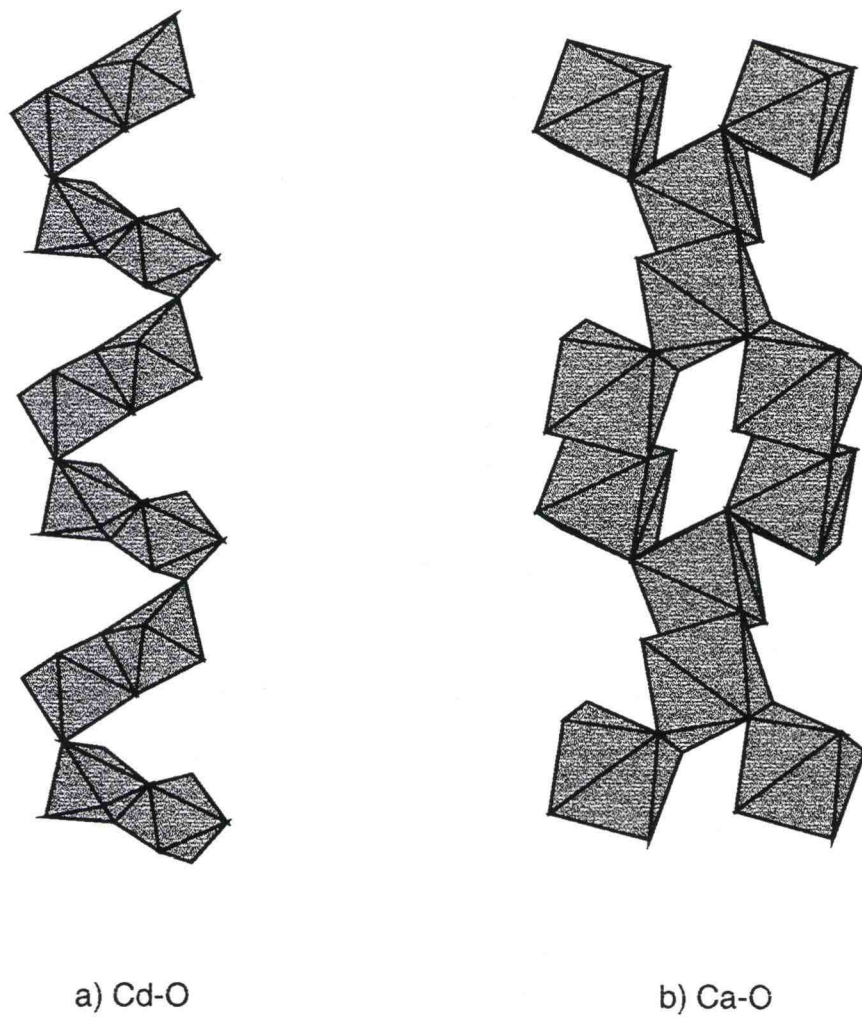
Figure 9.7. Cd-O layers in BiCdVO$_5$ and Ca-O layers in BiCaVO$_5$

9. 5. References

1. J. Huang and A. W. Sleight, *J. Solid State Chem.*, 104, 52 (1993)

2. J. Boje and Hk. Mueller – Buschbaum, *Z.anorg. allg. Chem.*, 619, 521 (1993)

3. XPREP, Ver. 5. 04/VMS, Siemens Analytical, Madison, WI, 1995.

4. SAINT, Ver. 5. 04/VMS, Siemens Analytical, Madison, WI, 1995

5. Z. Otwinowski and W. Minor, "Processing of X-Ray Diffraction Data in Oscillation Mode", in *Methods in Enzymology*, 276, C.W. Carter, Jr. and R.M. Sweet, Eds., Academic Press (1996)

6. A. Altomare, G. Cascarano, C. Giacovazzo, A. Guagliardi, M.C. Burla, G. Polidori and M. Camalli, *J. Appl. Cryst.*, 27, 435 (1994)

7. Oxford Crystals, D.J. Watkin, J.R. Carruthers and P.W. Betteridge, Chemical Crystallography Laboratory, University of Oxford, Oxford (1985)

8. R. D. Shannon, Acta Cryst., A32, 751 (1976)

9. I.D. Brown and D. Altermatt, *Acta Cryst.* Sect B 41, 244 (1985)

10. N.E. Brese and M. O'Keeffe, *Acta Cryst.* Sect B47, 192 (1991)

Chapter 10

A Comparative Analysis of the BiM_2AO_6 Structures

10. 1. Introduction

Structurally characterized phases of the BiM_2AO_6 family include $BiCa_2AO_6$ (A = V, As), $BiMg_2AO_6$ (A = V, As, P) and $BiCu_2AO_6$ (A = V, As, P). The compounds within the calcium series are isostructural and the compounds within the magnesium series are isostructural, while the three copper containing compounds all have different structures. $BiMg_2VO_6$ has also been found to undergo a phase transition between 300 K and 350 K. This leads to a total of six structure types observed to-date for the BiM_2AO_6 family. They are summarized in Table 10.1.

Two things are worth pointing out in regard to Table 10.1 and the subsequent content of this Chapter. Space group labels in Table 10.1 are not necessarily identical to those in which the individual structures have actually been reported. For ease of comparison, they are tabulated here in the standard space group settings. Secondly, the structure chosen to represent type I is

$BiMg_2VO_6$ at 350 K, while the representative for type III is $BiMg_2VO_6$ at 100 K; both structures are reported in Chapter 5 of this Thesis.

Table 10.1. Structure types in the BiM_2AO_6 family

Structure Type	Phase	Space Group	Z
I	High T $BiMg_2VO_6$	Cmcm	4
II	$BiCa_2VO_6$	$Cmc2_1$	4
III	Low T $BiMg_2VO_6$	Pnma	4
IV	$BiCu_2AsO_6$	Pnma	4
V	$BiCu_2PO_6$	Pnma	4
VI	$BiCu_2VO_6$	$P2_1/c$	12

The variety that these structure types exhibit, as well as certain similarities, can be most easily visualized by comparing their generated powder X-ray diffraction patterns. Patterns calculated from the structural refinements of this Thesis and, where appropriate, using literature coordinates are shown in Figure 10.1.

All of these structures can be viewed as consisting of three common building blocks: $(BiO_2)^-$ infinite chains, $(AO_4)^{3-}$ tetrahedra and interspersed M^{2+} cations. The goal of this comparative analysis is to use some simple crystal chemical arguments to account for the differences that the structures exhibit despite their similarities in stoichiometries.
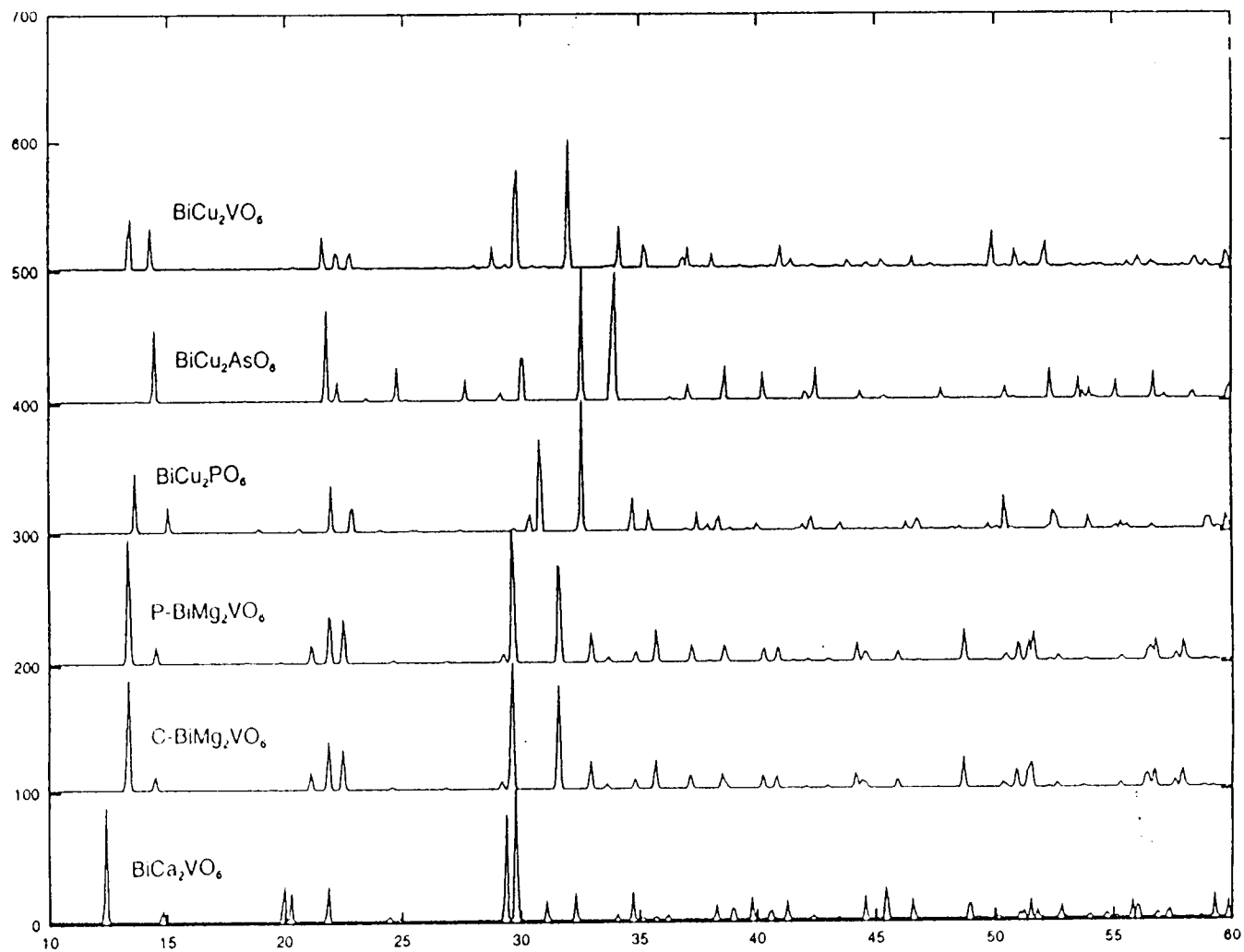
Figure 10.1. Calculated X-ray diffraction patterns for the six structural types in the BiM_2AO_6 family

10.2. Bismuth – Oxygen Chains, $(BiO_2)^-$

Table 10.2 gives a summary of relevant details of bismuth coordination environment in the six structure types.

Table 10.2. Details of Bismuth Coordination in BiM_2AO_6 Phases

Str. Type	Bi Site Sym	CN (Bi)	$<d_{Bi-O}^{chain}>$ (Å)	d_{Bi-O}^{other} (Å)	BV^{chain} (%)
I	m2m	4 + 4	2.21	4 × 3.36	96
II	m	4 + 3	2.21	2 × 3.00	92
				3.04	
III	m	4 + 3	2.21	3.02	95
				2 × 3.23	
IV	m	4 + 1 + 2	2.30	2.34	76
				2 × 2.90	
V	m	4 + 1 + 2	2.27	2.49	81
				2 × 2.86	
VI	1	2 × (4 + 2)	2.26	2.57, 2.84	88
			2.23	2.71, 3.08	
	1	4 + 3	2.25	2.69, 2.83,	
				2.93	

In all the structure types, bismuth forms short bonds to four oxygen atoms at about 2.20 Å – 2.30 Å forming a distorted square pyramidal coordination. The distorted square pyramids share edges, with bismuth atoms alternately above and below the mid-plane of oxygen atoms, to form infinite $(BiO_2)^-$ chains. When bismuth does not lie on any symmetry elements, these four bonds are of different lengths. When bismuth is on a mirror plane there are two pairs of short bonds. In the case of $BiCa_2VO_6$, they alternate along the polar axis of the crystal and can hence be viewed as a polar distortion. When bismuth is on the intersection of two mutually perpendicular mirror planes, the four chain oxygens are equidistant.

It is very typical of bismuth to have a coordination sphere that is clearly divided into short bonds on one side and long contacts on the opposite. In the BiM_2AO_6 phases, bismuth atoms have up to three long bonds on the side opposite the BiO_4 square pyramid. Data in Table 10.2 indicate a correlation between the two sets of bismuth – oxygen bonds: the more tightly bismuth is bonded in the chains, the longer its bonds to the tetrahedral oxygens. Figures 10.2.a – 10.2.e show different types of bismuth coordination environments found in the BiM_2AO_6 phases. A definition adopted for the purpose of this comparison is that those interactions that contribute to the total bond valence sum of bismuth at the 95% level are considered bonds. In each figure, the drawing on the left-hand side represents the view approximately perpendicular to the direction of propagation of the $(BiO_2)^-$ chains, while the one on the right shows the view along this direction.
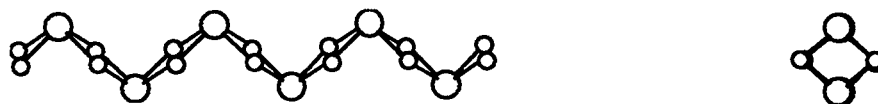
Figure 10.2.a. Bismuth – oxygen chains in structure types I and III
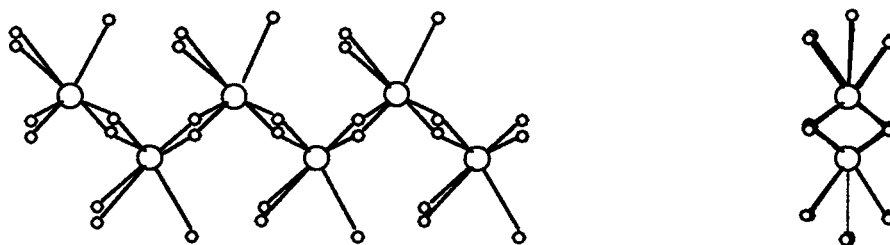
Figure 10.2.b. Bismuth – oxygen chains in structure type II
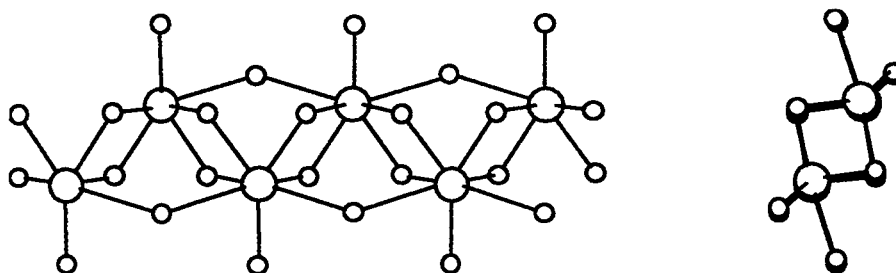
Figure 10.2.c. Bismuth – oxygen chains in structure type IV
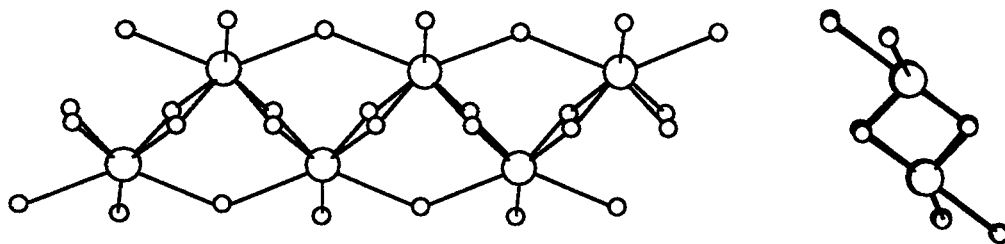
Figure 10.2.d. Bismuth – oxygen chains in structure type V
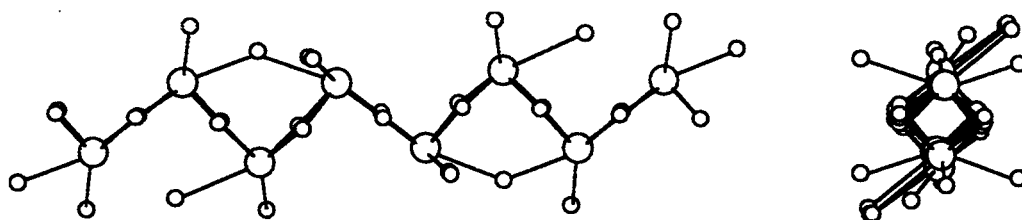
Figure 10.2.e. Bismuth – oxygen chains in structure type VI

The last column in Table 10.2 show the percentage contribution of the four bonds of bismuth to the chain oxygens to the total bond valence sum (1, 2) for this cation. In the case of structure type VI, which contains three crystallographically unique bismuth atoms, the average of the three is given.

If only four short bismuth – oxygen bonds are considered, it is interesting to compare the $(BiO_2)^-$ chains of the BiM_2AO_6 family with the $(Bi_2O_2)^{2+}$ layers found in Aurivillius phases described in some detail in Chapter 1.

Three different projections of the $(BiO_2)^-$ chains are depicted in the left-hand column of Figure 10.3. The smallest repetitive unit in the chains is marked on the drawing. It contains two bismuth atoms, two oxygens that are not shared and four more oxygens that are shared with two adjacent units. This leads to the chain stoichiometry of $(BiO_2)^-$. If these $(BiO_2)^-$ chains are connected laterally by corner sharing in such a way that they are staggered by one half of the repetitive unit, so that bismuth atoms are alternately above and below the oxygen mid-plane in both dimensions, two dimensional sheets are formed. They are shown in the right-hand column of Figure 10.3. The smallest repetitive unit of these sheets contains two bismuth atoms, two oxygens that are shared with two and four that are shared with four adjacent repetitive units. The stoichiometry of sheets is thus $(Bi_2O_2)^{2+}$, and these are the layers found in Aurivillius phases. While bismuth coordination remains unchanged, the coordination of oxygen atoms increases from 2 in the $(BiO_2)^-$ chains to 4 in the $(Bi_2O_2)^{2+}$ layers.
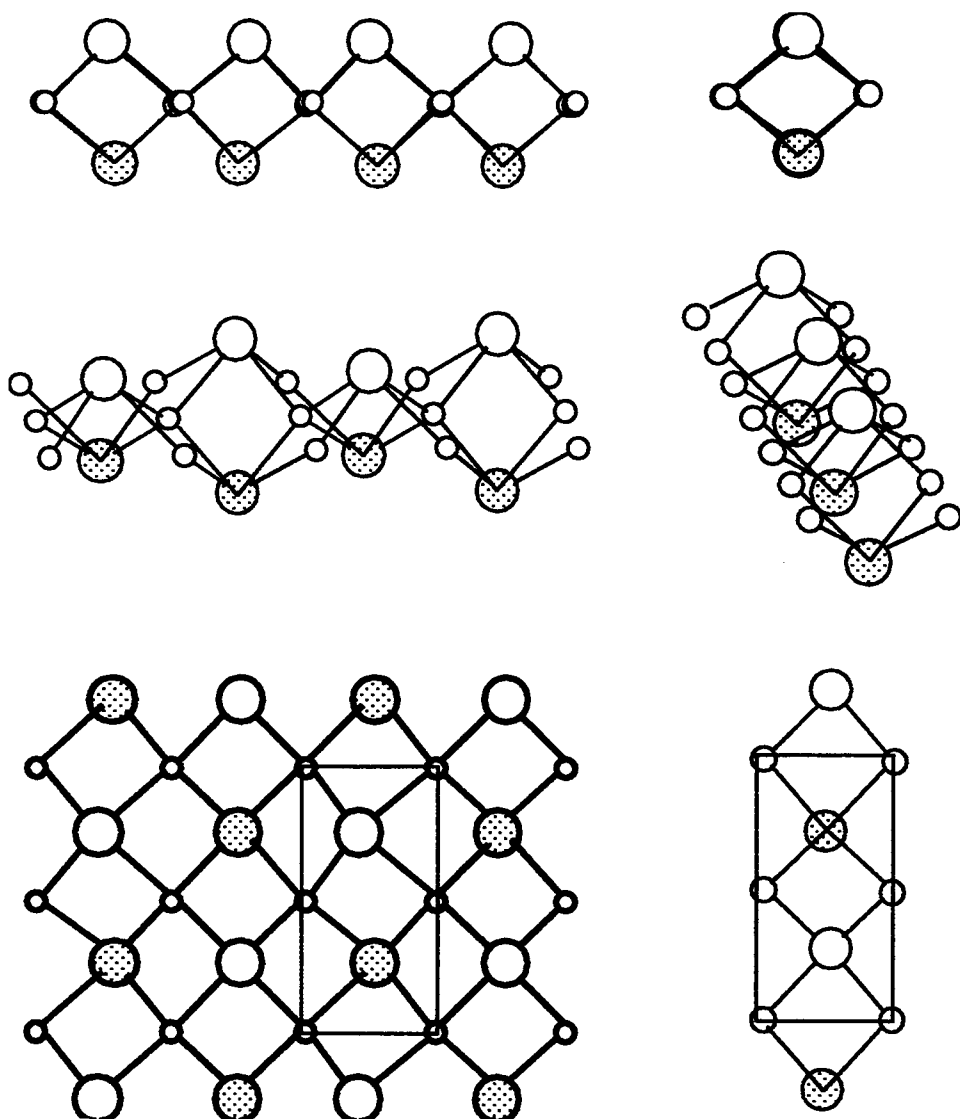
Figure 10.3. Comparison of $(BiO_2)^-$ chains and $(Bi_2O_2)^{2+}$ layers

10.3. M²⁺ Cations

The M^{2+} cations in BiM_2AO_6 phases are found in different types of environments, as illustrated by the data given in Table 10.3.

Table 10.3. Relevant Details of the M^{2+} Coordination Environments in BiM_2AO_6

Str. Type	M^{2+}	r_M^{2+} (Å) *	CN (M^{2+})	χ_M^{2+*}	Connectivity *	$d_{M-M, min}$ (Å)
I	Mg^{2+}	0.65	5	1.31	E	3.02
II	Ca^{2+}	1.06	7	1.00	F, E, C	3.56
III	Mg^{2+}	0.65	5	1.31	E	3.05
IV	Cu^{2+}	0.65	5	1.90	E	2.92
V	Cu^{2+}	0.65	5	1.90	E	2.90
VI	Cu^{2+}	0.65	5	1.90	E	2.82
		0.73	6	1.90	E, C	3.17

* Radii quoted here are those given by Shannon (3). Ionic radius for Mg in fivefold coordination is not known; the value listed here corresponds to the average of the radii for four- and six-coordinate magnesium

⁺Pauling's electronegativities

* Connectivity is here described in terms of shared elements of the M^{2+} coordination polyhedra and the following notation is used: C – corner sharing, E – edge sharing, F – face sharing

Magnesium is five coordinate in both structure types I and III. This coordination is unusual for magnesium, which is typically found in more symmetrical coordination environments, especially six-fold. Magnesium in the $BiMg_2AO_6$ compounds bonds to five oxygens, three of which are shared with three different VO_4 tetrahedra and two with the $(BiO_2)^-$ chains. Ionic bonding of magnesium to oxygens that are covalently bonded to other cations may be the basis of some rationalization of the unusual coordination number of magnesium. In other words, attaining a favorable coordination for bismuth and vanadium is the principal factor, while magnesium accomodates its resulting coordination, owing to its lower affinity towards directional bonding.

Calcium in structure type II is seven coordinate. The high coordination number and a geometrically irregular environment can be accounted for by the size of Ca^{2+} and the ionic character of its bonding to oxygen. Pairs of face sharing CaO_7 polyhedra connect along a common edge to form units of four polyhedra that share corners to build a three dimensional framework. These units are shown in Figure 10.4. Owing to the size of Ca^{2+} and the irregular geometry of its coordination polyhedra, the shortest calcium – calcium distance across the shared face is 3.6 Å.
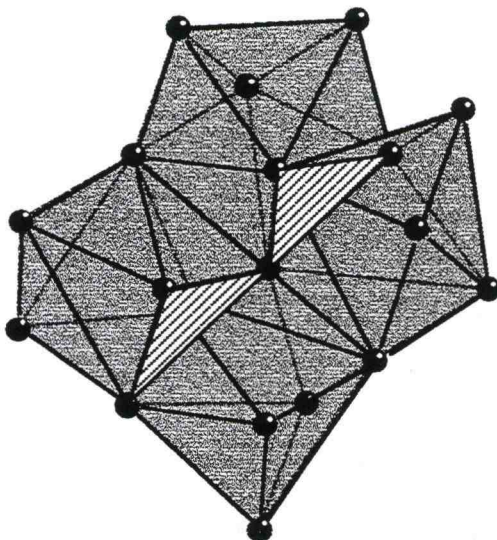
Figure 10.4. Connectivity of CaO_7 polyhedra in $BiCa_2VO_6$

Copper is five coordinate distorted square pyramidal in structure types Iv, V and VI. In structure type VI, however, one third of copper atoms are six coordinate distorted octahedral. While Cu^{2+} is a typical Jahn-Teller cation, the environment of Cu^{2+} in these phases cannot be explained solely by this effect. The coordination number of five and the departure of the coordination polyhedra from ideal geometries can be accounted for by considering the effects of the removal of a center of inversion from these systems. When the center of symmetry is removed, the parity of the d orbitals becomes equal to that of the p orbitals, thus facilitating their mixing and more efficient bonding. The formation of (Cu_2O_8) dimers found in all copper containing BiM_2AO_6 phases, with copper – copper bonds ranging from 2.82 Å to 2.92 Å, is consistent with the high degree of covalency of this cation.

10. 4. $(AO_4)^{3-}$ Tetrahedra

All BiM_2AO_6 phases contain $(AO_4)^{3-}$ tetrahedra, but the orientation of these units is very different in different structure types. In all cases, tetrahedral oxygens are shared with the other structural elements, but they do not share oxygens with each other. It appears that the tetrahedra are arranged in a way that makes it possible to achieve the most efficient packing possible for a given structure and still maintain the necessary connectivity. This is illustrated by the examples of structure types I and II in Figure 10.5.
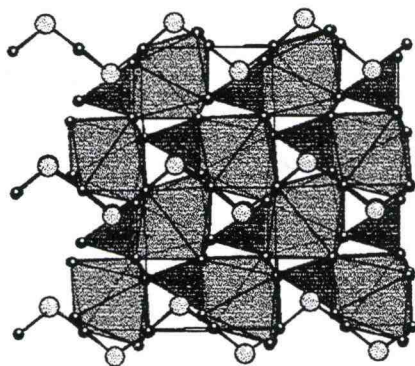
Figure 10.5.a. Packing of the (VO_4) tetrahedra in structure type II
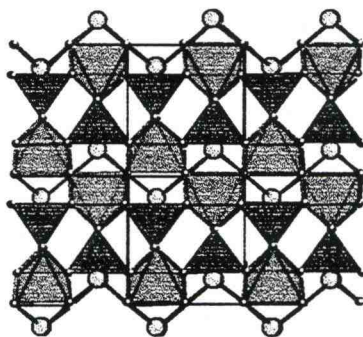
Figure 10.5.b. Packing of the (VO_4) tetrahedra in structure type I

10. 5. Comparison of Structure Types I and II

Atomic positions of $BiMg_2VO_6$ at 350 K (structure type I) and BiCa2VO6 (structure type II) are given in Table 10. 4.

Table 10. 4. Comparison of Atomic Position for Structure Types I and II

Atom	x/a	y/b	z/c
Bi	0.5	-0.5894(6)	0.75
	0.5	*-0.5918(2)*	*0.75*
V	0	0.681(2)	0.199(4)
	0.0	*0.6966(9)*	*0.25*
Ca	0.7999(4)	0.6073(3)	0.742(1)
Mg	*0.809*	*0.588(1)*	*0.75*
O (1)	0.1509(4)	0.0030(3)	0.992(1)
	0.167(3)	*0.0*	*0.0*
O (2)	0	0.6814(3)	0.199(1)
O (2)	*0*	*0.616(3)*	*-0.02(1)*
O (3)	0	0.4481(4)	0.568(1)
O (3)	*0.162(6)*	*0.784(4)*	*0.25*
O (4)	0.1548(4)	0.7472(3)	0.079(1)

Figure 10.6.a shows the view of $BiCa_2VO_6$ parallel to the (001) plane and

10.6.b the corresponding view of $BiMg_2VO_6$. These figures and the data in Table

10.4 show that bismuth, calcium, magnesium and the chain oxygen are

essentially in the same positions in the two phases. However, the analogous

atomic coordinates for the tetrahedral oxygens in the two structures cannot be

found. This difference becomes obvious when the structures are viewed parallel

to the (100) plane. This view is shown in Figures 10.7.a and 10.7.b. In the

noncentrosymmetric polar structure II all the tetrahedra point in the same

direction along the z axis, the polar axis of the crystal. In structure type I, the

orientation of the tetrahedra is dictated by the presence of inversion centers

located at (0,0,0), (1/2,0,0) and the symmetry generated positions. Adding a

center of symmetry onto the 2_1 axis generates a mirror plane perpendicular to

this axis, which is why two tetrahedral oxygens in the centrosymmetric structure

become symmetry equivalents.
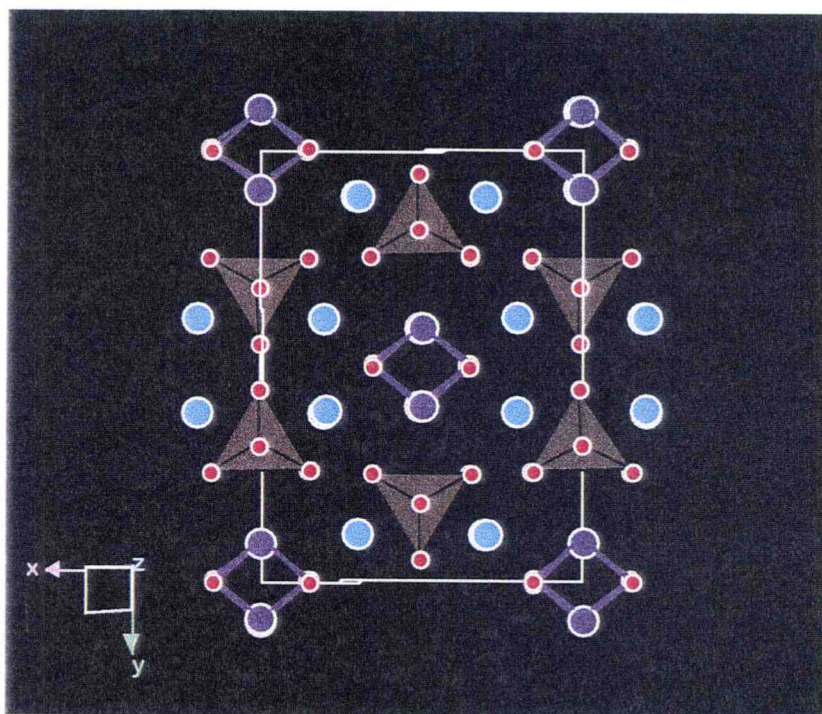
Figure 10.6.a. A view of BiCa$_2$VO$_6$ (type II) structure parallel to the (001) plane
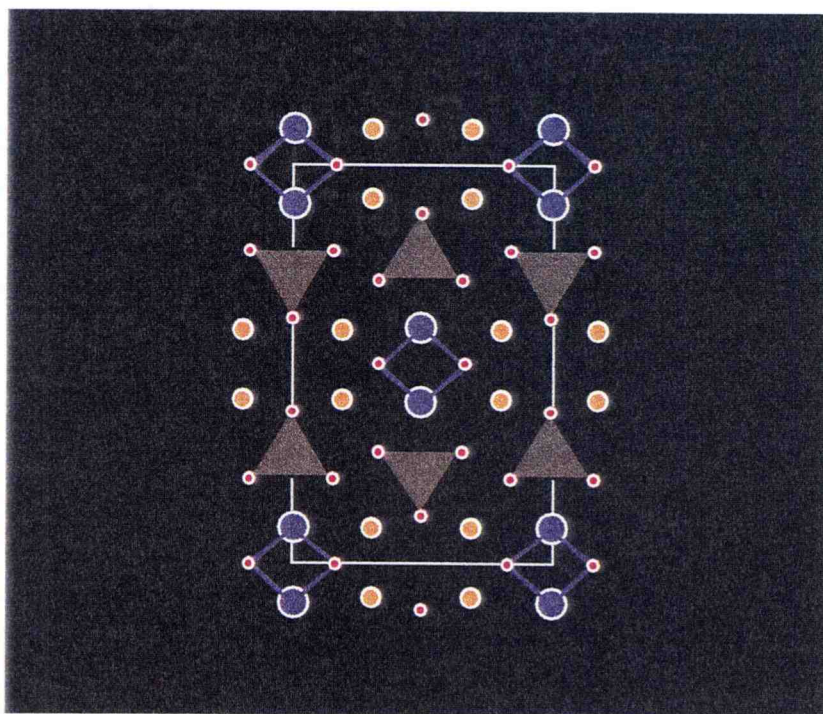
Figure 10.6.b. A view of BiMg$_2$VO$_6$ (type I) structure parallel to the (001) plane
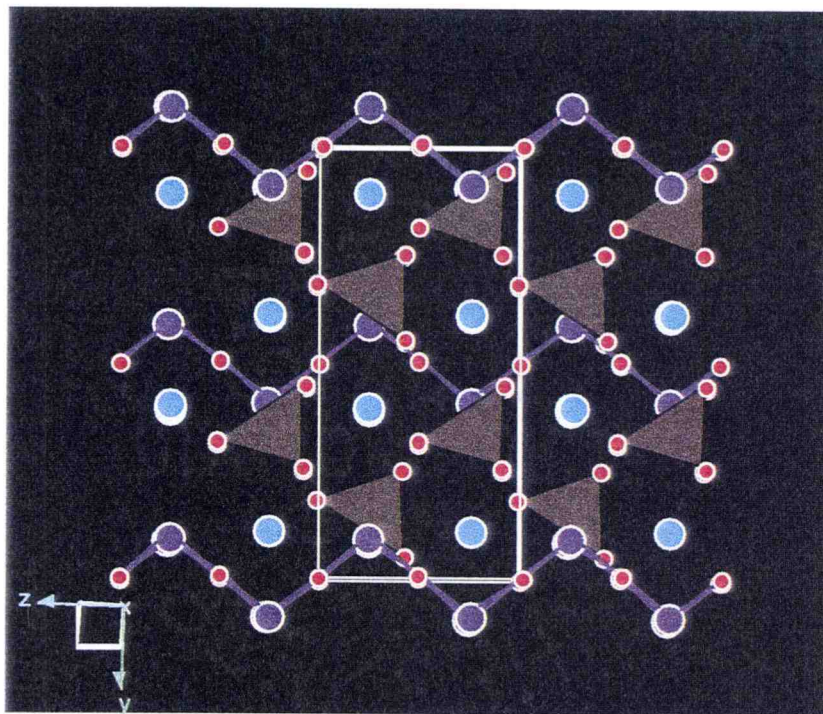
Figure 10.7.a. A view of BiCa$_2$VO$_6$ (type II) structure parallel to the (100) plane
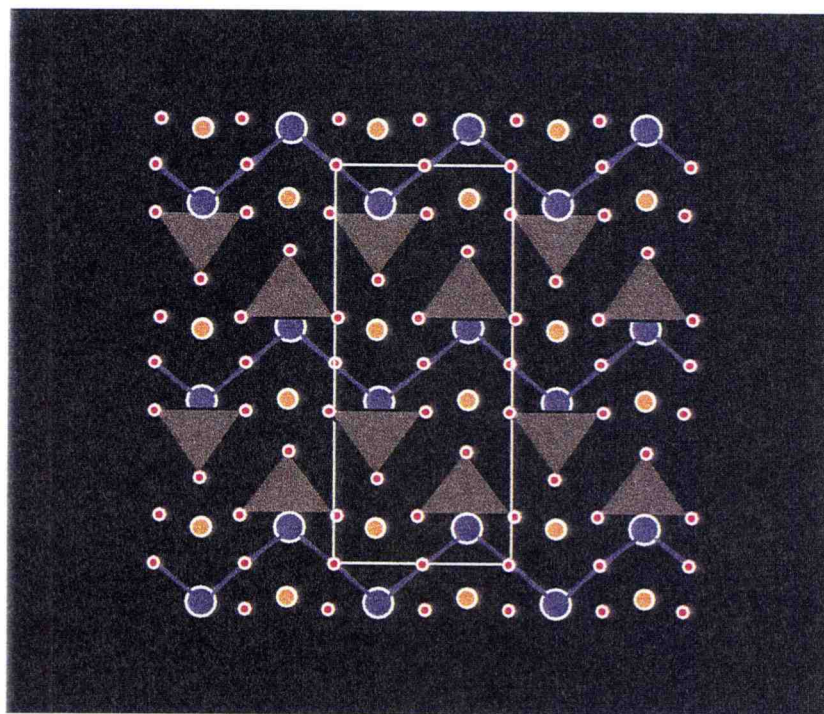
Figure 10.7.b. A view of BiMg$_2$VO$_6$ (type II) structure parallel to the (100) plane

10.6. Comparison of Structure Types I and IiI

BiMg$_2$VO$_6$ undergoes a phase transition between 300 K and 350 K. Atomic positions of BiMg$_2$VO$_6$ at 350 K and BiMg$_2$VO$_6$ at 100 K are given in Table 10.5.

Table 10.5. Comparison of Atomic Positions for Structure Types I and III

Str. Type	Atom	x/a	y/b	z/c
I	Bi	0.75	-1.0105(1)	0.90782(5)
III		0.75	-1.00	0.9082(2)
I	V	0.25	-0.9829(3)	0.6981(3)
III		0.25	-1.00	0.6962(9)
I	Mg(1)	0.75	-0.697(1)	1.0845(4)
III		0.75	-0.691(2)	1.088(1)
I	Mg(2)	1.25	-0.688(1)	0.9068(4)
III		1.25	-0.691(2)	0.912(1)
I	O(1)	-0.007(2)	-0.9937(7)	0.6172(9)
III		-0.019(8)	-1.00	0.617(3)
I	O(2)	1.001(1)	-0.8335(9)	0.9941(4)
III		1.00	-0.833(3)	1.00
I	O(3)	0.25	-1.140(1)	0.7928(9)
III		0.25	-1.160(6)	0.785(4)
I	O(4)	0.75	-1.292(2)	0.7409(9)
III		0.75	0.660(6)	0.715(4)

The positions given for structure type III are those obtained in the refinement in space group Pmcn with the necessary constraints to make the structure essentially centered. In other words, atoms Mg(1) and Mg(2), as well as O(3) and O(4) in Table 10.5 are not crystallographically unique.

Figures 10.8.a and 10.8.b show the views of the structure types I and III parallel to the (100) plane, while Figures 10.9.a and 10.9.b show the projection parallel to the (010) plane. The main differences arise from the difference in the symmetry elements present in the two space groups and the resulting differences in atom site symmetries . In the centered structure, bismuth lies on the mirror plane parallel to (010). The basal planes of the BiO_4 pyramids forming the (BiO_2)-chains are, consequently, constrained to be strictly perpendicular to this plane. In the primitive structure, bismuth atoms are very close to the (010) plane, which is not a mirror plane in this case, and the $(BiO_2)^-$ chains are therefore slightly tilted. Although the vanadium positions in the two structures are very similar, those of tetrahedral oxygens are different. In the centered structure, vanadium and two tetrahedral oxygens are located on the mirror plane parallel to (010), while the other two oxygens are symmetry equivalents related by this plane. In the primitive structure, vanadium and the tetrahedral oxygens are located off this plane and the tetrahedra are therefore tilted with respect to the cell edge. Magnesium atoms are in very similar positions in the two structures. However, in the centered form they become symmetry equivalents related by the mirror plane parallel to (010).
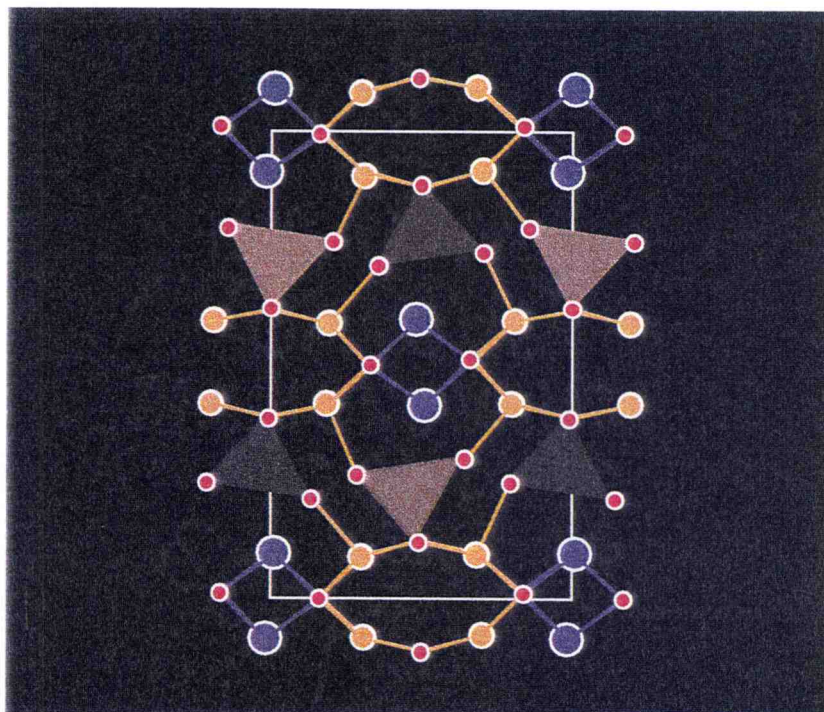
Figure 10.8.a. A view of BiMg$_2$VO$_6$ (type III) structure parallel to the (100) plane
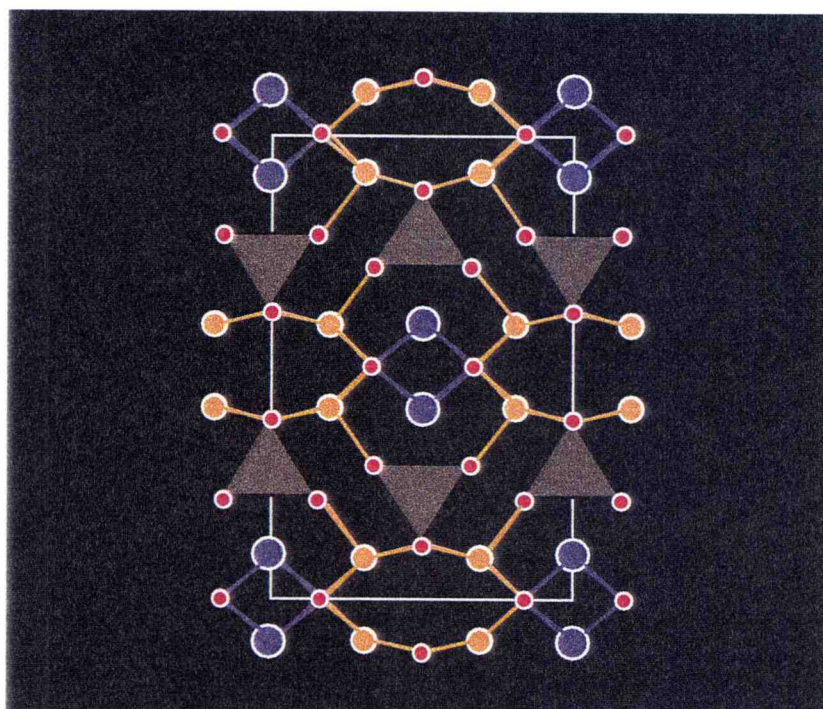
Figure 10.8.b. A view of BiMg$_2$VO$_6$ (type I) structure parallel to the (100) plane
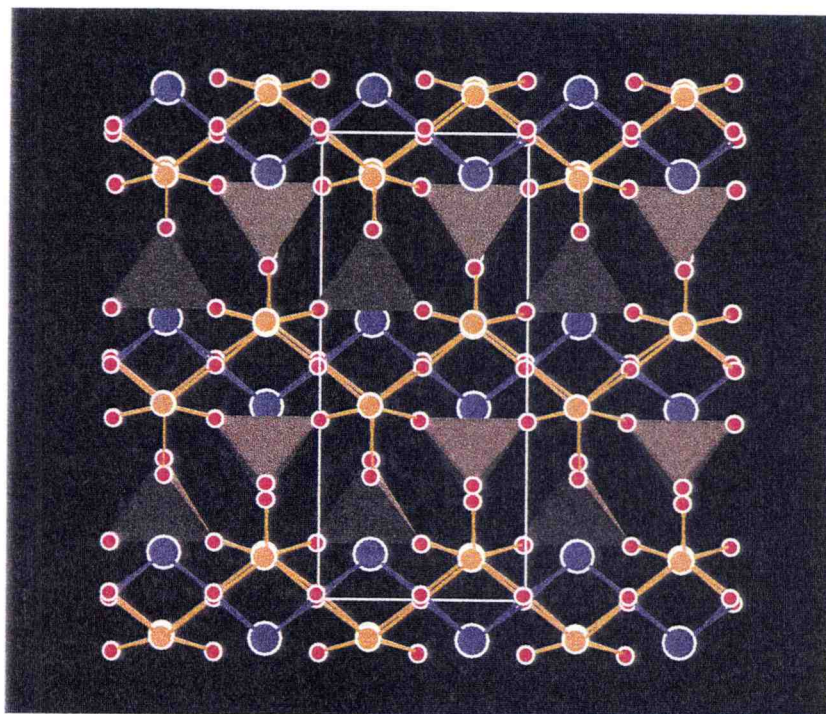
Figure 10.9.a. A view of BiMg$_2$VO$_6$ (type II) structure parallel to the (010) plane
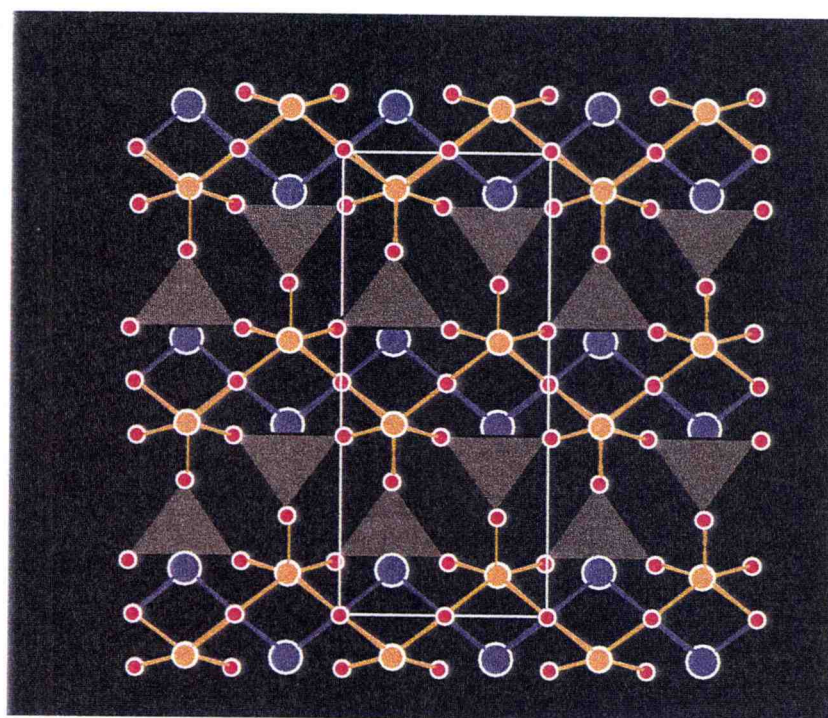
Figure 10.9.b. A view of BiMg$_2$VO$_6$ (type I) structure parallel to the (100) plane

## 10. 7. Relationship between BiMg$_2$VO$_6$ and BiCu$_2$PO$_6$ Type II Structures

Structure type III, represented by high-temperature BiMg$_2$VO$_6$ and type V, represented by BiCu$_2$PO$_6$ (4) are very similar. They belong to the same space group and the positions of the cations and the chain oxygens are very close, as shown in Table 10.6.

Table 10.6. Comparison of Atomic Positions for Structure Types III and V

Atom	x/a	y/b	z/c
Bi	0.90782(5)	0.75	0.9895(1)
	0.89287(3)	0.75	0.97640(5)
V	0.6981(3)	0.25	0.01714(3)
P	0.6972(2)	0.25	0.0342(4)
Mg (1)	0.0845(4)	0.75	0.303(1)
Cu (1)	0.0898(1)	0.75	0.6864(2)
Mg (2)	0.9068(4)	0.25	0.312(1)
Cu (2)	0.9278(1)	0.25	0.3156(2)
O(1)	0.6172(9)	0.993(2)	0.0063(7)
	0.6232(5)	0.9973(13)	0.0055(8)
O(2)	0.9941(4)	1.001(1)	0.1665(9)
	0.9944(5)	0.0040(12)	0.1760(7)
O(3)	0.7928(9)	0.25	0.860(1)
	0.7986(6)	0.25	0.9140(14)
O(4)	0.7409(9)	0.75	0.708(2)
	0.7655(8)	0.75	0.7218(11)
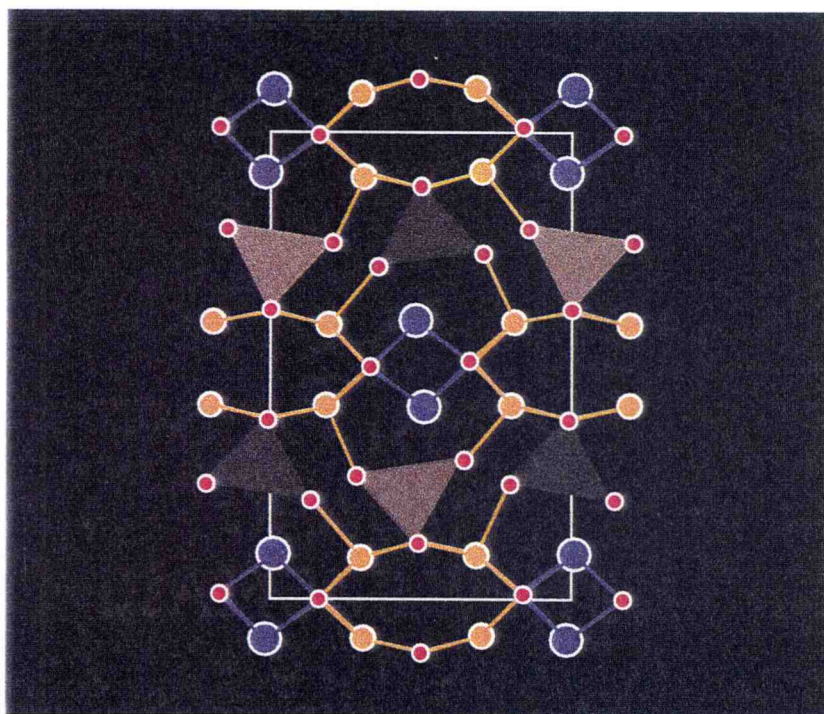
Figure 10.10.a. A view of BiMg$_2$VO$_6$ (type III) structure parallel to the (010) plane
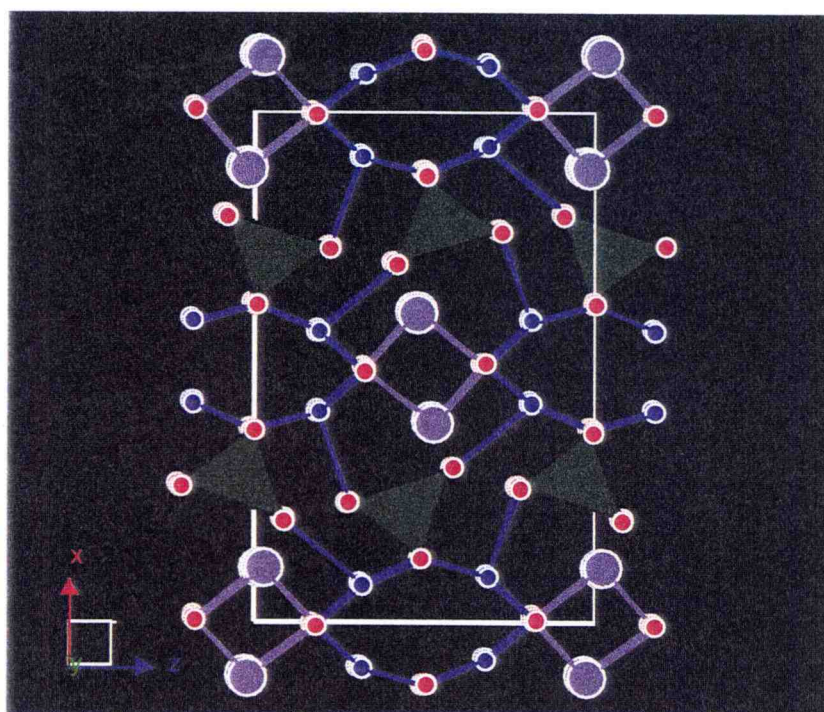
Figure 10.10.b. A view of BiCu$_2$PO$_6$ (type III) structure parallel to the (100) plane

Figure 10.10.a shows a view of the $BiMg_2VO_6$ (type III) parallel to the (100) plane and Figure 10.10.b represents the corresponding view of $BiCu_2PO_6$ (type V). Structure type V can be viewed as a continuation of the trend described in the comparison of structures I and III. The departure from the cell centering is in the case of $BiCu_2PO_6$ so pronounced that it affects the topology of the structure, reflected mainly in the number and lengths of bismuth – oxygen bonds, as described in section 10.2. By analogy with the $BiMg_2AO_6$ series, $BiCu_2PO_6$ may be expected to undergo a phase transition to the centered structure at high temperatures.

10. 8. Conclusions

This Thesis presents the synthesis of a number of new compounds and their structural characterization from X-ray and neutron diffraction data and, where appropriate, preliminary NLO measurements. Most of the prepared phases belong to the BiM_2VO_6 family of compounds. Some of the differences between them are accounted for by crystal chemistry concepts underlying the behavior of the constituent atomic species. Three compounds have been identified as active second harmonic generation materials and potential ferroelectrics.

In a recent article, Halasyamani and Poeppelmeier (5) have reviewed nearly 600 noncentrosymmetric oxides. They found that nearly 80% of them contain either a second order Jahn-Teller distorted cation or a tetrahedrally coordinated cation. Although these two factors cannot be viewed as solely responsible for the formation of noncentrosymetric structures, they certainly appear to facilitate it. According to these arguments, synthesis of new Bi(III) containing compounds presents a step in the right direction. While rational synthesis of new materials remains a challenge, synthetic solid state chemistry continues to be an exciting field in which to work.

10. 9. References

1. I.D. Brown and D. Altermatt, *Acta Cryst.* Sect B 41, 244 (1985)

2. N.E. Brese and M. O'Keeffe, *Acta Cryst.* Sect B47, 192 (1991)

3. R. D. Shannon, *Acta Cryst.* A32, 751 (1976)

4. F. Abraham, M. Ketatni, G. Mairesse and B. Memari, Eur. *J. Solid State Inorg. Chem.*, 31, 313 (1994)

5. P. S. Halasyamani and K. R. Poeppelmeier, *Chem. Mater.*, 10, 2753 (1998)

Bibliography

F. Abraham, J. C. Boivin, G. Mairesse and G. Nowogrocki, *Solid State Ionics*, 40-41, 934 (1190)

F. Abraham, M. Ketatni, G. Mairesse and B. Mernari, *Eur. J. Solid State Inorg. Chem.*, 31, 313 (1994)

S. C. Abrahams, *Mat. Res. Bull.*, 6, 881 (1971)

F. Abraham, M. F. Debruille-Gresse, G. Mairesse and G. Nowogrocki, *Solid State Ionics*, 28-30, 529 (1988)

K. Aizu, *J. Phys. Soc. Japan*, 27, 2, 387 (1969)

K. Aizu, *J. Phys. Soc. Japan*, 28, 3, 706 (1970)

E. Aleshin and R.Roy, *J. Am. Ceram. Soc.*, 45, 1, 18 (1965)

A. Altomare, G. Cascarno, C.Giacovazzo, A. Guagliardi, M. C. Burla, G. Polidori, M. Camalli, *J. Appl. Cryst.* 27, 435 (1994)

A. Altomare, M. C. Burla, G. Cascarno, C.Giacovazzo, A. Guagliardi, A. G. G. Moliterni and G. Polidori, *J. Appl. Cryst.* 28, 842 (1995)

J. P. Attfield, A. W. Sleight and A. K. Cheetam, *Nature*, 322 (1986)

B. Aurivillius, *Ark. Kemi*, 1, 54, 463 (1949)

B. Aurivillius, *Ark. Kemi*, 1, 58, 499 (1949)

B. Aurivillius, *Ark. Kemi*, 2, 37, 519 (1949)

D. N. Balducci et al., U. S. Patent N° 4,230,500, 1975.

C. E. Bamberger, H. W. Dunn, G. M. Begun and S. A. Landry, *J. Solid State Chem.*, 58, 114 (1985)

M. L. Barsukova, V. A. Kuznetsov, A. N. Lobachev and Yu. V. Shaldin, *J. Cryst. Growth*, 13/14, 530 (1972)

P. D. Battle, C. R. A. Catlow, J. Drennan and A. D. Murray, *J. Phys.* C16, L561 (1983)

A. I. Beskrovnyi, M. Dlouha, Z. Jirak and S. Vratislav, *Physica C*, 171, 19 (1990)

J. D. Bierlein and A. W. Sleight, *Solid State Comm.*, 16, 69 (1975)

T. Birchall and A. W. Sleight, *J. Solid State Chem.*, 13, 118 (1975)

J. Boje and Hk. Muller-Buschbaum, *Z. Anorg. Allg. Chem.*, 619, 521 (1993)

N.E. Brese and M. O'Keeffe, *Acta Cryst.* Sect B47, 192 (1991)

I. D. Brown, in Structure and Bonding in Crystals, ed. by M. O'Keffee and A. Navrotsky, Academic Press, New York, 1981.

I.D. Brown and D. Altermatt, *Acta Cryst.* Sect B 41, 244 (1985)

I. D. Brown and R. D. Shannon, *Acta Cryst.*, A29, 266 (1973)

A. Boultif and D. Louer, *J. Appl. Cryst.*, 24, 987 (1991)

M. J. Buerger, Crystal Structure Analysis, John Wiley and Sons, New York, N.Y., 1960.

D. J. Buttrey, T. Vogt, U. Wildgruber and W. R. Robinson, *J. Solid State Chem.*, 111, 118 (1994)

D. J. Buttrey, T. Vogt, G. P. A. Yap and A. L. Rheingold, *Mat. Res. Bull.*, 32, 7, 947 (1997)

A. A. Bush and Yu. N. Venetsev, *Russ. J. Inorg. Chem.*, 769, 31, 5 (1986)

A. Bystrom, *Ark. Kemi Min. Geol.*, 18A, 1 (1945)

H. Y. Chen and A. W. Sleight, *J. Solid State Chem.*, 63, 70 (1986)

W. I. F. David, A. M. Glazer and A. W. Hewat, *Phase Transitions*, 1, 155, (1979)

G. B. Deacon, B. M. Gatehouse and G. N. Ward, *Acta Cryst.*, C50, 1178 (1990)

L. E. Depero and L. Sangaletti, *J. Solid State Chem.*, 119, 428 (1995)

A. F. van den Elzek and G. D. Rieck, *Acta Cryst.* B29, 2433 (1973)

A. F. van den Elzek and G. D. Rieck, *Acta Cryst.* B29, 2436 (1973)

J. S. O. Evans and A. W. Sleight, in preparation

J. S. O. Evans and A. W. Sleight, in preparation

J. S. O. Evans, J. Huang and A. W. Sleight, in preparation

L. R. Falvello, *J. Chem. Soc., Dalton Trans.*, 4463 (1997)

J. Feldmann and Hk. Mueller Buschbaum, *Zeitschrift fur Naturforschung*, B50, 1163 (1995)

Fundamentals of Crystallography, ed. by C. Giacovazzo, Oxford University Press, Oxford, England, 1995.

H. von Gaertner, *Neues Jahrb. Mineral. Geol. Palaeontol.*, Ref. 61,1 (1930)

D. H. Galvan, S. Fuentes, M. Alvalosborja, L. Cotaaraiza, E. A. Early, M. B. Maple and J. Cruzreyes, *J. Phys. Condens. Matter*, 5, A217 (1993)

J. Galy, D. Lavaud, A. Casalot and P. Hagenmueller, *J. Solid State Chem.*, 2, 531 (1970)

J. Galy and D. Lavaud, *Acta Cryst.*, 27, 1005 (1971)

Y. Gao, P. Lee, P. Coppens, M. A. Subramanian and A. W. Sleight, *Science*, 241 954 (1988)

J. L. Garcia Munoz, J. Caravajal Rodriguez, F. Sapina, M. J. Sanchis, R. Ibanez and D. Beltran Porter, *J. Phys.*, 2, 2205 (1990)

G. Gattow and H. Schroeder, *Z. Anorg. Allg. Chem.*, 318, 176 (1962)

G. Gattow and D. Schuetze, *Z. Anorg. Allg. Chem.*, 328, 44 (1964)

L. C. Glaeser, J. F. Brazdil, M. A. Hazle, M. Mehicic and R. K. Grasseli, *J. Chem. Soc. Farad. Trans.*, 81, 2903 (1985)

R. K. Grasseli and J. F. Burrington, *Adv. Catal.*, 30, 133 (1981)

P. S. Halasyamani and K. R. Poeppelmeier, *Chem. Mater.*, 10, 2753 (1998)

H. A. Harwig, Thesis, State University Utrecht, The Netherlands, 1977.

H. A. Harwig, *Z. Anorg. Allg. Chem.*, 444, 151 (1978)

H. A. Harwig and A. G. Gerards, *J. Solid State Chem.*, 26, 265 (1978)

M. H. Hey and F. A. Bannister, *Mineral. Mag.*, 25, 41 (1938)

J. Huang, A. W. Sleight, *J. Solid State Chem.* 100, 170 (1992)

J. Huang and A. W. Sleight, *J. Solid State Chem.*, 104, 52 (1993)

J. Huang, Q. Gu, A. W. Sleight, *J. Solid State Chem.* 105, 599 (1993)

International Tables for Crystallography, Vol. 4, ed. by T. Hahn, D. Reidel Publishing Company, Dodrecht, The Netherlands, 1983.

Ismunandar, B. J. Kennedy and B. A. Hunter, *Mat. Res. Bull.*, in press

F. Izumi, H. Asano, H. Murata and N. Watanabe, *J. Appl. Cryst.*, 20, 411 (1987)

H. A. Jahn and E. Teller, *Proc. R. Soc. London, Ser. A*, 161, 220 (1937)

N. Jakubowicz, O. Perez, D. Grebille and H. Leligny, *J. Solid State Chem.*, 139, 194 (1998)

F. Jona, G. Shirane and R. Pepinsky, *Phys. Rev.*, 98, 4 (1955)

W. F. de Jong and J. J. de Lange, *Amer. Mineral.*, 21, 809 (1936)

O. Joubert, A. Jouanneaux and M. Ganne, *Mat. Res. Bull.*, 29, 12, 175 (1994)

K. Kato, E. Takayama Muromachi and Y. Kanke, *Acta Cryst.*, 45, 1841 (1989)

J. F. Keggin, *Nature*, 131, 908 (1933)

K. S. Knight, *Mineral. Mag.*, 56, 399 (1992)

O. Knop, F. Brisse and L. Castelliz, *Can. J. Chem.*, 13, 118 (1969)

O. Knop, F. Brisse and L. Castelliz, *Can. J. Chem.*, 47, 971 (1969)

A. C. Larson and R. B. von Dreele, LANSCE, Los Alamos National Laboratory, Los Alamos, N.M., 1994.

A. Lazoryak, L. O. Dmitrienko and S. V. Grechkin, *Russ. J. Inorg. Chem.*, 35, 5, (1990)

S. Lazure, Ch. Vernochet, R. N. Vannier, G. Nowogrocki and G. Mairesse, *Solid State Ionics*, 90, 117 (1990)

A. Le Bail, H. Duroy and J. L. Fourquet, *Mat. Res. Bull.*, 23, 447 (1988)

Y. Le Page, W. R. McKinnon, J. M. Tarascon and P. Barboux, *Phys. Rev. B*, 40, 10 (1989)

E. M. Levin and R. S. Roth, *J. Res. Nat. Bur. Stand.* 68A, 189 (1969)

A. A. Levin, Yu. I. Smolin and Yu. F. Shepelev, *J. Phys.:Condens. Matter*, 6, 3539 (1994)

J. M. Longo, P. M. Raccah and J. B. Goodenough, Mater. Res. Bull., 4, 191 (1969)

G. Mairesse, in Fast Ion Transport in Solids, ed. by B. Scrosati, Kluver, Amsterdam, The Netherlands, 1993.

G. Malmros, Acta Chem. Scand., 24, 384 (1970)

R. A. McCauley, J. Appl. Phys., 51, 1, 290 (1980)

R. A. McCauley and F. A. Hummel, J. Solid State Chem., 33, 99 (1980)

A. J. Millis, P. B. Littlewood and B. I. Shraiman, Phys. Rev. Lett., 74, 25, 5144 (1995)

R. E. Newnham, Structure – Property Relations, Springer – Verlag, New York, 1975.

R. E. Newnham, R. W. Wolfe and J. F. Dorrian, Mat. Res. Bull., 6, 1029 (1971)

L. G. Nikiforov, Sov. Phys. Cystallogr., 17, 2, 347 (1972)

M. O'Keffee, Structure and Bonding, 71, 162 (1989)

M. O'Keffee, Acta Cryst., A46, 138 (1990)

E. W. Ong, G. H. Kwei, R. A. Robinson, B. L. Ramakrishna and R. B. von Dreele, Phys. Rev. B, 42, 4255 (1990)

L. E. Orgel and J. D. Dunitz, Nature, 179, 462 (1957)

Z. Otwinowski and W. Minor, "Processing of X-Ray Diffraction Data in Oscillation Mode", in Methods in Enzymology, 276, C.W. Carter, Jr. and R.M. Sweet, Eds., Academic Press (1996)

Oxford Crystals, D.J. Watkin, J.R. Carruthers and P.W. Betteridge, Chemical Crystallography Laboratory, University of Oxford, Oxford (1985)

M. M. Qarashi and W. H. Barnes, Amer. Mineral., 37, 423 (1952)

M. M. Qarashi and W. H. Barnes, Amer. Mineral., 38, 489 (1953)

L. Pauling, J. Amer. Chem. Soc., 69, 542 (1947)

L. Pauling, The Nature of the Chemical Bond, Cornell University Press, Ithaca, New York, 1960.

G. S. Pawley, J. Appl. Cryst., 19, 440 (1981)

Profil Program, J. K. Cockroft, Department of Crystallography, Birkbeck College, London, 1994.

Profile Version 1.1, Diffract/AT Software Package Version 3.2, 1985.

I. Radosavljevic, J. S. O. Evans and A. W. Sleight, *J. Solid State Chem.*, 136, 63 (1998)

I. Radosavljevic, J. S. O. Evans and A. W. Sleight, *J. Solid State Chem.*, 137, 143 (1998)

I. Radosavljevic, J. S. O. Evans and A. W. Sleight, *J. Solid State Chem.*, 141, 149 (1998)

I. Radosavljevic, J. S. O. Evans and A. W. Sleight, *J. Alloya and Comp.*, in press

A. D. Rae, J. G. Thompson and R. L. Withers, *Acta Cryst.* B 47, 870 (1991)

B. Raveau, in High-T_c Superconductivity 1996: Ten Years after the Discovery, 109, Kluwer Academic Publishers, Amsterdam, The Netherlands, 1997.W. C. Schumb and E. S. Rittner, *J. Amer. Chem. Soc.*, 65, 1055 (1943)

Refcel Program, J. K. Cockroft, Department of Crystallography, Birkbeck College, London, 1985.

H. M. Rietveld, *J. Appl. Cryst.*, 2, 65 (1969)

The Rietveld Method, ed. by R. A. Young, Oxford University Press, 1993.

J. Rodriguez Caravajal, in Collected Abstracts of Powder Diffraction Meeting, p. 127, Toulouse, 1990.

SAINT, Ver. 5. 04/VMS, Siemens Analytical, Madison, WI, 1995.

H. L. Schlafer and G. Gliemann, Basic Principles of Ligand Field Theory, Wiley – Interscience, London, 1969.

R. D. Shannon and A. W. Sleight, *Inorg. Chem.*, 7, 1649 (1968)

R. D. Shannon, *Acta Cryst.* A32, 751 (1976)

S. Shimada, K. Kodaira and T. Matsushita, *J. Cryst. Growth*, 41, 317 (1977)

P. Shuk, H. D. Wiemhoefer, U. Guth, W. Goepel and M. Greenblatt, *Solid State Ionics*, 89, 179 (1996)

D. F. Shriver, P. Atkins and C. H. Langford, Inorganic Chemistry, Second Edition, W. H. Freeman and Company, New York, 1994.

L. G. Sillen, *Ark. Kemi Mineral. Geol.*, 12A, 1 (1937)

A. W. Sleight, *Inorg. Chem.*, 7, 9, 1704 (1968)

A. W. Sleight, J. L. Gillson and P. E. Bierstedt, *Solid State Commun.*, 7, 299 (1969)

A. W. Sleight, H. Y. Chen, A. Ferretti and D. E. Cox, *Mat. Res. Bull.*, 14, 1571 (1979)

A. W. Sleight, *Science*, 242, 1519 (1988)

A. W. Sleight and J. Huang, US Patent No 5202891 (1993)

D. Stewart and N. Walker, *Acta Cryst.* Sect. A 39, 158 (1983)

S. L. Sorokina and A. W. Sleight, *Mat. Res. Bull.*, 33, 7, 1077 (1998)

E. C. Subbarao, *J. Chem. Phys.*, 34, 2, 695 (1961)

E. C. Subbarao, *J. Amer. Chem. Soc.*, 45, 4, 166 (1962)

E. C. Subbarao, *J. Am. Ceram. Soc.*, 45, 564 (1962)

M. A. Subramanian, G. Aravamudan and G. V. Subba Rao, Prog. Solid State Chem., 15, 55 (1983)

M. A. Subramanian, C. C. Torardi, J. C. Calabrese, J. Gopalakrishnan, K. J. Morrissey, T. R. Askew, R. B. Flippen, U. Chowdry and A. W. Sleight, *Science*, 239, 1015 (1988)

M. A. Subramanian and A. W. Sleight, Handbook on the Physics and *Chemistry of Rare Earths*, Vol. 16, Elsevier Science Publishers B. V., 1993.

P. Suortti, *J. Appl. Cryst.*, 5, 325 (1972)

T. Takahashi and H, Iwahara, *Mat. Res. Bull.*, 13, 1447 (1978)

R. G. Teller, J. F. Brazdil, R. K. Grasseli and J. D. Jorgensen, *Acta Cryst.* C40, 2001 (1984)

F. Theobald, A. Laarif and A. W. Hewat, *Mat. Res. Bull.*, 20, 653 (1985)

C. C. Torardi, J. B. Parise, M. A. Subramanian, J. Gopalakrishnan and A. W. Sleight, *Physica C*, 157, 115 (1989)

C. C. Torrardi et al., *Phys. Rev. B*, 38, 225 (1988)

M. Touboul, J. Lokaj, L. Tessier, V. Kettman and V. Vrabel, *Acta Cryst.*, C48, 1176 (1992)

M. Troemel, *Acta Cryst.*, B39, 664 (1983)

T. Tsunoda, T. Hayakawa, T. Kameyama and K. Takehira, *J. Chem. Soc. Farad. Trans.*, 91, 1117 (1995)

K. B. R. Varma, G. N. Subbanna, T. N. Guru Row and C. N. R. Rao, *J. Mater. Res.*, 5, 2718 (1990)

M. J. Verkerk and A, J, Burggraaf, *J. Electrochem. Soc.*, 75, 128 (1980)

J. W. Visser, J. Appl. Cryst. 2, 89 (1969)

K. Waltersson, *Acta Cryst.*, A34, 901 (1978)

X. Wang, H. Wang and X. Yao, *J. Am. Ceram. Soc.*, 80, 10, 2745 (1997)

A. Watanabe, *Mat. Res. Bull.*, 15, 1473 (1980)

A. Watanabe, Y. Sekikawa and F. Izumi, *J. Solid State Chem.*, 41, 138 (1982)

A. Watanabe, *J. Solid State Chem.*, 41, 160 (1982)

A. Watanabe, *Mat. Res. Bull.*, 19, 877 (1984)

W. Weber, A. L. Shelankov and X. Zotos, *Phys. Rev. B*, 45, 5633 (1992)

P. E. Werner. L. Erriksson and M. Westdahl, *J. Appl. Cryst.*, 18, 367 (1985)

R. A. Wheeler, M. H. Whangbo, T. Hughbanks, R. Hoffmann, J. K. Burdett and T. A. Albright, *J. Amer. Chem. Soc.*, 108. 2222 (1986)

B. T. M. Willis, *Proc. Roy. Soc.*, A274, 134 (1963)

B. T. M. Willis, *Acta Cryst.*, 18, 75 (1965)

R. W. Wolfe, R. E. Newnham and M. I. Kay, *Solid State Comm.*, 7, 1797 (1969)

XPREP, Ver. 5. 04/VMS, Siemens Analytical, Madison, WI, 1995.

W. H. Zachariasen, *Acta Cryst.*, 16, 385 (1963)

W. H. Zachariasen and F. H. Ellinger, *Acta Cryst.*, 16, 5, 329 (1963)

Appendices

Appendix I

The Bond Valence Method – Principles and Applications

The concept of bond valence is historically derived from bond numbers and electrostatic valence rule (1, 2) as defined by Pauling and the definition of bond strengths used by Zachariasen (3). The bond valence method has developed into a powerful tool for verifying known crystal structures and making important predictions about new ones. The method relies on one basic assumption, namely that the total valence of an atom is distributed among the bonds that it forms. This is the formulation of the valence sum rule, which at the same time serves as the definition of bond valence. If atom i makes N bonds with atoms j, then:

$$\Sigma \upsilon_{ij} = V_i \qquad (1)$$

where: υ_{ij} = bond valence of the bond between atoms i and j

V_i = valence of atom i

A well defined correlation between bond valence and bond lengths has been empirically established (4).

The most widely used relationship is the logarithmic one (5):

$$\upsilon_{ij} = \exp\left[(R_{ij} - d_{ij})/b\right] \qquad (2)$$

where: d_{ij} = length of the bond between atoms i and j

R_{ij} = bond valence parameters for atoms i and j

b = fitted parameter

Brown and Altermatt have shown (6) that a universal value of b = 0.37 Å can be used for most practical applications. Bond valence parameters R_{ij} have been determined by Brese and O'Keeffe (7) from over 1000 known crystal structures.

Some important applications of the bond valence method stem directly from the correlation between bond valences and bond lengths; they include:

1. Predicting bond lengths

2. Distinguishing between oxidation states of transition metal atoms

3. Helping resolve structural ambiguities that cannot be resolved by X-rayray diffraction

4. Checking the accuracy of determined crystal structures

Bond lengths can be predicted if the connectivity of the structure is known. When it first started to be used for this purpose, the bond valence approach proved superior to the sum of radii method in that it was able to predict non-equivalent bond lengths between the same pairs of atoms and hence the

distortion of the coordination polyhedra from their ideal geometries. A simple illustration is the example of B_2O_3 (8), while the calculation algorithm for more complicated cases can be found in (9).

The bond valence method found use in distinguishing between the possible oxidation states of transition metal atoms. Two bond valence sums are calculated for the coordination environment of the atom, one for each possible oxidation state. The results of only one calculation will agree with the actual valence, indicating the correct oxidation state. Some examples of this approach include Ti(III)/Ti(IV) oxides (10) and Fe(II)/Fe(III) and Ti(III)/Ti(IV) in ilmenite (9).

Waltersson (11) used the bond valence method to locate Li atoms in the structure of lithium tungstates. He generated a map of the bond valences that Li would have at different sites in the unit cell. Regions of the map for which the calculated bond valences had a value equal to one revealed the locations of Li atoms.

The bond valence method can facilitate structural determinations in cases where X-ray diffraction faces difficulties, for example to distinguish between atoms of similar scattering powers that tend to be found in similar coordinations, such as Si and Al. Bond valence calculation can indicate the correct site for such atoms and also suggest any disorder between them. The method can also be used to distinguish between O and F sites in oxyfluorides, or between O, OH and H_2O when the positions of hydrogen atoms are unknown.

Finally, an equally important application of the bond valence method is verifying the reliability of determined crystal structures. The approach in this case is to start from the bond lengths predicted by the model and calculate the corresponding bond valences. Any obtained valence sums that significantly deviate from the expected valued for the atoms in question would indicate a possible error in the structural model.

References

1. L. Pauling, *J. Amer. Chem. Soc.*, 69, 542 (1947)

2. L. Pauling, The Nature of the Chemical Bond, Cornell University Press, Ithaca, New York, 1960.

3. W. H. Zachariasen, *Acta Cryst.*, 16, 385 (1963)

4. I. D. Brown and R. D. Shannon, *Acta Cryst.*, A29, 266 (1973)

5. I. D. Brown, in Structure and Bonding in Crystals, ed. by M. O'Keffee and A. Navrotsky, Academic Press, New York, 1981.

6. I. D. Brown and D. Altermatt, *Acta Cryst.*, B41, 244 (1985)

7. N.E. Brese and M. O'Keeffe, *Acta Cryst.*, Sect B47, 192 (1991)

8. M. O'Keffee, *Structure and Bonding*, 71, 162 (1989)

9. M. O'Keffee, *Acta Cryst.*, A46, 138 (1990)

10. M. Troemel, *Acta Cryst.*, B39, 664 (1983)

11. K. Waltersson, *Acta Cryst.*, A34, 901 (1978)

Appendix II

The Jahn Teller Effect

In 1937, Jahn and Teller (1) formulated a theorem stating that a non linear molecule with a partially occupied set of degenerate orbitals will distort to a form of lower symmetry and lower energy. They proved the theorem by mathematically strict group theoretical means, by showing that there always exists at least one vibrational mode that leads to the transformation of the totally symmetric nuclear configuration in the given point group to a more stable configuration of lower energy. Jahn and Teller also showed that the tendency towards distortion depends on the nature of the degenerate orbitals: the larger their effect on bonding, the larger the instability of the molecule with respect to distortion.

For a given set of degenerate orbitals, the theorem makes no a priori conclusions about the magnitude and the direction of distortion. It also does not distinguish between static distortions of coordination polyhedra and dynamic effects that involve resonance of several equivalent non-degenerate configurations. In the former case, the descent to lower symmetry and distortions of coordination polyhedra can be detected by crystallographic means. In the latter case, a higher average macroscopic symmetry is observed by

crystallographic experiments. Whether the Jahn Teller distortion will be static or dynamic in a given case depends on the potential barrier ΔE that needs to be surmounted for the molecule to undergo oscillations between the equivalent distorted configurations (2). If, for a given distortion at a given temperature, ΔE is larger than kT, the effect will be static. If ΔE is comparable to or smaller than kT, dynamic Jahn Teller effect will occur.

Coordination environments of Cu^{2+} reported in literature are distorted octahedral, square planar and tetrahedral (3). The first type is by far the most common and the rest of the decription of the Jahn Teller effect will apply to this particular coordination. Cu^{2+} has a d^9 electron configuration. In an octahedral ligand field, it has a set of partially filled degenerate e_g orbitals. Moreover, the e_g orbitals have a strong antibonding character compared to the non bonding character of the t_{2g} orbitals (4). This feature adds to the magnitude of the Jahn Teller distortion in Cu^{2+}.

The effect itself can be qualitatively described without the rigorous group theoretical considerations by using simple crystal field arguments. Let us assume the electron configuration of the degenerate e_g set to be $(d_z^2)^2 (d_{x^2-y^2})^1$. Since the lobes of the $(d_{x^2-y^2})$ orbital extend along the x and y axes, and this orbital is occupied by a single electron, the central ion will be less effectively shielded in these directions. The four ligands along the x and y axes will be attracted by a stronger effective nuclear charge than the two along the z axis. Consequently, a

distortion occurs by formation of four short and two long bonds relative to the totally symmetric octahedron.

By analogous arguments, the formation of a compressed octahedron can be explained if the initial electron configuration of the degenerate e_g set of $(d_{x^2-y^2})^2 (d_z^2)^1$ is assumed.

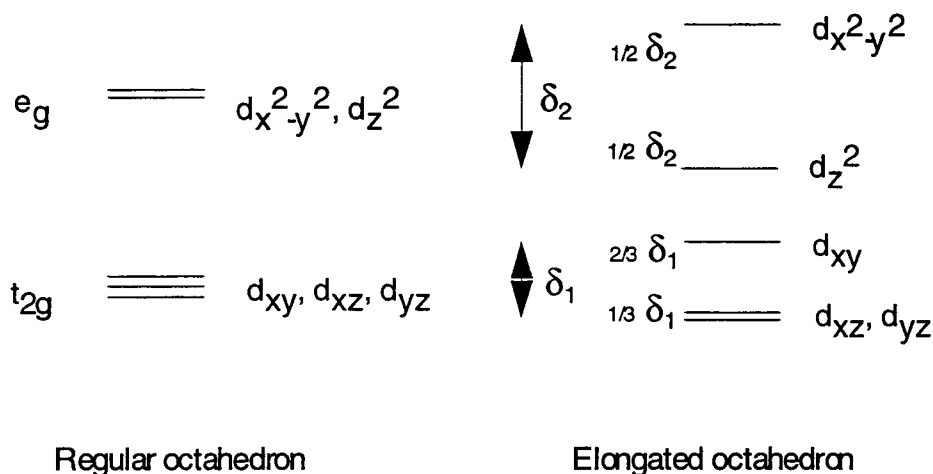The energetics of the process of formation of an elongated octahedron are represented in Figure II.1.

Figure II.1. An energy diagram for the Jahn Teller effect

The driving force for the distortion is the stabilization energy that, according to the diagram in Figure II.1, for the case of Cu^{2+} amounts to:

$$E_{stab} = -1/2 \, \delta_2 \times 2 + 1/2 \, \delta_2 \times 1$$

$$E_{stab} = -1/2 \, \delta_2$$

In the framework of the molecular orbital theory, the source of this stabilization energy can be qualitatively related to the removal of one electron from an antibonding orbital.

In addition to Cu^{2+}, typical Jahn Teller ions with e_g degenerate orbitals include high spin d^4 ions (Mn^{3+}, Cr^{2+}) and low spin d^7 ions (Co^{2+}, Ni^{3+}). Jahn Teller effects of slightly smaller magnitudes are found for ions with t_{2g} degenerate orbitals, such as d^1 (Ti^{3+}), d^2 (Ti^{2+}, V^{3+}), low spin d^4 ions (Mn^{3+}, Cr^{2+}), low spin d^5 ions (Mn^{2+}, Fe^{3+}), high spin d^6 ions (Fe^{2+}, Co^{3+}) and low spin d^7 ions (Co^{2+}, Ni^{3+}).

The Jahn Teller effect can be experimentally observed by diffraction and paramagnetic resonance techniques (5).

Two areas of important active research in solid state chemistry where the Jahn Teller effect has been proposed as an important factor are high T_c cuprate superconductors (6) and Mn^{3+} containing colossal magnetoresistive materials (7).

Second order Jahn Teller effect is manifested in the mixing of the highest occupied and lowest unoccupied molecular orbitals, when the energy difference between the two is small enough to allow it (8). It results in the lowering of coordination environment symmetry of the cation in question. A good example of the second order Jahn Teller effect is the lone pair stereochemical activity and the resulting asymmetric coordination environments of Bi(III).

References

1. H. A. Jahn and E. Teller, *Proc. R. Soc. London, Ser. A*, 161, 220 (1937)

2. H. L. Schlafer and G. Gliemann, Basic Principles of Ligand Field Theory, Wiley – Interscience, London, 1969.

3. L. E. Orgel and J. D. Dunitz, *Nature*, 179, 462 (1957)

4. D. F. Shriver, P. Atkins and C. H. Langford, Inorganic Chemistry, Second Edition, W. H. Freeman and Company, New York, 1994.

5. L. R. Falvello, *J. Chem. Soc., Dalton Trans.*, 4463 (1997)

6. W. Weber, A. L. Shelankov and X. Zotos, *Phys. Rev. B*, 45, 5633 (1992)

7. A. J. Millis, P. B. Littlewood and B. I. Shraiman, *Phys. Rev. Lett.*, 74, 25, 5144 (1995)

8. R. A. Wheeler, M. H. Whangbo, T. Hughbanks, R. Hoffmann, J. K. Burdett and T. A. Albright, *J. Amer. Chem. Soc.*, 108. 2222 (1986)